Bacteriophage M13 as a Template for Multi-Enzyme Assembly

By

Taylor May Urquhart

A thesis

presented to the University of Waterloo

in fulfillment of the

thesis requirement for the degree of

Doctor of Philosophy

in

Chemistry

Waterloo, Ontario, Canada, 2019

Examining Committee Membership

The following served on the Examining Committee for this thesis. The decision of the Examining Committee is by majority vote.

External Examiner	DR. JAN K. RAINEY Professor
Supervisor(s)	DR. JOHN F. HONEK Professor
Internal Member	DR. JOSEPH G. GUILLEMETTE Associate Professor
Internal Member	DR. JUEWEN LIU Professor
Internal-external Member	DR. DAVID R. ROSE Professor

Author's Declaration

I hereby declare that I am the sole author of this thesis. This is a true copy of the thesis, including any required final revisions, as accepted by my examiners. I understand that my thesis may be made electronically available to the public.

Abstract

An important aspect of bionanotechnology is the utilization of biomolecules to prepare controlled and defined arrangements of multiple components with nanoscale order. Bacteriophage M13 is a filamentous phage composed of five different coat proteins: with the minor coat proteins p3, p6, p7 and p9 each having five copies at the ends of the phage. The major coat protein p8 is a small alpha-helical protein and is present in approximately 2700 copies encapsulating the M13 ssDNA genome. The goal of this thesis research was to further develop methodologies for utilizing bacteriophage M13 as a scaffold for the purpose of binding multiple enzymes with nanoscale order to p8. The cellulase, Cel8A, was selected as the model protein to explore this system, as it exists as part of a multi-enzyme complex known to form in nature: the cellulosome.

Several different methodologies to load the bacteriophage with Cel8A were explored in order to determine the optimal way to prepare multi-enzyme complexes that were uniformly and densely loaded. In Chapter 2, an enzyme-mediated approach was taken to prepare an M13 construct with cohesin, a cellulosomal protein capable of binding to dockerin-containing cellulase, reacted to the p8 major coat proteins. The cohesin modules could then be used to bind the model protein, Cel8A. Under the conditions required for this enzyme-mediated reaction, cohesin was found to efficiently undergo a cyclization side reaction and an adduct to M13 could not be detected.

Of the approaches tested, the most successful approaches utilized highly efficient protein-ligand interactions. Streptavidin (a tetrameric protein which binds tightly to the small molecule biotin) served as an adaptor protein which could be bound to biotinylated p8. Two main strategies were explored for interacting Cel8A with the bacteriophage scaffold. In Chapter 3, a protocol for producing monovalent SA (single biotin-binding site) with three functional groups capable of binding to His6-tagged Cel8A was devised. However, dense enzyme loading was limited by the interaction between these functional groups and the His6-tagged protein.

In Chapter 4, covalently biotinylated Cel8A was utilized. The main challenge of this approach was binding all of the components (M13-biotin, SA and Cel8A) in a way that avoided aggregation. Surprisingly, it was found that under the appropriate conditions, SA on its own could efficiently coat the biotinylated bacteriophage without considerable crosslinking side interactions. It was furthermore found that the ionic strength of the solution impacted the stability of these SA-coated M13 complexes. Lastly, the constructs were tested for cellulase activity and were found to be active against both simple and complex cellulosic substrates. Over the course of this thesis, challenges which were encountered for each explored strategy are highlighted in order to improve future endeavors in preparing multi-enzyme complexes on virus-based nanoscale scaffolds.

Acknowledgments

I would like to first acknowledge my supervisor, John Honek, for guiding me through the process of designing and troubleshooting various difficult aspects of this project and giving me the opportunity to work on a challenging and complex system. In addition to this, being willing to impart some of his lifetime of experience in academia has helped me when I needed a shift in perspective.

I am grateful for Mishi Groh, for teaching me the finer points about electron microscopy and encouraging me to not settle for sub-par micrographs. I appreciate Dr. Richard Smith for giving his time and expertise in improving my theoretical understanding of mass spectrometry and granting me additional technical experience through my use of the equipment. Similarly, Val Goodfellow has provided very valuable technical assistance in using the mass spectrometers.

I would like to generally thank all of the Honek lab members throughout the years I've been here, with whom it was a pleasure to work with and have made the experience an interesting one. I am thankful for the friends I've made here and the support they have given me.

I would like to acknowledge my incredible partner, Kerith, who has helped to keep me centered and given me all the time and support I could ever need – and my family, who have always been available to show support and love when I needed it.

Table of Contents

List of Figures

List of Tables

List of Abbreviations

Acronym	Description
ADH	Alcohol dehydrogenase
Ald	Aldolase
AtoB	Acetoacetyl-CoA thiolase
B4F	Biotin-4-fluorescein
BSA	Bovine serum albumin
BXN	Biotin-X-NTA (N_{ε}-(*N-(+)*-Biotinyl-6-aminohexanoyl)-N_{α},N_{α}-bis(carboxymethyl)-*L*-lysine)
CBM	Cellulose-binding module
CBM-Coh	Cellulose-binding module-cohesin fusion protein
Cel8A	Endo-1,4-*β-D*-glucanase from *C. thermocellum* (UniProt: A3DC29)
CF	Correction factor
CMC	Carboxymethylcellulose
CNT	Carbon nanotube
Coh	Cohesin
Coh-Doc	Cohesin-dockerin
Coh2	Second cohesin domain from *C. thermocellum* CipA scaffoldin
DMSO	Dimethyl sulfoxide
DNS	Dinitrosalicylic acid
Doc	Dockerin
dtb	Desthiobiotin
EMS	Electrophoretic mobility shift

ESI-MS	Electrospray ionization mass spectrometry
F1,6BPase	Fructose 1,6-bisphosphatase
G6pDH	Glucose-6-phosphate dehydrogenase
GNP	Gold nanoparticle
GFP	Green fluorescent protein
HMGR	Methylglutaryl-CoA reductase
HMGS	Hydroxy-methylglutaryl-CoA synthase
HRP	Horseradish peroxidase
IEC	Ion exchange chromatography
IMAC	Immobilized metal affinity chromatography
IPTG	Isopropyl-B-*D*-1-thiogalactopyranoside
LB	Luria Broth
LC/MS-MS	Liquid chromatography tandem mass spectrometry
LDH	Lactate dehydrogenase
MDH	Malate dehydrogenase
MWCO	Molecular weight cut-off
MQH$_2$O	Ultra-pure (18 MΩ·cm resistivity) water
NADH	Nicotinamide adenine dinucleotide
NHS-TAMRA	*N*-hydroxy succinimidyl *5(6)*-carboxytetramethylrhodamine
NP	Nanoparticle
NTA	Nitrilotriacetic acid
PAGE	Polyacrylamide gel electrophoresis
PASC	Phosphoric-acid swollen cellulose

PBS	Phosphate-buffered saline
PEG	Polyethylene glycol
PEG-8000	Polyethylene glycol 8000 Da average MW
PFU	Plaque-forming units
PMSF	Phenylmethylsulfonyl fluoride
pNP	*p*-nitrophenol
PTA	Phosphotungstic acid
QD	Quantum dot
RFU	Relative fluorescence units
SA	Streptavidin
SA_{tet}	Streptavidin tetramer
SauSrtA	Sortase A from *S. aureus*
SD	Standard deviation
SDM	Site-directed mutagenesis
SDS	Sodium dodecyl sulfate
SEC	Size-exclusion chromatography
SpySrtA	Sortase A from *S. pyogenes*
SrtA	Sortase A
TAMRA	*5(6)*-carboxytetramethylrhodamine
TEM	Transmission electron microscopy
TFP-PEG_4-biotin	Tetrafluorophenyl-PEG_4-biotin

TFP-PEG$_{12}$-biotin	Tetrafluorophenyl-PEG$_{12}$-biotin
TIM	Triosephosphate isomerase
TMB	*3,3′,5,5′*-Tetramethylbenzidine
Tris	Tris(hydroxymethyl)aminomethane

Chapter 1 Introduction

Viruses are particles composed of proteins and nucleic acids capable of replication within a host organism. There exists a wide diversity of virus on Earth, with the oceans alone containing an estimated 200,000 different species of virus (Gregory et al. 2019). This variety, in addition to being important for understanding the role of viruses in different ecosystems, provides us with a plethora of viral architectures ranging in size and composition. Given the variety of virus species, future work on developing viruses as materials, or components in nanotechnologies, is one area that is expected to continue to evolve with the discovery of new viral architectures.

1.1 Bionanotechnology

Nanotechnology encompasses a very wide and interdisciplinary space that has been used to address a number of medical and technological challenges (Doll et al. 2013; Jinjun Shi et al. 2017). Nanotechnology deals with components or assemblies of components with features in the nanoscale. The types of research falling under the umbrella of nanotechnology might include those dependent on the positioning of just a few atoms (Eigler and Schweizer 1990) up to relatively "large" assemblies of components into nanoscale machines capable of self-assembling and performing a particular task (Douglas, Bachelet, and Church 2012; Ma et al. 2019). The types of materials that find use in various nanotechnological applications are wide-ranging, including: nanoparticles (**NP**), quantum dots (**QD**), organic polymers, and biological materials, such as DNA and RNA (Chidchob and Sleiman 2018), liposomes (Barile and Vassalli 2017; Malam, Loizidou, and Seifalian 2009), capsule proteins (He and Marles-Wright 2015; B.-R. Lee et al. 2016), structural proteins such as spider silks (L. Xu et al. 2013; Karan et al. 2018), nanocellulose (W. Chen et al. 2018; Kargarzadeh et al. 2018) and viruses (Molek and Bratkovič 2015; Petrescu and Blum 2018). Where the material components are biological in nature, the field can be more specifically referred to as bionanotechnology.

While there is considerable overlap in the types of applications to which these different biological materials find themselves applied, the structures and properties of each biomolecule allow them to fill different roles (**Figure 1.1**). Many of these materials have been applied to medical applications, including cell-targeting, drug delivery, diagnostic imaging and vaccination (Doll et al. 2013). In the context of drug delivery, there exist a number of FDA approved or clinical trials of systems of drug delivery based on liposomes as the vehicle (Jinjun Shi et al. 2017). The application of DNA is varied, given the massive design space made possible by being able to program precise shapes and geometries in an algorithmic way (Chidchob and Sleiman, 2018). In this way, DNA can be essentially "tailor-made" for a particular application. Specifically, nucleic acids with a designed or evolved affinity interaction (aptamers) or DNAzymes (DNA with catalytic activity) allow the design of varied biosensors with specific activity toward a particular analyte (Du and Dong 2017; Zhou, Saran, and Liu 2017). Proteins, inclusive of capsule proteins, viruses and virus-like particles, encompass a wide-range of potential applications including medical imaging tools, drug delivery vehicles, biocatalysts, and components that can impart new functionality to materials (E. J. Lee 2018). The nature of the application depends again on the possible geometries of proteins presented by nature – though there has been some work on building exact protein architectures from design principles (King et al. 2012; Glover and Clark 2016). Nanocellulose is a stable, biodegradable and renewable material that has found application to energy storage (W. Chen et al. 2018) or as a component in the preparation of nanomaterials (Hajian et al. 2017). There is much overlap in the applications of these biomaterials, and a thorough catalog of the nanoscale properties, and methodologies to properly incorporate these materials will aid in their optimal use in device designs and medical therapies.

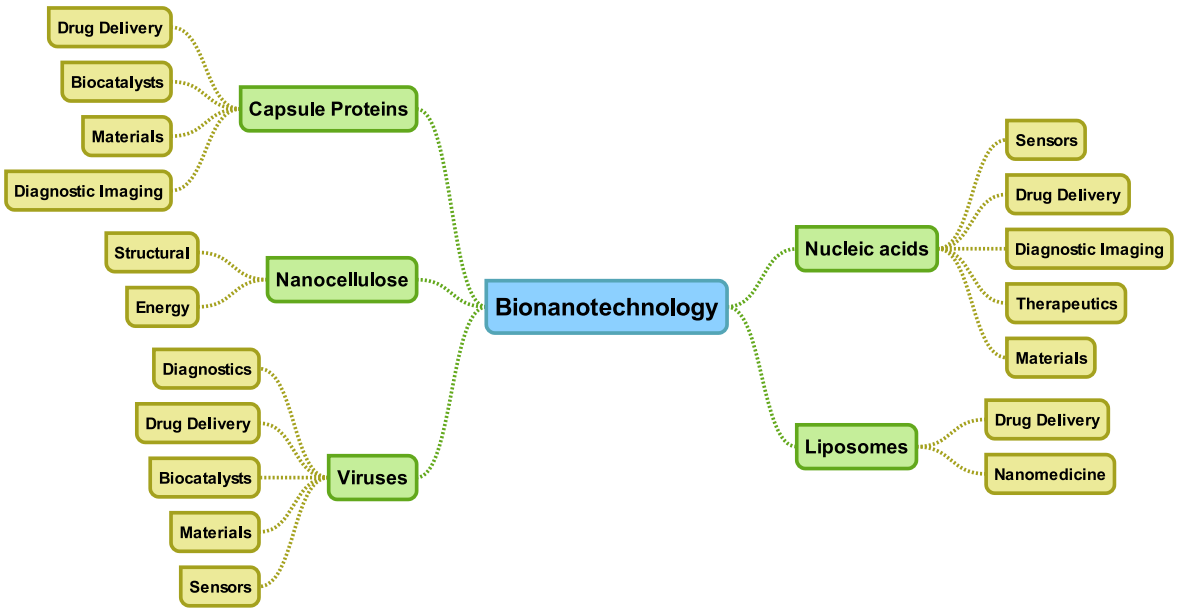

Figure 1.1: Overview of typical bionanomaterial applications.

Viruses have been noted to have several properties that would be beneficial to their use in bionanotechnology (L. A. Lee and Wang 2006). Namely, that they have: defined architecture with a variety of shapes and sizes, they are monodisperse, many have resolved structures, they can be produced in large-scale quantities, the surface chemistries of the viral coats can be manipulated by genetic methods, and in addition to genetic methods, chemical modification enables extensive possibilities for particle design. To elaborate on these points made by Lee and Wang, viruses have found their way into a number of very interesting nanotechnology applications beyond just biomedical applications. As illustrated in the cited review, there have been a number of sensor applications prior to 2014 (Hwang 2014). Further work on virus-based technological applications have continued since then (Petrescu and Blum 2018). While spherical viruses might share some common applications with capsule proteins and liposomes given their similar overall shape, filamentous viruses offer an interesting high-aspect ratio architecture to work from and has been taken advantage in a number of ways which will be highlighted in the following section.

1.2 Bacteriophage M13

1.2.1 Structure and properties

A virus that has found extensive use in bionanotechnological applications is the filamentous bacteriophage, M13. Bacteriophage M13 is a filamentous virus that infects enteric bacteria, such as *E. coli*. This phage has dimensions of ~7 x 900 nm and encapsulates a single stranded DNA genome (Day et al. 1988). M13 has five copies of each of its minor coat proteins, with p3 and p6 at one end and p7 and p9 at the other (**Figure 1.2**). Along the length of the phage is the major coat protein, p8, which is present in approximately 2700 copies (Day et al. 1988). The p8 coat protein has three general regions important to its assembly in the M13 coat: residues 1-20 consist of an amphipathic region, residues 21-39 compose a hydrophobic transmembrane region, and residues 40-50 compose the DNA-binding region (**Figure 1.3**) (D. Marvin 1998; K. A. Williams et al. 1995). The amphipathic region is composed of an alanine-rich face responsible for hydrophobic interaction with other pVIII in assembled M13 (K. A. Williams et al. 1995). The hydrophobic transmembrane portion of the helix keeps pVIII bound in the inner membrane of *E. coli* until re-assembly and is important for interaction between pVIII units in assembled M13. The DNA-binding region is composed of positively charged amino acids which interact with the phosphate backbone of DNA (Rakonjac et al. 2011).

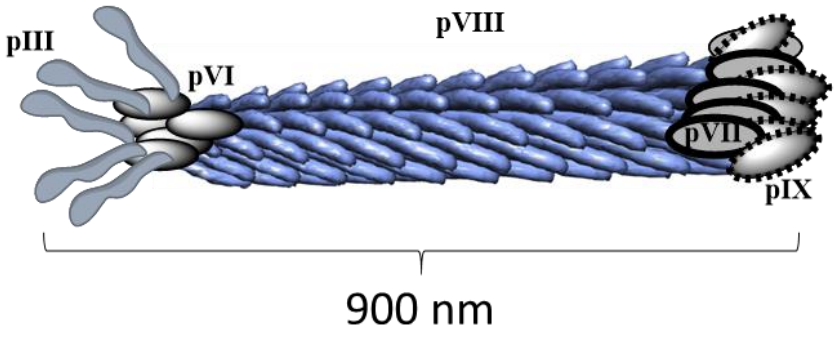

Figure 1.2: Structure of assembled bacteriophage M13.

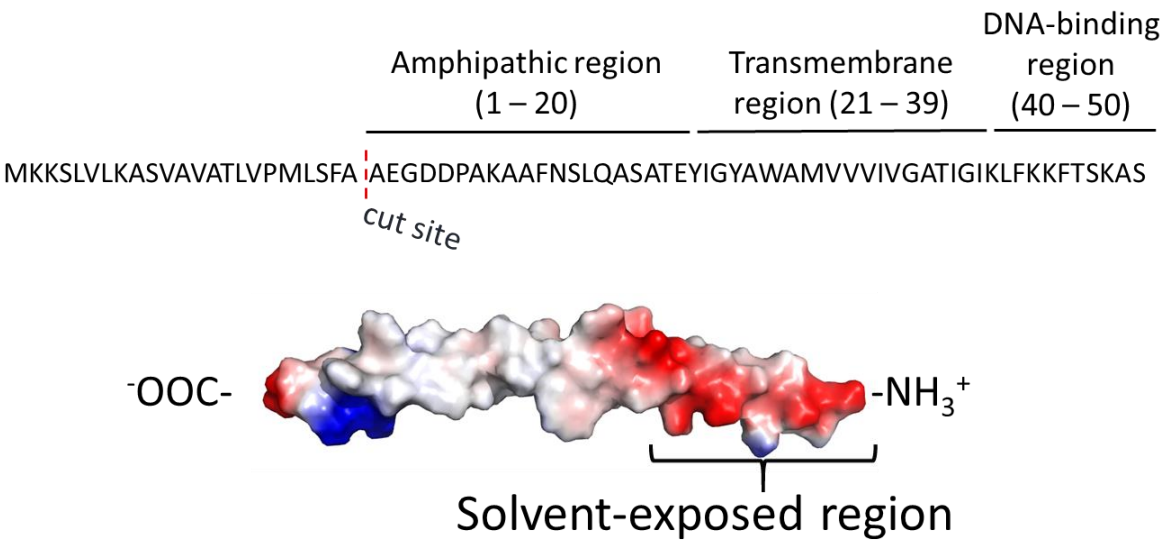

Figure 1.3: Major coat protein p8 sequence and structure. The sequence is of pro-p8 prior to removal of the 23 N-terminal residues by bacterial leader peptidase. Blue: basic residues, Red: acidic residues. PDB: 1IFJ (D. A. Marvin et al. 1994).

1.2.2 Life cycle

M13 is a non-lytic phage capable of sustaining its host while replicating in a controlled fashion that occurs without lysis or death of the host bacterium. This enables M13 to produce some of the highest occurring titers in nature (~10^{13} PFU/mL). The life cycle of M13 and the relevant experiments are very nicely summarized in the following two cited reviews (D. A. Marvin, Symmons, and Straus 2014; Rakonjac et al. 2011). Initially, the minor coat protein p3 is responsible for infection of its bacterial host by binding to the tip of the pilus. Therefore, there is the additional requirement that the host strain contain the F-plasmid which codes for the production of pili. In the absence of phage, the role of the pilus is to bring bacterium in close proximity to exchange DNA through conjugation (Clarke et al. 2008). This periodically extends and retracts, bringing the phage in close to the bacterial membrane to bind its secondary receptors, the TolQRA membrane protein complex, and initiate injection of its DNA into the host cell. After the ssDNA positive strand is injected into the cytoplasm, the host *E. coli* proteins synthesize the complementary strand (negative strand) of the DNA and the translation of phage proteins begins. In addition, more copies of DNA are replicated until p5, a DNA-binding protein, has been translated in sufficient quantity to bind up single stranded DNA for packing

into extruding M13 (**Figure 1.4**). The various membrane-bound M13 coat proteins assemble as the single-stranded DNA is extruded through a pore complex composed of M13 proteins p1, p4 and p11 (Rakonjac et al. 2011). A detailed description of this life cycle can be found in the following two reports which model the assembly of phage in a mathematical manner – taking into account the extensive data for M13 assembly from various sources (Smeal et al. 2017a; 2017b).

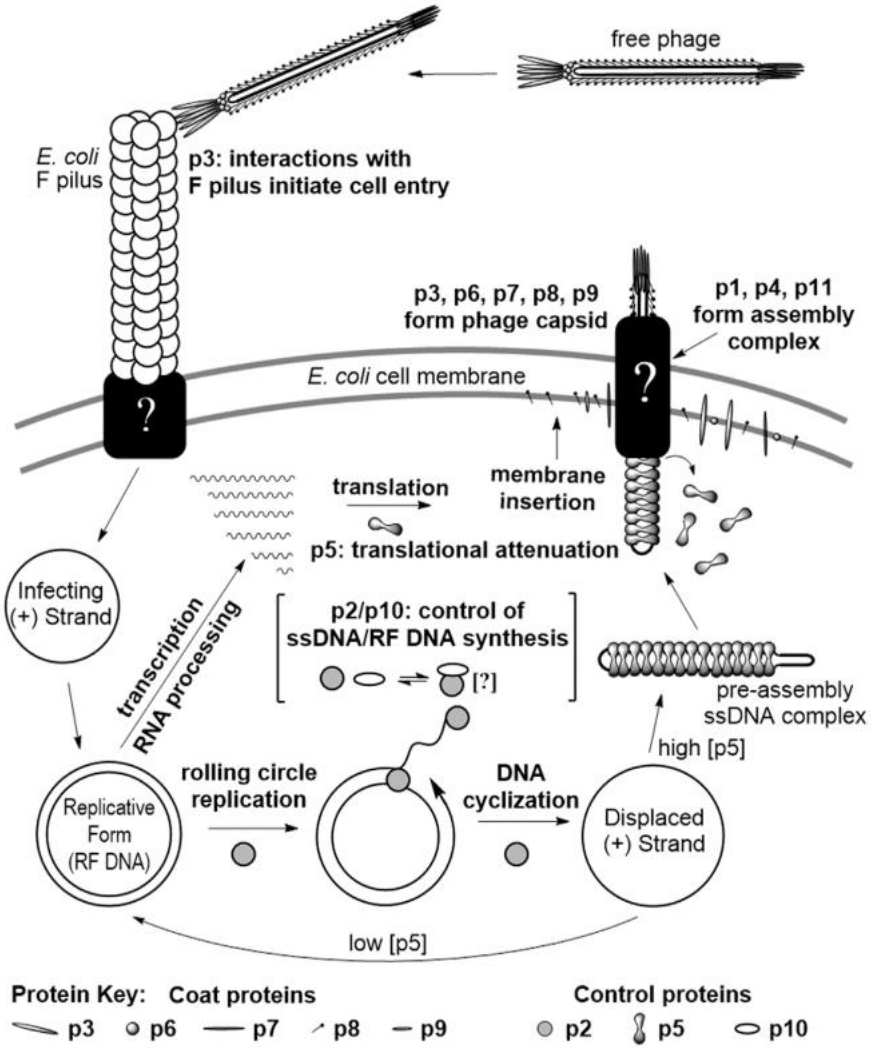

Figure 1.4: Life cycle of bacteriophage M13. Reproduced with permission from (Smeal et al. 2017a).

The major coat protein p8 is initially synthesized as pro-p8, a 73 amino acid protein (**Figure 1.5**). The N-terminal portion of pro-p8 destines the protein for transport to the inner membrane where it is then processed by leader peptidase to the mature coat protein with a single transmembrane helix; the N-terminus points toward the exterior of the cell (Rakonjac et al. 2011). Initially the protein is able to

associate with the inner leaf of the inner membrane by electrostatic attraction – its insertion into the inner membrane occurs without the requirement of the Sec translocase. Instead, the process occurs using the YidC invertase (Samuelson et al. 2001). However large p8 fusions have been observed to use the Sec translocase (Roos et al. 2001). After insertion into the inner membrane, there are two transmembrane domains with helices near to each other in the membrane (Eisenhawer et al. 2001). In the inner membrane, a leader peptidase cleaves the leader sequence, forming the mature p8 coat protein. By an unknown mechanism, p8 is able to associate with the extruded ssDNA of M13 as it passes through the p1/p4/p11 pore complex. Overall, much of the lifecycle of M13 has been well-studied – by having this level of detail on its assembly, it is possible to troubleshoot and better design engineered M13 bacteriophages for specific applications.

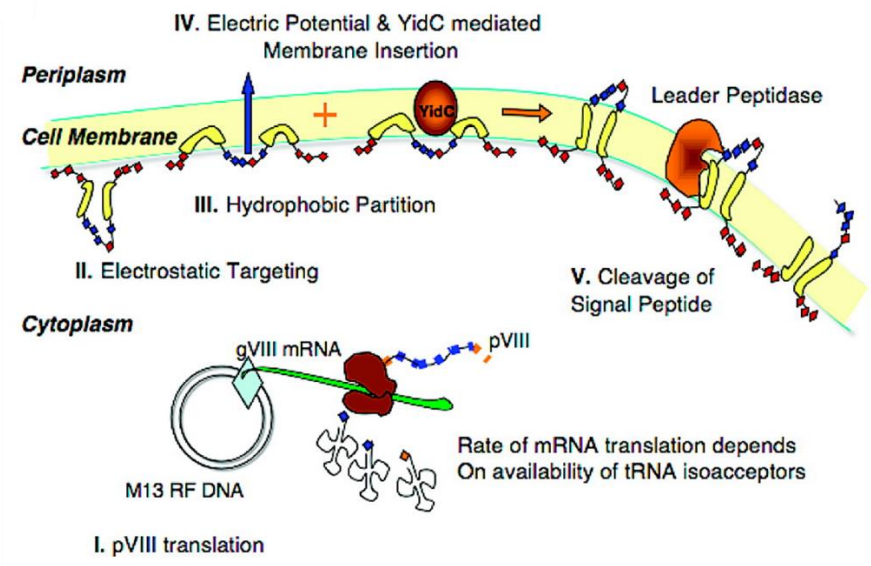

Figure 1.5: Fate of p8 during processing from pro-p8 to mature p8. Reproduced with permission from (Merzlyak and Lee 2009). Copyright (2009) American Chemical Society.

1.2.3 Applications

M13 has seen a great number of applications in the last few decades. These applications vary widely, including: application to medicine (Choi et al. 2014; DePorter and McNaughton 2014; J. Y. Lee, Chung, and Kim 2016; J. Wang et al. 2014; H.-S. Lee et al. 2018), energy (Nam 2006; B. Y. Lee et

al. 2012; P.-Y. Chen et al. 2013; Jeong et al. 2013; Shin et al. 2015), biosensor fabrication (H.-E. Lee et al. 2014; Oh et al. 2014; Adhikari et al. 2015; Brasino, Lee, and Cha 2015; Yan et al. 2016; J. H. Lee et al. 2017; Koh et al. 2018), functional materials (Niu et al. 2008; Courchesne et al. 2014; Jung et al. 2017; Devaraj et al. 2018) and nanomaterial synthesis (Mao 2004; Park et al. 2014; Zaman and Haberer 2014; Moradi et al. 2016; De Plano et al. 2018). These approaches have made use of different aspects of M13, including its architecture (7 x 900 nm slightly flexible rod) and surface properties (altering the major coat protein, given its high copy number, can greatly change the phage's properties). A selection of these applications will be highlighted in the following section, though the examples presented here are not exhaustive but representative of some of the different ways M13 has been utilized.

An early and still widely used technique utilizing M13 is phage display. Namely, by making modifications to the DNA genome of the virus, it is possible to produce fusion proteins of several of the virus's five mature coat proteins. This was initially demonstrated on p3 minor coat protein with the fusion of a protein fragment (G. P. Smith 1985). The ability to isolate phage bearing the fused protein by affinity interaction was demonstrated. The production of fusion proteins to p3 has been the most extensive and well known genetic manipulation of M13. Furthermore, gene libraries can instead be inserted producing a library of M13 phages with randomized stretches of amino acid sequences. This allows variants with a particular property to be isolated, amplified, and then sequenced to determine the identity of the insert (**Figure 1.6**). While it is possible to produce M13 with only coat proteins present as fusion proteins, by encoding the fusion protein on a phagemid and infecting with a helper phage (which provides the wildtype coat proteins), an M13 phage with a mix of wildtype and fusion coat protein can be obtained (Henry, Arbabi-Ghahroudi, and Scott 2015). Lowering the frequency of fusion protein can be useful in reducing avidity effects when performing selection (Chappel, He, and Kang 1998; Tsunoda, Tsutsumi, and Imai 2008). This results in higher affinity binders that can be isolated by biopanning. There are examples of phage display on all five of its coat proteins, though p3 and p8 display are most common.

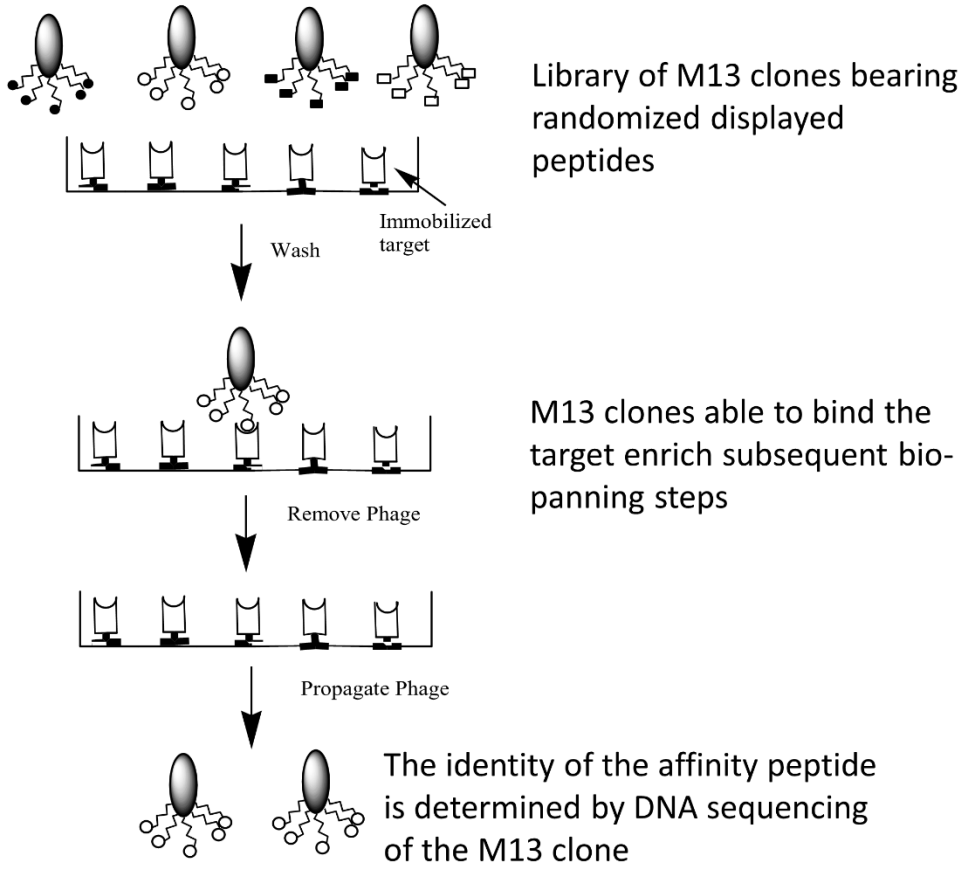

Figure 1.6: Schematic overview of biopanning using M13 phage display libraries.

Early applications of phage display envisioned the development of libraries of M13 fusions to isolate strong binding peptides to antibodies (G. P. Smith 1985). However, this technology has expanded and found utility beyond biological binding processes; quite interesting is its application to inorganic biological materials and non-biological materials – allowing a bridging of biological components and materials through affinity interactions (Seker and Demir 2011). For example, phage display against gold has led to the discovery of several gold-binding peptides (Huang et al. 2005; Jungok Kim et al. 2010; D. J. Lee et al. 2019; Tamerler et al. 2006). These could be used to target a complex to a gold surface, or allow gold nanoparticles (**GNP**) to bind to the viral surface. Related to the topic of interfacing biological components with materials was the discovery of a semi-conductor binding peptide (Whaley et al. 2000). Also related to nanomaterials was the discovery of a peptide with an affinity for single wall carbon nanotubes (**CNTs**) – also through phage display (Su, Leung, and

Honek 2006). At this point in time, there are many examples of p3-fusions that have been identified against a range of materials making for a substantial toolbox of phage variants to choose from in preparing engineered nanoscale constructs composed of M13 bacteriophage. Indeed, the idea of utilizing p3 as a targeting component, and p8 bound to a "cargo" molecule is an interesting one.

However, with the major coat protein of M13, p8, there exist limitations to the extent with which a fusion can be made. While fusions to p3 can be quite large, protein fusions made on p8 must be short (limited to 5 - 8 amino acids) (Henry, Arbabi-Ghahroudi, and Scott 2015). One approach to address this limitation has been to produce hybrid M13 with a mix of wildtype and fusion-p8; however, these typically yield low display rates at <1 protein/M13 (Sidhu, Weiss, and Wells 2000). Furthermore, even short amino acid fusions to p8 can produce non-viable phage if they interfere with the processing of pro-p8 protein (Merzlyak and Lee 2009). In particular, the bacterial leader peptidase can have trouble with processing p8 if there is too much positive charge near the mature N-terminus (**Figure 1.5**). This can cause the external loop to associate to the negatively charged extracellular leaf of the *E. coli* inner membrane which makes it difficult for leader peptidase to cleave pro-p8. Despite the difficulties of genetic fusion to p8, there exist libraries of p8 fusions that allow for different sorts of interactions to be discovered due to the different mode of binding to an antigen. In particular, the multiple p8 interactions that result from the many copies of p8 can result in lower affinity interactions that can be enhanced by avidity (Knez et al. 2013). Furthermore, the display of short peptides on p8 can greatly change the properties of the entire phage, as there are 2700 copies and these proteins make up the majority of the mass of M13.

Despite the limitations of p8 display, chemical modification of the major coat protein is a good alternative with a great deal of work done with characterization and application. A thorough examination of native p8 has found reactivity from several exposed amino acids: Gly1 (amine), Glu2, Asp4/5, Lys8, Tyr21 and Tyr24 were all capable of chemical modification (K. Li et al. 2010). Furthermore, the incorporation of orthogonally reactive, non-canonical amino acids for phage display,

or for the purpose of utilizing M13 as a nanoscale scaffold has expanded its reactivity (Tian, Tsao, and Schultz 2004; Urquhart, Daub, and Honek 2016). The filamentous structure of M13 was used to prepare a light-responsive nanowire by modifying Tyr residues with a photo-reactive component (Murugesan et al. 2013). Building up on the idea of M13 as a scaffold for adding components onto, this has been carried out with several minerals.

A number of different approaches have been taken to accomplish controlled mineralization or formation of nanoparticles with M13. M13 without any kind of modification has been shown to be suitable for the reduction of metal salt solutions directly onto the filamentous phage (Avery, Schaak, and Schaak 2009). The electrostatics of M13 have been further tuned in a number of cases by engineering several glutamates on the N-terminus of p8 – aiding the electrostatic attraction of cationic metals for nucleation along the length of intact M13. Nanodimensional MnO_2 nanowires formed on E4-M13 was employed in a novel glucose oxidase biosensor (Han et al. 2016). E3-M13 phages were used to form TiO_2 nanowires in solution, which were then formed into a network (P.-Y. Chen et al. 2015). E4-M13 with bound Co_3O_4 in solution, which was reduced with $NaBH_4$, was used to form the anode of a flexible battery (Nam 2006). The M13 used for this was a hybrid formed with a mixture of p8 displaying the EEEE (E4) motif, and some p8 showing a specific gold-binding motif. M13 with defined metal-binding properties has also been used – taking advantage of the capability of displaying short peptides along the length of M13 (on the p8 major coat protein). Several different peptides selected for binding to ZnS, CdS, FePt and CoPt have been used to form different crystalline nanowires (Mao 2004).

One of the most intriguing and surprising applications of M13 has been its utilization in technological applications. Elaborating upon the fundamentals of how one could prepare mineralized M13 phages, these concepts have been further applied to more elaborate device designs. M13 has been used in the construction of energy producing materials using a few different strategies which both utilize the architecture of the virus in unique ways. In one example, the filamentous structure of the

virus was useful as a template for the mineralization of $BaTiO_3$ which allowed the material to be better dispersed and utilized more efficiently as a flexible generator (**Figure 1.7A**) (Jeong et al. 2013). Again, using the architecture of the phage itself to template the mineralization of a material, this time the formation of gold clusters and dye molecules were utilized for a dye-sensitized solar cell design (**Figure 1.7B**) (P.-Y. Chen et al. 2013). Further exploring the use of M13 in energy devices, energy generation was realized by using the piezoelectric properties of the p8 major coat proteins to create a material which would generate a current when flexed (B. Y. Lee et al. 2012). These applications of M13, a scaffold which can been separately and controllably modified by genetic and chemical methods, demonstrate some of the potential that a precisely manipulated and designed nanoscale scaffold can have.

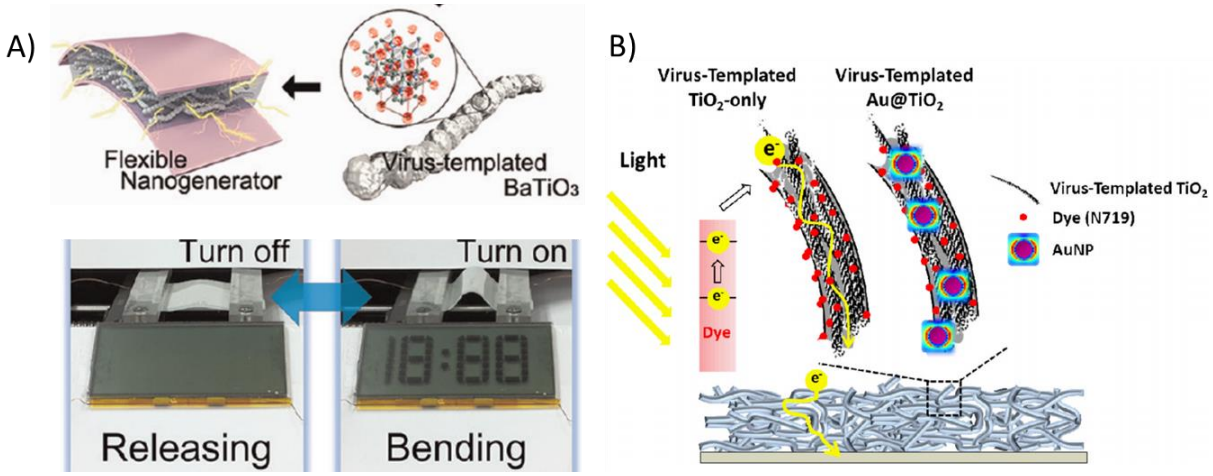

Figure 1.7: Examples of M13 utilizing in device designs. A) M13 used to template mineralization of $BaTiO_3$ in a flexible nanogenerator design. Reproduced with permission from (Jeong et al. 2013). Copyright (2013) American Chemical Society. B) M13 utilized as a component in a dye-sensitizes solar cell design. Reproduced with permission from (P.-Y. Chen et al. 2013). Copyright (2013) American Chemical Society.

1.3 Multi-enzyme complexes

A number of important industrial applications such as biofuel production, production of pharmaceuticals or precursors, and sensing devices can be aided or made possible through the use of multi-enzyme biocatalysts. Furthermore, enzyme-based catalysts are considered a green technology since they are biodegradable (Sheldon 2007). Considerable research into the development of such

biocatalysts has involved the use of nanoscale architectures to alter and improve the function of these enzymes. Some advantages of enzymes immobilized onto scaffolds include improved stability, the ability to more easily remove and recycle enzyme catalysts, and the capability of carrying out more efficient multistep reactions (Lin, Palomec, and Wheeldon 2014). In this field of research many different types of nanoscale architectures have been utilized to immobilize enzymes of interest. Some of these different types of scaffolds, which will be elaborated on in the following sections, include nanomaterials, DNA scaffolds, and protein-protein interactions. Concepts such as changes to enzyme stability and how the rates of multi-enzyme reactions change when bound to a nanoscale architecture are highlighted below with specific examples.

1.3.1 Nanomaterial scaffolds

Nanoparticles (**NPs**) include a wide range of carbon-based and inorganic nanomaterials, such as quantum dots and silica NPs. For physical adsorption of proteins to NPs, both the properties of the protein and the surface are important in explaining protein adsorption behavior. For example, protein adsorption to increasingly chemically reduced graphene oxide surfaces showed varying structural changes (Y. Zhang et al. 2012). As the hydrophobicity of the surface was increased, protein structure determined by circular dichroism and relative activity both decreased (**Figure 1.8**). Therefore, for physical adsorption, understanding how proteins interact with a particular surface is important for maintaining the activity of the biocatalyst.

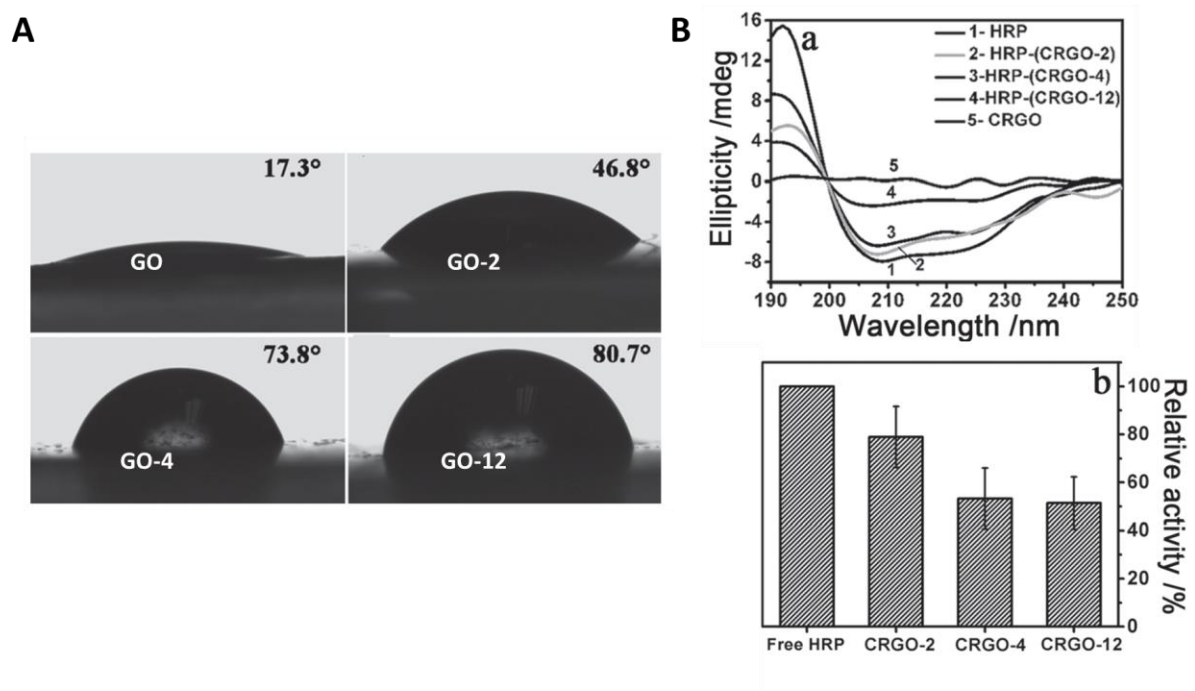

*Figure 1.8: Horseradish peroxidase (**HRP**) binding to graphene oxide (**GO**) and chemically reduced graphene oxide (**CRGO**) surfaces. A) Contact angles of different GO and CRGO surfaces. Higher contact angles indicate greater hydrophobicity. B) Top: Circular dichroism spectra of HRP adsorbed to different GO/CRGO surfaces. Bottom: Residual HRP activity after adsorption onto CRGO surfaces. Adapted with permission from (Y. Zhang et al. 2012).*

Predicting the orientation of a protein on a surface is difficult by physical adsorption. A mass spectrometry based approached was used to determine the orientation of RNase A physically adsorbed to silica surfaces and highlighted factors important for protein adsorption to a NP surface. At low protein concentrations of RNase A, the orientation of the enzyme on silica indicated a role of arginine residues in adsorption (Wei et al. 2014). At high protein concentrations, though, the orientation of RNase A on the surface suggested that the enzyme underwent considerable rearrangement as the previously surface bound arginine residues became solvent accessible. For a biocatalyst design, orientation of the enzyme component is important as blocking of the active site, or denaturation of the protein would greatly reduce activity. So not only do the properties of the protein and the surface need to be considered, but protein-protein interactions of adsorbed proteins can further change the orientation of surface-bound proteins.

Controlled methods for modifying a surface with proteins are valuable to biocatalyst designs. A peptide-mediated approach to enzyme binding to NPs could be used to better control orientation on the surface. Histidine tags commonly used in protein purification can also serve to provide affinity interactions with CdSe-ZnS quantum dots (Kang et al. 2014). Alternatively, Zbasic2, a 7 kDa protein tag, binds to silica surfaces (Bolivar and Nidetzky 2012). It was rich in arginine residues which were expected to interact with the negatively charged silica surface. Additionally, covalent attachment of an enzyme to a surface can allow orienting the enzyme active site such that it is still accessible upon surface attachment (Y. Liu et al. 2013). In comparison to the physically adsorbed enzyme, they found that covalent attachment afforded nearly the same activity as in solution.

The use of nanomaterial-based scaffolds offers several approaches for stabilizing enzyme(s). There have been results reported on enzymes that have been encapsulated within inorganic NPs or polymers having increased stability (Sheldon 2007). Penicillin G amidase encased in polymerized acrylamide followed by mesoporous silica encapsulation retained more activity after incubation at 37 ^{o}C for 24 hours than non-encapsulated enzyme (**Figure 1.9A**) (F. Zhang et al. 2014). In another example, alcohol dehydrogenase (**ADH**) was encapsulated within silica nanoparticles (**Figure 1.9B**) (Jiafu Shi and Jiang 2014). The evidence of encapsulation was the absence of leeching of enzymatic activity even in the presence of high salt. Salt titration can help to determine the extent to which protein interaction with a surface is from electrostatic interactions (Boulos et al. 2013). It is possible though, that electrostatics are only responsible for a percentage of the total free energy change of a protein adsorbing to the surface. Therefore, this single experiment of incubating silica NPs with 1M KCl might not rule out other non-electrostatic contributions to protein adsorption (Xia, Monteiro-Riviere, and Riviere 2010). Despite this, their silica NP-enzyme constructs did have greater stability over one month than the free enzyme in solution and had comparable activity to the free enzyme (Jiafu Shi and Jiang 2014). They showed evidence that the silica-NP microcapsules could be recycled with less loss of activity but this may be due to lower recovery of the lower mass biocatalysts.

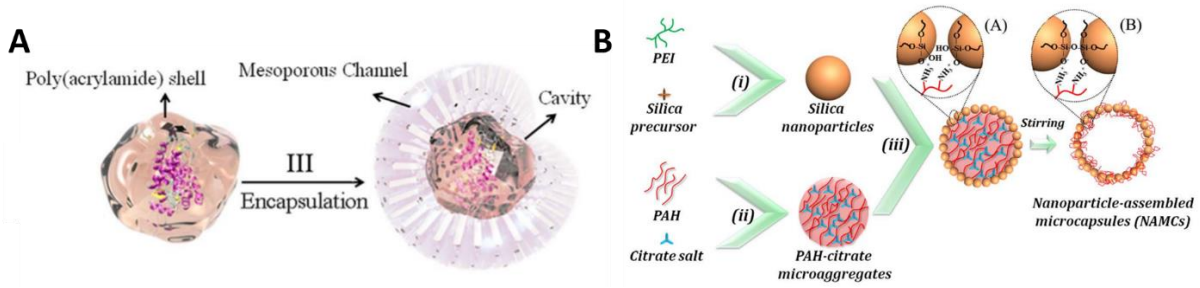

Figure 1.9: Examples of enzyme/nanomaterial complexes with altered properties. A) Penicillin G amidase was modified with N-acryloxysuccinimide. Monomers of acrylamide and bis-acrylamide were added and polymerized to Penicillin G amidase with N'-tetramethylethylenediamine and ammonium persulfate initiators. Mesoporous silica was encapsulated around the acrylamide Penicillin G amidase. This biocatalyst retained ~80% activity after 24 hours at 37 ºC whereas free Penicillin G amidase only retained ~5% activity at 24 hours. (B) Synthesis scheme for the fabrication of enzyme-silica NPs. (i) Silicate, alcohol dehydrogenase and polyethyleneimine were reacted forming enzyme-silica NPs. (ii) Aggregates of polyallylamine hydrochloride were mixed with (iii) enzyme-NPs to form hollow catalytic microcapsules. After 30 days the catalytic microcapsules had ~90% activity while free enzymes did not have activity after 30 days. The image in panel A) was adapted from (F. Zhang et al. 2014) under a Creative Commons Attribution 3.0 Unported License(http://creativecommons.org/licenses/by/3.0/). The image in panel B) was reproduced from (Jiafu Shi and Jiang 2014) with permission from The Royal Society of Chemistry.

A study evolving from work on NPs grown in the presence of an enzyme was the co-encapsulation of two enzymes, glucose oxidase and horseradish peroxidase, to catalyze a cascade reaction for a glucose sensor (J. Sun et al. 2014). Both higher stability and glucose sensitivity were observed in this biocatalyst. The improvement of sensitivity over free enzymes was attributed to the closer proximity of co-embedded enzymes. In another study using these two enzymes, they were encapsulated within a polymer matrix, and the increased stability of the enzyme pair was attributed to the reduction of entropy in the unfolded state (Zore et al. 2015). This reasoning might be extended to enzymes captured within an inorganic NP to explain the high stability observed in those studies. Overall, enhanced stability of enzymes prepared within or on NP scaffolds is a common theme and can be a potential advantage with this type of scaffold.

1.3.2 DNA-based scaffolds

DNA origami technology has enabled many biocatalyst designs and fundamental studies of their kinetics by allowing the design of a diverse set of architectures. DNA origami involves folding a strand of circular ssDNA using small DNA oligonucleotides called "staple strands" (**Figure 1.10**). These can be designed using an algorithmic approach to create a particular geometry (Rothemund

2006). Recent research in this field demonstrates the high level of precision possible with this technology by developing a DNA scaffold capable of tunable separation of two molecules with up to 0.04 nm displacement (Funke and Dietz 2016). Given the ability to easily design different shapes from DNA origami the ability to precisely position proteins is quite high.

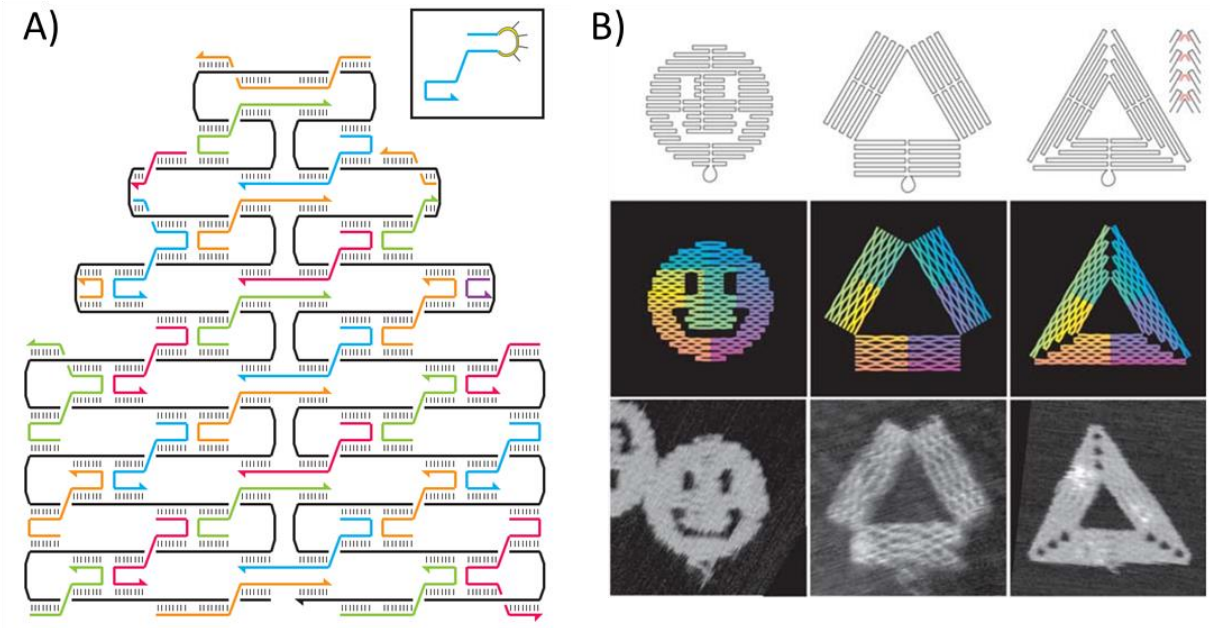

Figure 1.10: Overview of DNA origami. A) Schematic of a finalized DNA origami design. Single-stranded, circular template DNA is shown in black and staple strands are shown in colour. B) Several examples of different folded DNA origami designs. Adapted with permission from (Rothemund 2006).

Interfacing proteins with DNA scaffolds can be achieved in a few different ways. By modifying the protein with a DNA oligonucleotide one can use the base complementarity of DNA bases to position the protein. The DNA origami structure would then have to contain staple strands with the complementary sequence as an overhang. Alternatively, producing a protein or enzyme of interest as a fusion with a DNA-binding protein, such as the Zif268 and PE1A zinc-finger proteins, is another approach (Q. Sun et al. 2014). A weakness of this approach is the relative low affinity of this DNA-protein interaction. RNA-binding domains that bind to specific RNA aptamers were used in a different approach to attach proteins of interest to nucleic acid scaffolds (Sachdeva et al. 2014). Interestingly, this approach could be used *in vivo* and showed association of a split fluorescent protein in cells. DNA

offers an easily tunable framework that one would expect to be ideal in studying the parameters that affect the enhancement of enzyme activity on scaffolds.

The programmable nature of DNA makes it particularly suitable toward the development of nanoscale devices and in-depth exploration on how physically constrained enzymes or co-factors with very exact positioning impacts enzyme rates. A DNA tweezer, for example, was designed to separate glucose-6-phosphate dehydrogenase (**G6pDH**) from nicotinamide adenine dinucleotide (**NADH**) under certain conditions (M. Liu et al. 2013). The presence of appropriate strands of ssDNA can open or close the device, therefore bringing G6pDH in contact with its NADH cofactor and causing a detectable signal (**Figure 1.11A**). The authors were able to further optimize their design in a more recent paper where they redesigned the scaffold to have more complete closure and increase the activity in the closed state by an additional 3-fold (Dhakal et al. 2016). In a different example, the separated domains of P450 BM3, which catalyzes monooxygenation reactions when assembled, were attached to a DNA scaffold to reconstitute enzymatic activity (Erkelenz, Kuo, and Niemeyer 2011). Proximity of the two domains was required for electron transfer between domains and therefore, successful catalysis. Using strand displacement, the authors could controllably separate the two domains resulting in abolishment of activity.

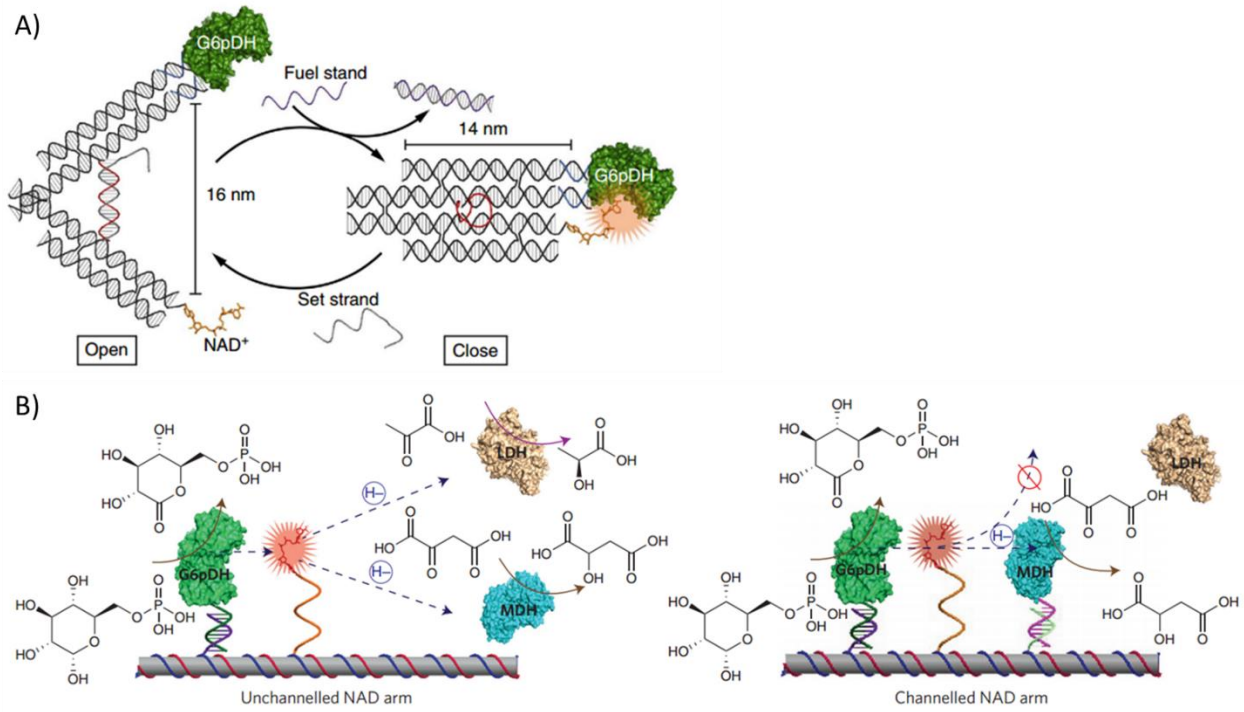

*Figure 1.11: Schematics of DNA-based sensors and devices. (A) A DNA tweezer-based device utilizing glucose-6-phosphate dehydrogenase (**G6pDH**) and NAD$^+$. When fuel strand oligonucleotides are added, the tweezers close allowing oxidation of glucose-6-phosphate (**G6P**). Adding the set strand oligonucleotide opens up the structure again, reducing catalysis. (B) Different configurations of a DNA scaffold with a tethered NAD$^+$ cofactor. DNA scaffold bound to G6pDH and tethered NAD$^+$ cofactor with lactate dehydrogenase (**LDH**) and malate dehydrogenase (**MDH**) in solution (unchannelled NAD arm; left). In this configuration, the hydrides from NADH are preferentially transferred to LDH. A DNA device bound to G6pDH and MDH with a tethered NAD+ cofactor (right). In this configuration, the hydrides from NADH are preferentially transferred to MDH. Panel A was adapted with permission from (M. Liu et al. 2013). Panel B was adapted with permission from (Fu et al. 2014).*

In another example of spatially-constrained enzymes and cofactors, a DNA origami scaffold was used to explore the creation of a biocatalyst utilizing a tethered NADH that could transfer hydrides between the active sites of two different enzymes, G6pDH and malate dehydrogenase (**MDH**) (Fu et al. 2014). The rate enhancement of tethered NADH cofactor compared to freely diffusing NADH was an impressive 91-fold increase. Further optimization was carried out by adjusting the stoichiometry of NADH to enzyme. Noting that G6pDH activity continued to increase linearly with additional NADH it was found that the most optimal configuration had G6pDH:NADH as 4:1 and MDH:NADH as a 1:1 ratio. An interesting part of their work was that having the enzymes tethered together in proximity with their cofactor greatly increased the specificity of the reaction (**Figure 1.11B**). When in competition with freely diffusing lactate dehydrogenase (**LDH**), the reaction proceeded down the MDH pathway

preferentially only when MDH was spatially confined near NADH. This could potentially be an approach to channel or detect a substrate from a complex mixture of molecules down a particular pathway of interest in the presence of competing enzymes.

1.3.3 Protein-based scaffolds

Designing protein-based scaffolds to have a desired architecture is a challenge given the complexity of protein-protein binding interfaces. Although protein scaffolds are far behind the level of design of DNA scaffolds (Chidchob and Sleiman 2018) there is some work on design principles for creating novel protein scaffolds (King et al. 2012; Glover and Clark 2016). Protein-based scaffolds found in nature offer another source of stable and well-defined architectures. An excellent naturally occurring example of this is the cellulosome which is produced by cellulose-degrading bacteria for the purpose of breaking cellulose down to simpler sugars (Bayer, Setter, and Lamed 1985; Fontes and Gilbert 2010; Yael Vazana et al. 2013). The biological role and more detailed concepts concerning the cellulosome and its function will be discussed in the following section, **Section 1.4**. For this particular discussion on multi-enzyme scaffolds, the scaffolding proteins of the cellulosome are of particular relevance and will be introduced here first. The cellulosome is composed of a mixture of non-catalytic scaffolding proteins, called scaffoldins, and various cellulases (**Figure 1.12A**). Artificial cellulosome scaffolds were developed to understand how the cellulosome functions in nature and for biofuel applications (Borne et al. 2013; Stern et al. 2015; Yael Vazana et al. 2013). By improving the rate of cellulose hydrolysis down to simpler sugars for fermentation, one can access the energy found in cellulosic biomass efficiently.

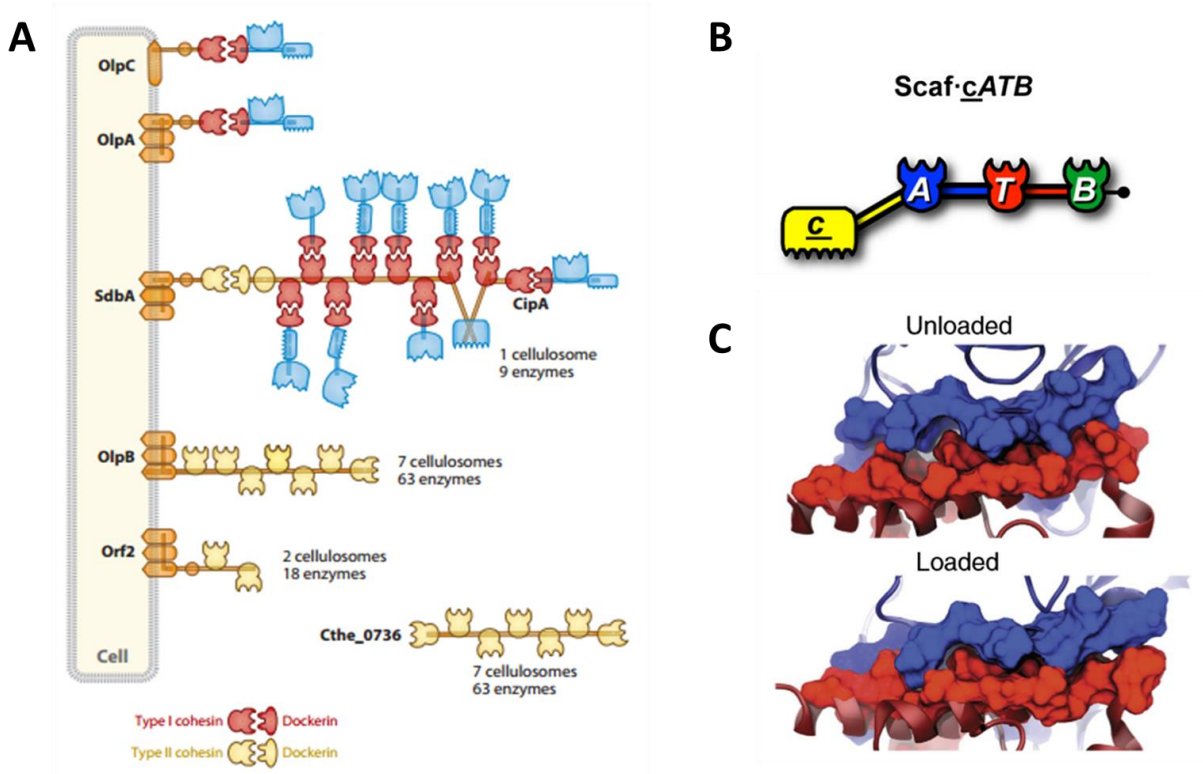

Figure 1.12: Cellulosome structural features. A) Schematic showing cellulosome structural organization. CipA is a scaffoldin from Clostridium thermocellum. B) Schematic showing domains on chimeric scaffoldin. "c" refers to the cellulose binding module, "A" is the cohesin from A. cellulolyticus, "T" is the cohesin from C. thermocellum, and "B" is the cohesin from B. cellulosolvens. C) Molecular dynamics simulation of cohesin:dockerin interface in the absence or presence of an applied force. Cohesin is shown in blue and dockerin is shown in red. Panel A was reproduced with permission from (Fontes and Gilbert 2010). Panel B is modified from (Yael Vazana et al. 2013) under Creative Commons Attribution License 2.0 (http://creativecommons.org/licenses/by/2.0). Panel C is modified from (Schoeler et al. 2014) under Creative Commons Attribution 4.0 International License (http://creativecommons.org/licenses/by/4.0/).

In the course of artificial cellulosome research, a useful nanoscale scaffold was developed due to the nature of orthogonal dockerin and cohesin proteins. The orthologs from *Clostridium thermocellum*, *Bacteroides cellulosolvens* and *Acetivibrio cellulolyticus* do not bind to the orthologs of the other species (Yael Vazana et al. 2013). It was found that the two major areas of the binding interface that were crucial for specificity were a hydrophobic patch and H-bonding network (Slutzki et al. 2015). Chimeric scaffoldin combines these orthogonal cohesin domains into a single protein scaffold (**Figure 1.12B**). In addition to the specificity of the interaction, cohesin bound to dockerin has considerable mechanical strength (Schoeler et al. 2014). In this study, researchers found that the mechanical strength of the intermolecular interaction was about 600 pN. This is approximately half the rupture force required to break a gold-thiol bond. Interestingly, the cohesin:dockerin interface tightens

in response to applied force by rearrangement of several residues (**Figure 1.12C**). This factor could make such a scaffold very suitable for application in the construction of continuous flow devices or biosensors.

There are several good examples of multi-enzyme complexes employing protein scaffolds that demonstrate higher catalytic rates through substrate channeling. Substrate channeling is the concept of enhancing the efficiency of a pathway of multiple enzymes by having an intermediate diffuse directly to the next active site without entering the bulk solvent (Miles, Rhee, and Davies 1999). To examine the effects of spatial configuration on substrate channeling, chimeric scaffoldins have been used to spatially confine pathway-related enzymes. These biocatalysts were reported to enhance rate through substrate channeling (F. Liu, Banta, and Chen 2013; You, Myung, and Zhang 2012). In a particular example, chimeric scaffoldin was used to explore effects on rate using a model system of glycolysis enzymes (**Figure 1.13A**). Triosephosphate isomerase (**TIM**), aldolase (**Ald**) and fructose 1,6-bisphosphatase (**F1,6BPase**) were arranged on this scaffold by expressing them as dockerin fusion proteins to control their spatial positioning relative to each other (You, Myung, and Zhang 2012). Rate enhancement as high as 21.1-fold greater compared to freely diffusing enzymes was observed. The authors noted that by dynamic light scattering that the size of the assembled complex was larger than expected. A mechanism pointed out by the authors for larger aggregate formation could involve TIP, Ald and F1,6BPase, which can exist as dimers and tetramers. By virtue of this fact, there may be additional factors that contribute to the rate enhancement they observed.

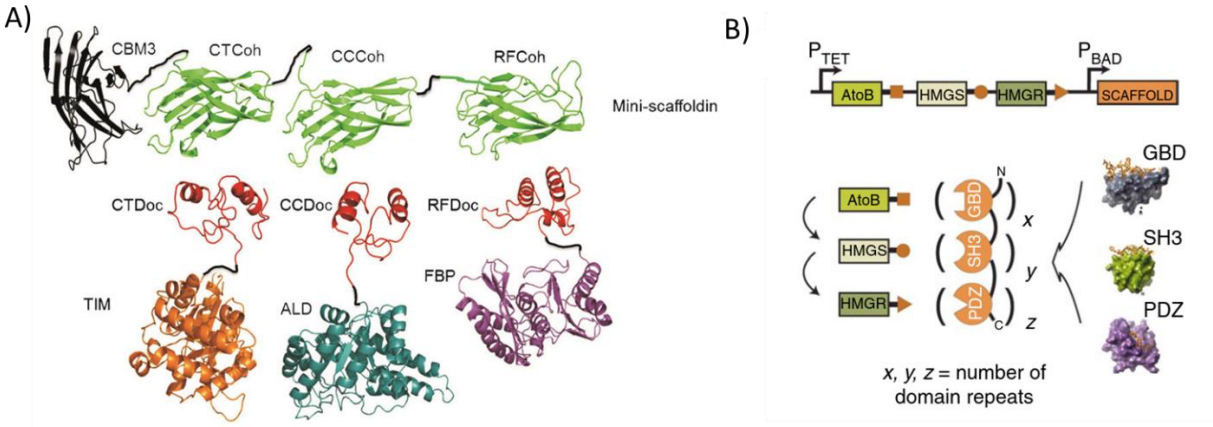

*Figure 1.13: Examples of protein-based nanoscale scaffolds. A) Glycolysis pathway enzymes bound to a protein scaffold using divergent cohesin:dockerin interactions. Triosephosphate isomerase (**TIM**), aldolase (**Ald**) and fructose 1,6-bisphosphatase (**F1,6BPase**) are shown bound to cohesin domains from C. thermocellum (**CTCoh**), Clostridium cellulolyticum (**CCCoh**), and Ruminococcus flavefaciens (**RFCoh**). B) Mevalonate biosynthesis pathway enzymes bound to a scaffold comprised of three different protein-protein interaction domains. The image in panel A was adapted with permission from (You, Myung, and Zhang 2012). The image in panel B was adapted with permission from (Dueber et al. 2009).*

Another example which utilized protein-protein interactions was the design of a scaffold with three distinct modules to bind up three different pathway-related enzymes. In particular, expressing these components such that they assembled onto a designed scaffold in *E. coli* was found to greatly enhance the formation of mevalonate, a precursor for several types of therapeutic molecules (Dueber et al. 2009). The scaffold utilized three different protein domains with specific and distinct protein-protein interactions separated by flexible glycine linkers (**Figure 1.13B**). Peptides with affinity to each of the different domains on the scaffold were fused to pathway related enzymes: acetoacetyl-CoA thiolase (**AtoB**), hydroxy-methylglutaryl-CoA (**HMGS**) and methylglutaryl-CoA reductase (**HMGR**). By altering the number of times each domain on their scaffold was repeated, the number of recruited enzymes could be tailored – a single AtoB and two each of HMGS and HMGR was found to be the optimal arrangement. This system expressed in *E. coli* and mevalonate biosynthesis was enhanced by up to 77-fold through better flux of metabolites through substrate channeling (Dueber et al. 2009). Thus, unlike nucleic acids which are particularly well-suited to rationally designed interactions, there

exists a palette of protein-protein interaction pairs in nature that can be selected for a particular application.

1.3.4 Rate enhancement in multi-enzyme complexes

As already highlighted in some of the examples above, binding multi-enzymes to a nanoscale scaffold can improve their catalytic activity. Simply having small aggregates of pathway-related enzymes may in and of itself may be enough for rate enhancement through substrate channeling; a theory-based study showed that small clusters of enzymes may be kinetically advantageous with respect to substrate channeling occurring (Castellana et al. 2014). The proximity of enzymes gives more potential targets for a diffusing intermediate to react with before escaping to the bulk solvent (**Figure 1.14A**). The model constructed included enzyme clusters of two or three pathway-related enzymes of defined radius, within a basin of larger volume (**Figure 1.14B**). For two enzymes, the optimized effect of clustering was a 6-fold improvement compared to evenly distributed enzymes. For three related enzymes the expected increase in pathway efficiency was calculated to be 110-fold. In contrast to engineering studies that place importance on defined spatial positioning of pathway components, this study suggested the relative unimportance of precise spatial positioning but rather that dense clustering is more important for substrate channeling by proximity to occur.

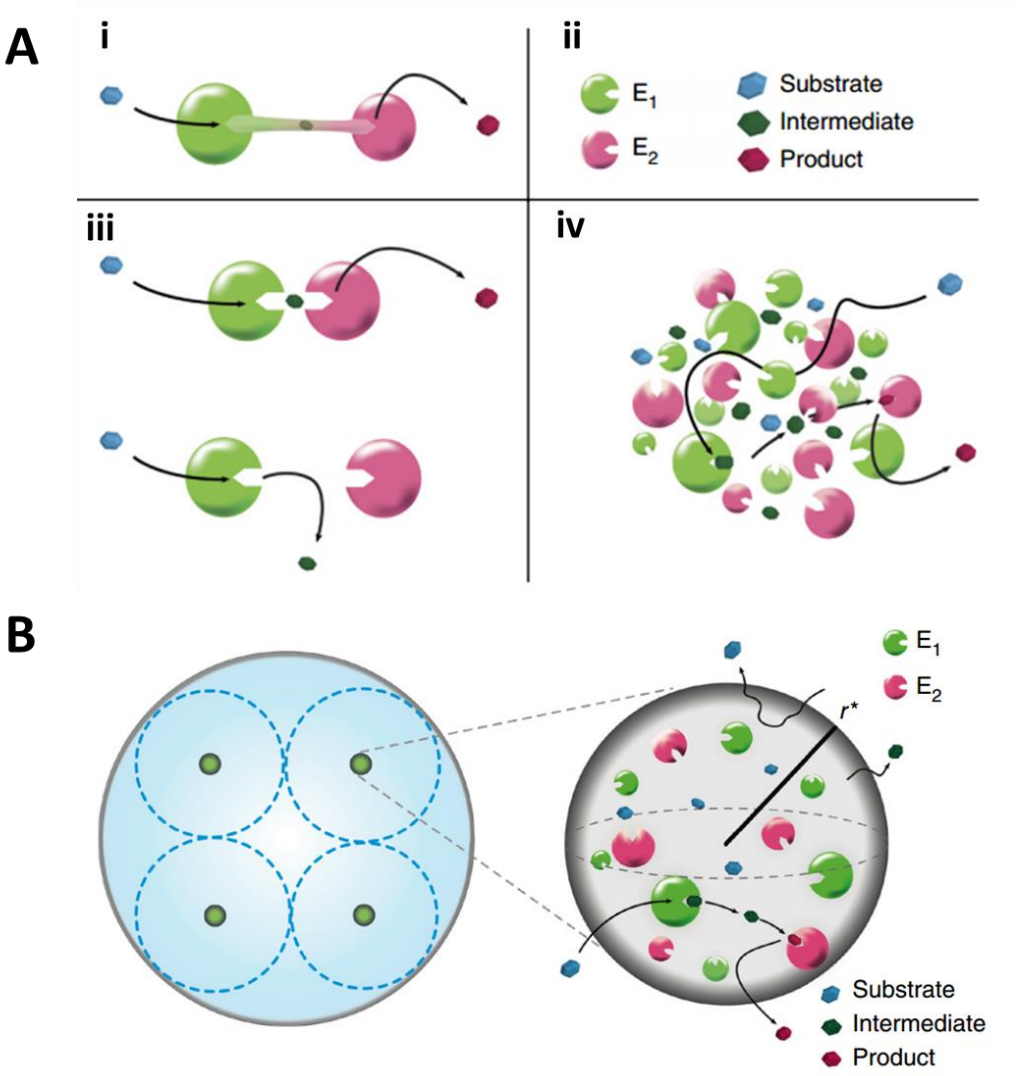

Figure 1.14: Schematic representations of substrate channeling. A)(i) Channeling of substrates through a physical channel. (ii) Legend; E_1 represents enzyme 1 and E_2 represents enzyme 2. (iii) Channeling of substrates by proximity. This only occurs when the active sites are sufficiently close to each other. (iv) Substrate channeling within clusters of enzymes. B) Model used to simulate rate enhancement from dense clusters of enzymes. Clusters of enzymes of radius r were separated at a defined distances. These clusters are separated by basins of radius, R (dashed lines). Adapted with permission from (Castellana et al. 2014).*

Another theory-based study on substrate channeling set up two enzymes at fixed distance and carried out simulations of diffusion from one enzyme to the other (**Figure 1.15A**) (Idan and Hess 2013). It was found that spatially constraining the enzymes only improved the rate for a limited time. At a certain point the intermediate product will accumulate sufficiently in the container that the concentration gradient will dissipate (**Figure 1.15B**). Therefore, only in a system where an intermediate is unstable and decomposes might one expect to see rate enhancement merely from close proximity of

two enzymes. Additionally, when an attractive force was included between the target protein and substrate, acceleration due to channeling was observed. In theory, it seems that proximity without a physical tunnel or mechanism for channeling should not be expected to allow for substrate channeling. Indeed, when three pathway related enzymes were covalently crosslinked to each other no rate enhancement observed despite their spatial configuration (Schoffelen et al. 2013). Therefore, it may be important to look critically at cases where substrate channeling by proximity is used as the reason for rate enhancement as other mechanisms may be involved in the rate enhancements observed.

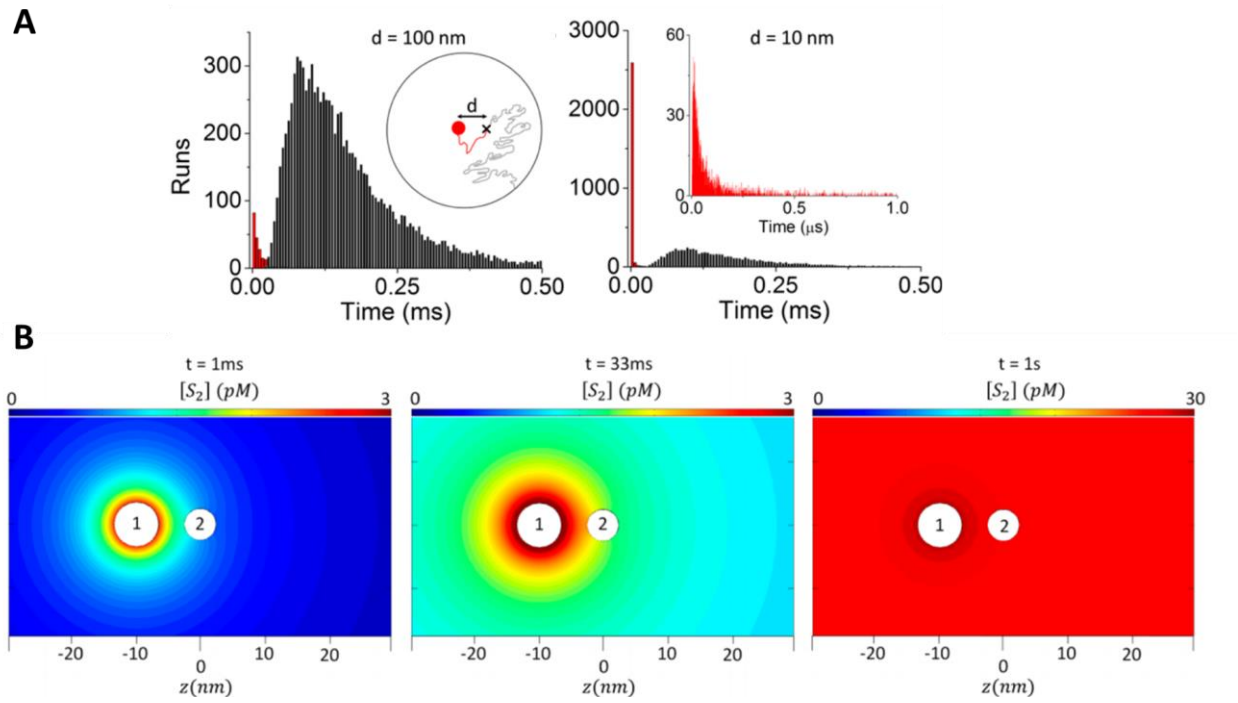

Figure 1.15: Simulations used to model substrate channeling between two enzymes from just diffusion effects. A) Histograms of 10000 random walk simulations from a point at (left) 100 nm or (right) 10 nm from a red sphere which represents a hypothetical reference. Red bars represent trajectories that collided with the red sphere and black bars represent trajectories that reached the limits of the basin. B) Diffusion simulations of a reaction at time-points (1 ms, 33 ms and 1 s) after initiating a reaction at point "1". Colours indicate the concentration of diffused intermediate. At t=1s the diffusion gradient dissipates. Adapted with permission from (Idan and Hess 2013). Copyright (2013) American Chemical Society.

Electrostatics are known to play an important role in substrate channeling for enzymes proximal to each other. *In vivo* crosslinking of citric acid cycle enzymes gave evidence of multi-enzyme structures in nature and a model was constructed (Wu and Minteer 2015). In this model, there was a possible path of positive electrostatics connecting the active sites of the two enzymes. Some older

research based upon computational modelling suggested that electrostatic effects could contribute considerably to substrate channeling effects (Elcock and McCammon 1996). In a more recent study of thymidylate synthase, which has a history of research regarding electrostatic channeling, pulse-chase type kinetics suggested channeling occurs (Sharma et al. 2013). In this experiment the channeled intermediate had a radiolabel which was expected to be detected in the absence of channeling. In combination with the structure of the enzyme, the authors suggested that electrostatic channeling occurred and does not necessarily require a continuous pathway of charge from one active site to the next and that a concentration of appropriate charge near the active site may be sufficient. In contrast to this, the human version of the enzyme may have such a pathway according to docking simulations (N. Wang and McCammon 2016). Given these additional experiments and the various studies predicting the kinetics of scaffolded enzymes, it seems that for substrate channeling to occur, that close proximity of enzymes may not be sufficient to cause channeling. Therefore, in the cases where several pathway-related enzymes are bound together on a scaffold, other factors such as electrostatic effects and aggregation should also be considered.

1.3.5 Conclusions

For the different types of scaffolds discussed, each have their own advantages and it might not be correct to say that a single type of scaffold would be optimal for all applications. Protein scaffolds, for example, are not as expensive to produce as DNA origami scaffolds, whose assembly requires the synthesis or purchase of hundreds of different oligonucleotide staple strands. On the other hand, the ease of designing a particular architecture from DNA with precision might make it particularly useful for more fundamental studies on how different parameters affect biocatalyst designs. Lastly, the properties of NP scaffolds of enable biocatalyst recovery by centrifugation and improved stability, which would be valuable to industry. Different NPs or materials though, vary in how they impact enzymatic activity depending on both surface and protein properties. In the following section, a

naturally occurring multi-enzyme system for which there is a good theoretical understanding of the mechanism of its rate enhancement will be further discussed.

1.4 Cellulosomes

Cellulose is a polymer of glucose monomers joined by β(1 → 4) glycosidic linkages (**Figure 1.16**). The repeating unit is cellobiose, which is composed of two β-*D*-glucose units. Cellulose polymer chains have two distinct ends depending on the placement of the anomeric carbon of the terminal sugar. In the case where the anomeric carbon is a hemi-acetal, and not a acetal, then the end is considered the "reducing end". Conversely, the other end of the cellulose chain is the non-reducing end. These polymers are roughly linear and strands of about 10000 – 15000 glucose units (depending on the source), which are assembled into large, super-molecular arrangements with intra and inter-chain hydrogen-bonding. These form fibrils which are 5 – 50 nm in diameter (Moon et al. 2011). These fibrils contain regions of high crystallinity, termed crystalline regions, and amorphous regions which contain more disordered arrangements of fibrils. Some of the important characteristics of cellulose from differing sources have been summarized in the following reference, which include: the crystallinity, length of cellulose chains, exposed surface area, pore distribution on surface and dimensions of cellulose fibrils (Mansfield, Mooney, and Saddler 1999). Cellulose comes from a variety of sources including the cell wall of plants and bacteria, where these factors vary (Langan et al. 2011).

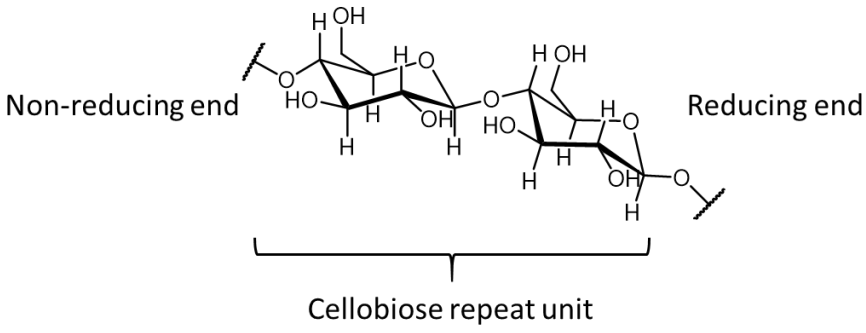

Figure 1.16: Structure of repeat unit of cellulose, cellobiose, which is composed of two β-D-glucose units.

Cellulose encompasses a large quantity of energy bound up in the biomass of plants but due to its nature, being recalcitrant to hydrolysis, it is difficult to liberate that energy (Langan et al. 2011). Enzymes capable of the hydrolysis of cellulose exist naturally and are referred to as cellulases. These enzymes exist in a large category with many varieties, and different types of activity. Overall these enzymes catalyze the release of glucose or oligomers of glucose as shown in the overall reaction presented in **Figure 1.17**. Since cellulose is not a simple, soluble substrate, there exists a large space for cellulases with different modes of action against this substrate. In reality, the liberation of simpler sugars from biomass has an additional complexity, that of additional cell-wall components that are not cellulose which need to be removed by some pre-treatment step followed by the more specific digestion of cellulose by added cellulases (Chundawat et al. 2011).

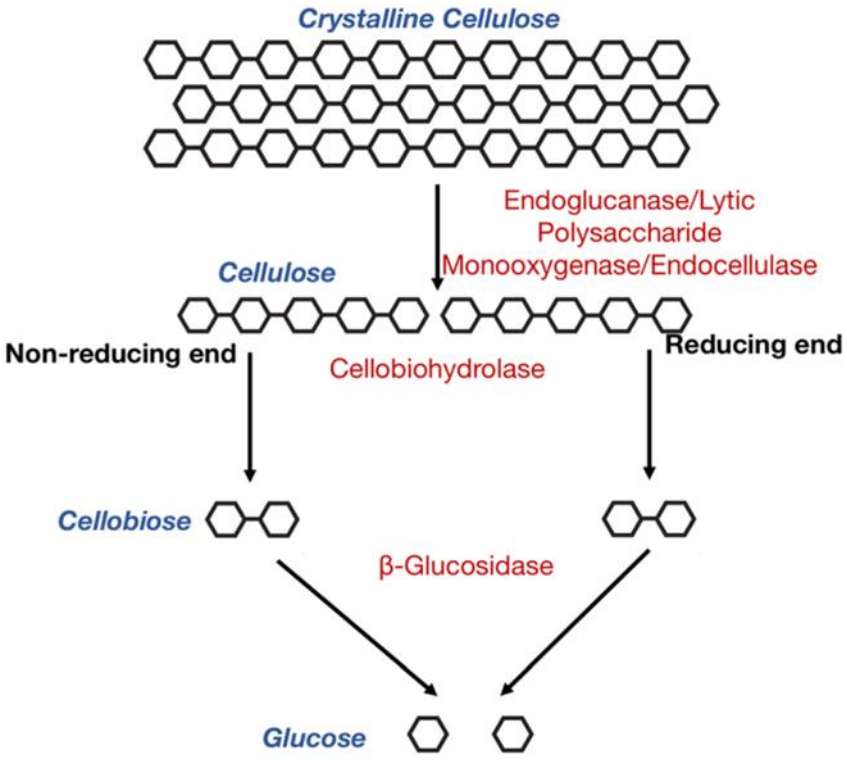

Figure 1.17: Simplified scheme of cellulose breakdown by various cellulases. Adapted with modifications from (Arora, Yennamalli, and Sen 2018) under Creative Commons Attribution 4.0 International License (http://creativecommons.org/licenses/by/4.0/).

1.4.1 Cellulosome structure

In particular, a complicated arrangement of cellulases exists in nature – cellulosomes. In 1983, a cellulase-containing complex with cellulose binding functionality was discovered in *Clostridium thermocellum* (Lamed, Setiter, and Bayer 1983). This was later discovered to be a multi-cellulase complex bound in nodules on the surface of the organism that was named the cellulosome (**Figure 1.18A**) (Bayer, Setter, and Lamed 1985). The cellulosome is a multi-enzyme complex produced naturally by cellulose-digesting bacteria, such as *C. thermocellum* (Artzi, Bayer, and Moraïs 2017). The multi-enzyme complex has attracted the attention of biofuels researchers looking to harness its very high cellulolytic activity, and better understand the principles through which such high conversion can be achieved, in order to access the massive energy stored in the world's biomass waste.

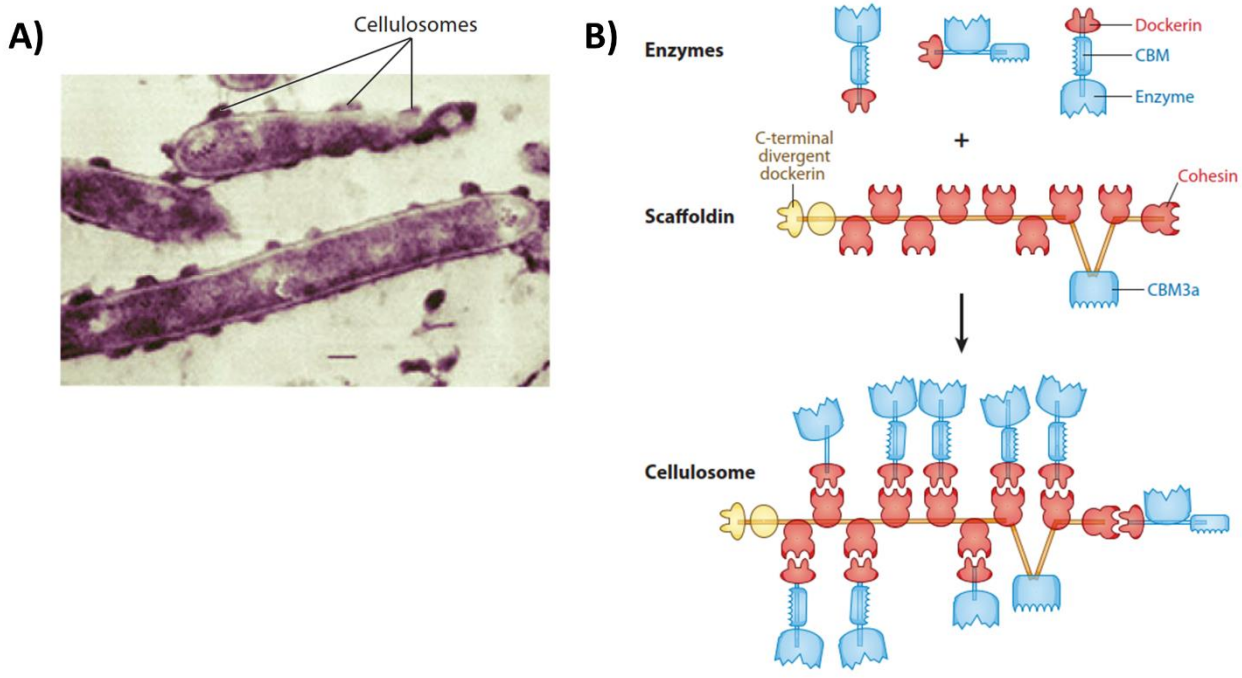

Figure 1.18: Structural organization of the cellulosome. A) Micrograph of cellulosome anchored on C. thermocellum cell surface. B) Structural organization of the cellulosome highlighting the scaffolding proteins, scaffoldin, and modular enzymatic components. Images were reproduced with permission from (Fontes and Gilbert 2010).

The cellulosome is composed of a mixture of scaffolding proteins and cellulose-degrading enzymes (Artzi, Bayer, and Moraïs 2017). The main protein-protein interaction that allows for hierarchical ordering of the various cellulosome components is the cohesin-dockerin interaction

(**Figure 1.18B**). In the *C. thermocellum* cellulosome, there are two main types of Coh and Doc that are distinct and play different roles. Type 2 Coh and Doc are responsible for binding of the whole scaffoldin complex to the cell-surface and type 2 Coh bind type 2 dockerin domains present on various cellulosomal cellulases. The specificity of the Coh-Doc interaction has been taken advantage of for further tailoring and engineering of cellulolytic assemblies. In particular it has been noted that Coh and Doc homologs from different species bind specifically to the same-species homologs, which has had important implications for synthetic biology applications of cellulosomal proteins (Pagès et al. 1997; Slutzki et al. 2015). Furthermore, the Coh-Doc interaction has been found to be particularly tight, with a K_d of less than 1×10^{-9} M (H.-P. Fierobe et al. 2005). As highlighted previously, this interaction is speculated to further tighten under externally applied force (Schoeler et al. 2014). This may have been an evolutionary adaptation to the shear forces found in the environments these bacteria grow in.

There exist several arrangements of cellulosomal components which depend on the species of cellulolytic bacterium, with varying levels of complexity. These may be free cellulosomes or those which are tethered to the bacterial membrane (Artzi, Bayer, and Moraïs 2017). Typically, there is some kind of scaffolding protein, called scaffoldin. The role of this is structural in nature, and allows for several dockerin-bearing enzymes to be brought into close vicinity to each other. In the case of the *C. thermocellum* scaffoldin, CipA, there is also a single cellulose-binding module (**CBM** – also called, carbohydrate-binding module – other papers refer to cellulose-binding domain **CBD**) that is responsible for interacting and binding to cellulose. The complexity and arrangement of components is specific to the number of cohesion modules present (and whether any secondary scaffoldins are included in the complex). In the case of *C. thermocellum*, CipA scaffoldin is capable of binding up to 9 dockerin-bearing components with a Type 2 dockerin present to bind to the cell surface (Krauss, Zverlov, and Schwarz 2012). In particular, an important aspect of the cellulosomes high degree of catalytic activity against cellulose is the presence of cellulases with differing modes of action which allow for synergistic processing of the cellulosic substrate (Hirano et al. 2016).

Having several types of cellulases in close proximity has been shown to be a critical factor in the function of the cellulosome. In particular, researchers have identified several core concepts that are important to the rate enhancement observed. These are synergism between enzyme types and adsorption to cellulose (Mansfield, Mooney, and Saddler 1999). Specifically, the synergism is that between endo- and exo-cellulases on cellulose, and beta-glucosidases, which act on produced cellobiose and prevent inhibition of other cellulases. Several theoretical models have been put forth to describe the nature of this synergy (Asztalos et al. 2012; Kostylev and Wilson 2013; Kumar and Murthy 2013). Given the complex nature of the substrate, there is a continuous evolution of concepts and parameters considered in such models. The basic concept is that endoglucanases act internally on cellulose chains, increasing the concentration of cellulose chain termini that exoglucanases act on, liberating cellobiose in a processive manner; the freed cellobiose, which is known to inhibit many cellulases, is acted upon by a β-glucosidase. Then, with respect to adsorption, since cellulose is insoluble, the enzymes must adsorb onto the cellulose surface – this is facilitated by CBM. The role of these components is to 1) increase local concentration of cellulase, and 2) liberate the cellulose chains from the surface of the substrate in a non-hydrolytic manner that makes the chains more accessible for hydrolysis (Shoseyov, Shani, and Levy 2006). There are many factors that contribute to the high rate of cellulose hydrolysis in cellulosomal systems, and in understanding this, one might be able to better tailor or enable more efficient cellulose hydrolysis for biofuel applications.

1.4.2 Artificial cellulosomes

Building upon the concepts that have been learned while studying the mechanisms behind the efficient cellulolytic activity of the cellulosome, several groups have applied these concepts to developing artificial cellulosomes – mixtures of scaffolding components and select cellulases of varying types. Some of the goals set out to meet using artificial cellulosomes include mimicking, or improving, the high activity of the natural cellulosome against cellulose. Alternatively, some groups have envisioned constructs more precisely tailored to hydrolyse cellulose for a particular application –

favoring certain types of cellulases over others (Fontes and Gilbert 2010). The basic strategy involves the careful design of a scaffold that may then be further applied for the specific binding or arranging of different cellulases: typically a combination of exocellulases, endocellulases and CBMs.

The types of scaffolds that have been explored are varied and extend beyond just the natural components that typically make up the cellulosome. These types of scaffolds include synthetic/chimeric scaffoldins, multimeric proteins, DNA, inorganic nanoparticles, and protein-coated nanoparticles (**Figure 1.19**). Some of the cellulases that have been employed in artificial cellulosome designs are summarized in **Table 1-1**. Often, these consist of a mixture of endo- and exo-cellulases in order to obtain synergy between the two components as discussed above. Furthermore, CBM domains are also a common inclusion in these artificial cellulosome constructs.

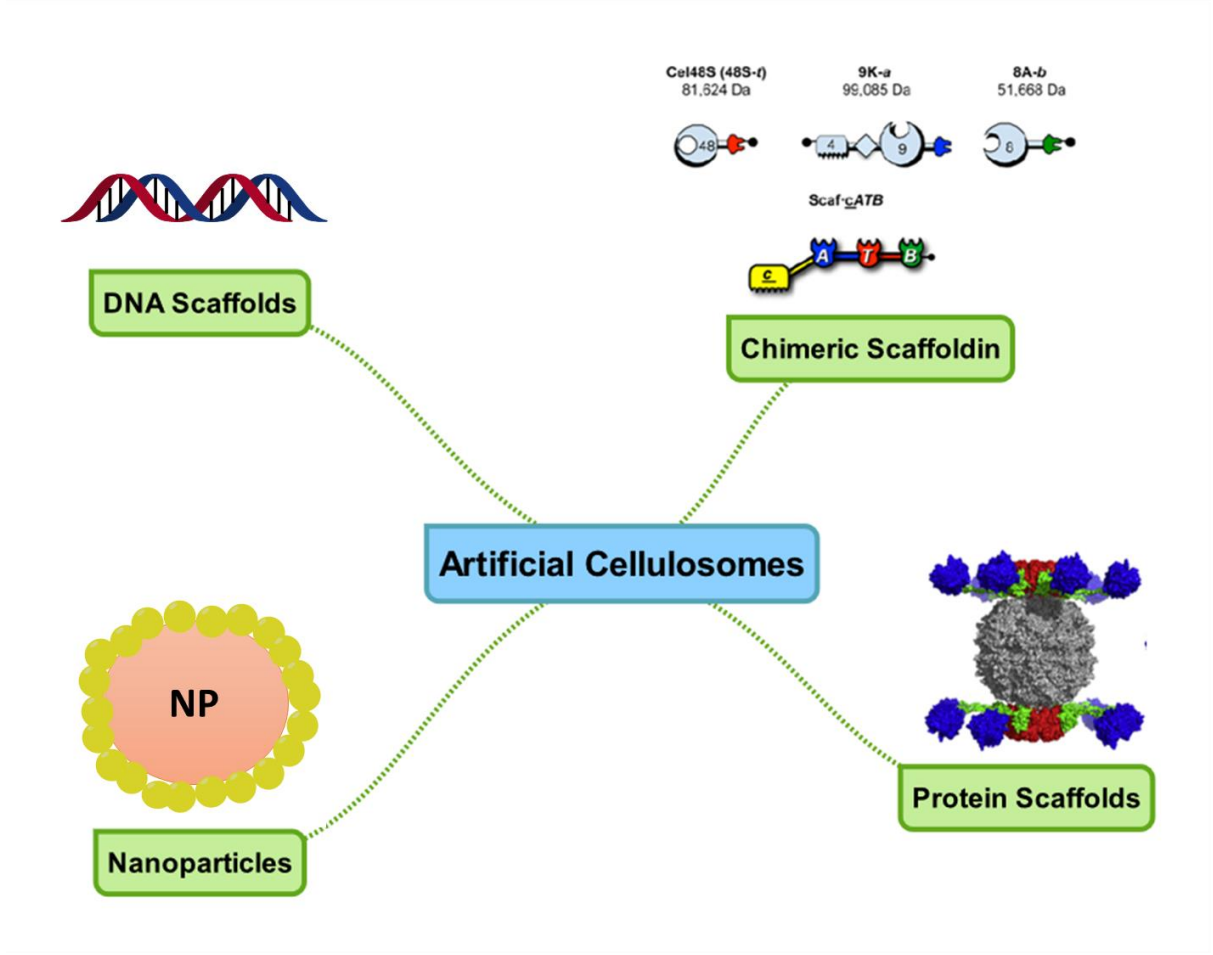

Figure 1.19: Types of scaffolds that have been commonly used to prepare artificial cellulosomes. Chimeric scaffoldin example – chimeric scaffoldin to bind dockerin-bearing cellulases from (Yael Vazana et al. 2013) under Creative Commons Attribution License 2.0 (http://creativecommons.org/licenses/by/2.0). Protein scaffold example – model of cohesin-rosettasome adapted with permission from (Mitsuzawa et al. 2009).

*Table 1-1: Cellulases employed in artificial cellulosome designs. CMCase activity denotes activity against carboxymethylcellulose (**CMC**). pNPase activity denotes activity against p-nitrophenol (**pNP**) derivatives of cello-oligosaccharides.*

Organism	ID	UniProt	Function	Mature Size (Da)	Domains	CMCase activity (μmol/min/μmol enzyme)	Avicel (μmol/min/μmol enzyme)	pNPase activity (μmol/min/μmol enzyme)	Type of scaffold used in design
A. niger	EglA	D3YC02; see also: A2R322	Endoglucanase	26000	Cellulase	753 (Pham et al. 2011), 1820 (commercial source: Megazyme. CAS: 9012-58-4)	Yes (D.-M. Kim et al. 2011); no specific activity reported	?	Streptavidin-coated quantum dots (D.-M. Kim et al. 2011)
C. cellulolyticum	Cel9E	B8I7V4	Exoglucanase	93791	CBM4, Ig-like, Cellulase, Dockerin	13.5 (Gaudin et al. 2000)	5.8 (Gaudin et al. 2000)	34.8 ((Gaudin et al. 2000); pNP-cellobiose)	Quantum dots (Tsai, Park, and Chen 2013)
C. cellulolyticum	celCCA	P17901	Endoglucanase	50710	Cellulase, Dockerin	2500 (H. P. Fierobe et al. 1991)	5.4 (H. P. Fierobe et al. 1991)	1.5 ((H. P. Fierobe et al. 1991); pNP-cellobiose)	Magnetosome (Honda, Tanaka, and Yoshino 2015)
C. thermocellum	Cel8A	A3DC29	Endoglucanase	49212	Cellulase, Dockerin	30208 (Schwarz, Gräbnitz, and Staudenbauer 1986)	5 (Schwarz, Gräbnitz, and Staudenbauer 1986)	?	Zinc-finger DNA (Q. Sun et al. 2014), QDs (Tsai, Park, and Chen 2013), rosettasome (Chundawat et al. 2016), DNA (Q. Sun and Chen 2016), Mini-scaffoldin (Yael Vazana et al. 2013)
C. thermocellum	Cel9R	Q70DK3	Processive Endoglucanase	79277	Cellulase, CBM3c, Dockerin	1250 (Zverlov, Schantz, and Schwarz 2005)	Yes (Y. Vazana et al. 2010); no specific activity reported	2.53 ((Zverlov, Schantz, and Schwarz 2005); pNP-G4)	Rosettasome (Chundawat et al. 2016; Mitsuzawa et al. 2009)
C. thermocellum	Cel9F	P26224	Processive Endoglucanase	79293	Cellulase, CBM3, Dockerin	Not detected, but 42.5 on PASC (Reverbel-Leroy et al. 1997)	13.4 (Reverbel-Leroy et al. 1997)	?	Rosettasome (Chundawat et al. 2016; Mitsuzawa et al. 2009)
C. thermocellum	Cel5B	P04956	Endoglucanase	61063	Cellulase, Dockerin	258 (Hirano et al. 2016)	?	?	Rosettasome (Chundawat et al. 2016)
C. thermocellum	Cel9K	A3DCH1	Exoglucanase, Processive Endoglucanase	97628	CBM4, Cellulase, Dockerin	2.9 (Hirano et al. 2015)	0.28 (Hirano et al. 2015)	?	Rosettasome (Chundawat et al. 2016; Mitsuzawa et al. 2009), Mini-scaffoldin (Yael Vazana et al. 2013)

C. thermocellum	Cel48S	A3DH67	Exoglucanase	80671	Cellulase, Dockerin	0.003 (Hirano et al. 2016)	Yes; but altered to have CBM domain (Q. Xu et al. 2013).	?	Rosettasome (Chundawat et al. 2016; Mitsuzawa et al. 2009), Mini-scaffoldin (Yael Vazana et al. 2013)
C. thermocellum	Cel9A	A3DDN1	Endoglucanase	67993	Cellulase, Dockerin	?	?	?	Streptavidin-coated quantum dots (Nakazawa et al. 2013)
T. fusca	Cel5A	Q01786	Endoglucanase	46383	CBM2, Cellulase	2840 (Irwin et al. 1993)	0.83 ((Irwin et al. 1993); filter paper)	14.8 ((Irwin et al. 1993); pNP-cellobioside)	DNA scaffold (Mori et al. 2013)

There have been several designs that have utilized native-like cellulosomal scaffolding proteins (i.e. scaffoldin, predominantly) or variants of those proteins (highlighted in **Figure 1.19**). In some cases, this has been to dissect and understand the behavior of the cellulosome, for example, using divalent (H.-P. Fierobe et al. 2002) or trivalent (H.-P. Fierobe et al. 2005) chimeric scaffoldin scaffolds to highlight important synergistic effects. Alternatively, these have been used to head toward optimizing many different parameters, such as: spacing of the cellulase components and relative positioning (Yael Vazana et al. 2013). This chimeric scaffoldin included an exo-cellulase, an endo-cellulase and a processive endo-cellulase and the positions were shuffled by preparing 56 different scaffoldins. Thus, the positioning of the cohesin module determined the final positioning of the components. The presence of a linker was found to be the main factor affecting activity, with longer linker lengths producing the highest activities. These studies utilizing chimeric scaffoldin have been very informative; getting away from native-like proteins, a number of scaffolds have been tested in preparing artificial cellulosomes.

Other stable proteins have been used in place of scaffoldin variants for the purpose of preparing artificial cellulosomes. The rosettasome – an 18-mer protein (protein structure highlighted in **Figure 1.19**) – was engineered as a genetic fusion to cohesin such that the final assembled protein would be a multimer capable of binding up to 18 dockerin-containing enzymes (Mitsuzawa et al. 2009). Four different cellulases from *C. thermocellum* were used in this study. For single components, there was only a minor increase in activity when complexed to rosettazyme scaffold; however, there was an approximately 2.4-fold increase of activity against Avicel® when different cellulase types were bound to the complex. In a further elaboration of this scaffold, more "naturally-occurring" amounts of 12 different cellulases were used to further enhance degradation of crystalline cellulose (Chundawat et al. 2016). These complexed cellulases showed enhanced activity on crystalline cellulose – though the authors noted some possible reasons for slightly lowered activity including limited flexibility and geometry of the scaffold not permitting optimal orientation of all cellulase components.

Transitioning from protein-only scaffolds, there has been some work over the years on using a protein coating on NPs. Instead of utilizing the native Coh-Doc interaction of cellulosomal cellulases, the specific interaction is now mediated by a different ligand pair. In this design, cellulolytic components expressed with a biotin-acceptor peptide were bound to a streptavidin-coated CdSe QDs (D.-M. Kim et al. 2011). Notably, this study found rate enhancement against cellulosic substrates with only a fungal endoglucanase, and CBM domain complexed together. A later study using this platform explored a slightly more elaborate setup with an endocellulase, processive endocellulase and two different types of CBMs (Nakazawa et al. 2013). In an alternate approach to complexation of enzymes to CdSe QDs, an oligo-His tag on an endo- and exocellulase was used to bind both components to NPs of differing sizes (Tsai, Park, and Chen 2013). The oligo-His tag was used to directly bind the components to the NP surface. It was found that the size of the NPs did not matter as much as having the two different types of enzymes complexed together. Finally, a magnetic NP used to template the binding of a endocellulase and β-glucosidase was explored (Honda, Tanaka, and Yoshino 2015). The authors combined two orthologous cohesins to a protein that could bind to the magnetosome – a membrane-bound magnetic particle produced by certain bacteria. Due to the magnetic nature of the complex, the construct was capable of several cycles where the enzyme-bound particles could be reused (shown for 5 cycles).

Several designs have utilized DNA as the scaffolding component. In contrast to NP designs, DNA has additional flexibility and can be very easily tailored to space and bind components at specific positions. Furthermore, DNA differs from some of the protein and NP-based scaffolds in the flexibility of the scaffold – which could be a factor important for orienting cellulases on the cellulose surface. In an early design, an endocellulase/CBM fusion protein was joined to a DNA scaffold by a transglutaminase reaction (Mori et al. 2013). Despite only having an endocellulase and CBM component (no exo-cellulase), there was observed rate enhancement upon complexation – presumably the rate enhancement was from targeting effects. The authors furthermore found that there existed an

optimal amount of cellulase bound to their DNA scaffold – and that further complexation hindered activity. Later, a method using Zn-finger proteins was used to position cellulolytic components to the DNA scaffold (Q. Sun et al. 2014). This artificial cellulosome similarly found rate enhancement, though assembled cellulases were only tested against phosphoric acid swollen cellulose (**PASC**) – not more recalcitrant cellulosic substrates, such as Avicel®. Lastly, an approach using DNA base pair complementarity to exactly position components was used to bind 4 components: endocellulase, exocellulase, β-glucosidase, and CBM (Q. Sun and Chen 2016). Though again, activity was only tested against more digestible substrates, carboxymethylcellulose (**CMC**) and PASC.

Overall, there have been modest enhancements to the rate of hydrolysis of various cellulose substrates using different scaffolds for binding of cellulolytic components. Of the different cellulases that have been used, they vary in both mode of action (exo- or endo-) and source organism. Interestingly, while it has been shown that synergy between different cellulase functionalities is an important factor to enhanced hydrolysis of cellulose, a few of these designs have included only endocellulase activity, and a targeting component (CBM). Even so, the authors reported a rate enhancement, possibly due to the proximity effect imparted to a cellulase when complexed to the cellulose-targeting component. The endo-1,4-β-*D*-glucanase from *C. thermocellum* (**Cel8A**; UniProt: A3DC29) has ended up in many of these designs as a component. The enzyme has been crystallized and had the structure of its catalytic domain determined (Guérin et al. 2002). Given the wealth of information available for this enzyme, and evidence of its effectiveness in artificial cellulosomes, this enzyme was chosen as a model protein for developing an M13-based nanoscaffold in this thesis work.

1.5 Streptavidin

Streptavidin (**SA**) is a tetrameric protein originally discovered as a synergistic component for an antibiotic factor produced by the *Streptomyces avidinii* (Chaiet and Wolf 1964). The protein was

named in part after the organism it was discovered in and its similar activity to avidin, a protein that was discovered previously (Tausig and Wolf 1964). SA binds very tightly to the vitamin, biotin, with one of the strongest non-covalent interactions known in nature (**Figure 1.20**). The dissociation constant for the biotin/SA interaction is about 4 x 10^{-14} M (Chilkoti and Stayton 1995). Its biotin-binding activity is approximately an order of magnitude weaker than the interaction of avidin with biotin (~1.3 x 10^{-15} M) (Green 1963). Some additional differences - apart from avidin being purified from chicken eggs, and SA being isolated from a bacterial source - is that avidin is heavily glycosylated (~10% by MW) (Hiller et al. 1987; Spolaore et al. 2014). Several systems for producing SA recombinantly have been realized enabling the production and study of variants produced of the protein (Gallizia et al. 1998; Sano and Cantor 1990a). There has been some work tailoring the activity of avidin, for example: through nitration of binding site residues producing a pH-sensitive avidin called "captavidin" (García-Aljaro, Muñoz, and Baldrich 2009). The ability to produce SA recombinantly allows further engineering of SA leading to the development of multiple strategies to change the nature of the tight biotin-binding interaction of this protein. This has led to the development of several SA variants: "traptavidin" (Chivers et al. 2010; 2011), dimeric SA (Sano et al. 1997), and "switchavidin" (Taskinen et al. 2014). A more complete description of variants of SA/avidin produced are summarized here (Laitinen et al. 2006). Namely, the high specificity and tightness of binding to its ligand has enabled SA to be used in numerous applications that require tight and specific binding or recognition.

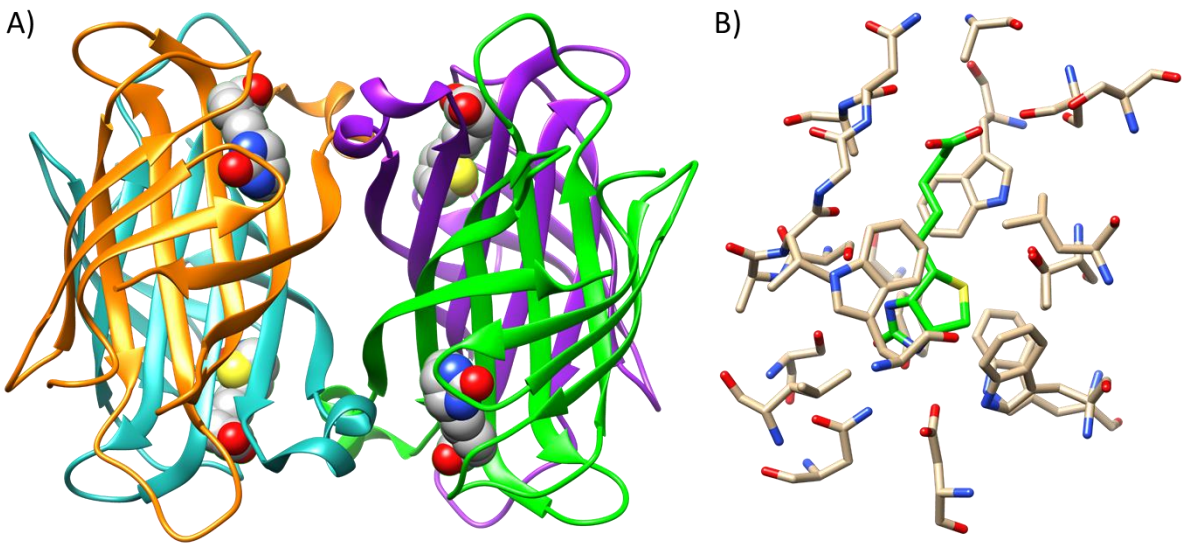

*Figure 1.20: Overview of the structure of streptavidin (**SA**). A) SA (ribbon structure) showing biotin (spheres) bound in each of the four monomers shown. B) Close-up of biotin-binding pocket showing residues within 0.5 nm of biotin (green).*

The unique tight-binding nature of biotin to SA/avidin has enabled many applications utilizing this protein. The following cited review highlights several applications of SA/avidin: engineered variants, SA-based enzymes, live cell imaging, proteomics applications, targeted drug delivery, and SA-based sensors (Dundas, Demonte, and Park 2013). Particularly interesting variants of SA include "monovalent SA" (SA with a single "active" biotin-binding site) which is particularly beneficial for applications where the multivalent nature of SA could be a hinderance. Studies on the quaternary structure of SA have highlighted that the tetrameric form of the protein is essential for high affinity, as the biotin-binding site is found at the interface between subunits, thus ruling out the possibility of producing a truly tight-binding, monomeric form of SA. Indeed, a monomeric variant of SA can be produced from two mutations, T90A and D128A, resulting in a protein with a K_d of $1.3x10^{-8}$ M (Qureshi and Wong 2002). In particular, a useful modification of SA was developed making the protein essentially "monomeric" for biotin binding (Howarth et al. 2006). This was initially done to solve a fluorescence microscopy artifact that resulted from the multivalent nature of SA biotin binding. In particular, the protein of interest, a neuronal membrane protein, would "crosslink" as a side reaction. In their approach, the authors were able to utilize a mutation that abolished biotin-binding – this was

denatured and allowed to refold in the presence of active monomers such that SA with a single active subunit, and three "dead" subunits could be isolated (Howarth et al. 2006). However, when it comes to stable surface attachment (e.g., to a biotinylated surface), a single, high-binding site may be inadequate for a long-lived interaction with such a surface (Dubacheva et al. 2017). It was found that SA bound to the surface with only a single ligand-binding site could be washed away under the flow conditions used in their experiment. Thus, the optimal valency of a particular SA variant is very much dependant on the application.

In addition to affinity staining techniques (biotin blotting, microscopy) SA itself has been used as a scaffold for organizing protein components on the nanoscale. In particular, one of the highlighted artificial cellulosome designs included SA, as well as SA-coated QDs used to bridge the NP scaffold to the cellulase and CBM components (D.-M. Kim et al. 2011; Nakazawa et al. 2013). Further elaborating on SA-based scaffold designs, modification of SA subunits themselves were designed such that 4 tetramers could self-assemble into a construct with 12 available biotin-binding sites in order to prepare a 56 component nanoscale assembly of a signalling protein of interest (Fairhead et al. 2014). To accomplish this, 1 of 4 SA monomers were fused to the SpyCatcher/SpyTag affinity pair. In another example of this, crosslinking of SA with a tag that permits HRP-mediated Tyr coupling was done to produce SA capable of both biotin-binding and further "dual-modification" using sortase-mediated coupling (Matsumoto et al. 2016). Binding an endo- and exo-cellulase on crosslinked SA variants was done, though rate enhancement was only modest. Using SA as a mediator to bind a protein of interest to a scaffold (virus) has been done using biotinylated tobacco mosaic virus (**TMV;** 2130 coat protein per virus) (M. L. Smith et al. 2006; Klug 1999). The SA was produced as a genetic fusion to the protein of interest and up to 2200 copies of the protein displayed (~710 tetramers of SA were estimated to be loaded).

The ability to precisely build and position components, allowing bottom-up fabrication schemes, can be useful in the fabrication of devices. One approach is to use a biotinylated surface to be

functionalized with SA covalently attached to some biomolecule component. For example, biotinylated TMV was used as a component in a field-effect transistor device for detecting penicillin G (Poghossian et al. 2018). The TMV served the role of being a mediator to which a penicillinase-SA fusion protein was indirectly bound to the sensor surface to avoid issues with direct enzyme adsorption. In the reverse case, surfaces modified with SA might be used to bind biotinylated components. A pH-sensitive SA variant was used to bind molecules of interest for capture of an analyte to a biosensor chip (Pollheimer et al. 2013). The surface could be regenerated by a combination of low pH and detergent for re-use. In summary, SA is a particularly useful addition to the nanoscale assembly "toolbox" as it can act as a sort of molecular glue for the positioning of components in devices, sensors or nanoscale assemblies in general.

1.6 Summary

Bionanotechnology has a wide selection of biological materials with which new technological designs can be brought forth from. The different biological building blocks outlined in **Section 1.1** each have their own benefits and optimal uses. To reiterate, the interest in viruses as biological building blocks stems from their monodispersity, variety of architectures, high production and exact positioning of reactive functional groups. The fact that the particles are composed of DNA and protein packaged together enables modification of the coat proteins themselves through molecular biological techniques. Knowledge of virus structure and positioning of reactive amino acids furthermore enables chemical modification – opening up many possibilities for designs in the context of using viruses as nanoscale scaffolds.

It is the goal of this thesis to further explore and enable the application of viruses to bionanotechnological designs through exploring methods with which large multi-enzyme assemblies may be prepared using filamentous bacteriophage as a nanoscale scaffold. In a broader context, multi-enzyme complexes may be applied to the fields of technology and synthetic biology. With respect to technology, having methodologies whereby dense arrangements of enzymes can be prepared and

directed to a surface (refer to phage display **Section 1.2.3**) may expand upon available "bottom-up" device fabrication strategies in which biological components are required. With respect to synthetic biology, methodologies for preparing large multi-enzyme complexes may be useful in creating model systems which may be used to study naturally occurring multi-enzyme complexes (such as the cellulosome, referred to in **Section 1.4**). Several approaches have been explored with respect to this end goal. In exploring these approaches several design challenges and concepts important to controllable nanoscale assembly on this platform were found. In preparing a multi-enzyme complex on M13, a cellulosomal cellulase was chosen to examine the effects of high-density enzyme loading on the platform. Given the large amount of literature exploring the assemblies of cellulases, and how the cellulolytic activity of such enzymes can be affected by targeting and synergy effects, this was a relevant enzyme to explore. Cel8A from *C. thermocellum* was chosen as the model enzyme given its prevalence in artificial cellulosome designs (Chundawat et al. 2016; Q. Sun and Chen 2016; Q. Sun et al. 2014; Tsai, Park, and Chen 2013; Yael Vazana et al. 2013).

A number of approaches were taken to preparing enzyme modified M13. As highlighted in the section on the M13 lifecycle and p8 display methods, direct fusions to the major coat protein are poorly displayed (Sidhu, Weiss, and Wells 2000). Given the difficulties in preparing direct genetic fusions, alternate means were explored. Briefly, a sortase-mediated platform was tested to see if a Coh-bearing M13 could be produced and then used to bind Cel8A via the Coh-Doc interaction (**Figure 1.21**). Further approaches utilized a combination of other affinity interactions to prepare multi-enzyme complexes on M13. SA was utilized as a mediator to complex Cel8A onto biotinylated-M13. Though initially a simple concept, experimentation with this approach highlighted several important design principles that were not initially evident and uncovered over the course of exploring the preparation of this multi-enzyme platform. Model systems exhibiting cellulolytic activity were discovered and the design principles elucidated herein should provide critical information for the future fabrication of complex multi-enzyme supramolecular complexes.

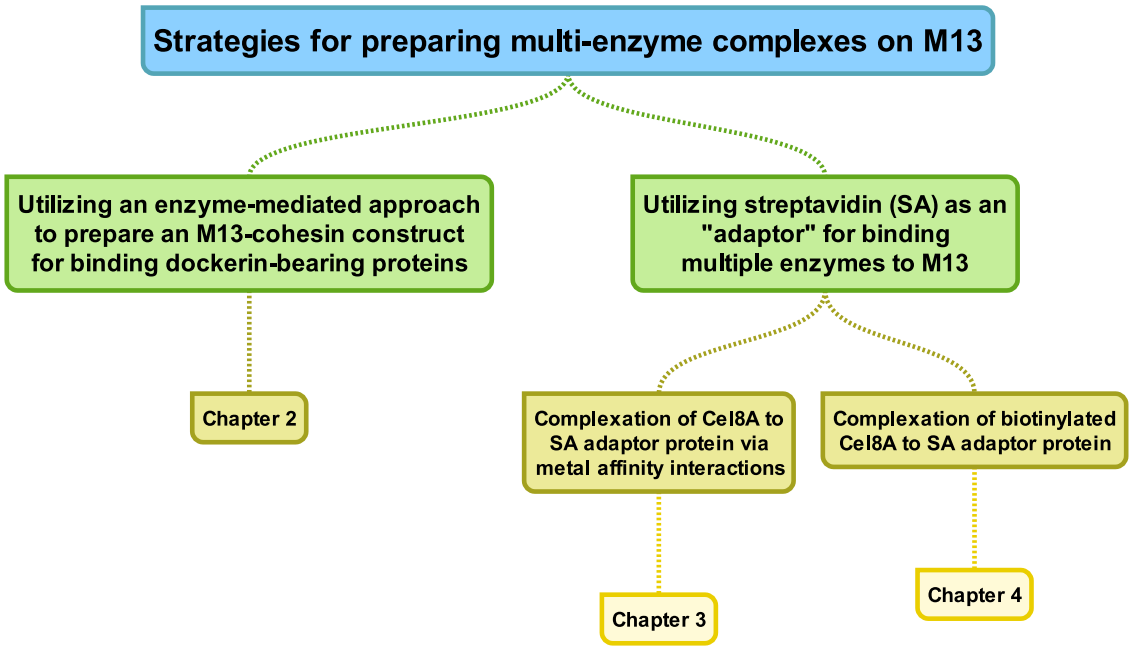

Figure 1.21: Overview of thesis topics.

Chapter 2 Sortase-mediated approach to form Coh-M13 construct

2.1 Introduction

The first strategy used to prepare a multi-enzyme complex on M13 was to utilize the native Coh-Doc interaction in the cellulosome (**Section 1.4**) to load Doc-bearing cellulase onto M13. Given the limitations of directly displaying genetic fusions of large proteins on p8, the proteins were joined enzymatically. The target M13 nanoscale scaffold was an M13 displaying Coh subunits along its length (**Figure 2.1**). The bound Coh modules would then be used to bind enzymes that have Doc domains, such as Cel8A. CipA, the scaffoldin from *C. thermocellum*, contains nine Coh domains with similar sequence identity (Jindou et al. 2004). The second Coh domain of CipA (**Coh2**), has been well-studied and characterized, and was selected as the Coh to be used in preparing this complex (Caspi et al. 2009; Yaron et al. 1995). Therefore, preparation of this complex would be done in two steps: first the M13-Coh2 scaffold must be prepared, and 2) the docking of Cel8A would be carried out in a second step. Therefore, the preparation of the initial M13-Coh2 construct should be done in a way that efficiently reacts multiple Coh2 molecules to the phage.

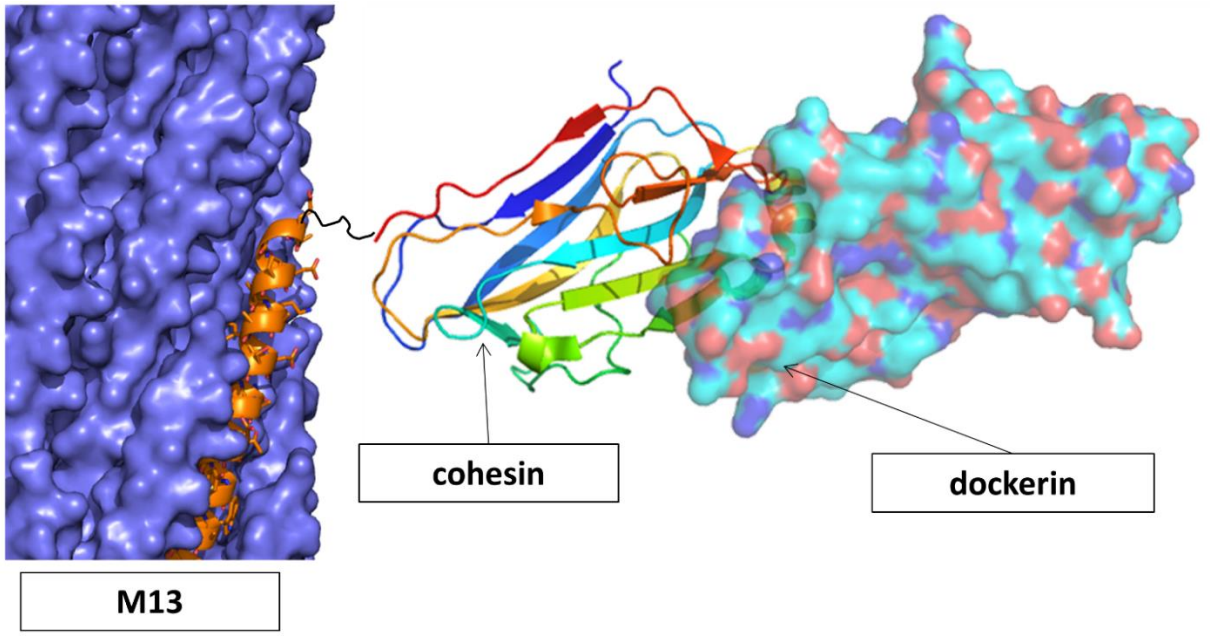

Figure 2.1: Concept image of Coh2 fused to the N-terminus of the p8 major coat protein of M13. To the Coh2 module is a dockerin-containing protein shown bound. M13 – PDB: 2MJZ (Morag et al. 2015), Coh2/Doc complex – PDB: 2B59 (Adams et al. 2006).

One method that has been cited in literature for post-translationally preparing p8 fusions utilizes the enzyme, sortase (Hess et al. 2012). Natively, sortase is responsible for taking proteins with a C-terminal signal peptide and attaching them to the bacterial cell wall peptidoglycan layer (Marraffini, DeDent, and Schneewind 2006). Specifically, the enzyme initially reacts with a recognized peptide to form a covalent acyl-enzyme intermediate in the first step, followed by reaction with an appropriate nucleophile to liberate the peptide from the enzyme. In particular, two sortases have found use in protein engineering applications: sortase from *S. aureus* (**SauSrtA**) which is Ca-dependent and recognizes a LPXTG motif, and sortase from *S. pyogenes* (**SpySrtA**) which has no calcium requirement and recognizes a LPXTA motif (Guimaraes et al. 2013; Theile et al. 2013). The development of an M13 p8 variant with the ability to act as a nucleophile in the SpySrtA reaction has been demonstrated with small molecules and model proteins (Hess et al. 2012). To make this possible, this p8 variant has a mutated N-terminus with an insertion of AAGGGG (**p8-A2G4**). Therefore, in adapting this methodology for preparing a multi-M13-Coh2 scaffold, the following scheme was devised (**Figure**

2.2). Coh2 with a C-terminal LPETAG motif will be prepared and reacted with SpySrtA in the presence of A2G4-p8 to covalently join the two proteins with a native peptide bond.

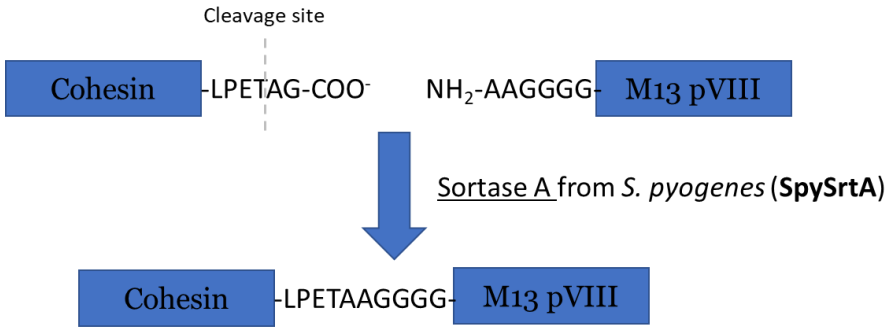

Figure 2.2: Reaction schematic for SpySrtA reaction with Coh2-LPETAG substrate.

As this methodology involved the purification of several proteins, the different proteins that were produced and used will be introduced first (**Figure 2.3**). Following this, initial experiments with a model fluorescent SpySrtA substrate were carried out to confirm that all purified components were active. Furthermore, the importance of SpySrtA concentration is illustrated. Then, moving on to the reactions with the Coh2-LPETAG substrate, several methods were explored for detecting a p8-Coh2 adduct. Lastly, it was observed that a cyclization side-reaction was occurring – further modifications to the Coh2-LPETAG variant were made to try and reduce this side reaction. While this methodology was unable to produce an efficiently modified M13 scaffold, the efforts to utilize this approach highlight some of the potential difficulties with enzyme-mediated approaches to modify M13-p8 with high efficiency.

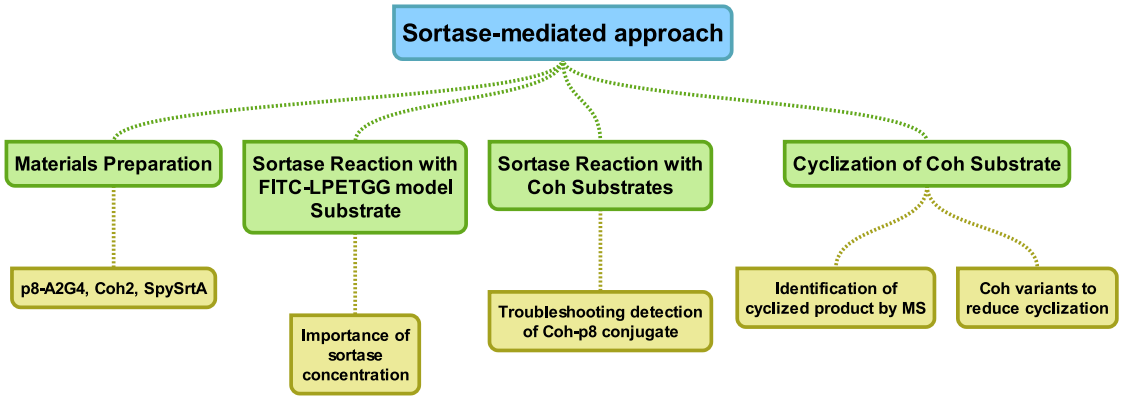

Figure 2.3: Chapter 2 overview.

2.2 Materials and methods

2.2.1 General methods

2.2.1.1 *General M13 amplification and purification*

M13 (M13KE strain from New England Biolabs, Whitby, Canada) was amplified by inoculating a 1:100 diluted overnight culture of *E. coli* K12 ER2738 (New England Biolabs, Whitby, Canada) in Luria Broth (**LB**) media (1% (w/v) peptone, 0.5% (w/v) yeast extract, 1% NaCl (w/v)) supplemented with 8 µg/mL tetracycline. M13 was inoculated to a final titer of ~10^6 plaque-forming units (**PFU**) per mL and amplified for 4.5 – 5.5 h at 37 °C with shaking for aeration. *E. coli* were pelleted by centrifugation at 12000 *g* for 10 min and 4 °C.

M13 was concentrated by polyethylene glycol with 8000 Da average MW (**PEG-8000**) precipitation with PEG-8000/NaCl solution (20% PEG-8000 Da, 2.5 M NaCl). The resulting supernatant was mixed with a 1/5 volume of PEG-8000/NaCl solution and precipitated for 18 h at 4 °C. The precipitated M13 was centrifuged at 12000 *g* for 15 min at 4 °C. The pellet was resuspended in a solution of 1x phosphate-buffered saline (**PBS**; 10 mM Na_2HPO_4, 1.8 mM KH_2PO_4, 137 mM NaCl, 2.7 mM KCl) pH 7.4 that was 1/20 the volume of the initial culture volume. A 1/6 volume of PEG-8000/NaCl solution was added for a second round of precipitation for 30 min on ice. The phage was

pelleted by centrifugation at 15000 *g* for 10 min. The final pellet was resuspended in a volume of 1x PBS that was 1/100 the initial culture volume. If the solution was cloudy, it was centrifuged at 15000 *g* for 1 min to clear the supernatant. The resulting phage solutions were flash frozen in liquid nitrogen and stored at -80 ^{o}C.

The M13 stocks were quantified by measuring the absorbance at 269 nm. The absorbance at 320 nm is included to account for light scattering. This can be converted to a measure of M13 concentration in particles/mL using **Equation 2.1**. N_{bases} is the number of bases in the M13 ssDNA genome which is 7222 bp for M13KE. The 6 x 10^{16} coefficient can be derived from the literature extinction coefficient of 3.84 mg^{-1} cm^{-1} mL and the mass of M13 (Berkowitz and Day 1976).

$$[M13] = \frac{(A_{269} - A_{320}) \times 6 \times 10^{16}}{N_{bases}} \quad (2.1)$$

2.2.2 Materials preparation

2.2.2.1 *Coh2 variants*

The initial construct for Coh2 (Coh2-LPETG) was cloned in a pET28b(+) vector (Genscript, Piscataway, USA). This construct was cloned with a LPETG C-terminal tag to act as a SpySrtA substrate. Several modifications were made to this plasmid to improve its role as a SpySrtA substrate. These modifications were made using standard molecular biological techniques (**Table 2-1**). To clone Coh2-LPETAG, Ala was inserted into the C-terminal tag to produce Coh2-LPETAG by site-directed mutagenesis (**SDM**).

Table 2-1: Mutagenesis strategies for preparing variants of Coh2 for use as a SpySrtA substrate.

Variant	Method	Forward Primer	Reverse Primer
Coh2-LPETAG	SDM; Insertion (A)	5' – CCT GCC GGA AAC CGC AGG CTA ACT CGA GC – 3'	5' – GCT CGA GTT AGC CTG CGG TTT CCG GCA GG – 3'
Coh2-A2S	Two-Step SDM; Mutation (A2S)	5' – GGA GAT ATA CCA TGT CGC ACC ACC ATC AC-3'	5' – GTG ATG GTG GTG CGA CAT GGT ATA TCT CC-3'
A2S-Coh2-GGGGS	Two-Step SDM; Insertion (GGGGS)	5' – GTG AAT GTG GGT GGA TCC **GGT GGT GGC GGT TCT** CTG CCG GAA AC-3'	5' – GGA TCC ACC CAC ATT CAC GCC ACC ATC AAT AAA GC-3'

Expression and purification conditions were the same for each variant. The plasmid was transformed in BL21 *E. coli* which were grown to 0.4 – 0.5 OD at 37 ºC in LB media with 40 µg/mL kanamycin. Protein expression was induced at 23 ºC with 1 mM isopropyl-B-*D*-1-thiogalactopyranoside (**IPTG**) for 18 h, at which point the cells were collected by centrifugation at 5000 *g* for 15 min at 4 ºC.

To 1 L of cell pellet, 30 mL of lysis buffer (50 mM tris(hydroxymethyl)aminomethane (**Tris**) pH 7.5, 150 mM NaCl, 10 mM imidazole) supplemented with 1 mM phenylmethylsulfonyl fluoride (**PMSF**) was added. The resuspended pellet was passed three times through a high-pressure homogenizer to lyse the cells. The lysate was centrifuged at 15,000 *g* for 30 min at 4 ºC. The protein was purified by immobilized metal affinity chromatography (**IMAC**). The cleared lysate was loaded onto a 1 mL HisTrap™ (GE Healthcare, Chicago, USA), washed with 5 mL of wash buffer (50 mM Tris-HCl pH 7.5, 150 mM NaCl, 10 mM imidazole), and eluted over a 5 mL gradient from 20 to 300 mM imidazole. The eluted fractions were dialyzed 3 x 2 L into 200 mM HEPES pH 7.5. The purified protein was flash frozen in liquid nitrogen and stored at -80 ºC. Coh2 was quantified by measuring its absorbance at 280 nm and using its theoretical extinction coefficient of 7450 M^{-1} cm^{-1} calculated by ProtParam (Gasteiger et al. 2005).

2.2.2.2 *SpySrtA*

The SpySrtA was expressed from pET28a-SpySrtA (Addgene plasmid # 51139) from Hidde Ploegh (Guimaraes et al. 2013). The plasmid was transformed in BL21 *E. coli* which was grown to 0.5 – 0.6 OD at 37 ºC in LB media with 40 µg/mL kanamycin. Protein expression was induced at 23 ºC with 1 mM IPTG for 18 h, at which point the cells were collected by centrifugation at 5000 *g* for 15 min at 4 ºC.

To the cell pellet from 1 L of culture, 30 mL of lysis buffer (50 mM Tris-HCl pH 7.5, 150 mM NaCl, 10 mM imidazole) supplemented with 1 mM PMSF was added. The resuspended pellet was passed three times through a high-pressure homogenizer (>10,000 psi) to lyse the cells. The lysate was centrifuged at 15,000 *g* for 30 min at 4 ºC. The protein was purified by IMAC. The cleared lysate was loaded onto a 1 mL HisTrap™ (GE Healthcare, Chicago, USA), washed with 5 mL of wash buffer (50 mM Tris-HCl pH 7.5, 150 mM NaCl, 10 mM imidazole), and eluted over a 5 mL gradient from 10 to 300 mM imidazole. The eluted fractions containing SpySrtA were pooled and concentrated with a 10 kDa molecular weight cut-off (**MWCO**) spin concentrator. The concentrated sample was loaded onto a Superdex® 75 size-exclusion column and eluted with 50 mM Tris-HCl pH 7.5, 150 mM NaCl. The purified protein was flash frozen in liquid nitrogen and stored at -80 ºC. SpySrtA was quantified by measuring its absorbance at 280 nm and using its theoretical extinction coefficient of 10430 M^{-1} cm^{-1} calculated by ProtParam (Gasteiger et al. 2005).

2.2.2.3 *A2G4 M13*

M13 double stranded DNA was prepared by inoculating a 1:100 diluted overnight culture of *E. coli* K12 ER2738 (New England Biolabs, Whitby, Canada) in Luria Broth (**LB**) media (1% (w/v) peptone, 0.5% (w/v) yeast extract, 1% NaCl (w/v)) supplemented with 8 µg/mL tetracycline. M13 was inoculated to a final titer of ~10^6 plaque-forming units (**PFU**) per mL and amplified for 4.5 – 5.5 h at 37 ºC with shaking for aeration. Aliquots of 1 mL were centrifuged at 15000 *g* for 1 min to collect the cell pellet which was processed with GenElute™ Plasmid Miniprep Kit (Millipore Sigma, Oakville, Canada) according to manufacturer's protocol.

Mutagenesis of M13KE DNA to prepare M13-A2G4 for SpySrtA reactions was carried out using primers synthesized at Millipore Sigma (Millipore Sigma, Oakville, Canada). For insertion of sequences to the N-terminus of p8, the M13KE vector was prepared by mutating T1372A and C1381G to introduce PstI and BamHI sites respectively (**Table 2-2**) (Petrenko et al. 1996). Additionally, there was a PstI site that was removed from M13KE by mutation of A6249T. M13-A2G4 (M13 p8 variant for reaction with SpySrtA) was prepared by insertion of A2G4 with complementary oligos according to (Hess et al. 2012). Amplification and purification were carried out using general M13 amplification and purification (**Section 2.2.1.1**).

Table 2-2: Primers used in preparing M13-A2G4 as described in the Methods.

Variant	Method	Forward Primer	Reverse Primer
A6249T	SDM	5' – GCT TGC ATG CCT GCT GGT CCT CGA ATT CAC – 3'	5' – GTG AAT TCG AGG ACC AGC AGG CAT GCA AGC – 3'
C1381G	SDM	5' – CTG CAG AGG GTG AGG ATC CCG CAA AAG – 3'	5' – CTT TTG CGG GAT CCT CAC CCT CTG CAG – 3'
T1372A	SDM	5' – CTG TCT TTC GCT GCA GAG GGT GAC GAT CC – 3'	5' – GGA TCG TCA CCC TCT GCA GCG AAA GAC AG – 3'
A2G4	Subcloning (from annealed insert)	5' – (phos)GCT GGC GGG GGA GGG – 3'	5' – (phos)GAT CCC CTC CCC CGC CAG CTG CA – 3'

2.2.3 SpySrtA reaction conditions

2.2.3.1 *Reaction with SpySrtA substrates*

The synthetic peptide FITC-LPETGG(N2) (**Figure 2.4**) was purchased from GenScript (95.9 % purity; GenScript, Piscataway, USA). The peptide was prepared as a 10 mg/mL working stock in dimethyl sulfoxide (**DMSO**). Coh2 substrates were purified and stored as indicated above.

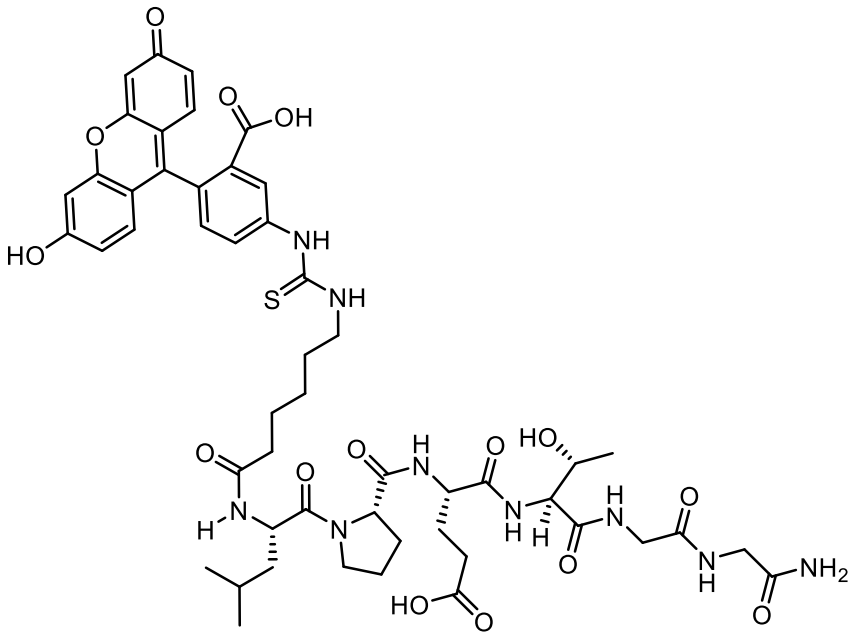

Figure 2.4: Structure of FITC-LPETGG-N2.

Typical reaction conditions with SpySrtA were prepared with 50 µM p8-A2G4, 500 µM substrate (FITC-LPETGG or Coh2 variant), 25 µM SpySrtA in 1x sortase reaction buffer (50 mM Tris-HCl pH 7.5, 150 mM NaCl) incubated at 37 ºC up to 18 h. The reaction conditions and 1x sortase reaction buffer were adapted from (Theile et al. 2013). Aliquots of the reaction were removed and mixed with sodium dodecyl sulfate polyacrylamide gel electrophoresis (**SDS-PAGE**) loading buffer (containing β-mercaptoethanol) to stock the reaction. The gels were analyzed in a gel imager with 534 nm excitation source and 537 nm filter to image FITC fluorescence. For detection of adducts by Western blotting, the primary antibody used was a mouse monoclonal antibody against the M13 major coat protein (RL-ph1; Santa Cruz Biotechnology, Dallas, USA). The secondary antibody was goat anti-mouse conjugated to horseradish peroxidase (Santa Cruz Biotechnology, Dallas, USA). The HRP was detected using *3,3′,5,5′*-Tetramethylbenzidine (**TMB**) substrate for membranes (Millipore Sigma, Oakville, Canada).

2.3 Results and discussion

In the initial design for a multi-enzyme complex built from bacteriophage M13, native cellulosomal proteins were used. By coating bacteriophage M13 with Coh from the *C. thermocellum* scaffoldin protein, a nanoscale scaffold with the capability of binding multiple Doc-bearing enzymes (such as native cellulases) could be accomplished. There are a number of ways that a Coh-bearing M13 could be prepared. One of the main difficulties in displaying large proteins onto p8 is that this occurs very inefficiently (Sidhu, Weiss, and Wells 2000). In particular, large genetic fusions on p8 likely interfere with the assembly of phage particles. When preparing genetic fusions, it has been necessary for groups to grow hybrid phage with genes coding for wildtype p8 and the p8-fusion protein (Sidhu, Weiss, and Wells 2000). However, display of proteins in this way is still very inefficient – leading to <1 displayed protein per M13. A group developed an enzyme-mediated approach to preparing fusion proteins attached to M13 p8 protein using sortase (SpySrtA) – a bacterial cell-wall sorting enzyme (Hess et al. 2012). This method has been demonstrated to be useful for the display of a model protein, green fluorescent protein (**GFP**), onto p8. Thus, this approach was used here for the attachment of Coh to M13.

2.3.1 Component purification

Three components needed to be prepared to carry out this procedure: Coh2-LPETAG, SpySrtA and M13-A2G4. Coh2-LPETAG was expressed and purified with a N-terminal His6-tag for IMAC. SpySrtA was also expressed with a His6-tag for IMAC – however, IMAC was not adequate to purify the protein and subsequent size-exclusion chromatography (**SEC**) was required. Lastly, M13-A2G4 was purified by typical methods using PEG-8000 precipitation.

In order to be recognized by sortase from *S. pyogenes* LPETAG was fused to the C-terminal end of the construct (this construct will be referred to as **Coh2-LPETAG**). Coh2-LPETAG was separated solely by IMAC, eluting as expected over the course of the imidazole gradient (**Figure 2.5A**). Based on the intensity of the bands, the protein expressed very well. Coh2-LPETAG was purified only using IMAC with an initial wash of 10 mM imidazole. The purified Coh2 was analyzed by electrospray

ionization mass spectrometry (**ESI-MS**) and the resulting deconvoluted spectrum showed a reconstructed mass slightly lower than the theoretical MW of 16734.88 Da (**Figure 2.5B**). However, the reconstructed mass was exactly consistent with the mass of Coh2-LPETAG without its N-terminal Met.

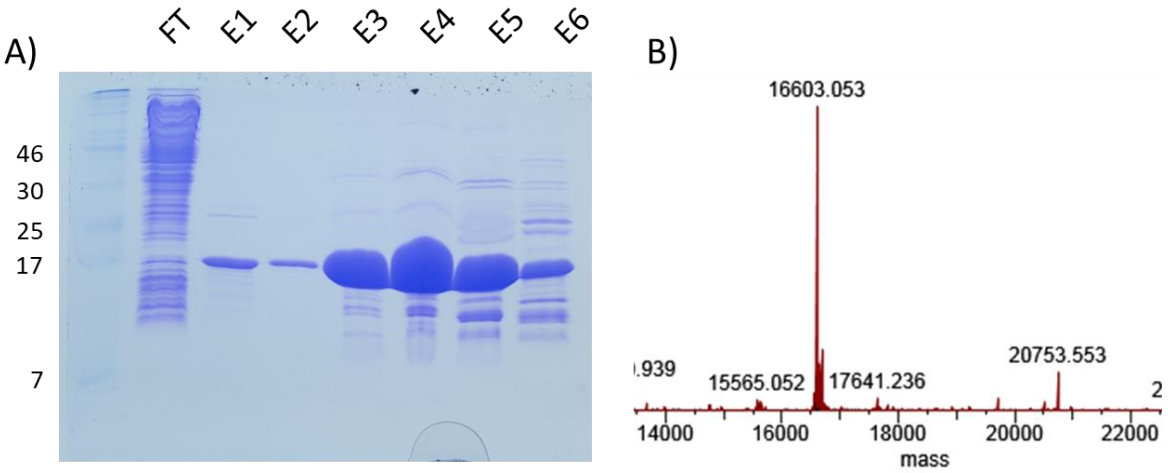

Figure 2.5: Purification of Coh2-LPETAG starting material. A) SDS-PAGE of IMAC separation of Coh2-LPETAG as described in the Methods. FT is the flowthrough, and E1-6 are fractions eluted during the imidazole gradient. B) Deconvoluted ESI-MS of purified Coh2-LPETAG in 1:1 MeOH:H_2O + 0.1% FA run on a ThermoFisher Q-Exactive and deconvoluted using BioPharma Finder™ (ThermoScientific, v.3.0).

Initially, the concentration of Coh2-LPETAG was estimated using the Bradford assay; however, it was found that the assay grossly underestimated the concentration of Coh2-LPETAG. The concentration estimated by the Bradford assay was 338 µM (~5.6 mg/mL). The concentration estimated from the calculated extinction coefficient (ProtParam) and UV-Vis spectroscopy was found to be 7.72 mM (129.2 mg/mL). The Bradford assay therefore underestimated the concentration by more than 20-fold. The yield ended up being about 60 mg of protein per liter. Typically, differences between the protein being assayed and the protein used for the standard curve (bovine serum albumin (**BSA**)) can result in such inaccuracies (Kruger 1994). Though the Coh construct used has 4 Arg and 8 Lys residues, which should facilitate binding to the dye, thermostable proteins tend to have a network of ionic interactions on their surface stabilizing the protein (Chan et al 2011). Perhaps these make basic residues

unavailable for interaction with the Bradford dye. Regardless, this ended up being one of those cautionary examples where the protein being studied is poorly assayed with this method.

SpySrtA was purified initially by IMAC, however the resulting protein was inadequately purified by this method alone. This has been noted in the literature, and SEC following IMAC was recommended (Guimaraes et al. 2013). Therefore, fractions collected from IMAC were concentrated and then applied to SEC to further clean-up the protein (**Figure 2.6A**). The yield of this protein was quite poor, as only 3 mg/L of culture was ultimately purified. This protein was also analyzed by ESI-MS and the reconstructed mass was consistent with the expected mass of 20556.35 Da (**Figure 2.6B**). Ultimately, this protein would also be tested with a model substrate in the following section to confirm that it was indeed active.

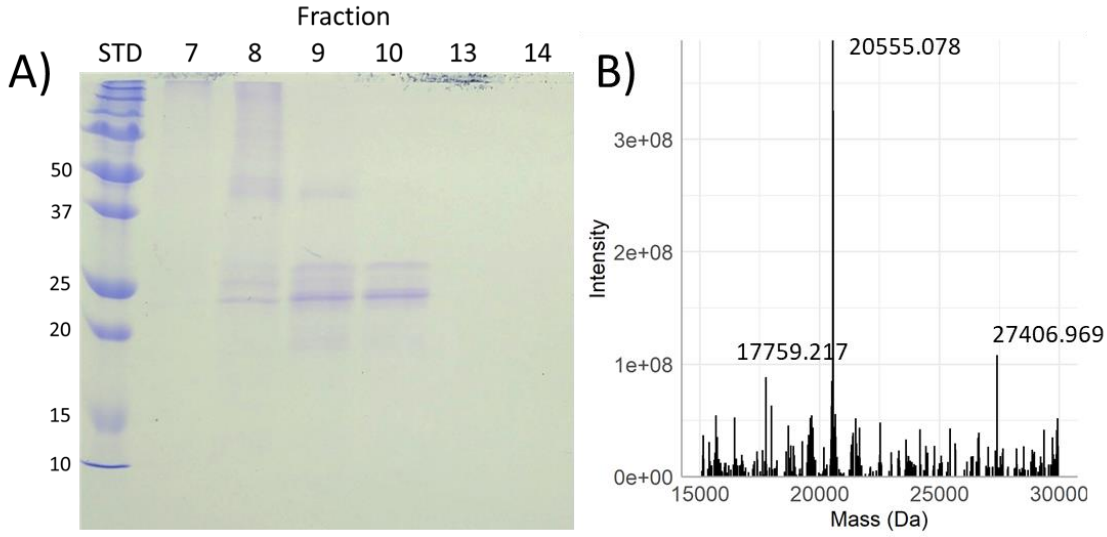

Figure 2.6: Purification of SpySrtA. A) SDS-PAGE of SEC of SpySrtA fractions pooled from IMAC on Superdex® 75 as described in the Methods. B) Deconvoluted ESI-MS of purified SpySrtA in 1:1 MeOH:H_2O + 0.1% FA run on a ThermoFisher Q-Exactive and deconvoluted using BioPharma Finder™ (ThermoScientific, v.3.0).

Lastly, M13-A2G4 was cloned according to the Methods and then amplified using standard M13 purification protocols. Typically, the yields from these preparations were around $1 – 2 \times 10^{13}$ particles/mL, as estimated by their absorbance spectra (**Equation 2.1**). The solutions were centrifuged until they were clear to remove any aggregated protein (15,000 *g* for 5 min). As a side observation, this variant of M13 was more prone to aggregation than M13KE, as the phage tended to settle to the bottom

of tubes when stored at 4 ºC after a few days. Furthermore, when preparing this variant for ESI-MS it was particularly sensitive to dilution into the ESI-MS solvent (50% MeOH) and tended to precipitate at higher concentrations. However, diluting M13-A2G4 to a p8 concentration of ~1 µM was suitable for preparing the sample without visible precipitates.

Interestingly, the ESI-MS did not show the major coat protein to be the expected monoisotopic mass. The major peak observed on the spectrum was at 5274.75 Da (**Figure 2.7A**). The expected monoisotopic mass for p8-A2G4 was 5232.77 Da based on its expected mature sequence (**Figure 2.7B**). The difference between the observed mass and expected mass corresponded to the mass change expected for acetylation. Furthermore, the sequence was confirmed to be the correct one by DNA sequencing of the M13-A2G4 stock. While acetylation of proteins is typically thought to be a eukaryotic phenomenon, it has been observed extensively in bacteria such as *E. coli* (Kuhn et al. 2014). Based on the consensus sequence published, the altered p8 sequence in A2G4 does make the protein appear as a suitable substrate for acetylation of Lys (**Figure 2.7C**). This was not noted in the original paper for the M13-A2G4 framework; however, no intact mass spectra of p8-A2G4 were included in this report (Hess et al. 2012). As liquid chromatography tandem mass spectrometry (**LC/MS-MS**) spectra of digested p8-adducts were analyzed in their work, an acetylated fragment may have gone unnoticed. Regardless, it is not expected that N-acetylation of the Lys residue would affect the role of p8-A2G4 as a nucleophile in the sortase reaction. It is also unlikely that N-terminal acetylation occurred, as reactions with the model substrate, FITC-LPETGG were positive.

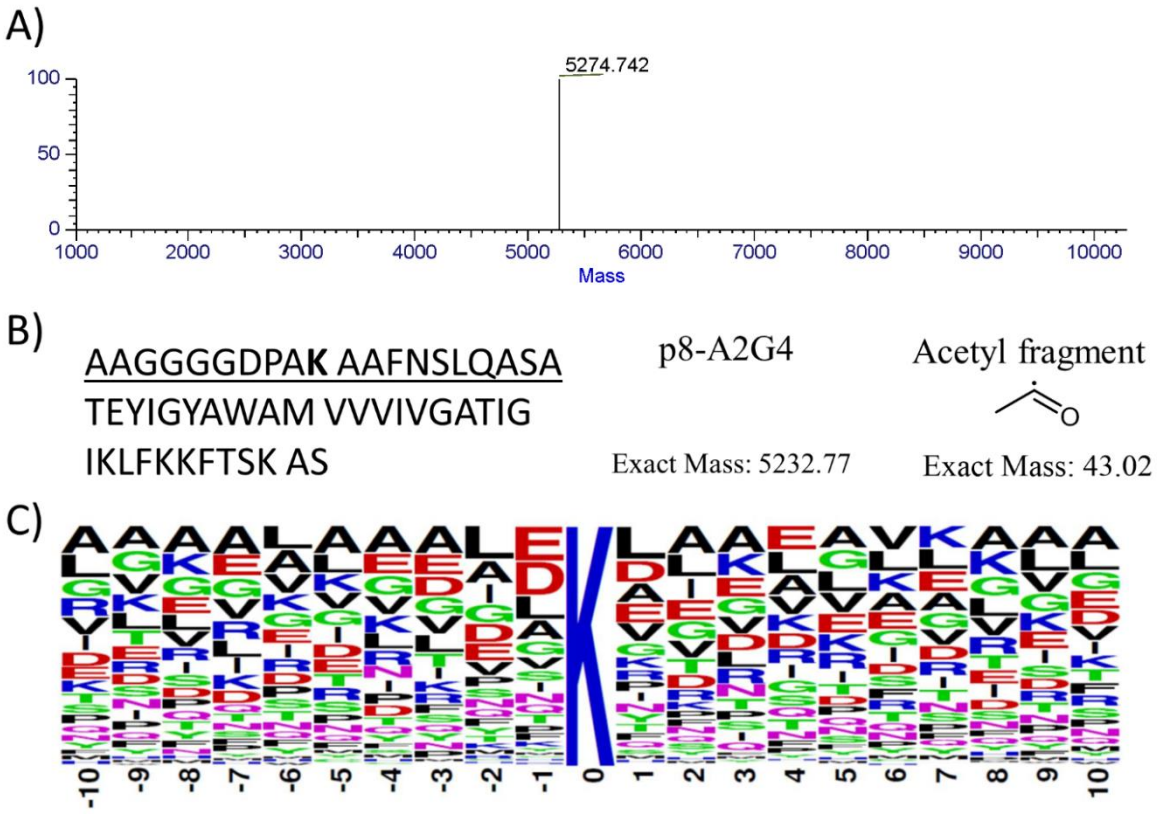

Figure 2.7: Characterization of M13-A2G4 starting material by ESI-MS. A) Deconvoluted ESI-MS of M13-A2G4 run in 1:1 MeOH:H_2O + 0.1% FA on a ThermoFisher Q-Exactive. B) Sequence of mature p8-A2G4 with expected monoisotopic masses of protein and acetyl modification. C) Consensus sequences for acetate kinase (ackA) Lys acetylation in E. coli from (Kuhn et al. 2014) under a creative commons license (https://creativecommons.org/licenses/by/4.0/).

2.3.2 Reactions with FITC-LPETGG

There are several sets of conditions that have been successfully used to perform reactions using sortase. One such publication presents a protocol for the use of sortase (both *S. pyogenes* and *S. aureus* sortases) to join a peptide-containing probe to the N-terminus of a protein (Theile et al. 2013). They provide a range of component concentrations to set up reactions: 0.5 – 1 mM peptide, 10 - 50 µM target protein, 20 – 150 µM sortase A in 1x sortase buffer and 37 °C. The final concentrations for the reaction buffer are 50 mM Tris pH 7.5 and 150 mM NaCl ($CaCl_2$ can be omitted for SpySrtA). What is particularly noticeable is the recommended high enzyme concentration.

The purified components were first tested to confirm that they were indeed reactive and that the reactions would proceed as described in the literature. To test the SpySrtA enzyme and the A2G4-M13

strain that were prepared as described in the Methods, the fluorescent peptide FITC-LPETGG was used. This particular substrate had an amidated "C-terminus", rather than the usually carboxy-terminus. Such small molecule substrates have previously been reported as successful sortase substrates (Nelson et al. 2010). It was necessary to use high concentrations of both the substrate, FITC-LPETGG, and SpySrtA. At 500 µM FITC-LPETGG and 2.5 µM SpySrtA, there was very little product detected by denaturing PAGE at several time points (**Figure 2.8A**). However, at 25 µM SpySrtA labelling of p8 was observed. The acyl-enzyme intermediate (SpySrtA/FITC) could also be detected throughout the reaction. The gel was stained and imaged to confirm the bands ran at their expected MW (**Figure 2.8B**). Overall, the components were active – however, the reaction was inefficient and proceeded slowly. It was clear from these tests that high substrate concentrations and enzyme concentration would be necessary for effective reaction. High substrate concentration is typically recommended to offset the hydrolysis side reaction that can occur (Levary et al. 2011). More specifically, it is recommended to have the sortase enzyme at 1/10th the concentration of the substrate.

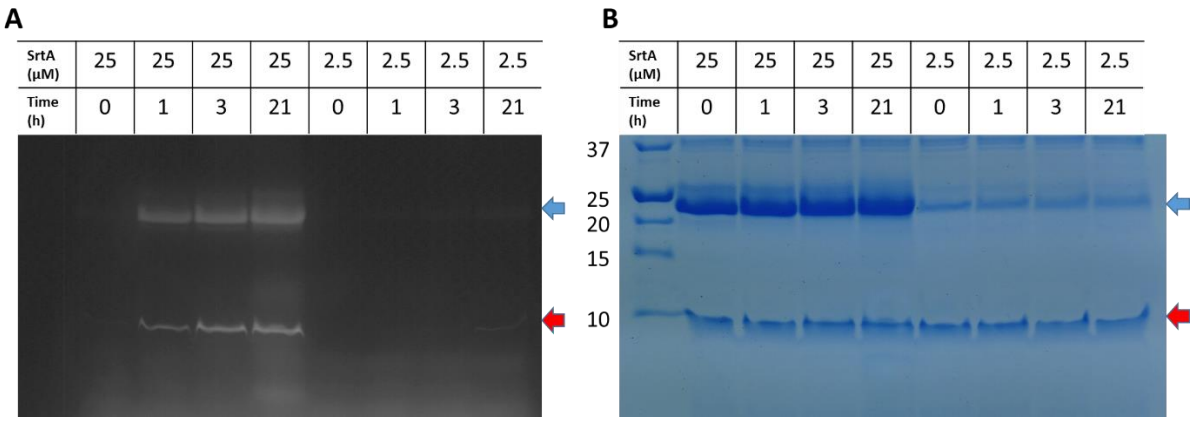

Figure 2.8: Monitoring reaction of SpySrtA, M13-A2G4 and FITC-LPETGG fluorescent substrate over time. Aliquots were taken at 0 and 1, 3 and 21 h. Tricine-PAGE gel of FITC-LPETGG/M13-A2G4 reactions with variable amounts of SpySrtA under A) fluorescence imaging, and B) after staining with Coomassie stain. The red arrow indicates the location of the p8 band. The blue arrow indicates the location of the SpySrtA band.

Based on the observed reactions with the small, fluorescent peptide FITC-LPETGG, the purified SpySrtA was indeed active and the M13-A2G4 capable of being modified by SpySrtA as

described in literature. These conditions would be used to inform on those necessary for reaction with the protein substrate, Coh2-LPETAG.

2.3.3 Reactions with Coh2-LPETAG and M13-A2G4

After testing the SpySrtA enzyme preparations with FITC-LPETGG, reactions with M13-A2G4 and Coh2-LPETAG were tested. Unlike FITC-LPETGG which was easily detected by its fluorescence, identification of the Coh-p8 adduct by denaturing PAGE was not possible due to the similar MW of some of the components (**Table 2-3**). In particular, the expected MW of the Coh2-p8 adduct and SpySrtA enzyme were similar – 21.9 and 20.6 kDa respectively. As it was unlikely that the adduct would be confirmed by denaturing PAGE only, some alternate methods were tested.

Table 2-3: Average molecular weight of components used as substrates for SpySrtA-mediated reactions and estimated masses of possible products.

Component	MW
Coh2-LPETAG	16.7
SpySrtA	20.6
P8	5.2
Coh2-LPET-p8	21.9
SpySrtA acyl-enzyme intermediate	37.3*

In the purification of M13, the filamentous phage is typically precipitated by PEG-8000 and NaCl. This method has been used in several literature approaches to purify M13 reacted with various small molecules (Chung, Lee, and Yoo 2014; Jinsu Kim et al. 2015). This was tested here to determine the extent to which the M13 and any formed adducts might be separated from unreacted components. Reactions were carried out with a 10-fold excess of substrate to SpySrtA (500 µM Coh2-LPETAG). As determined from initial testing with FITC-LPETGG test substrate, an excess of substrate was required in addition to a high enzyme concentration. Prior to PEG precipitation, the excessive amount of substrate required for reaction made the reactions difficult to analyze directly by SDS-PAGE (**Figure 2.9A**). To clean-up the reaction mixtures and make it clearer to identify possible products, the reaction mixtures were fractionated by PEG precipitation and the supernatant and pellets analyzed by SDS-

PAGE (**Figure 2.9B**). The precipitation method did not adequately remove unreacted Coh2-LPETAG, though the M13 p8 band was clearly separated to the pellet fraction. While the SpySrtA band was effectively removed by PEG precipitation according to the control lane, there was no clear band that might correspond to the p8-Coh2 adduct.

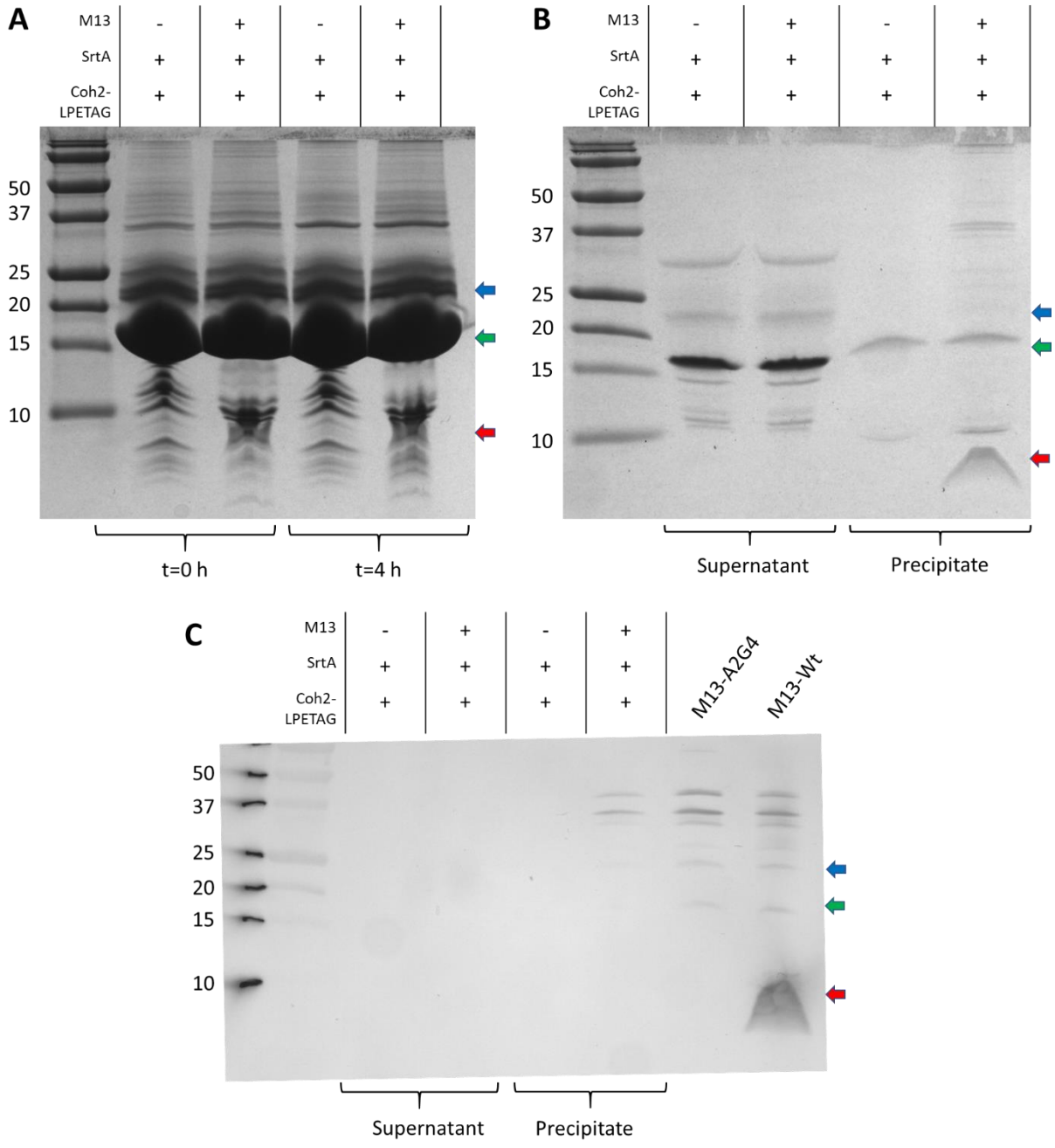

Figure 2.9: Monitoring reaction progress of M13-A2G4 and Coh2-LPETAG via the SpySrtA-catalyzed transpeptidation reaction. A) Tricine-PAGE gel of sortase reaction of 500 µM Coh2, 25 µM SpySrtA and 50 µM p8-A2G4 at 0 and 4 h with

control lacking M13-A2G4. B) Tricine-PAGE gel of precipitated SpySrtA reactions in A). Aliquots were taken of the supernatant and resuspended pellets after overnight precipitation. C) Western blot of precipitated SpySrtA reactions in B) using anti-p8 primary antibody and HRP-conjugated secondary antibody. The arrows correspond to the positions or expected positions of SpySrtA (blue), Coh2-LPETAG (green) and p8-A2G4 (red).

It was briefly tested whether the adduct (containing p8) might be a suitable antigen for an anti-p8 antibody, as a possible way to distinguish the Coh2-p8 adduct from other components. Western blotting to try and detect attached p8 was not possible given that the antibody did not recognize p8 with the N-terminal modifications (p8-A2G4) (**Figure 2.9C**). Several other bands in M13-containing samples were reactive toward the anti-p8 antibody. In the control lanes for WT M13 and A2G4-M13, the inability to detect A2G4-p8 was most obvious – showing that M13-A2G4 is not antigenic toward antibodies prepared for WT M13. Overall, there was no clear evidence of Coh2-LPET-p8 having formed. It would therefore be recommended that in designing substrates for this procedure that they be designed with an additional specific tag for the purpose of antibody detection in order to avoid the complication of similar MW components.

It was furthermore apparent that the expected yield of adduct (if formed) would be quite low. Even assuming that levels of adduct formation comparable to those observed in the literature were obtained, this would not be suitable for preparing a large, densely clustered multi-enzyme complex on M13. In particular, the literature values estimate about 3.4 % of p8 subunits reacted with GFP-LPETG to form an adduct via the sortase-mediated reaction (Hess et al. 2012). If considering this an approximate expected yield for the reaction, there would need to be a sensitive method to detect the adduct. While mass spectrometry is highly sensitive, direct analysis of reaction mixtures with intact proteins was later shown to be inappropriate for detecting an adduct, as the major coat protein of M13-A2G4 suppressed the ionization of other components (see **Section 2.3.4**).

In summary, the p8-LPET-Coh2 adduct was not easily detected, and the following two considerations should be taken: 1) that the substrate, for the purpose of confirming successful reaction, should be designed with a specific immunoreactive tag, as direct identification of p8-adducts are

unlikely given their expected low yields and, 2) as an alternate means to ESI-MS of intact proteins, it is likely necessary that more elaborate methods, such as LC-MS/MS following digestion of the proteins be done to reduce ionization suppression from p8. Given the low expected yields, the approach was not extensively pursued to use as the main method for assembling multiple cellulases on the surface of M13 – however, a few aspects were investigated further.

2.3.4 Cyclization of Coh2-LPETAG by SpySrtA

Over the course of trying to detect a p8-Coh2 adduct, it became apparent that there was also a side-reaction occurring in the reaction mixtures containing Coh2 and SpySrtA (presence or absence of M13). Initial reactions containing SpySrtA, p8-A2G4 and Coh2-LPETAG resulted in the formation of a lower MW band over time (**Figure 2.10**). Initially it was hypothesized that this might be a hydrolysis (or reaction with Tris buffer) side-reaction at an internal amino acid sequence that resembled a sortase substrate close enough to react. To test for cross-reaction of Tris with the acyl-enzyme intermediate, the FITC-LPETGG test substrates were reacted in either Tris, or HEPES buffer – however, no difference of in-gel fluorescence was noted (not shown). However, it was later confirmed by ESI-MS that the mass of a reaction mixture consisting of both SpySrtA and Coh2-LPETAG was instead consistent with a cyclization reaction occurring with the N-terminus of the Coh2-LPETAG protein (**Figure 2.11**). This was identified by a mass peak corresponding to Coh2-LPET without its N-terminal Met1 and furthermore, missing mass corresponding to water (18 Da). The formation of a cyclized protein was consistent with the formation of a lower MW band on denaturing PAGE in figure 10, since the cyclized protein would be expected to run at an apparent lower MW.

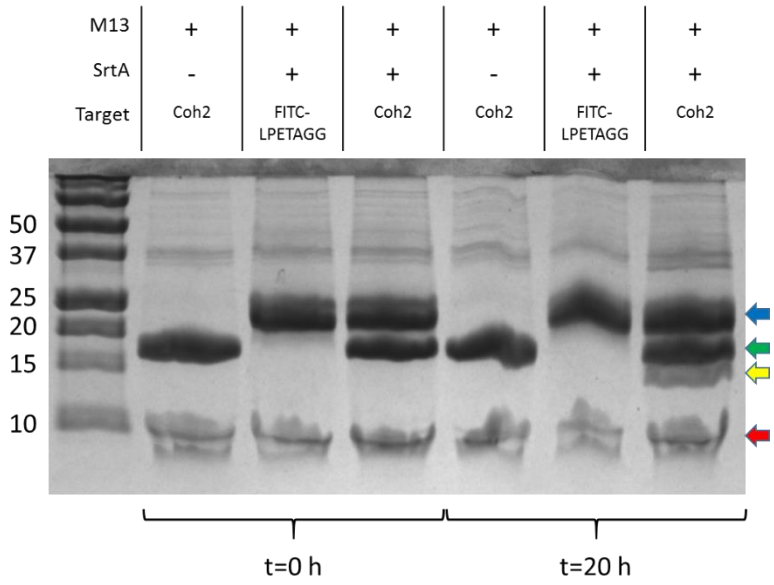

Figure 2.10: Tricine-PAGE gel of 50 µM Coh2-LPETAG, 50 µM p8-A2G4 or 500 µM FITC-LPETGG reactions and control without 25 µM SpySrtA. Aliquots were taken at 0 and 20 h. The arrows correspond to SpySrtA (blue), Coh2-LPETAG (green), cyclized Coh2-LPETAG (yellow) and p8-A2G4 (red).

A) Coh2 only mass spec

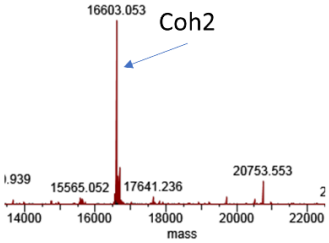

AHHHHHHAAG VVVEIGKVTG SVGTTVEIPV YFRGVPSKGI
ANCDFVFRYD PNVLEIIGID PGDIIVDPNP TKSFDTAIYP DRKIIVFLFA
EDSGTGAYAI TKDGVFAKIR ATVKSSAPGY ITFDEVGGFA
DNDLVEQKVS FIDGGVNVGG SLPETAG

Average MW

Linear: 16603.68 Da

B) Coh2 + SpySrtA mass spec

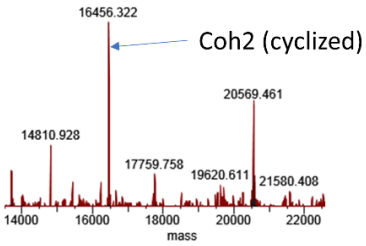

AHHHHHHAAG VVVEIGKVTG SVGTTVEIPV YFRGVPSKGI
ANCDFVFRYD PNVLEIIGID PGDIIVDPNP TKSFDTAIYP DRKIIVFLFA
EDSGTGAYAI TKDGVFAKIR ATVKSSAPGY ITFDEVGGFA
DNDLVEQKVS FIDGGVNVGG SLPET

Average MW

Linear: 16475.55 Da

Cyclized: 16457.55 Da

Figure 2.11: ESI-MS evidence of Coh2-LPETAG cyclization catalyzed by SpySrtA. A) Deconvoluted ESI-MS of Coh2-LPETAG only. B) Deconvoluted ESI-MS of Coh2-LPETAG in the presence of SpySrtA. Also shown are the expected sequences of the highlighted primary peaks in the spectra.

This has been seen with other proteins where Ala is the second residue and the N- and C-termini are in close proximity. In fact, for many of the proteins for which there are structures available, about 2/3 have N- and C-termini in close proximity (Antos et al. 2009). Inspection of the structure of Coh2 indicates that the N- and C-termini are indeed close to each other and could conceivably react

(**Figure 2.12**). The exact distance cannot be estimated due to the missing portions of the sequence in the structure shown. It has been suggested that in the case of proteins with Ala2 as the residue following the N-terminal Met that it be mutated to Ser to reduce the potential for this occurring (Guimaraes et al. 2013). The mutation Ala2Ser was planned for a future Coh2 construct to eliminate this side-reaction that could be reducing the amount of p8-adduct forming. Though, it has been shown that addition of a small peptide (i.e.. GGG (Antos et al. 2009)), can shift the equilibrium back to a linear product, p8-A2G4 on intact M13 would be considerably more hindered as a nucleophile compared to a small peptide and may not effectively do so.

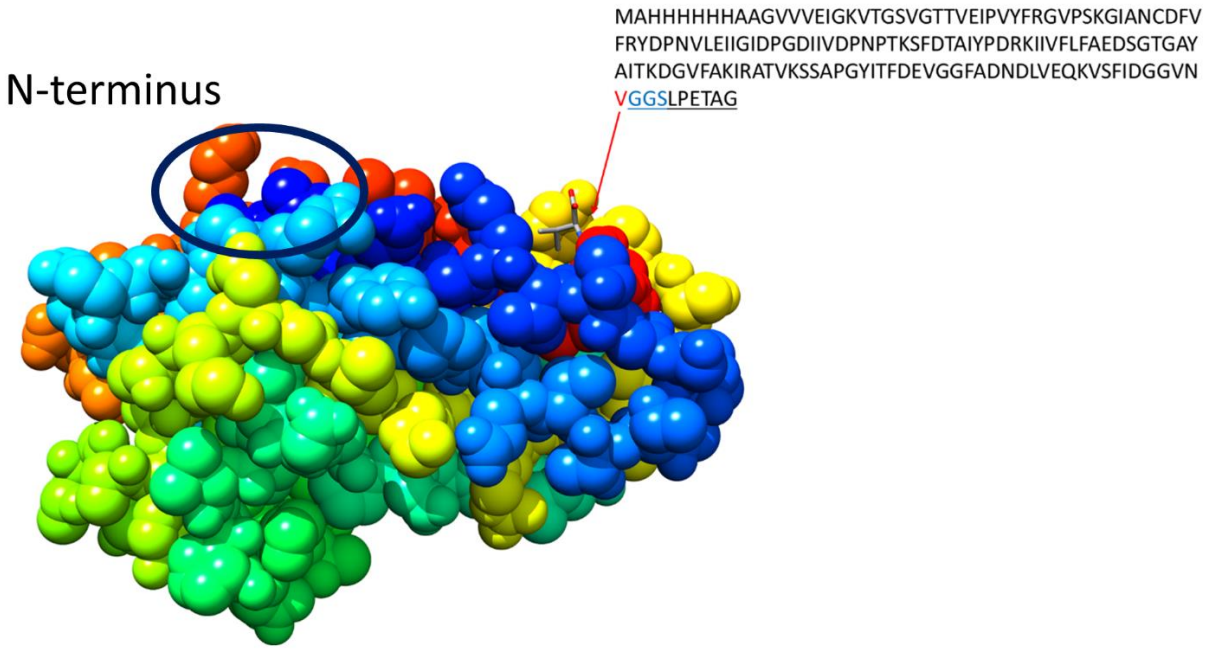

Figure 2.12: Structure of Coh2 with the C-terminal residue indicated. The sequence shown has the amino acids not included in the structure underlined. Additionally, Coh2-LPETAG has the following N-terminal residues that are not present in this structure: "AHHHHHHAAG". Structural data comes from PDB:1ANU (Shimon et al. 1997).

In addition to the planned Ala2Ser mutation to reduce cyclization, an additional mutation was made to the C-terminus in an effort to make the substrate more likely to react with p8-A2G4. Recall, the reactions with the test substrate, FITC-LPETGG, confirmed that the purified SpySrtA was active, and that p8-A2G4 was capable of reaction with it. As mentioned above, the approach of p8-A2G4 to liberate Coh2 from the covalent SpySrtA intermediate would be more hindered in comparison to its

approach to react with a FITC/SpySrtA covalent intermediate (**Figure 2.13**). Therefore, the ability of M13-A2G4 to be positioned to react with the acyl-enzyme intermediate might be further improved with an additional extension to its C-terminal linker. With this in mind, a GGGGS spacer was also added by mutagenesis between the protein and the C-terminal LPETAG motif.

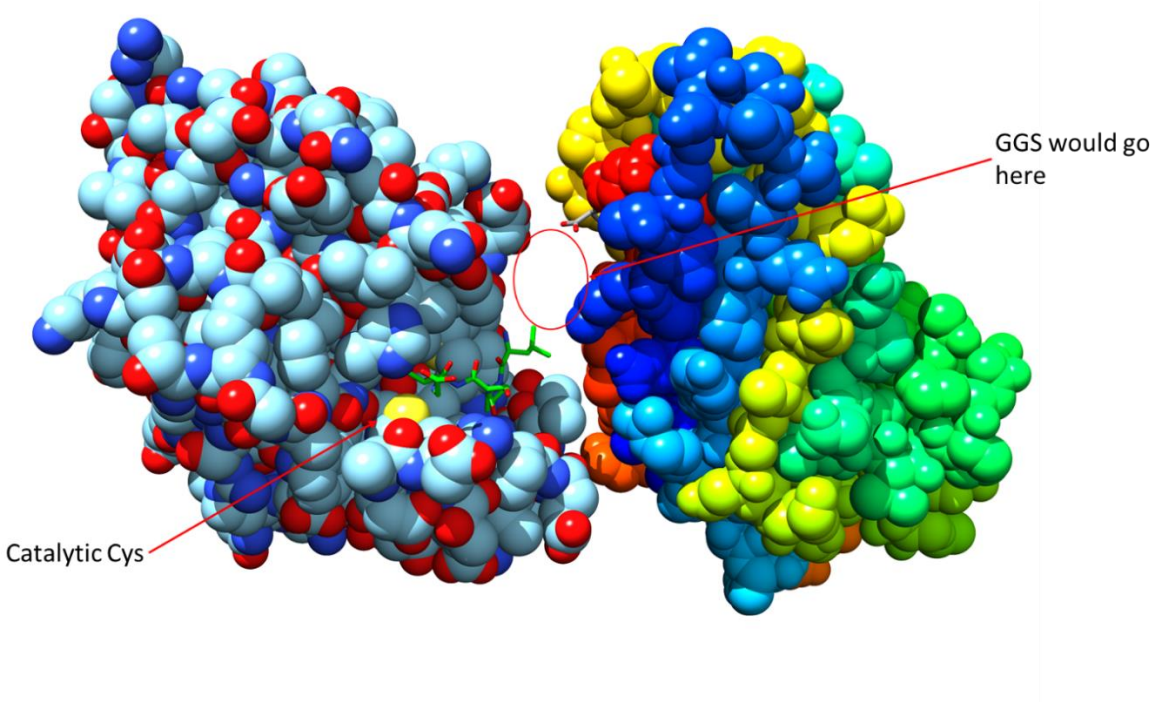

Figure 2.13: Steric considerations for reaction of Coh2-LPETAG to M13 using SpySrtA. Comparison of (right) experimental structure of Coh2 and (left) computational structure of SpySrtA with a LPSTG peptide docked into its active site (shown in green; from (Race et al. 2009)). The Coh2 structure is coloured such that it goes from blue to red for N- to C-terminus.

2.3.4.1 *Mutation of Coh2 N-terminus to reduce cyclization*

Ala2 was mutated to Ser in order to reduce the extent to which the protein could react with itself via SpySrtA. Furthermore, Coh2-LPETAG was further modified to have an extended GGGGS linker added to the C-terminus. Despite the modification to the N-terminus, the Coh2 construct was still quite capable of cyclization (**Figure 2.14A**). ESI-MS confirmed that the product could still cyclize. Formation of cyclized product was also apparent by SDS-PAGE analysis of SpySrtA and A2S-Coh2-GGGGS-LPETAG over time (**Figure 2.14B**). Approximately 15 % of the Coh2 was cyclized at 3 hours

when reacted at 37 ºC, according to densitometry. In one source, A2S mutations have been recommended suggested to prevent cyclization reaction from occurring (Guimaraes et al., 2013). From these results, it was apparent that this is not adequate to completely prevent the cyclization side reaction. A more drastic change in the second amino acid from the N-terminus should be considered instead. Val has been used to prevent this cyclization side reaction; the authors mutated the N-terminus such that the 2nd amino acid after Met would be Val and found that hydrolysis of acyl-enzyme intermediate could be detected, but not cyclization (Antos et al., 2009). However, with the modifications here, it was possible that cyclization was reduced and so it was briefly examined whether M13-A2G4 could react with a higher efficiency and be more easily detected.

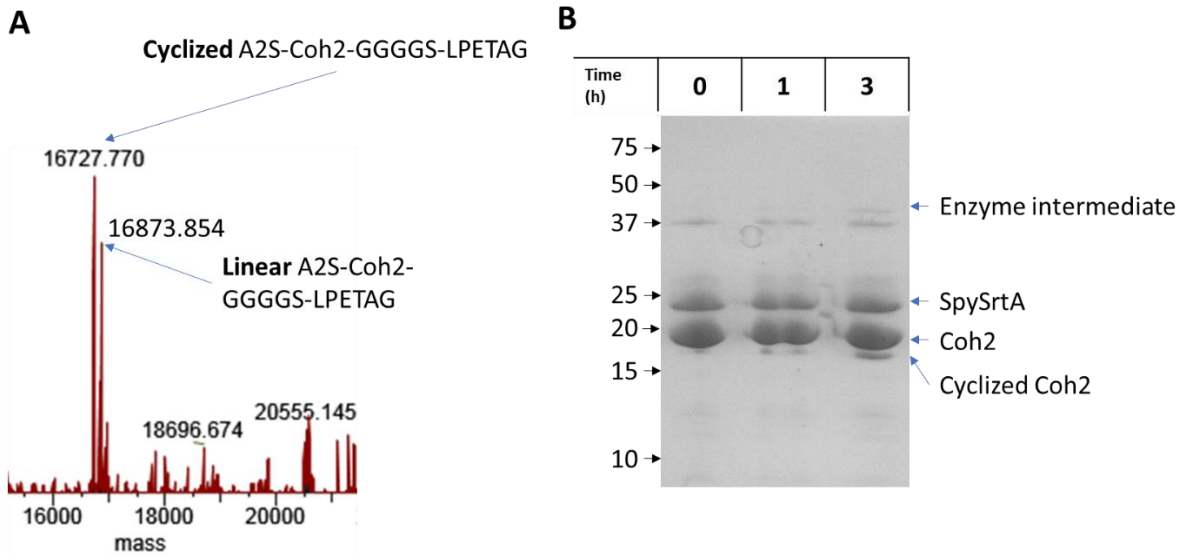

Figure 2.14: Reaction of 25 µM SpySrtA with 50 µM A2S-Coh2-GGGGS-LPETAG to check for cyclization. A) Deconvoluted ESI-MS of mixture at 3 h reaction time. B) SDS-PAGE gel of reaction mixture at indicated time points.

Again, without re-engineering the substrate to contain a specific tag for immunodetection, formation of an adduct could not be unambiguously identified. Indirectly, there was indication that the mutations were favorable in aiding the formation of p8-LPET-Coh2 product. A sortase reaction with the new substrate was set up and aliquots were removed during the course of the reaction to analyze possible products by SDS-PAGE (**Figure 2.15A**). If M13-A2G4 was included as a competing nucleophile, any reduction in the formation of the cyclized Coh2 band could be an indication of some

kind of competing reaction – such as p8-Coh2 adduct formation. When M13-A2G4 was present in the reaction, the formation of cyclized Coh2 was reduced by about 33% by densitometry.

The reactions were also analyzed by ESI-MS of the intact proteins. An aliquot was removed at 3 h and desalted for ESI-MS. It should be noted that intact protein analysis by ESI-MS was not an appropriate method for analysis of the products of this reaction with M13. When complete reactions were desalted and analyzed by ESI-MS, it became apparent that M13-A2G4 signal suppressed ionization of Coh2 and SrtA signals (**Figure 2.15B**). When comparing the signal of Coh2 and SpySrtA without M13-A2G4 present – the charge envelope in the raw spectrum was clearly visible. However, with M13-A2G4, only a signal corresponding to the major coat protein could be seen in the raw spectrum despite having the same concentration of Coh2 variant. No signal corresponding to a p8-Coh2 adduct could be detected.

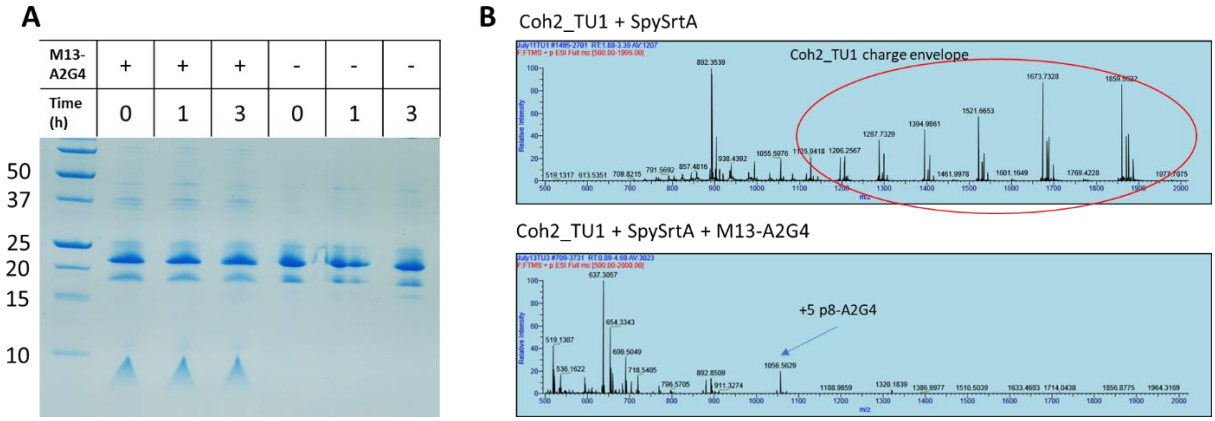

Figure 2.15: Testing reaction with of modified Coh2 variant with M13-A2G4 to compete with cyclization. Reaction conditions were 25 µM SpySrtA with 50 µM A2S-Coh2-GGGGS-LPETAG with 25 µM p8-A2G4 at 37 °C. A) SDS-PAGE gel of reaction with or without p8-A2G4. Raw ESI-MS of reaction B) without M13-A2G4 or C) with M13-A2G4. The m/z species that were relevant to either A2S-Coh2-GGGGS-LPETAG or p8-A2G4 are highlighted.

2.4 Conclusions

A desirable nanoscale multienzyme scaffold is one that is uniformly and highly concentrated with some binding or adhesive moiety on the surface to ensure uniform distribution and high loading of enzyme. It became apparent while working with this enzyme-mediated approach that it would likely be insufficient in meeting these goals. In particular, the efficient cyclization of Co2-LPETAG (with A2S

mutation as well), and the expected low yields of adduct based on literature values describing the same system, indicated that alternate methods should be pursued. Though the SrtA reaction has seen broad and effective applicability over the years (Dai, Böker, and Glebe 2019), it seems as though the approach of the SrtA enzyme to the phage surface might be too hindered to achieve the high and uniform degree of labelling desired for this particular nanoscale scaffold. Furthermore, as the reaction progresses one might expect the surface to become even more difficult for the enzyme-substrate intermediate to approach. In the following sections, a re-design of the nanoscale scaffold was instead pursued to reduce the potential steric limitations of enzymatic modification: M13 was instead modified densely with a small molecule via bioconjugate techniques that could bind a high affinity adaptor protein.

Chapter 3 Multi-enzyme assembly using streptavidin as an adaptor molecule mediated by His6-tag interactions

3.1 Introduction

In the previous chapter, an enzyme-mediated approach was used to prepare multi-enzyme complexes on M13. In exploring that approach however, it was determined that the resulting scaffold would be unlikely to be densely loaded with protein. This chapter will cover the approaches taken utilizing streptavidin (**SA**) as an adaptor molecule to bind multiple enzymes to the major coat protein (p8) of M13. The main interaction used in the approaches discussed in this chapter then, is the tight binding between SA and biotin (**Section 1.5**). In all cases, the approaches in this chapter utilize covalently biotinylated M13 which was then used to bind to SA (**Figure 3.1**). This was then further complexed with the cellulase, Cel8A from *C. thermocellum*, utilizing a non-covalent interaction between the His6-tag present on the enzyme and a biotin analogue attached to three of the four SA ligand-binding sites.

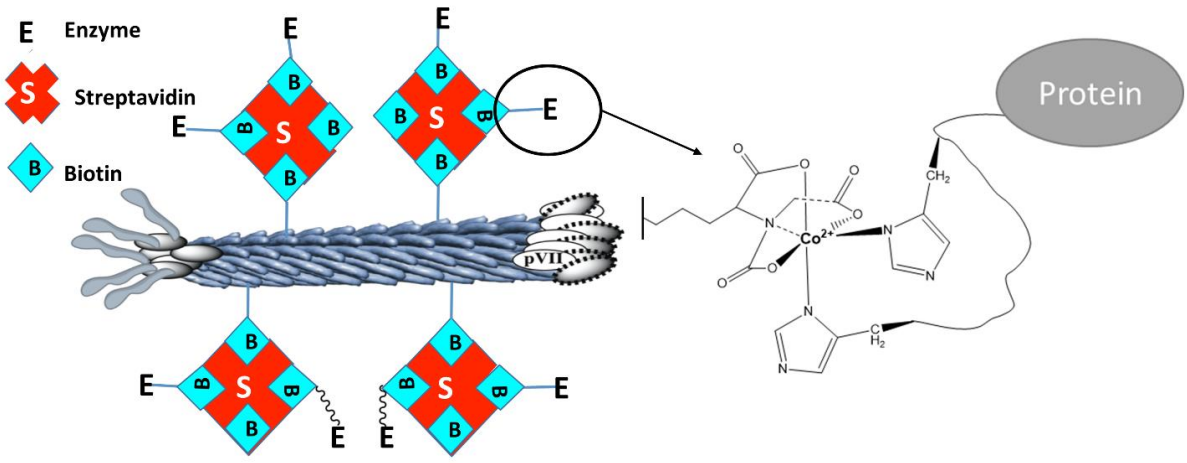

Figure 3.1: Schematic representation of multi-enzyme complex assembly using biotinylated enzyme and SA as an adaptor molecule.

M13 was covalently labelled with biotin which was used to bridge the p8 coat protein with the SA adaptor molecule. It has been demonstrated that acylation of primary amines of the major coat protein p8 (Ala1 and Lys8) with an activated ester is an efficient strategy. With *N*-hydroxysuccinimidyl

5(6)-carboxytetramethylrhodamine (**NHS-TAMRA**), as high as ~1600 *5(6)*-carboxytetramethylrhodamine (**TAMRA**) per M13 phage was obtained when reacted (K. Li et al. 2010). The authors found that both Lys8 and Ala1 were modified, though Ala1 was modified more readily. This approach was therefore deemed appropriate for preparing multiply and efficiently biotinylated M13. Thus, M13 was labelled by acylation of primary amines with an activated ester of biotin to serve as a connector between the intact bacteriophage and SA (**Figure 3.2**). This would serve as one of the main components used in building M13 complexes in this chapter and **Chapter 4**.

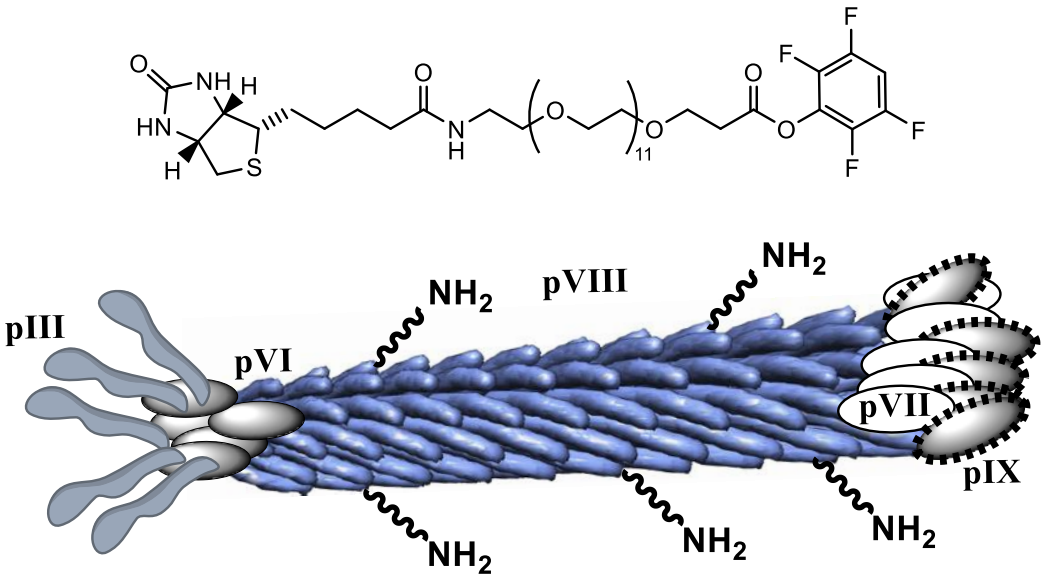

Figure 3.2: Structure of activated ester, TFP-PEG$_{12}$-biotin, used to biotinylated M13 at the primary amines of p8.

As alluded to, an affinity interaction between the His6-tag on Cel8A and a chelated metal was used to attach Cel8A to the SA adaptor. Loading Cel8A onto SA in this way was done to make this approach generally applicable to any His-tagged protein/enzyme of interest. Although this introduced an additional step in preparing this complex, the general applicability would make the resulting scaffold far more useful. In this design, SA was complexed to His6-tagged Cel8A via biotin-X-NTA (**BXN;** N_ε-(*N-(+)*-Biotinyl-6-aminohexanoyl)-N_α,N_α-bis(carboxymethyl)-*L*-lysine) bound to SA (**Figure 3.3**). The nitrilotriacetic acid (**NTA**) group is able to mediate binding to the His6-tagged protein via a chelated metal which results in a coordination complex between the protein of interest and the biotin

moiety on BXN. In this design, Co(II) is bound to the NTA and His6-tagged Cel8A; however, this can be further oxidized to Co(III) resulting in a kinetically stable complex (Wegner and Spatz 2013). In their work, Wegner and coworkers demonstrated that by oxidizing Co(II) to Co(III) after equilibration with a His-tagged protein, the off-rate of the resulting coordinated complex was decreased by many orders of magnitude down to 1.1 x 10^{-6} s^{-1}. As a reference point, this is the same order of magnitude as the off-rate of the SA/biotin interaction. The metal affinity interaction was therefore used here to form a stable arrangement of Cel8A onto the SA adaptor protein. Mentions in this chapter to complexes prepared via the "Co(III)-mediated approach" are in reference to this methodology, adapted for His6-tagged Cel8A.

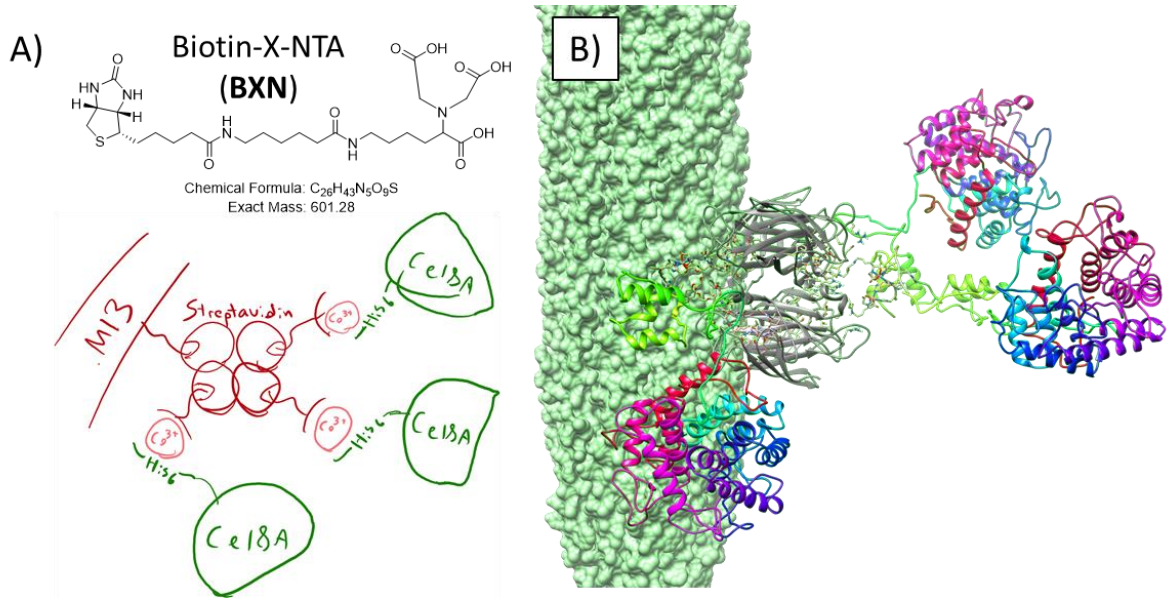

Figure 3.3: Schematic representation of M13/SA(BXN):Co(III):Cel8A complexes. A) Cartoon representation of M13/SA(BXN):Co(III):Cel8A complex showing intended stoichiometry. The interaction shown between SA and Cel8A is the molecule, biotin-X-NTA (BXN) shown above. B) Relative size of components with M13-PEG$_{12}$-biotin (green; PDB: 1IFJ, (D. A. Marvin et al. 1994)), SA (white; PDB: 3RY2, (Le Trong et al. 2011)), and three Cel8A (rainbow; PDB: 1CEM, (Alzari, ne Souchon, and Dominguez 1996)) attached via BXN coordinated to Co(III) and His6-tag of Cel8A (built using Maestro (Schrödinger)).

The sections in this chapter will be presented as outlined in the chapter overview. A commonality to the various approaches in this chapter (and the following chapter) is the utilization of the SA/biotin non-covalent interaction as the primary interaction holding the complex together. Therefore, the first topic that will be discussed are some experiments and considerations regarding the

binding of biotin to SA for the purpose of forming multi-protein complexes (**Figure 3.4**). These include the formation, stability and dynamic nature (at higher temperatures) of the biotin/SA bond. This is presented early on in the chapter such that some of the behaviors observed when preparing M13 complexes with a SA adaptor can be discussed within that context.

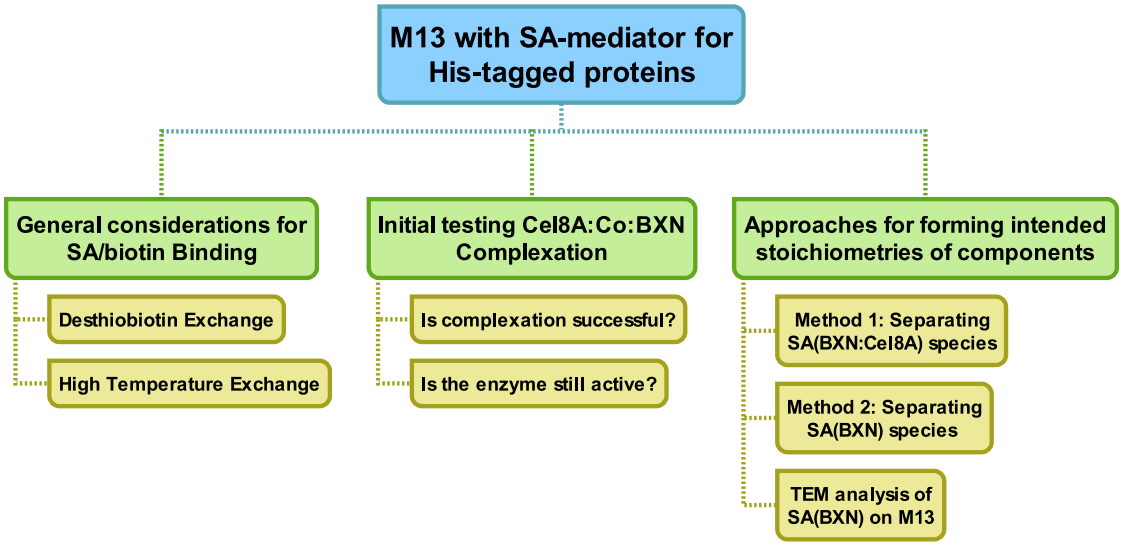

Figure 3.4: Organization of topics in Chapter 3.

Next, given the very defined arrangement of each component in the design, the main challenge was in devising a methodology that directed the self-assembly of each component toward the final structure depicted in **Figure 3.3**. Initially, the interaction between just Cel8A and BXN via the Co(III)-mediated interaction was tested to ensure it would function correctly and that Cel8A would still be active under the conditions used to oxidize Co(II) (**Figure 3.4**). After confirming that the Co(III)-mediated approach was suitable for Cel8A and BXN, further complexation to SA was explored – producing SA with a single open biotin-binding site remaining to allow binding to M13-biotin. However, given that SA has four biotin-binding sites, it was expected that a mixture of SA species with differing valencies (of unoccupied biotin-binding sites) would form.

There were two main strategies tested for preparing the M13/Cel8A complex with a single free biotin-binding site: 1) preparing a mixture of SA(BXN:Co(III):Cel8A)$_N$ complexes and separating species by size-exclusion chromatography (**SEC**), and 2) preparing SA(BXN)$_N$ and separating species by ion exchange chromatography (**IEC**) followed by complexation with Cel8A using the Co(III)-mediated approach (**Figure 3.5**). The former approach was not viable as individual SA(BXN:Co(III):Cel8A)$_N$ species could not be resolved; however, the latter approach was able to successfully isolate the SA(BXN)$_3$ species for further complexation with M13-biotin. Then in a final step, the complexation of Cel8A to this scaffold via the Co(III)-mediated approach was examined in a series of transmission electron microscopy (**TEM**) experiments. Though ultimately, there were some drawbacks to utilization of the Co(III)-mediated approach for docking Cel8A onto the scaffold, some of the methodologies involved in isolating a "monovalent" SA highlight successful strategies to ensure multi-valent adaptors (i.e.. SA) have the desired arrangement of components. Furthermore, the efficient docking of SA(BXN)$_3$ to M13 highlights the interesting interplay of how viral subunit symmetry and packing translates to how the resulting adaptor is spaced on this nanoscale scaffold.

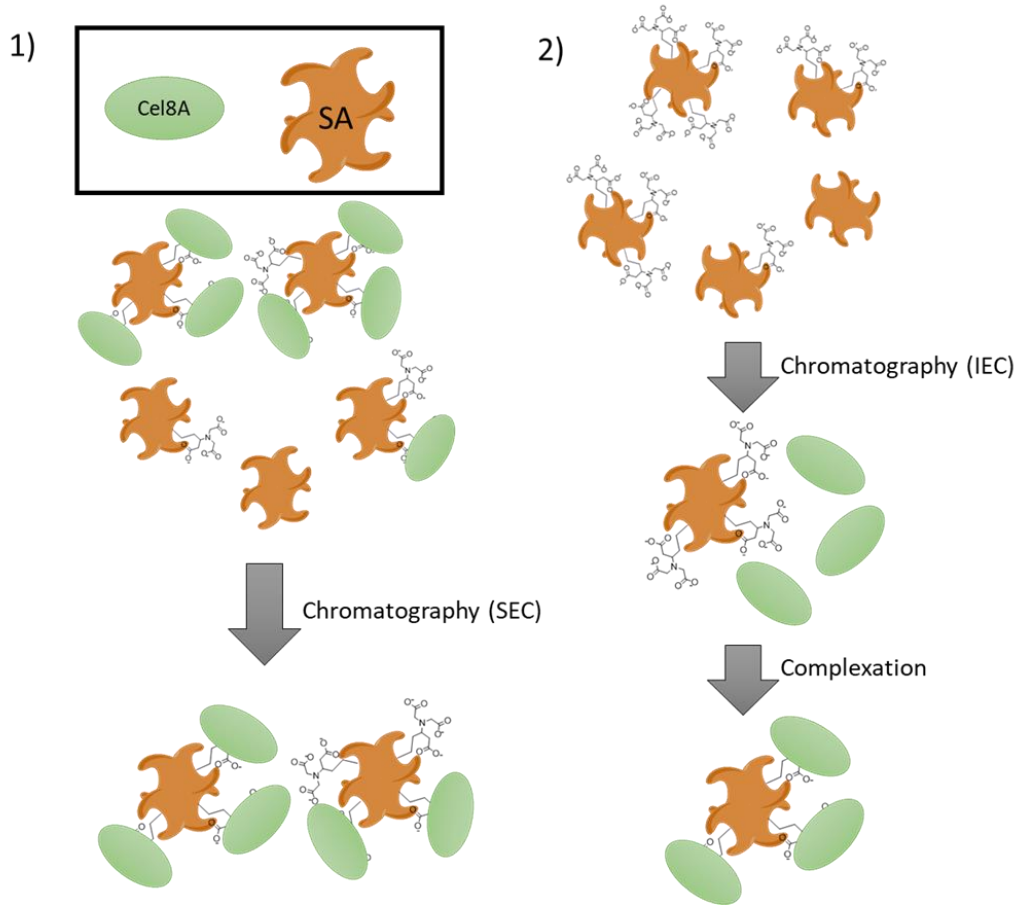

Figure 3.5: Overview of schemes for isolating SA(Cel8A-biotin) of the desired stoichiometry from the chelated metal affinity interaction between BXN and His6-Cel8A.

3.2 Methods

3.2.1 General

SA (>95% purity according to the supplier; Cedarlane, Burlington, Canada) was supplied as a lyophilized protein (from 10 mM potassium phosphate buffer pH 6.5) and was resuspended up to 5 mg/mL in ultra-pure (18 MΩ·cm resistivity) water (**MQH$_2$O**). The concentration of SA was determined by its estimated monomer extinction coefficient at 280 nm of 41940 M^{-1} cm^{-1} (ProtParam, ExPASy). Low viscosity carboxymethylcellulose (**CMC**) sodium salt (Millipore Sigma, Oakville, Canada) was prepared freshly as a 1% (w/v) solution in 0.1 M sodium citrate pH 5.8.

3.2.2 Phage amplification and protein expression

3.2.2.1 *M13 amplification*

M13KE was amplified by inoculating a 1:100 diluted overnight culture of *E. coli* K12 ER2738 (New England Biolabs, Whitby, Canada) in Luria Broth (**LB**) media (1% (w/v) peptone, 0.5% (w/v) yeast extract, 1% NaCl (w/v)) supplemented with 8 µg/mL tetracycline. M13KE was inoculated to a final titer of ~10^6 plaque-forming units (**PFU**) per mL and amplified for 4.5 – 5.5 h at 37 ºC with shaking for aeration. *E. coli* were pelleted by centrifugation at 12000 *g* for 10 min and 4 ºC.

M13 was concentrated by PEG precipitation with PEG/NaCl solution (20% PEG-8000, 2.5 M NaCl). The resulting supernatant was mixed with a 1/5 volume of PEG/NaCl solution and precipitated for 18 h at 4 ºC. The precipitated M13 was centrifuged at 12000 *g* for 15 min at 4 ºC. The pellet was resuspended in a solution of 1x phosphate-buffered saline (**PBS**; 10 mM Na_2HPO_4, 1.8 mM KH_2PO_4, 137 mM NaCl, 2.7 mM KCl) pH 7.4 that was 1/20 the volume of the initial culture volume. A 1/6 volume of PEG/NaCl solution was added for a second round of precipitation for 30 min on ice. The phage was pelleted by centrifugation at 15000 *g* for 10 min. The final pellet was resuspended in a volume of 1x PBS that was 1/100 the initial culture volume. If the solution was cloudy, it was centrifuged at 15000 *g* for 1 min to clear the supernatant. The resulting phage solutions were flash frozen in liquid nitrogen and stored at -80 ºC.

The M13 stocks were quantified by measuring the absorbance at 269 nm. This can be converted to a measure of M13 concentration in particles/mL using **Equation 3.1**. N_{bases} is the number of bases in the M13 ssDNA genome which is 7222 bp for M13KE. The 6 x 10^{16} coefficient can be derived from the literature extinction coefficient of 3.84 mg^{-1} cm^{-1} mL (Berkowitz and Day 1976).

$$[M13] = \frac{(A_{269} - A_{320}) \times 6 \times 10^{16}}{N_{bases}} \quad (3.1)$$

3.2.2.2 *Cel8A expression and purification*

The sequence of Cel8A from *C. thermocellum* was cloned in a pET28b(+) vector (GenScript, Piscataway, USA). The cellulase was cloned with a C-terminal His6-tag as has been done previously in the literature (Anbar et al. 2012). The protocol for expression and purification was adapted from the literature for this enzyme (Anbar et al. 2012). Briefly, the protein was overproduced from transformed BL21 *E. coli* which was grown to ~0.8 OD at 37 ºC in LB media with 50 µg/mL kanamycin. Protein expression was induced at 37 ºC with 1 mM IPTG for 3 h, at which point the cells were collected by centrifugation at 5000 *g* for 15 min at 4 ºC.

To 1 L worth of cell pellet, 30 mL of lysis buffer (25 mM Tris, 137 mM NaCl, 2.7 mM NaCl, 5 mM imidazole) supplemented with 0.5 mM phenylmethylsulfonyl fluoride (**PMSF**). The resuspended pellet was passed three times through a high-pressure homogenizer (>10,000 psi) to lyse the cells. The lysate was incubated at 60 ºC for 30 min and then centrifuged at 20,000 *g* for 30 min at 4 ºC. The protein was purified by immobilized metal affinity chromatography (**IMAC**). The cleared lysate was loaded onto a 1 mL HisTrap™ (GE Healthcare, Chicago, USA), washed with 5 mL of wash buffer (25 mM Tris, 137 mM NaCl, 2.7 mM NaCl, 10 mM imidazole), and eluted over a 5 mL gradient from 5 to 250 mM imidazole. The sample was dialyzed against 50 mM sodium acetate pH 6 using a 12400 Da MWCO dialysis membrane (Millipore Sigma, Oakville, Canada). The purified protein was flash frozen in liquid nitrogen and stored at -80 ºC. Cel8A was quantified by measuring its absorbance at 280 nm and using its theoretical extinction coefficient of 104420 M^{-1} cm^{-1} calculated by ProtParam (Gasteiger et al. 2005).

3.2.3 Bioconjugation methods

3.2.3.1 *Reaction of M13 with TFP-PEG$_{12}$-biotin*

Tetrafluorophenyl-PEG_{12}-biotin (**TFP-PEG_{12}-biotin**) was first prepared as a 10 mM stock in anhydrous dimethyl formamide (**DMF**). The final reaction concentrations were 100 µM p8, 1 mM TFP-PEG_{12}-biotin in 1x PBS pH 7.46 with 20% DMF. Reactions were carried out over 18 h at 4 ºC. These were then dialyzed 6 times against 2 L of 1x PBS pH 7.46 in 12.4 kDa MWCO regenerated cellulose dialysis tubing (Millipore Sigma, Oakville, Canada). M13-PEG_{12}-biotin were flash frozen with liquid nitrogen and stored at -80 ºC. The concentration of M13-PEG_{12}-biotin was determined according to its A_{269} absorbance as described in **Section 3.2.2.1**.

3.2.3.2 *Reaction of Cel8A with TFP-PEG_{12}-biotin*

Cel8A was diluted to 160.8 µM in 100 mM sodium phosphate buffer pH 7.46. To this solution, 800 µM TFP-PEG_{12}-biotin was added to initiate the reaction. The total amount of DMF present in the reaction was 10% (v/v). The reaction was carried out for 18 h at 4 ºC. After reaction, the labeled Cel8A samples were dialyzed for a total of three 2 L dialysis exchanges (6 h minimum, 23 ºC) in 12400 kDa MWCO dialysis tubing (Millipore Sigma, Oakville, Canada) against 1x PBS pH 7.4. Labelled protein was flash frozen with liquid nitrogen and stored at -80 ºC. The protein was quantified as described in **Section 3.2.2.2**.

3.2.3.3 *Reaction of Cel8A with NHS-TAMRA*

Cel8A was diluted to 80.4 µM in 100 mM sodium phosphate buffer pH 7.9. To this solution, 400 µM NHS-TAMRA in DMSO was added to initiate the reaction. The total amount of DMSO present in the final reaction mixture was 10 % (v/v). The reaction was carried out for 3 h at 23 ºC. After reaction, the labeled Cel8A samples were dialyzed for a total of three 2 L dialysis exchanges (6 h minimum, 23 ºC) in 12400 kDa MWCO dialysis tubing (Millipore Sigma, Oakville, Canada) against 1x PBS pH 7.9. Labelled protein was flash frozen with liquid nitrogen and stored at -80 ºC. The quantity of Cel8A-TAMRA recovered was calculated using the theoretical extinction coefficient of 104420 M^{-1} cm^{-1} with an additional correction factor (**CF**) of 0.3 to account for the absorbance of the dye at 280 nm.

The extinction coefficient of the dye used was 65000 M^{-1} cm^{-1} (Meadows, Shafer, and Schultz 1991). The correction factor was calculated from the ratio of (280/517) nm absorbances for the free dye.

3.2.4 Characterization of SA/biotin binding

3.2.4.1 *Desthiobiotin exchange*

Desthiobiotin (**dtb**) stock was prepared as a 40 mg/mL dimethyl sulfoxide (**DMSO**) stock. This was further diluted to a working concentration of 1 mM in water. SA at a tetramer (**SA_{tet}**) concentration of 10 µM was mixed with 40 µM desthiobiotin in 1x phosphate-buffered saline (**PBS**: 10 mM Na_2HPO_4, 1.8 mM KH_2PO_4, 137 mM NaCl, 2.7 mM KCl) pH 7.4. This was further diluted to a working stock concentration of 2.5 µM SA_{tet}. In preparing each displacement experiment, SA/desthiobiotin was first added to 1x PBS pH 7.4 buffer in a quartz fluorescence cuvette to final concentrations indicated in the relevant figures. Biotin-4-fluorescein (**B4F**; **Figure 3.6**) was then added to a final concentration ranging from 25 to 300 nM and the exchange was monitored using 490 nm excitation, 525 nm emission with a 515 nm cut-off filter at 23 °C. Controls without SA present were similarly prepared and monitored for a shorter time (~2 min) to determine fluorescence of B4F at t = 0 h. Fluorescence data was collected on a SpectraMax® M5 (Molecular Devices, San Jose, USA) with the photomultiplier tube sensitivity set to high.

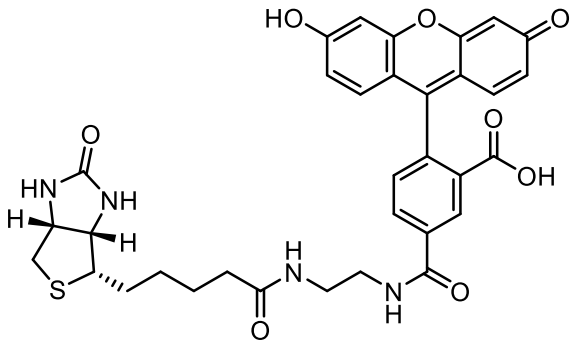

*Figure 3.6: Structure of biotin-4-fluorescein (**B4F**).*

Conversion of fluorescent data in relative fluorescence units (**RFU**) to molar amounts of B4F was done by creating a standard curve of fluorescence over a range of 0 – 544 nM B4F. A standard

curve was prepared for each experiment using the same prepared buffers. Concentrations of B4F stocks were determined in 1x PBS pH 7.4 by measuring the absorbance at 494 nm and literature extinction coefficient of 68000 M^{-1} cm^{-1} (Ebner et al. 2008).

The kinetic exchange was described using a model that considered the following two equilibria (**Figure 3.7**).

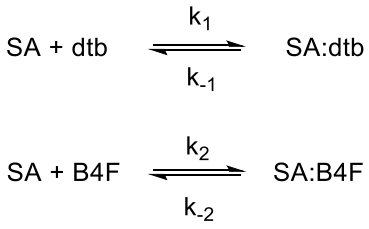

*Figure 3.7: Competing equilibria used to model desthiobiotin (**dtb**)/B4F exchange process.*

This model is simplified, in that the four biotin-binding sites per SA tetramer are treated as equal. This follows from literature evidence which shows all four sites are equivalent and that there is no cooperative binding (Deng, Kitova, and Klassen 2013). The equilibria were therefore described by the following system of ordinary differential equations (**Equations 3.2 – 3.6**) that were solved by numerical methods using DynaFit4 to perform the analysis (Kuzmič 2009).

$$\frac{d[SA{:}dtb]}{dt} = k_1[SA][dtb] - k_{-1}[SA{:}dtb] \quad (3.2)$$

$$\frac{d[SA]}{dt} = k_{-1}[SA{:}dtb] - k_1[SA][dtb] - k_2[SA][B4F] + k_{-2}[SA{:}B4F] \quad (3.3)$$

$$\frac{d[B4F]}{dt} = k_{-2}[SA{:}B4F] - k_2[SA][B4F] \quad (3.4)$$

$$\frac{d[dtb]}{dt} = k_{-1}[SA{:}dtb] - k_1[SA][dtb] \quad (3.5)$$

$$\frac{d[SA{:}B4F]}{dt} = k_2[SA][B4F] - k_{-2}[SA{:}B4F] \quad (3.6)$$

3.2.4.2 *B4F/BXN thermal exchange*

This experiment was to test dynamic binding and rebinding of biotin to SA by competitive binding between pre-bound biotin analogue, BXN, with fluorescent analogue, B4F. First, 10 µM SA_{tet}

was mixed with 40 µM BXN in 1x PBS pH 7.4 to form 10 µM $SA(BXN)_4$. This was further diluted down to 100 nM $SA(BXN)_4$ in 1x PBS pH 7.4. B4F was added to a final concentration of 400 nM to initiate the exchange in separate tubes (obscured from light) which were incubated at either 23 ^oC or 50 ^oC in a temperature-controlled water bath. The fluorescence was read in 96-well opaque (black) plates at 490 nm excitation, 525 nm emission (515 nm cutoff) at 0, and 18 h incubation time at each temperature.

3.2.5 Cobalt-mediated approach to prepare multi-enzyme complexes

3.2.5.1 *Co(II):NTA complexes with Cel8A*

This protocol was adapted for complexation of Cel8A and NTA with Co(II) followed by oxidation to Co(III) (Wegner and Spatz 2013). $CoCl_2$ and biotin-X-NTA were mixed at a 1:1 ratio at 2.5 mM in MQH_2O. Cel8A at a final concentration of 20 µM and BXN:Co(II) at 100 µM were incubated together in 1x PBS pH 7.4 for 2.5 h to equilibrate. A working stock solution of 500 mM H_2O_2 was prepared fresh from a 30% (9.8 M) stock solution and added to a final concentration of 10 mM to the Cel8A:Co(II):BXN solution above. A control without H_2O_2 was also prepared.

To assess complexation, the resulting solutions were separated by IMAC. Samples were loaded onto a 1 mL HisTrap™ column in wash buffer (25 mM Tris, 137 mM NaCl, 2.7 mM KCl, 10 mM imidazole pH 7.4). The samples were eluted with a 10 – 100 mM imidazole gradient over 10 mL at 0.5 mL/min. Afterward, the individual fractions of Cel8A which were recovered were assayed using the Bradford assay with purified Cel8A for the standard curve using Bradford 1x dye reagent (Bio-Rad, Hercules, USA) according to the manufacturer.

Collected fractions from IMAC were assayed for endocellulase activity against model cellulose substrate, CMC. A CMC stock solution was first prepared at 1 % (w/v) in 0.1 M sodium citrate pH 5.8. These solutions were stored no longer than a week at 4 ^oC. Hydrolysis of CMC was monitored by end-point analysis with a dinitrosalicylic acid reagent (**DNS**; Millipore Sigma, Oakville, Canada) to detect

the reducing ends present in solution. The DNS reagent was prepared in the proportions described (Aiba, Kitai, and Imanaka 1983). First, 25 mL of a 60% w/v solution of sodium potassium tartrate (gently heated to dissolve). Separately, 0.5 g DNS solution was prepared in 15 mL water. The tartrate solution was added slowly to this solution (a yellow precipitate forms). Upon adding 10 mL 2 M NaOH, the precipitate will dissolve, and the resulting orange solution is brought up to 50 mL with water and stored at 23 ºC. To assay for reducing ends, an equal volume of this solution was added to CMC reactions at the end points of the reaction. The solutions were boiled 5 min to develop the colour, and absorbance was read at 540 nm. These were compared to a standard curve of *D*-glucose to determine the reducing ends present in the solution.

3.2.5.2 *Separating SA(NTA):Co(III):Cel8A complexes by SEC*

SA was bound with BXN followed by Cel8A via the Co(III)-mediated interaction to prepare complexes of SA and Cel8A. $CoCl_2$ and biotin-X-NTA (**BXN**) were mixed at a 1:1 ratio at 2.5 mM in MQH_2O. BXN:Co(II) at 20 µM was bound to SA_{tet} at 20 µM in 1x PBS pH 7.4. Cel8A at a final concentration of 80 µM and $SA(BXN:Co(II))_4$ at 20 µM were incubated together in 1x PBS pH 7.4 to equilibrate. A working stock solution of H_2O_2 of 500 mM was prepared from a 30% (9.8 M) stock solution and added to a final concentration of 10 mM to the $SA(BXN:Co(II))_4$/Cel8A solution above. A control with 4 µM SA_{tet} and 12 µM Cel8A-biotin (prepared as described in **Section 3.2.3.2**) was assembled in 1x PBS pH 7.4. The samples were separated on either a Sephacryl® S-300 or Superdex® 75 SEC column. Fractions were collected from SEC and assayed for endocellulase activity as described in **Section 3.2.5.1**.

3.2.5.3 *Separating $SA(BXN)_N$ by IEC*

SA_{tet} at 20 µM was mixed with 0 – 80 µM BXN in 20 mM Tris pH 8.0. The samples prepared this way were loaded onto a MonoQ® anion exchange column with 20 mM Tris pH 8.0 running buffer. An elution gradient of 0 – 200 mM NaCl was applied to elute $SA(BXN)_N$ species. Collected fractions

were concentrated using 10 kDa MWCO spin concentrators (Millipore Sigma, Oakville, Canada) and the concentration of SA estimated using its theoretical monomer extinction coefficient of 41940 M^{-1} cm^{-1} calculated by ProtParam (Gasteiger et al. 2005). The number of biotin-binding sites per tetramer was determined by B4F titration as described below in **Section 3.2.6.1**.

3.2.6 Analysis methods

3.2.6.1 *B4F forward titration*

B4F titrations were carried out for two main purposes: to determine the number of biotin-binding sites present in a solution of SA, and to determine the extent of biotinylation of labelled biomolecules. First, determining the number of biotin-binding sites in solution was carried out according to the "forward titration" technique for determining the biotin-binding sites present in a solution of strept(avidin) (Ebner et al. 2008). B4F was diluted 250-fold from a 4 mM DMSO stock into 1x PBS pH 7.4 and standardized using its extinction coefficient of 68000 M^{-1} cm^{-1} at 495 nm (Ebner et al. 2008). B4F was protected from light as much as possible, as exposure to light has been observed to oxidize the biotin moiety of B4F (Haack et al. 2017). For titration, B4F was titrated into a quartz cuvette containing sample diluted down to approximately 100 to 400 nM biotin-binding sites. The fluorescence of this mixture was measured at 490 nm excitation and 525 nm emission with a 515 nm cut-off filter after each addition of B4F. B4F was added until a breakpoint (intersection of two lines fit to the data) was clearly observed.

The breakpoint represents the point in the titration at which all available biotin-binding sites have been titrated (Ebner et al. 2008). The location of the breakpoint was determined by linear regression using R with the "segmented" library (Muggeo 2003; Vm 2008). An example of a B4F titration and subsequent regression in R is shown (**Figure 3.8**).

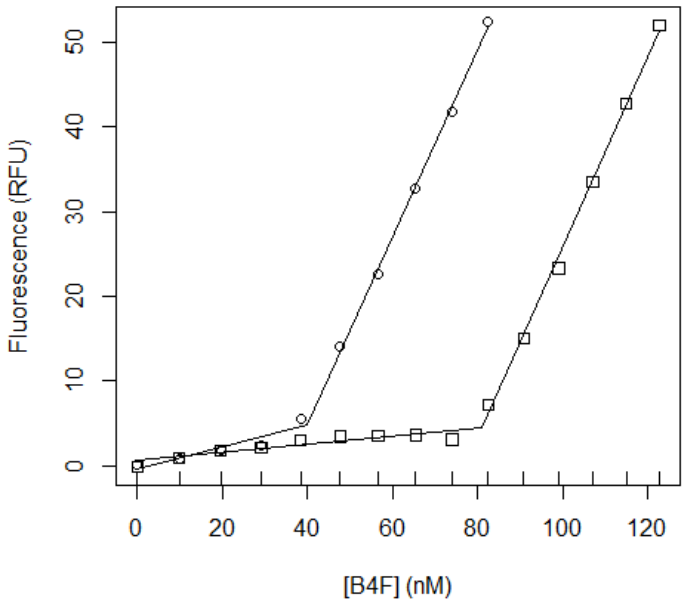

Figure 3.8: Example B4F titration and linear regression using "segmented" module in R. Titrations are carried out with SA only (open squares) and with SA mixed with biotinylated sample (open circles). The difference between the location of the breakpoints gives the amount of biotin present in the sample. Produced in R (v.3.5.1).

B4F titrations were also carried out to estimate the extent of biotinylation of biomolecules. The procedure used here was adapted from a "forward titration" technique for estimating the amount of (strept)avidin in unknown samples, with some modifications (Ebner et al. 2008). In particular, rather than determining the concentration of an unknown sample of SA, this titration was used to determine the total number of biotin present by measuring the total number of biotin-binding sites in a known solution of SA before and after adding biotinylated sample. The estimated amount of biotin present in the sample is determined by the straightforward relation:

$$[biotin\ in\ sample] = breakpoint_{control} - breakpoint_{sample}$$

For the titration, M13-PEG_{12}-biotin samples were first mixed with SA at a concentration of 2.5 µM SA_{tet} and 5 µM p8 (or 2.5 µM for Cel8A-PEG_{12}-biotin) in 1x PBS pH 7.4. The complexed protein was further diluted into 1x PBS pH 7.4 to a SA_{tet} concentration of 25 nM at a final volume of 500 µL in a quartz cuvette. The fluorescence of this mixture was measured at 490 nm excitation and 525 nm emission with a 515 nm cut-off filter after each 5 µL addition of 1 µM B4F. B4F was added until a

breakpoint was clearly observed. A control titration with just SA to determine the number of open biotin-binding sites in the absence of biotinylated protein was also carried out as described above. Along with the total concentration of p8 in the titration, the extent of biotinylation can be estimated.

3.2.6.2 *TEM staining conditions (regular staining with PTA)*

Phosphotungstic acid (**PTA**) stain was prepared fresh before each experiment by diluting PTA in water to 1% (w/v) and then adding 1.12 mL 2 M NaOH per 1 g of PTA that was weighed out to neutralize the stain (Phillips 1950).

M13 phage containing samples were typically adhered to transmission electron microscopy (**TEM**) grids at a concentration of 1.5 – 4.5 x 10^{11} M13 particles/mL in sterile MQH_2O (M13 typically exchanged into MQH_2O from 1x PBS buffer by dilution of ~100-fold). Grids used were carbon/formvar 400 mesh (Ted Pella, etc.) or ultrathin carbon film supported by lacey carbon 400 mesh (Ted Pella, etc.) where indicated. Grids were prepared by placing grids onto prepared drops of sample/wash solution. A typical grid preparation is as follows: a 10 µL drop of M13 was adhered to the grid for 1 min, followed by two brief washes (a few seconds) on 50 µL drops of sterile MQH_2O, and lastly, staining for 20 sec on a 20 µL drop of 1% PTA. Excess solution was wicked away with filter paper after each step. Grids were dried overnight. TEM samples were imaged at 60 kV using a CM10 Philips microscope modified with an Advanced Microscopy Techniques image capturing CCD camera.

3.2.6.3 *TEM staining conditions (TEM immunostaining procedure)*

This staining procedure was carried out to specifically bind 5 nm gold nanoparticles (**GNP**) to the TAMRA reacted to Cel8A (**Section 3.2.3.3**). The primary antibody was an anti-TAMRA monoclonal mouse IgG antibody (Abcam, Toronto, Canada). The stock solution was at 1 mg/mL. The secondary antibody was goat anti-mouse IgG 5 nm GNP conjugate (Cytodiagnostics, Burlington, Canada). The stock solution was at 3 OD (~1.64 x 10^{14} particles/mL according to the manufacturer).

The protocol for immunogold staining was adapted from literature methods with some changes (X. Li et al. 2016). The TEM grids used were carbon/formvar 400 mesh. In order to adhere phage samples to the grid, M13 was diluted down to 1.5 – 4.5 x 10^{11} M13 particles/mL in sterile MQH_2O, and a 10 µL droplet to each grid and let sit for 1 min before removing the excess with filter paper. The grid was touched to 50 µL water droplets (~2 sec) to wash and the excess was removed with filter paper. The grid was blocked by incubation of the grid with 50 µL droplet of blocking buffer (0.1 % BSA in 1x TBS pH 7.4) for 10 min to prevent non-specific binding of antibodies. The excess solution was removed with filter paper. The grid was incubated on 50 µL droplet containing primary antibody (diluted 1:20 into blocking buffer) for 60 min. This was washed 5 x 3 min on 50 µL droplets of blocking buffer. The grid was incubated on 50 µL droplet containing the secondary antibody GNP conjugate (diluted 1:30 into blocking buffer) for 60 min. This was washed 3 x 3 min on 50 µL droplets of blocking buffer, followed by 3 x 3 min on 50 µL droplets of 1x TBS pH 7.4, and lastly, with 4 x 30 s on 50 µL droplets of sterile MQH_2O. The excess solution was removed with filter paper. Lastly, the grids were stained on 20 µL droplets of 1% (w/v) PTA for 1 min and then the excess stain was removed with filter paper.

3.3 Results and discussion

3.3.1 General considerations for SA/biotin complexation

As mentioned, some general considerations for SA/biotin complexation will be discussed in this chapter. The results in this section are applicable to both this chapter, and **Chapter 4**, where the SA/biotin interaction is again employed. The purpose of presenting this here is to provide some context on the distribution of $SA(biotin)_N$ species (SA with biotin bound at N ligand-binding sites) that form when mixing SA and BXN (or biotin-Cel8A; particularly in Chapter 4). Binding of biotin to SA, due to its slow off-rate, results in a distribution of occupied biotin-binding sites that is not statistical in nature (Jones and Kurzban 1995). Initially it was thought that binding of biotin to SA was cooperative since

the resulting mixture of SA(biotin)$_N$ species appeared biased toward the SA(biotin)$_0$ and SA(biotin)$_4$ species (Sano and Cantor 1990b). In fact, there have been several papers disagreeing on whether the nature of biotin-binding to SA was cooperative or not. However, several experiments have since shown that binding to SA is not cooperative, and the non-statistical distribution of species is due to the slow off-rate and limits of mixing quickly enough (Deng, Kitova, and Klassen 2013; Jones and Kurzban 1995). Regardless, this context highlights one of the subtleties involved in working with biotin and SA – that is, it is very difficult to mix biotin with SA without biasing the distribution of biotin-bound species toward either the fully bound, or fully unbound SA(biotin) species.

3.3.1.1 *Desthiobiotin Exchange Kinetics*

To overcome a non-statistical mixture of species resulting from mixing biotin (or biotinylated enzyme), desthiobiotin has been used here to slow the binding of biotin (requiring that desthiobiotin first dissociate from SA) and therefore, make the distribution closer to what one would statistically expect. For binding of biotin to SA with four equivalent sites, the resulting mixture of SA(biotin)$_N$ should have a binomial distribution. However, because of the slow off-rate of SA this is typically not the case (Jones and Kurzban 1995). Furthermore, by reducing the need for rapid mixing, the resulting mixture of species should be more predictable between experiments. In order to test the feasibility of this approach with biotinylated enzyme, a model system using desthiobiotin-saturated SA and a fluorescent biotin was used to monitor this exchange process over time. In this section, some of the details of the exchange of desthiobiotin with biotin will be discussed.

The goals of these experiments were to: 1) determine the time-frame that exchange of desthiobiotin for biotin would expected to occur over, and 2) show that desthiobiotin can indeed be used to form a more statistically predictable distribution of SA(biotin)$_N$ species. In order to probe this ligand exchange process, the fluorescent biotin analogue biotin-4-fluorescein (**B4F**) was used as the biotin-containing probe for these experiments. The fluorescence of the attached fluorescein is quenched

upon binding to SA (Kada, Falk, and Gruber 1999). Therefore, upon adding B4F to desthiobiotin-saturated SA, the initial fluorescence of free B4F should decrease over time as it binds to SA.

Pre-incubation of SA with desthiobiotin slows the binding of B4F. Binding of 300 nM B4F to 100 nM SA_{tet} either without or with pre-bound desthiobiotin at 400 nM was carried out at 23 ^{o}C. SA_{tet} binds B4F more quickly when not already bound to desthiobiotin, as expected (**Figure 3.9A**). The binding was reduced when SA was pre-saturated with desthiobiotin, as expected. Importantly, even with desthiobiotin present, B4F does eventually displace the desthiobiotin completely. Binding was 90% complete at 50 s for SA only and 480 s for SA pre-bound with desthiobiotin. As a side note, the binding of B4F to SA on its own was slower than expected in theory. For a protein/ligand pair with an on-rate on the order of 10^8 M^{-1} s^{-1} (Deng, Kitova, and Klassen 2013), complete binding is expected to be reached in under 1 second (**Figure 3.9B**). There was likely a limit in how rapidly the solution could be mixed manually that reflects this discrepancy. Regardless, this served as an initial indication that pre-binding with desthiobiotin could indeed slow biotin-binding.

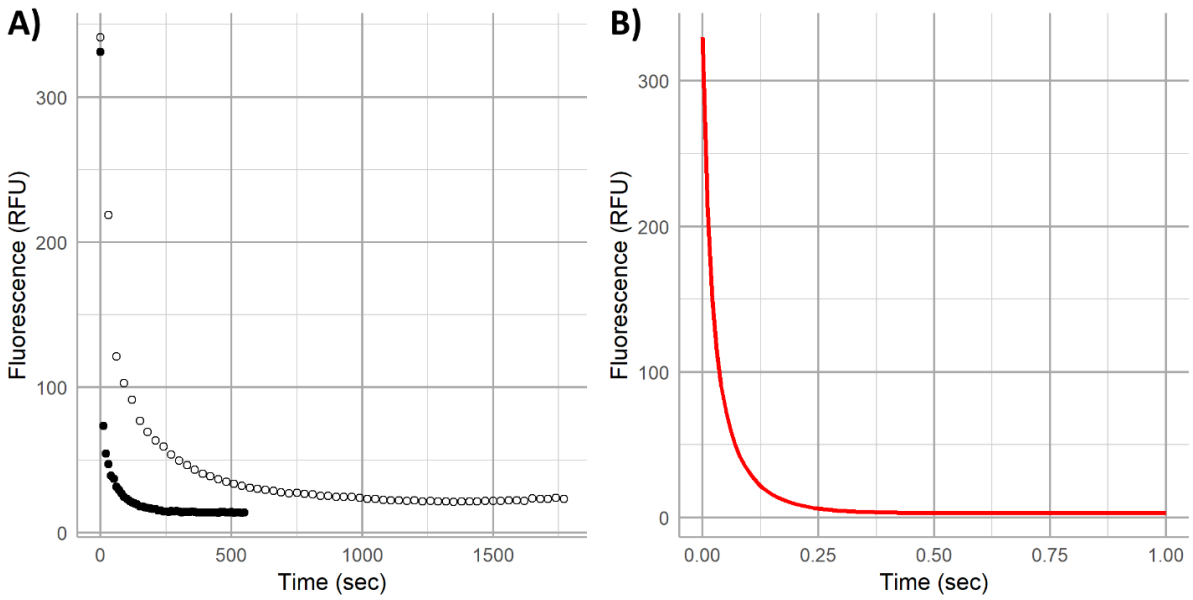

Figure 3.9: Relative time to reach equilibrium for SA mixed with B4F using desthiobiotin pre-incubation. A) 100 nM SA_{tet} mixed with 300 nM B4F either (black circles) SA without pre-bound desthiobiotin, or (open circles) with 400 nM pre-bound desthiobiotin (average of three trials). B) Simulated data for binding of 300 nM B4F to 100 nM SA_{tet} using an association rate constant of 130 x 10^6 M^{-1} s^{-1} (Deng, Kitova, and Klassen 2013) and dissociation rate constant of 5.5 x 10^{-6} s^{-1} (Deng, Kitova, and Klassen 2013) and simple protein-ligand binding model (described by equilibrium 2 in Section 3.2.4.1).

To get a better sense of the amount of time that should be given to allow a biotin analogue or biotinylated-protein to displace desthiobiotin (**dtb**) from $SA(dtb)_4$, several B4F/desthiobiotin exchange experiments were carried out at different concentrations of B4F. The purpose here was to qualitatively capture the time frame of incubation required for this exchange process to occur, not to extensively characterize the kinetics of the process; however, some kinetic considerations were included to determine if the results produced were reasonable within the wealth of kinetic data available for biotin/SA kinetics. The exchange rate was quite fast and the very first seconds of the exchange were missed during mixing and placing the cuvette in the fluorimeter (**Figure 3.10A - C**). At the higher concentrations of B4F, it took longer for complete binding of B4F, while the lower concentrations tested were rapidly bound over the course of a few minutes.

In order to better understand the process of desthiobiotin exchange, the data was fit to a model considering the dissociation of desthiobiotin from SA:dtb and binding of B4F to SA (as described in the Methods **Section 3.2.4.1.**). Only the 100 nM B4F trace was able to capture enough of the initial portion of the exchange process to fit the desthiobiotin binding and dissociation parameters (**Figure 3.10A**). Using the parameters for the on-rate and off-rate of desthiobiotin estimated from this fit, some simulated data sets were run to get an idea of the trend expected for differing B4F concentrations **Figure 3.10D**). The decreased time it took to completely bind the biotin probe in the simulated data followed a similar trend to that observed in Figure 3.10 traces A – C, where decreasing initial [B4F] resulted in the system more rapidly reaching equilibrium. This makes sense if one considers that as more B4F binds to SA (forming SA(B4F) which dissociates from SA very slowly), the concentration of SA(dtb) with which to exchange with decreases; this is more apparent when the [B4F] is stoichiometric to the number of biotin-binding sites. This would be expected to be less impactful where the initial [B4F] << [SA(dtb)], as even when the majority of B4F has bound, there would still be considerable SA(dtb) left to exchange with.

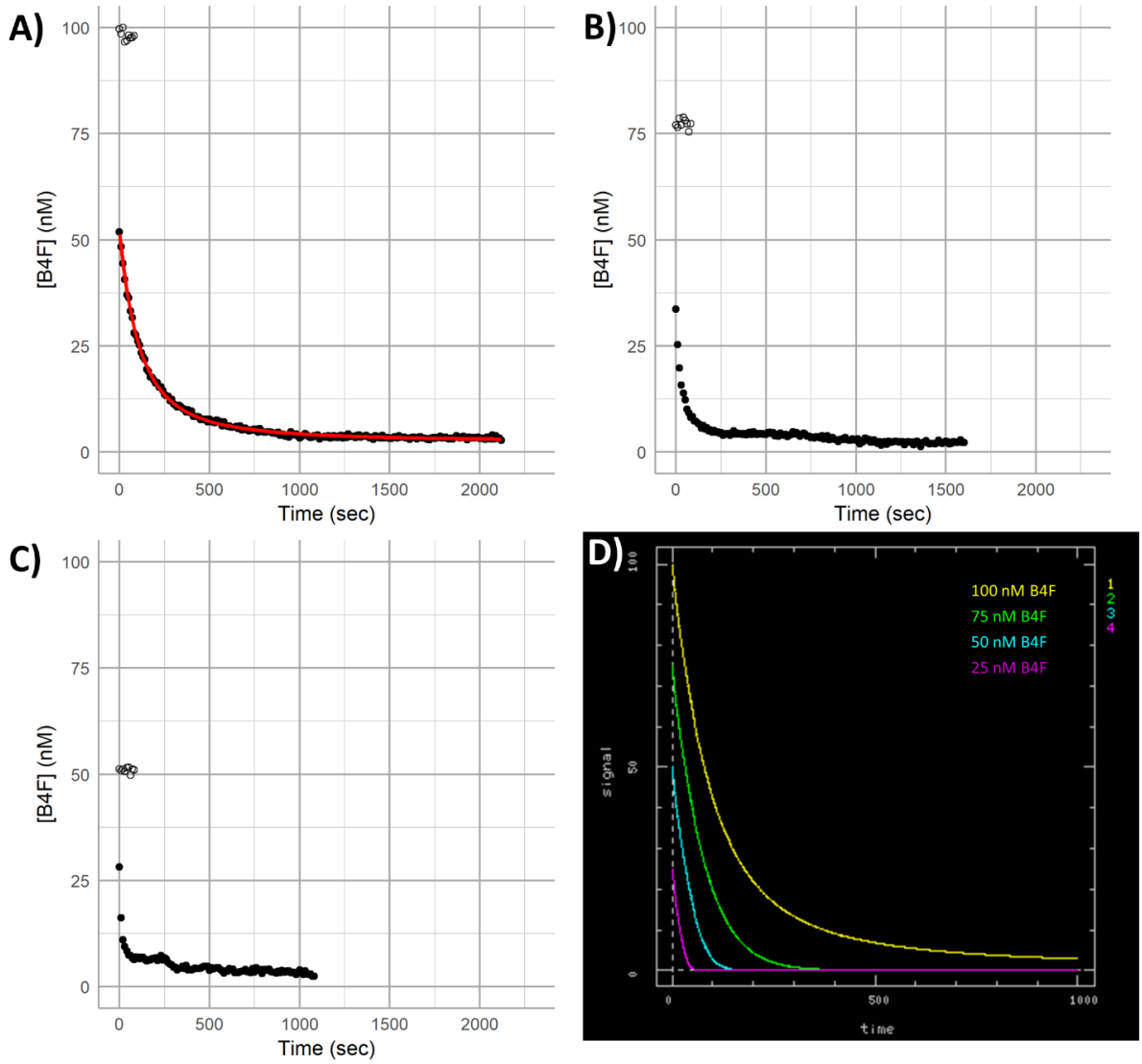

Figure 3.10: Displacement of desthiobiotin from SA active site by B4F. SA_{tet} (25 nM; 100 nM biotin-binding sites) was mixed with 100 nM B4F and the exchange was monitored reading the fluorescence at 490 nm excitation and 525 nm emission with a 515 nm cut-off filter at 23 °C. B) SA (100 nM biotin-binding sites) was mixed with 75 nM B4F. C) SA (100 nM biotin-binding sites) was mixed with 50 nM B4F. D) Simulated data using parameters fitted from A), K_{on} = 24.09 μM^{-1} s^{-1} K_{off} = 0.009505 s^{-1}. K_d = ~3.95 x 10^{-10} M. Single traces (n = 1) were done to qualitatively explore the time-frame necessary for the exchange to reach equilibrium.

The kinetics of biotin binding to SA has been well-established and studied. The K_d of SA is on the order of 10^{-15} – 4 x 10^{-14} M (Chilkoti and Stayton 1995; Hofmann et al. 1982). A fairly recent estimate utilizing ESI-MS to study the dissociation of biotin from SA determined the on- and off-rates to be 1.3 x 10^{8} M^{-1} s^{-1} and 5.5 x 10^{-6} s^{-1} at 22.1 °C (Deng, Kitova, and Klassen 2013). There were relatively fewer estimates available for the dissociation constants of desthiobiotin from SA, though several papers have cited a value of 10^{-11} M for the dissociation constant (Wong et al. 2013; M. Zhang

et al. 2016). The values estimated (k_{on} ~24 x 10^6 M^{-1} s^{-1}, k_{off} ~0.0095 s^{-1}, **K_D ~4 x 10^{-10} M**) to simulate a theoretical desthiobiotin/biotin exchange seem reasonable, in terms of magnitude, within the context of the 10^{-11} M literature estimates available. For the purposes of simulating the data and understanding the trends observed this was suitable; however, the estimate should not be taken to be a definitive determination of desthiobiotin/SA rate constants. The goal here was not to extensively characterize the exchange kinetics of biotin/desthiobiotin, but rather to obtain some reasonable values to simulate the exchange process and get a sense of the time frame required for subsequent experiments that utilized this approach for binding biotinylated proteins to SA. Importantly, the exchange occurs over a useful time frame (not requiring extensive incubation) and desthiobiotin was found to be completely displaced by B4F.

Lastly, the question of whether the distribution of biotin-bound SA species changes as a result of using SA pre-saturated with desthiobiotin was tested. The electrophoretic mobility shift (**EMS**) that occurs between SA and SA(biotin)$_N$ can be taken advantage of to determine the resulting mix of SA species (Sano and Cantor 1990b). Biotin-X-NTA (**BXN**) was used because it gave a good EMS and was used in experiments later in this chapter. Thus, mixtures of SA with or without desthiobiotin bound initially were mixed with aliquots of BXN and run on native PAGE. The binding of desthiobiotin to SA itself induced a slight EMS initially (**Figure 3.11A**). There was an additional transition that occurred upon adding 3 – 4 equivalents to SA. Treating the 4:1 dtb:SA lane as a starting point, addition of equivalents of BXN induced a further EMS. The shift from the addition of desthiobiotin made it more challenging to identify individual bands as the migration range between 4:1 dtb:SA and 4:1 BXN:SA was shorter compared to SA only. However, in comparing SA with 2 equivalents of BXN added (either with or without pre-bound desthiobiotin), the distributions of species were visibly quite different (**Figure 3.11B, C**). In particular, adding BXN directly to SA biases the distribution toward fully occupied and fully unoccupied SA species, as seen previously (Sano and Cantor 1990b). The pre-

saturation of SA with desthiobiotin appears to be a viable strategy for producing a more predictable distribution of SA(biotin)$_N$ species.

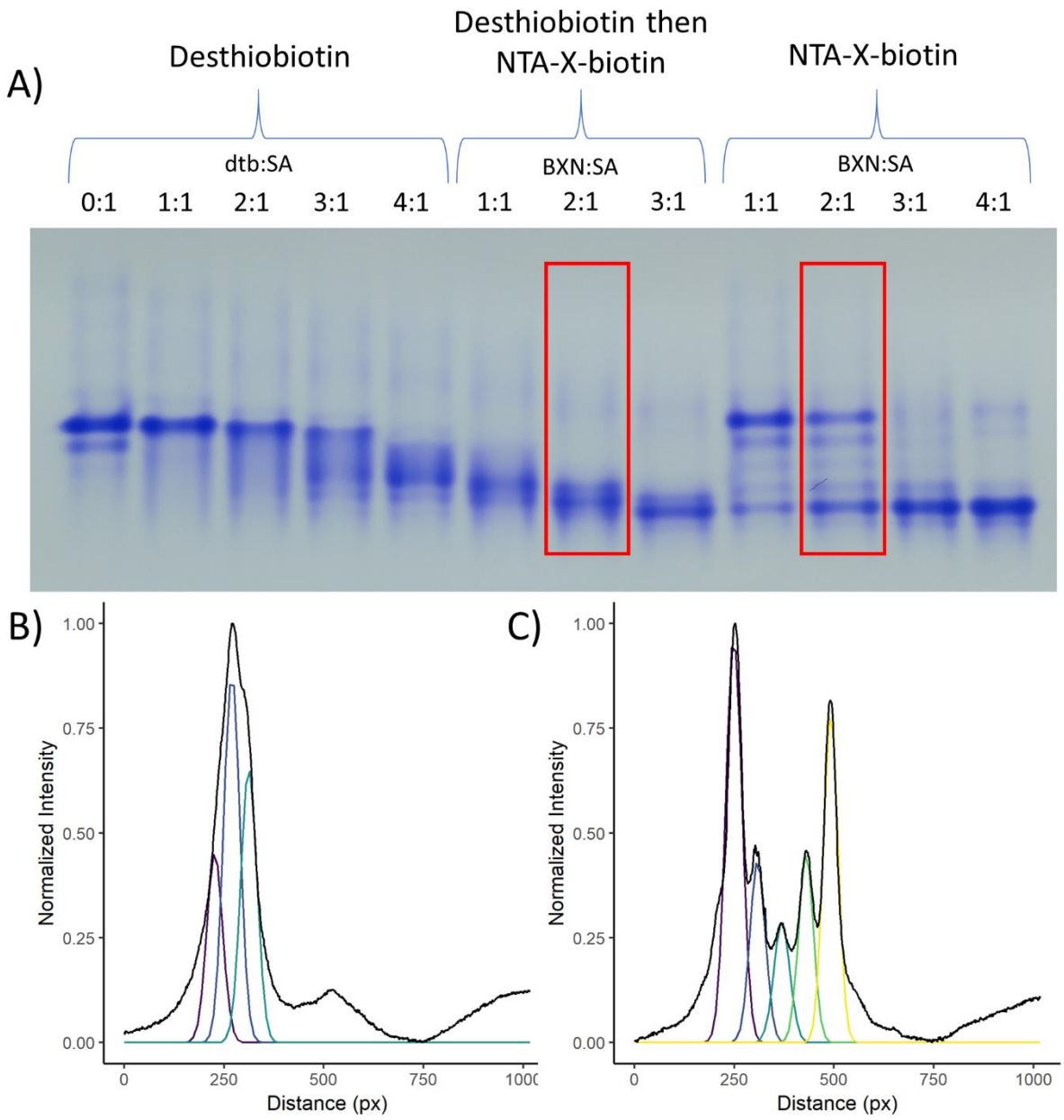

Figure 3.11: Comparison of preparing SA/biotin complexes with or without pre-incubation with desthiobiotin (prepared at a [SA] = 20 µM). Plotted lane profiles of B) 2:1 BXN:SA (with desthiobiotin) and C) 2:1 BXN:SA lanes fitted with a multiple Gaussian distribution in R (version 3.5.1).

This desthiobiotin/biotin exchange approach offers an alternate method to fine tune the association of biotinylated molecules to a SA scaffold. While not explicitly used to affect the distribution of SA(biotin)$_N$ species, displacement of desthiobiotin has been used in other applications.

The reversibility of SA binding to desthiobiotin has been used for regenerating functionalized surfaces (Yoon, Hong, and Kim 2001), and for the purpose of gently dissociating SA from labelled proteins in affinity chromatography or labelling applications (Hirsch et al. 2002). The exchange of desthiobiotin and biotin bound to SA has also been utilized in a DNA tile designed to reveal a message after incubating with a "decoder molecule" (biotin) (Wong et al. 2013). While utilizing the reversibility of desthiobiotin is not a novel idea, the use of it to subtly alter the distribution of $SA(biotin)_N$ species immediately formed upon mixing offers a novel approach to controlling the self-assembly of components onto SA-based scaffolds.

3.3.1.2 *SA/BXN thermal exchange*

Cellulase assays for *C. thermocellum* enzymes are typically run at higher temperature (50 – 65 ^oC). Though the SA/biotin interaction is relatively long-lived, the lifetime of the interaction is expected to be shorter at higher temperature. The following experiment was devised to quickly confirm whether there would be dynamic unbinding and rebinding of loaded Cel8A expected when utilizing the designed scaffold at higher temperature. To test whether this was occurring, SA was pre-saturated with a stoichiometric amount of biotin in the form of biotin-X-NTA (**BXN**) to form $SA(BXN)_4$. If BXN dissociates from SA in the presence of a competing biotin-analogue, there will be competition between the two molecules to bind to open biotin-binding sites; in this case, B4F was used as the competing biotin reagent. The assay then measured the loss of B4F fluorescence from binding to SA at either 23 or 50 ^oC.

At the end of an 18 h incubation, the residual B4F fluorescence in the samples were compared. Firstly, the control (B4F only) in both cases showed a slight increase in fluorescence over time for the fluorophore by itself (**Figure 3.12**). This could be due to slight concentration due to evaporation of aqueous phase over 18 h. There was a clear decrease in measured fluorescence for the 50 ^oC samples incubated together suggesting displacement of BXN with B4F (~50 % displacement from the residual

fluorescence detected). That there was no detected loss of fluorescence for the 23 ºC samples suggested that little exchange occurs at 23 ºC over 18 hours.

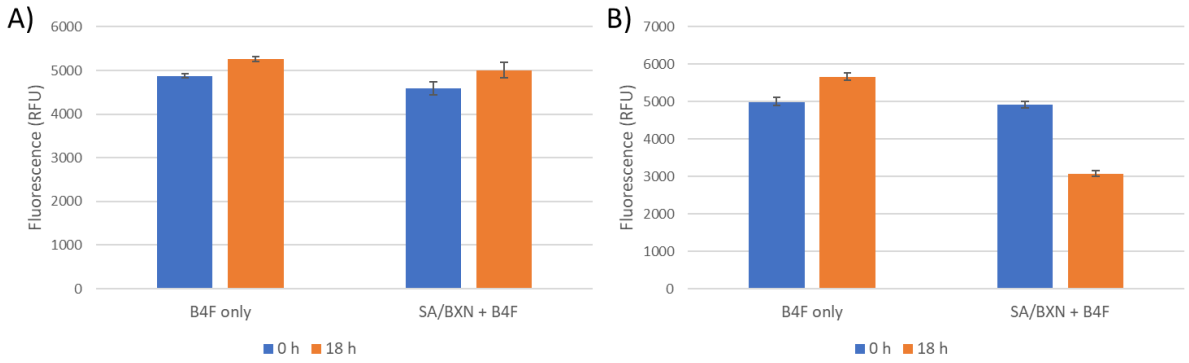

*Figure 3.12: B4F exchange assay to examine whether there is significant exchange of biotin molecules bound to SA at 50 ºC. B4F (400 nM) either with or without SA(BXN)$_4$ at 100 nM incubated at A) 23 ºC, or B) 50 ºC. (average with standard deviation (**SD**) shown, n = 3).*

In summary, these results indicate that there is exchange of biotin analogues between SA binding sites at 50 ºC showing that the system would be expected to be dynamic at this temperature. Therefore, any complexes formed on M13 utilizing the biotin/SA interaction should be expected to be dynamic at higher temperatures, though stable at 23 ºC for longer periods of time. Given the dynamic nature of the SA/biotin bond at higher temperature, it should be expected that this also exists for M13-biotin/SA/Cel8A complexes that are designed here. For comparison, the half-life (calculated from the cited off-rates) of SA/biotin interaction at 44.8 ºC is roughly 46.2 min compared to 35 h at 22.1 ºC (Deng, Kitova, and Klassen 2013). Despite dynamic unbinding and rebinding at higher temperature, it is expected that the SA mediator would increase the localized concentration of enzyme to the vicinity of the nanoscale scaffold. Consider that in the native cellulosome, the components are held together by non-covalent interactions via the Coh modules bound to Doc-containing cellulases; these interactions are likely to be much weaker than a SA/biotin interaction (K_D ~10^{-10} M (Sakka et al. 2011)), yet this is adequate for cellulosome assembly and its resulting high cellulase activity.

3.3.2 Preparing M13 SA scaffold for binding His-tagged proteins

One approach to preparing a multi-enzyme scaffold on M13 was to prepare a SA molecule with BXN which would further be complexed to a His-tagged protein via a metal affinity interaction. In this approach, the BXN serves as a mediator between the SA molecule and the protein of interest via the NTA moiety. This approach utilizes a metal affinity interaction whereby a coordination complex between the His-tag of the protein of interest, Co(II) and NTA is allowed to equilibrate (**Figure 3.13**). Oxidation to Co(III) by the addition of H_2O_2 results in a coordination complex with a very slow exchange rate (Wegner and Spatz 2013). In this way, Cel8A would be stably complexed onto SA, which itself is furthermore complexed onto M13 via biotin-binding. The result would be a nanoscale scaffold that could be generalized to any His-tagged protein/enzyme of interest. One of the main challenges to be addressed in this section is how one can effectively prepare these types of complexes in the stoichiometry shown, such that a single biotin-binding site is available to bind to M13.

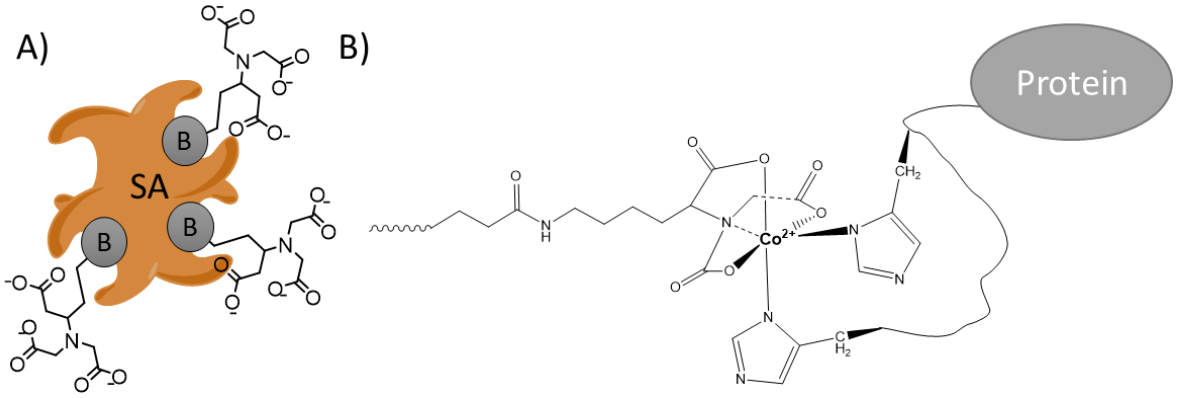

Figure 3.13: Representation of SA(BXN) scaffold to attach i) M13-biotin and ii) Cel8A via Co(III)-mediated interaction. A) SA bound with 3 BXN molecules which can chelate Co(II)/Co(III). B) The His6-tagged protein of interest is complexed with the NTA-bearing SA scaffold via the Co(III)-mediated interaction.

3.3.2.1 *Co-NTA Complexes with Histidine*

First, the applicability of this method to Cel8A was tested using BXN, Co(II), His6-tagged Cel8A (referred to as just "Cel8A") and H_2O_2 to oxidize the Co(II) to Co(III). Oxidation of Co(II) to Co(III) requires incubation with 10 mM H_2O_2 – given the susceptibility of some proteins to oxidation, the activity of Cel8A was first determined before and after treatment with H_2O_2. One approach to confirm that stable complex has formed is to run the resulting mixture on IMAC (Wegner and Spatz

2013). They observed that earlier elution peaks corresponded to His6-tagged protein complexed to Co(III) and NTA – that methodology was used here as confirmation that complexation was successful. Thus, Cel8A:Co(III):BXN is expected to interact poorly with the IMAC resin as it would have two less His residues available with which to interact with the immobilized metal resin in contrast to free Cel8A.

After incubating Cel8A with all components (including H_2O_2) for 3 hours, the samples were resolved by IMAC. For the Cel8A sample without H_2O_2 added, the protein eluted as a single peak during the imidazole gradient (**Figure 3.14A**). However, the sample that had been treated with H_2O_2 had several peaks which eluted earlier (**Figure 3.14B**). The first peak to elute during the imidazole gradient (fraction 18) was expected to be Cel8A complexed to BXN via the Co(III)-mediated interaction, as complexation of the His6-tag in a coordination complex would reduce the interaction with the immobilized metal of the resin. Some of the Cel8A in this sample eluted later in the gradient where Cel8A eluted in the control without H_2O_2 (fraction 21). The sharp peaks early in the elution profile were from trapped air bubbles.

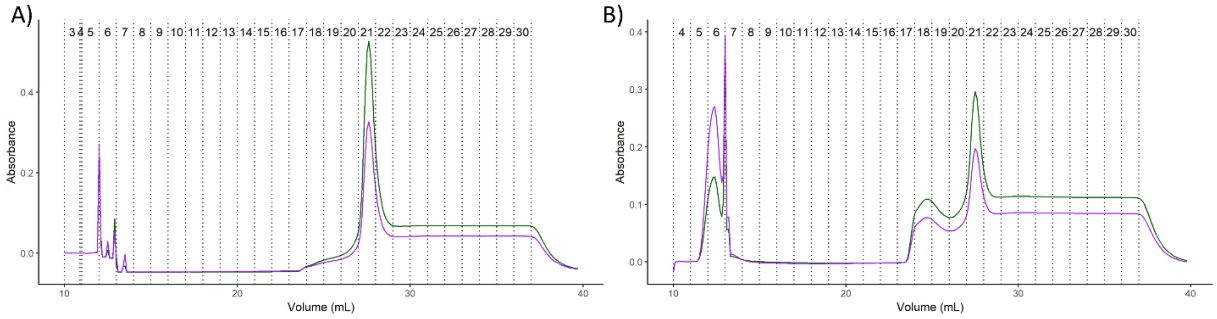

Figure 3.14: Testing Co(III)-mediated BXN complex with Cel8A by IMAC. IMAC chromatogram of 100 µM BXN and 20 µM Cel8A with 100 µM $CoCl_2$ A) without and B) with the addition of 10 mM H_2O_2. The absorbance at 280 nm (green) and 260 nm (purple) are shown. The imidazole gradient starts at fraction 17.

The first eluted peak in the Cel8A:Co(III):BXN chromatogram (fraction 6) was likely mostly composed of excess Co(III):BXN. It was found separately that BXN mixed with $CoCl_2$ and treated with 10 mM H_2O_2 absorbed at 260 nm, and more weakly at 280 nm (not shown). Also, when assayed for protein content by the Bradford assay, the low signal indicated that little protein was present (**Table 3-1**). Thus, the higher A260 absorbance of this peak is consistent with elution of the unreacted small

molecules in the mixture. For the fractions containing Cel8A, it was found that approximately 50% of the protein applied to the column was recovered in total (20 nmol Cel8A applied). It is possible that the other protein can be found spread out throughout the rest of the fractions in low amounts to account for the missing 50% of protein. About 30% of the collected protein was recovered as Cel8A:Co(III):BXN (**Table 3-1**). In contrast, about 61% of the recovered protein was uncomplexed. It was not expected that there would be 100% complexation, as initially, it is necessary for Cel8A to equilibrate with Co(II) and BXN before oxidation to Co(III). The formation constants for His6-tag complexes with Co(II) are typically poorer than for the metals typically used for immobilized metal affinity interactions, such as Ni(II) or Zn(II) (Mehlenbacher et al. 2015). Overall, these results indicated that the complexation was not complete under these conditions, but that a fraction of Cel8A was complexed with BXN. This served as a positive indication that complexation with BXN and Cel8A would occur according to literature methods in further experiments employing SA(BXN) complexes.

Table 3-1: Recovered components from IMAC of Cel8A complexed with BXN via Co(III)-mediated interaction (n=3).

Component	**Without H_2O_2 (% recovery ± SD)***	**With H_2O_2 (% recovery ± SD)***
Excess Co(III):BXN (F-6)	-	0.06
Cel8A:Co(III):BXN (F-18)	1.3 ± 1.5	15.2 ± 5.2
Cel8A (F-21)	47.5 ± 6.7	30.5 ± 5.7

**Percent recovery calculated by moles of recovered protein detected by Bradford assay divided by the total moles of Cel8A applied to the column.*

Lastly, to determine whether the Co(III)-mediated strategy would be appropriate for this particular enzyme, endocellulase activity was tested with the Cel8A fractions collected from the columns. Cel8A isolated from fractions 18 and 21 (with H_2O_2) and fraction 21 (without H_2O_2) were diluted to 100 nM and tested for endocellulase activity with 0.5% (w/v) CMC at 65 ^oC for 1 h. Over the course of 1 hour, a similar amount of reducing ends were produced for all fractions compared to the control (**Figure 3.15A**). This indicated positively that endocellulase activity was present; however, the reaction with CMC was found to be complete at this time point when a time course reaction was carried out under the same conditions with Cel8A (**Figure 3.15B**). Thus, this can only serve as an indicator that Cel8A treated in this way retained some activity– not as a diagnostic of the relative activity of the

samples. Overall, this was an adequate indicator that this treatment did not abolish endocellulase activity and that further experiments could be carried out.

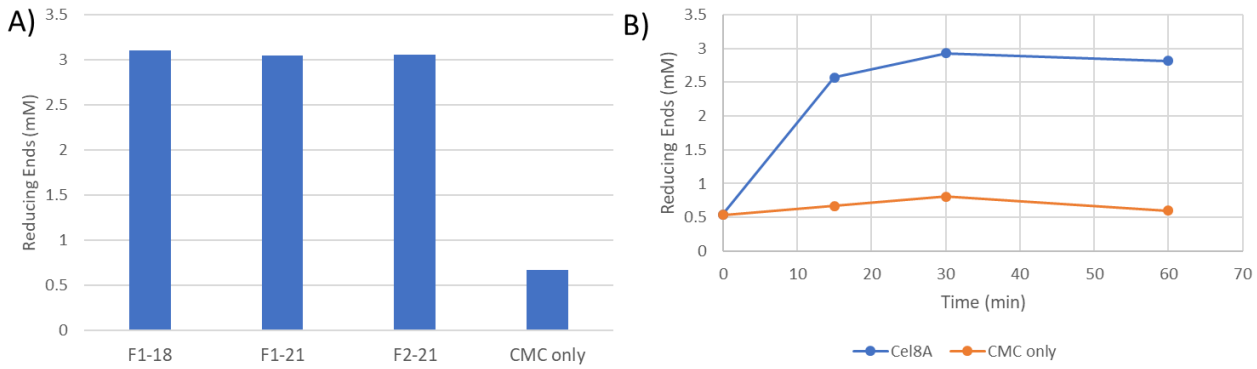

Figure 3.15: Endocellulase activity of Cel8A, BXN and $CoCl_2$ treated with or without H_2O_2 after IMAC. The reaction conditions were 0.5% CMC reacted with 100 nM Cel8A at 65 °C for 1 h. A) Activity of fraction eluted from IMAC (F1-18 Cel8A:Co(III):BXN, F1-21 Cel8A (with H_2O_2), F2-21 Cel8A (no H_2O_2) (n = 1). B) Time course of CMC hydrolysis by Cel8A. Reducing ends were detected using DNS and comparing to glucose standard curve (n = 1).

3.3.2.2 *Preparing and separating an ensemble of SA(NTA):Co(III):Cel8A complexes*

The main goal was to ultimately prepare a stable arrangement of Cel8A onto SA which could be further complexed onto M13-biotin. One approach to prepare complexes onto M13 of defined stoichiometry is to first prepare a mixture of Cel8A bound to $SA(BXN)_N$ via the Co(III)-mediated interaction and separate $SA(BXN)_N$ with the desired stoichiometry as discussed in the introduction (**Figure 3.16**). SEC was used as a method to distinguish between the different components, and ideally, between $SA(BXN:Co(III):Cel8A)_N$ complexes of differing stoichiometry.

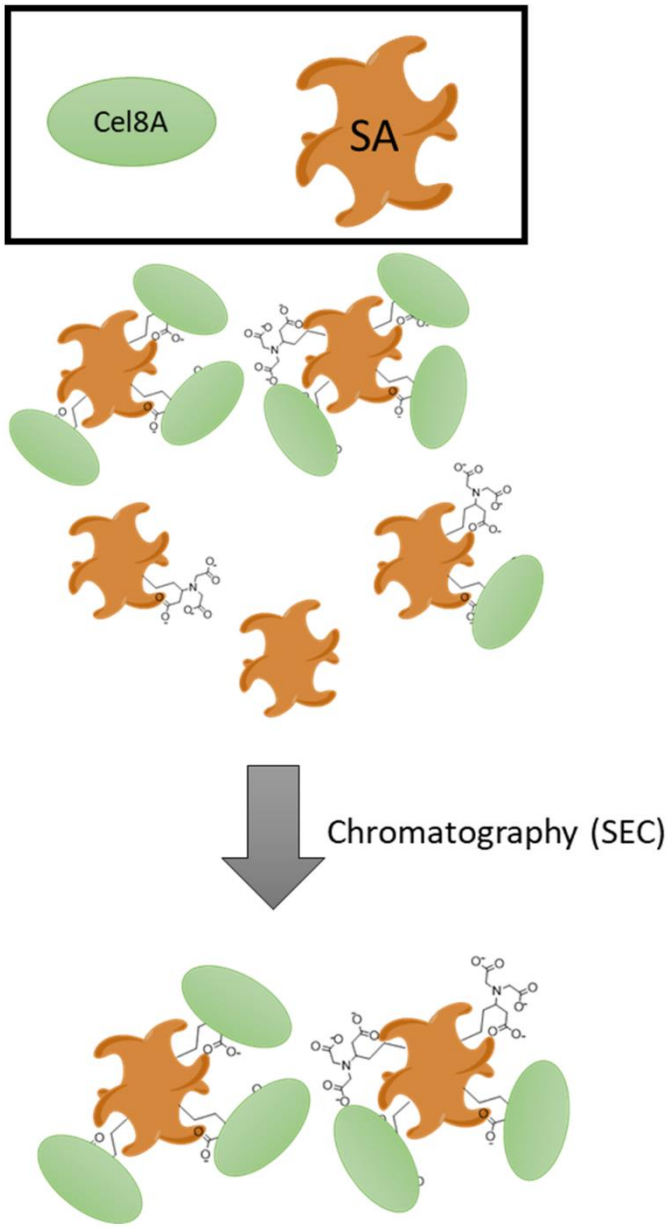

Figure 3.16: Schematic representation Cel8A assembly onto SA(BXN) followed by SEC. SA(BXN:Co(III):Cel8A complexes are prepared and then separated by SEC to obtain a species with a single biotin-binding site for further complexation to M13-biotin.

The SA(BXN:Co(III):Cel8A) complexes were prepared in the following way: first BXN:Co(II) was prepared at a 1:1 ratio in water, this was next incubated with SA at a ratio of 1:4 SA_{tet}:BXN, followed by Cel8A at a ratio of 1:4 SA_{tet}:Cel8A and then ultimately the entire mixture was reacted with 10 mM H_2O_2. Note that for this procedure that all of the biotin-binding sites would be expected to be occupied (i.e., all SA should exist as $SA(BXN)_4$ with some of this further complexed to Cel8A via

Co(III)). Though the end goal was to prepare a SA(Cel8A) complex with a single free biotin-binding site, fully saturated SA was tested here. Since the previous experiments with Cel8A and BXN separated on IMAC indicated that complexation would be incomplete, using SA fully occupied with BXN was expected to simplify the interpretation of the chromatograms.

The separation of any formed complexes by size-exclusion was initially tested on a Sephacryl® S-300 resin but the resolution was poor and there was very little separation between SA and Cel8A components (**Figure 3.17**). There was an observed shift toward higher MW observed for the SA(BXN:Co(III):Cel8A) sample compared to either SA_{tet} (52 kDa) or Cel8A (50 kDa) run on their own. The separation range of the Sephacryl® S-300 resin used was specified to be 10 – 1500 kDa and therefore any formed complexes (expected to range from 52 – 252 kDa based on the masses of the individual components) would be expected to be well within this range.

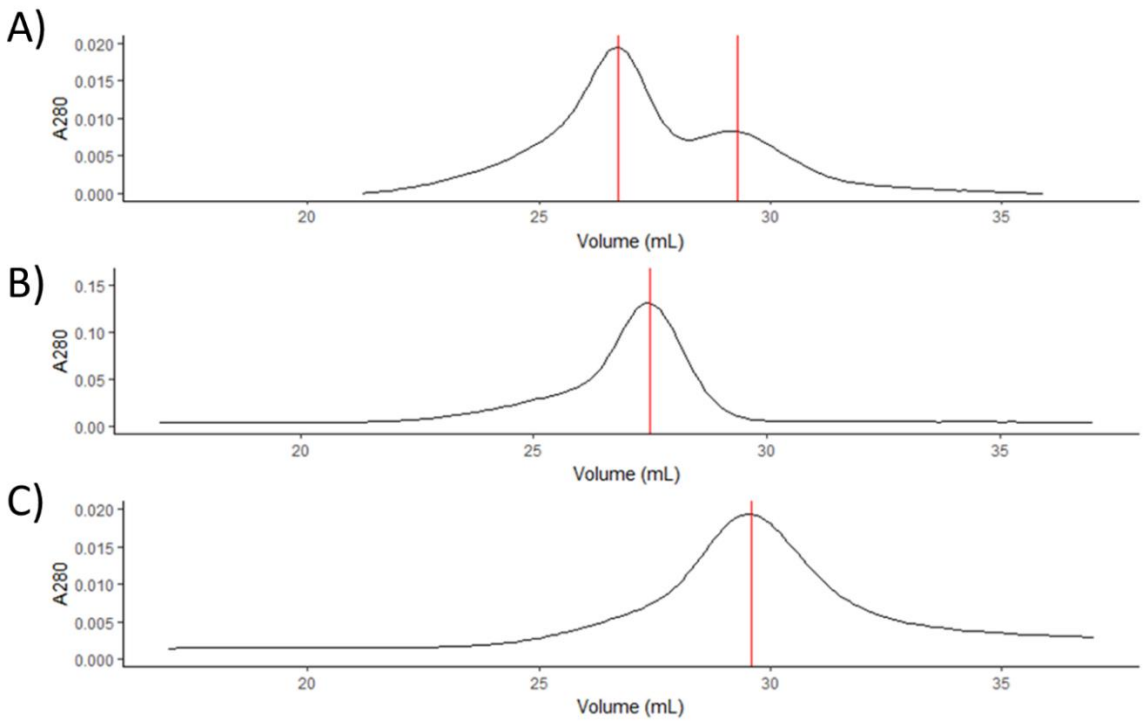

Figure 3.17: SEC separation of $SA(BXN)_4$ complexed to Cel8A via Co(III)-mediated interaction on a Sephacryl® S-300 column. Chromatogram of A) 20 µM $SA(BXN:Co(II))_4$ complexed to 80 µM Cel8A followed by treatment with 10 mM H_2O_2, B) SA only and C) Cel8A only.

In order to get a better sense of how complexed samples should be expected to run on this particular column, a further control with biotinylated Cel8A (**Cel8A-PEG$_{12}$-biotin**; prepared by acylation of Lys residues as described in the Methods) was used to provide an additional comparison between elution profiles. The main difference between the sample and this control is that the biotin is covalently reacted to Cel8A, and therefore, would be suitable as a positive control to see how these complexed components would be expected to separate. The chromatogram of SA and Cel8A-PEG$_{12}$-biotin was similar to the one performed with the Co(III)-mediated complex of Cel8A and SA above (**Figure 3.18**). The main eluted peak was shifted toward a higher MW and was presumed to be from complexation of Cel8A-biotin to SA. The first peak to elute was broader than that seen in the Co(III)-mediated complex, perhaps indicative of a wider range of SA-complexed species of varied size (the larger of those species eluting earlier). Once again, any potential complexed species were poorly separated from their starting components (SA and Cel8A). Given the poor resolution, a resin with a smaller fractionation range would be tested next.

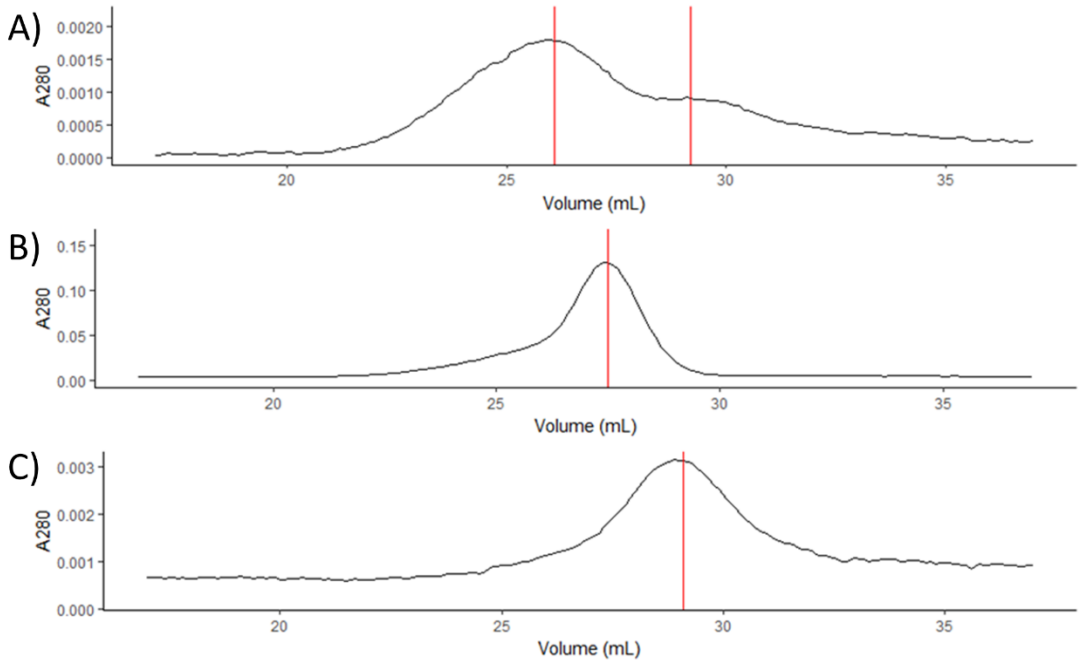

Figure 3.18: SEC separation of SA complexed to Cel8A-PEG$_{12}$-biotin on a Sephacryl® S-300 column. Chromatogram of A) 4 µM SA complexed to 12 µM Cel8A-PEG$_{12}$-biotin, B) SA only and C) Cel8A-PEG$_{12}$-biotin only.

A Superdex® 75 column with a fractionation range of 3000-70,000 Da was next used. Though the assembled complex would be expected to be much larger than 70 kDa (SA_{tet} = 52 kDa, Cel8A = 50 kDa), Cel8A is composed of several small globular domains with flexible linker regions and therefore would be expected to run differently than a single globular protein of the same MW (**Figure 3.19**). Therefore, it was expected that an assembled complex might still elute within the fractionation range of the column. For a direct comparison the SA(BXN:Co(III):Cel8A) complexes run above on the S-300 resin, the complexes were prepared the same way.

Figure 3.19: Cel8A with linker region and dockerin domain. Built from Cel8A cellulase domain (PDB: 1KWF), and dockerin domain (built from ModBase with template structure PDB: 4FL4) and sequence from Cel8A (UniProt A3DC29) (Pieper et al. 2014). The linker was built in from the primary sequence of Cel8A in Maestro (Schrödinger).

The Superdex® 75 column was able to better resolve the different species after complexation via the Co(III)-mediated interaction. Cel8A was run on its own and was found to elute latest of all the individual components (**Figure 3.20A**). As an additional control, Cel8A incubated with $CoCl_2$ and BXN (but no SA), was then oxidized with H_2O_2 was run on this column as well. This was found to run at a slightly higher MW that Cel8A on its own (**Figure 3.20B**). This could be from a subtle change in conformation with how the cellulase and dockerin domains are positioned relative to each other. When complexed with SA, three peaks were observed – one with a very obvious shift to a higher MW (**Figure**

3.20). The first eluted peak was expected to be various complexes of SA(BXN:Co(III):Cel8A) eluting together at a higher MW. The third peak was Cel8A as determined from the controls. Therefore, the second (and largest peak) was likely SA(BXN) species eluting as a single peak.

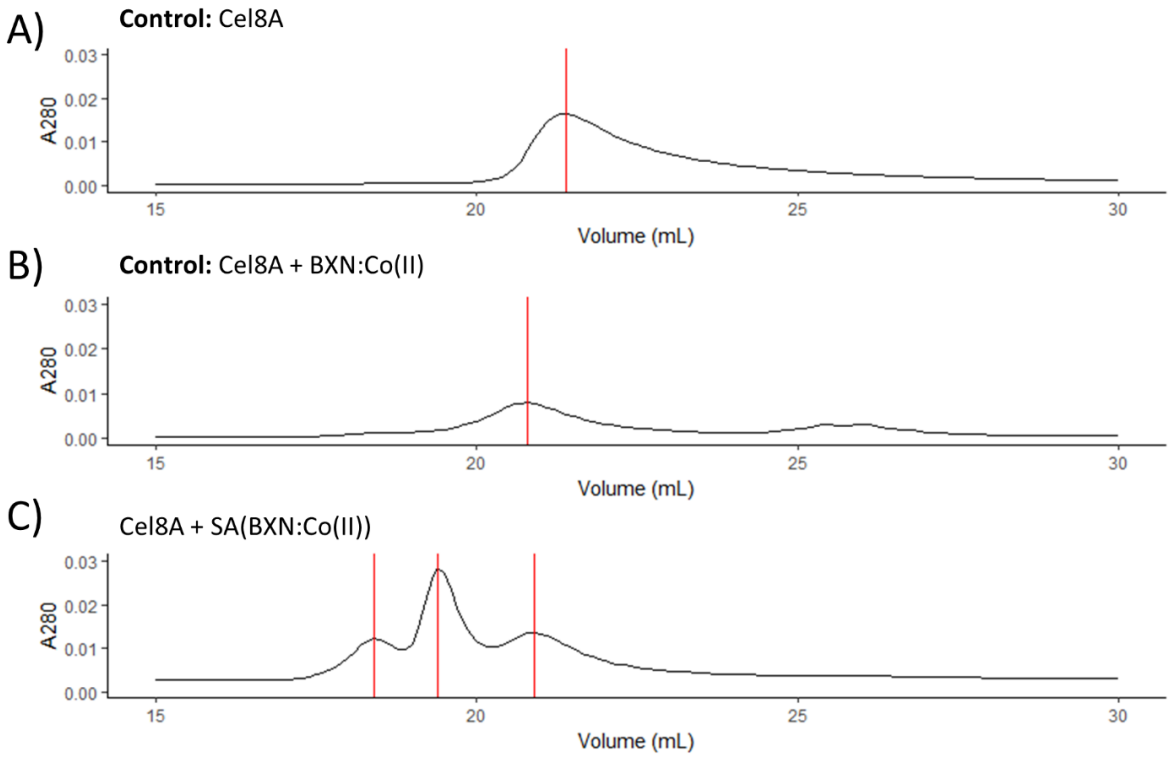

Figure 3.20: SEC separation of SA(BXN)$_4$ complexed to Cel8A via Co(III)-mediated interaction on a Superdex® 75 column. Chromatogram of (top panel) Cel8A only, (middle panel) 80 µM Cel8A and 80 µM BXN:Co(II) followed by treatment with 10 mM H_2O_2, (bottom panel) 20 µM SA(BXN:Co(II))$_4$ complexed to 80 µM Cel8A followed by treatment with 10 mM H_2O_2.

To further confirm the suspected assignments of these peaks, Cel8A-biotin was again used as a control to see what one should expect from the Superdex® 75 column for SA complexed to Cel8A. This could then be compared to the elution profile of the Co(III)-mediated complex to see if the assignment of peaks was reasonable. Like the complexes prepared using the Co(III)-mediated approach, when the SA(Cel8A-biotin) positive control was run, there was again a very obvious shift to higher MW (**Figure 3.21A**). As with the S-300 column, the first peak to elute was quite broad and likely consisted of various SA(Cel8A-biotin)$_N$ complexes. The suspected SA peak was not observed in this control, suggesting the complexation of Cel8A-biotin to SA does not leave much SA that is not complexed. Additionally, a protein MW standard was run on this column (**Figure 3.21C**). Of the

components in these mixtures, SA was the only protein with a single globular domain; therefore, it should be expected to run true to its MW. Indeed, when compared to the protein standards, the peak suspected of being uncomplexed $SA(BXN)_4$ ran near to its expected MW of 52 kDa – suggesting that the assignment was reasonable. Noticeably, the Cel8A does not run true to its MW; however, this was discussed above as likely being due to the two domains and flexible linker present on the protein. Alternatively, the cellulase may have some affinity for the crosslinked agarose and dextran which compose the column resin which might alter the retention time. From the comparison of Cel8A complexed via the Co(III)-mediated interaction with Cel8A-biotin, it was apparent that some complexation does likely occur with the Co(III)-mediated approach; however, there was a considerable amount of uncomplexed SA(BXN).

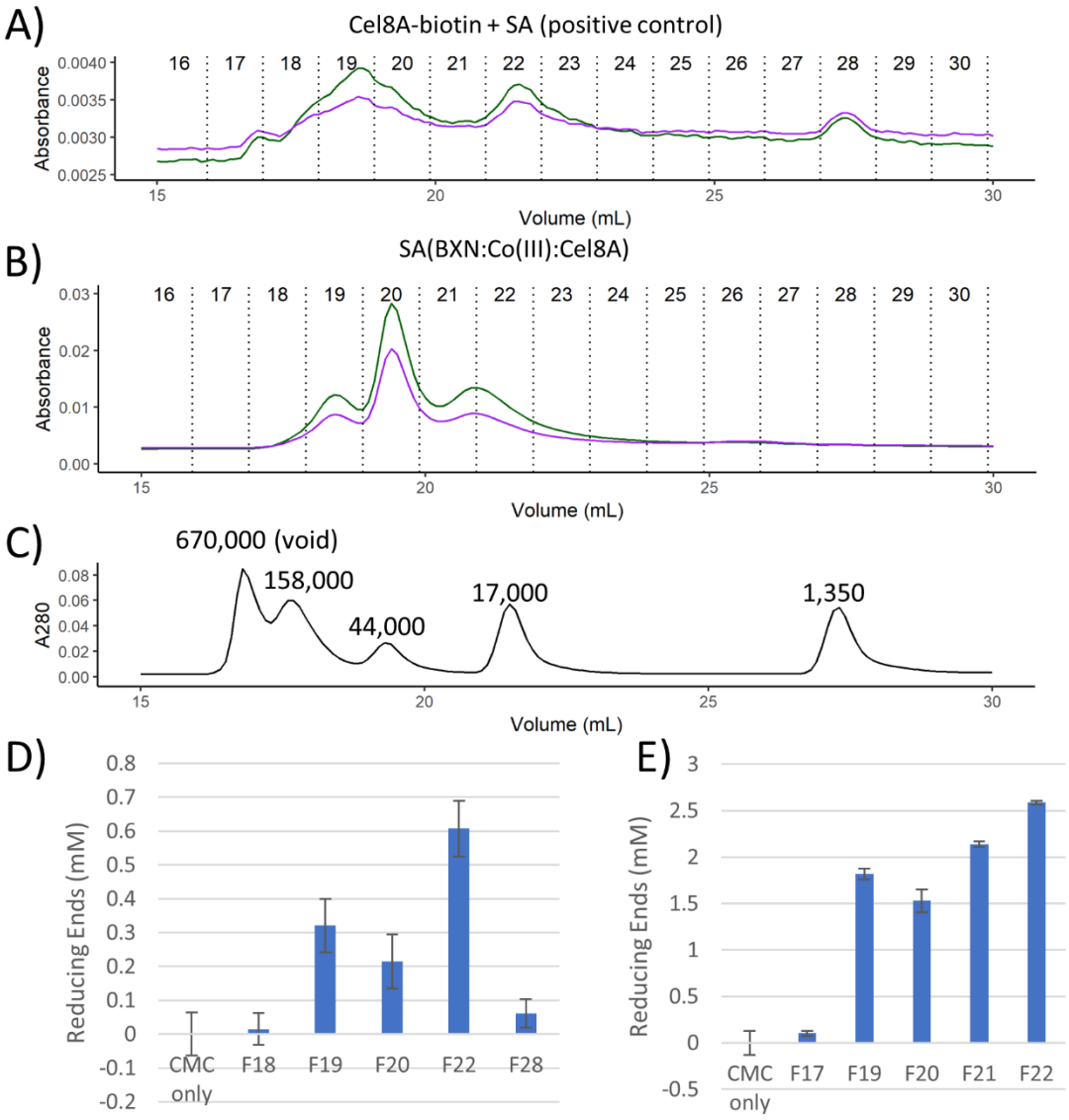

Figure 3.21: Comparison of SA(BXN:Co(II))$_4$ with Cel8A complex with Cel8A-PEG$_{12}$-biotin control on a Superdex® 75 column. Chromatogram of A) 4 µM SA and 12 µM Cel8A-PEG$_{12}$-biotin, B) 20 µM SA(BXN:Co(II))$_4$ complexed to 80 µM Cel8A followed by treatment with 10 mM H_2O_2, C) Bio-Rad gel filtration standard showing 280 nm absorbance. The purple traces show the absorbance at 260 nm, and the green traces show the absorbance at 280 nm. DNS detection of reducing ends after 15 min reaction of 0.5 % CMC in 0.1 M citrate pH 5.8 at 65 °C with SEC fractions corresponding to D) complexation of Cel8A-PEG$_{12}$-biotin with SA (mean and SD shown; n = 2), E) Co(III)-mediated approach (mean and SD shown; n = 3). Fractions were either assayed directly (for D), or diluted 4-fold (E), before reacting with CMC. Values were converted to reducing ends by comparison to a DNS standard curve of D-glucose.

To further confirm the assignment of the elution profile, the endocellulase activity of Cel8A was assayed as it eluted from the column to identify which eluted peaks might be associated with Cel8A (or some complex of Cel8A). The fractions were diluted at the same fold-dilution and assayed against CMC at 65 °C giving a measure of relative activity in each fraction. The first peak to elute for

both the SA(BXN:Co(III):Cel8A) mixture and the SA(Cel8A-biotin) positive control had endocellulase activity (**Figure 3.21D, E**). This would be consistent with that peak containing SA and Cel8A complexed together either through BXN:Co(III) or biotin (for the control). Some activity was detected in fraction 20 (which was suspected to be SA); however, this likely comes from slight overlap of the preceding and following peaks. The last peak eluted in each spectrum around fraction 22 was also consistent with the expectation that the peak corresponded to uncomplexed Cel8A.

In summary, SEC was tested as a potential approach to separate individual species of SA(BXN:Co(III):Cel8A) for the purpose of later binding these complexes on M13-biotin in a controllable way. The Superdex® 75 resin did give better resolution than the S-300 column; however, the column was still only able to resolve the complexed species, and the individual components (SA and Cel8A). The lack of resolution could in part be due to the flexible linker on Cel8A giving a wide range of possible conformations that a formed complex might exist in, resulting in broad and unresolved peaks by SEC. Therefore, this approach was not considered viable for separation of a SA loaded with enzyme at a particular stoichiometry. As one of the goals of this project was to explore ways of producing defined, and well-ordered arrangements on the nanoscale, a second approach was pursued to obtain SA(Cel8A) complexes with the desired arrangement of components.

3.3.2.3 *Isolating SA(BXN)$_N$ species of defined stoichiometry*

In order to overcome the challenge of preparing a multi-enzyme complex with the kind of defined stoichiometry of components outlined in the design presented in **Figure 3.3, Section 3.1**, a different approach was taken where SA(BXN)$_3$ was prepared and isolated first by IEC (**Figure 3.22**). As the NTA moiety has several negatively charged carboxylate groups, the interaction of SA(BXN)$_N$ with an anion exchange column would be expected to increase with additional bound BXN. The isolated SA(BXN)$_3$ would have a single unoccupied biotin-binding site for further complexation to M13-biotin. Additionally, the NTA groups from the BXN bound to SA could be used for complexation with the His6-tag of Cel8A via the Co(III)-mediated interaction explored in the previous section. It was

found that this method was suitable for isolating the various SA(BXN) species that form from mixing the two.

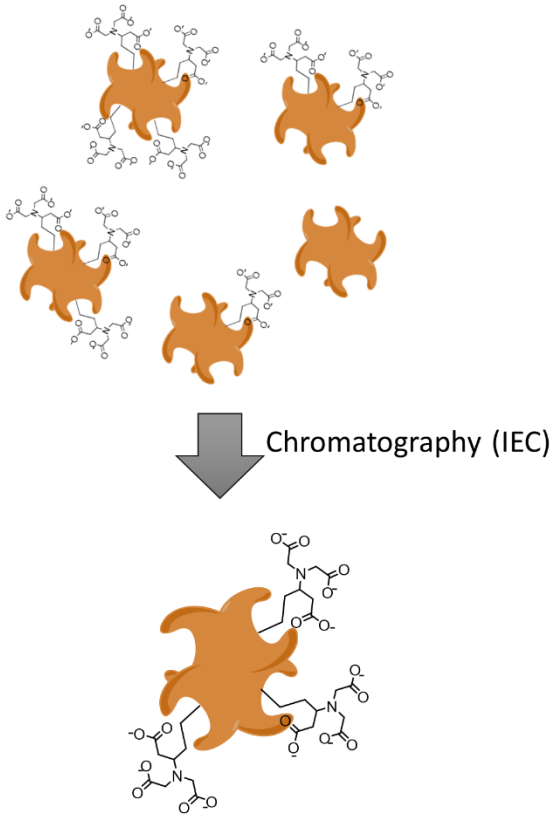

Figure 3.22: Schematic representation showing isolation of SA(BXN)$_3$ prior to complexation with Cel8A. A mixture of SA(BXN)$_N$ are first prepared and then separated by IEC to obtain a species with a single biotin-binding site and three bound BXN to complex with the His6-tag of Cel8A via the Co(III)-mediated interaction.

Briefly, the ability to separate different species of SA bound to BXN was tested with two extremes: SA with nothing bound to it, and SA saturated with BXN to form SA(BXN)$_4$. Due to the additional negative charge introduced by BXN, this separation was carried out on an anion exchange column. It was found that all species would be expected to elute over the range of 5 – 20 mS/cm when a NaCl gradient was used for elution (**Figure 3.23**). As expected, the SA fully saturated with BXN eluted later than the unmodified SA.

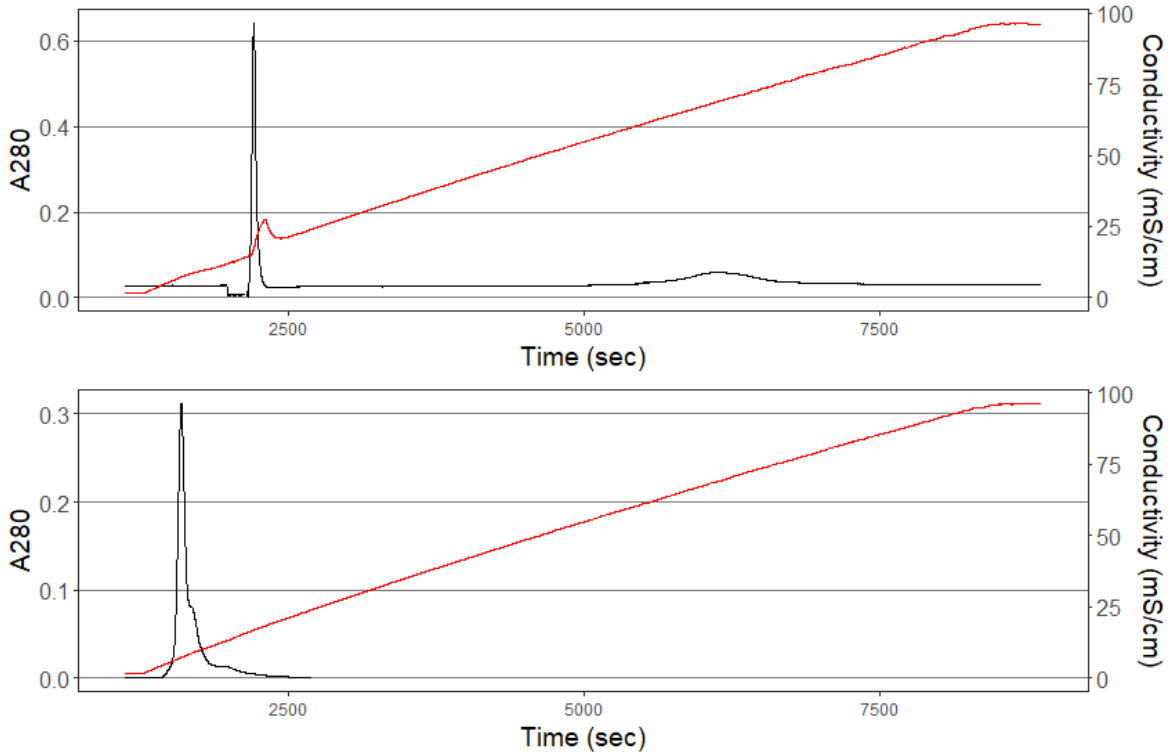

Figure 3.23: IEC separation of SA complexed with BXN on a MonoQ® anion exchange column in 10 mM Tris pH 8.0 and eluted with a gradient of 0 – 1 M NaCl. Chromatogram of A) 20 µM SA and 80 µM BXN, B) 20 µM SA.

As discussed in **Section 3.3.1**, desthiobiotin can be used to alter the distribution of $SA(BXN)_N$ species that form by pre-incubation with desthiobiotin. However, it was also observed that desthiobiotin bound to SA itself resulted in an electrophoretic mobility shift on native PAGE. It was expected that pre-incubation in this specific case would not be suitable, as it might affect the resolution of the anion exchange chromatogram. Therefore, $SA(NTA)_N$ prepared at different ratios of BXN:SA tetramer (1:1 to 4:1) were separated together by IEC. This was to ensure that there would be a good distribution of species to separate and identify once separated. When the prepared mixture of $SA(BXN)_N$ species was run on a MonoQ® IEC column, six potential $SA(BXN)_N$ peaks were observed (**Figure 3.24A**). It was expected that the SA species with more BXN bound would elute later based on the additional negative charge present from the NTA moieties.

In order to confirm that the tentatively assigned peaks had the predicted stoichiometry of bound BXN, the unoccupied biotin-binding sites were assayed as described in the Methods (**Section 3.2.6.1**).

Briefly, a fluorescent biotin analogue, biotin-4-fluorescein (**B4F**), is titrated into a solution of SA and is quenched upon binding (Ebner et al. 2008). When an amount of B4F equivalent to the number of free biotin-binding sites is added, a sharp breakpoint is observed in the titration curve. A clear pattern identifying the different isolated peaks was observed (**Figure 3.24B**). The concentrations isolated from the column were low, making the accuracy a little lower, but the positioning of the breakpoints relative to each other qualitatively supported the peak fraction assignments made. Interestingly, the shoulder that elutes immediately after the $SA(BXN)_0$ peak does appear to be SA-related, as it does bind four equivalents of biotin per tetramer (**Figure 3.24B; orange trace**). Each subsequent peak was confirmed to have an additional BXN bound.

To confirm that each isolated fraction corresponded to a single $SA(BXN)_N$ species, they were analyzed by native PAGE (**Figure 3.24C**). For comparison, mixtures of SA and BXN were prepared without separation, alongside the fractions isolated by IEC. For the mixtures of SA and BXN, there was a clear shift in electrophoretic mobility upon each subsequent addition of a BXN equivalent. Importantly, the fractions isolated from IEC ran as single species, rather than a distribution of species. This showed that $SA(BXN)_N$ with defined stoichiometry can indeed be isolated using this strategy.

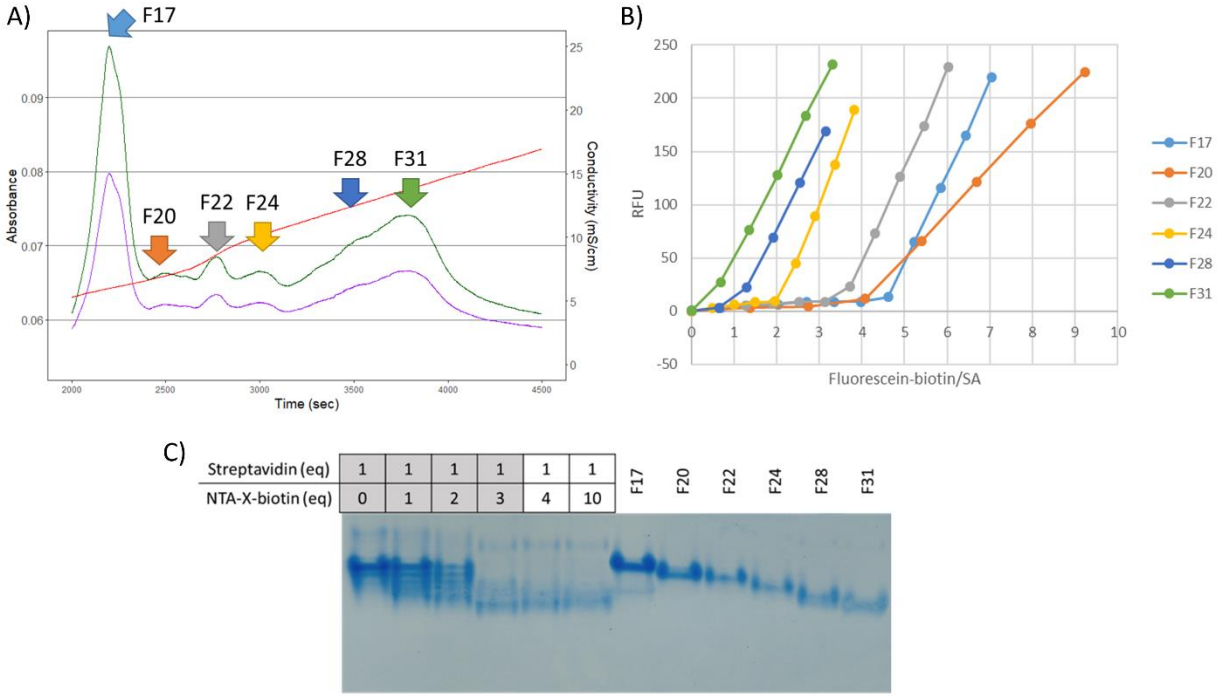

Figure 3.24: IEC separation of SA(BXN)$_N$ species on a MonoQ® anion exchange column in 10 mM Tris pH 8.0 and eluted with a gradient of 0 – 200 mM NaCl. A) Chromatogram of equal volumes of SA(BXN) separately prepared at SA:BXN ratios of 1:0, 1:1, 1:2, 1:3 loaded together. B) B4F fluorescence (490 nm excitation, 525 nm emission) titration of SA(BXN)$_N$ fractions isolated from IEC. C) A 7% native PAGE gel of prepared mixtures of SA and BXN and fractions eluted from IEC of SA(BXN)$_N$ mixture.

A scaled-up separation was carried out to obtain SA(BXN)$_3$ for use in complexation with M13-biotin. Although the SA(BXN)$_0$ – SA(BXN)$_2$ species were well-resolved, the SA(BXN)$_3$ and SA(BXN)$_4$ species were not well separated from each other (**Figure 3.25A**). Despite this, fractions could still be isolated that would correspond to SA with either no or one biotin-binding site open (**Figure 3.25B**). Several approaches to improve the resolution were attempted including: shallower elution gradients and cleaning the column; however, the best resolution obtained was that shown in **Figure 3.25**. Given that it was still possible to obtain SA(BXN) with a single biotin-binding site using these conditions, it was deemed suitable for producing SA(BXN)$_3$ for further complexation with M13-biotin.

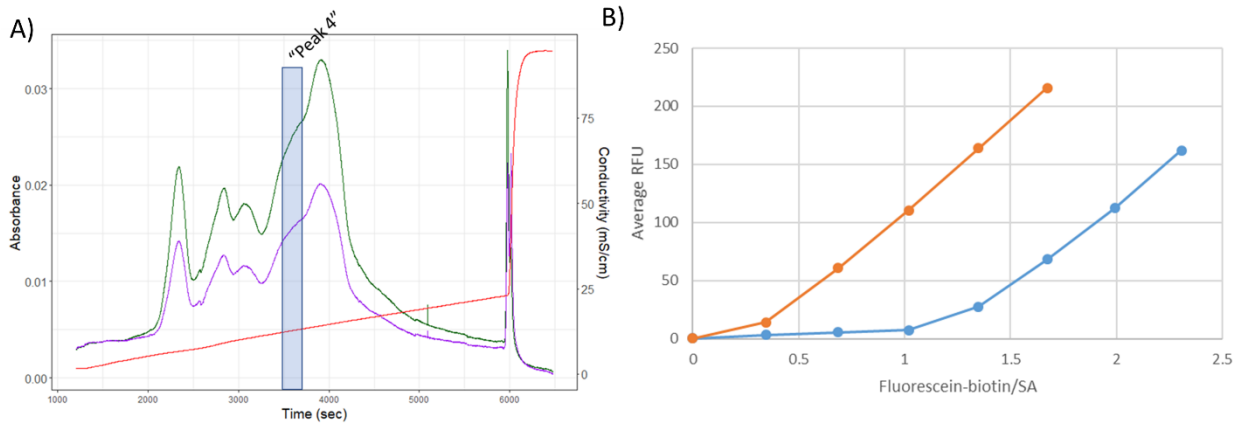

Figure 3.25: IEC separation of SA(BXN)$_N$ species on a MonoQ® anion exchange column in 10 mM Tris pH 8.0 and eluted with a gradient of 0 – 200 mM NaCl. A) Chromatogram of SA(BXN) prepared at a SA:BXN ratios of 1:2. Peak 4 indicates the elution time of SA(BXN)$_3$ species. B) B4F fluorescence (490 nm excitation, 525 nm emission) titration of SA(BXN)$_3$ and SA(BXN)$_4$ isolated from IEC. The x-axis is reported in terms of B4F added per SA monomer concentration (average, n = 3).

Possible future improvements to this methodology can be easily conceived. When mixing BXN and SA, a wide distribution of SA(BXN)$_N$ forms – with only a fraction of this being SA(BXN)$_3$. This is due to the rapid binding of biotin to SA and slow off-rate, which results in a non-equilibrium distribution of species (Jones and Kurzban 1995). However, over time the distribution of SA(biotin) species would shift to one that better reflects the relative quantities of biotin and SA in the solution. Therefore, it should be possible to favour formation of a particular species by incubation of SA/BXN mixtures at higher temperature, followed by separation by IEC. As noted in **Section 3.3.1.2**, at increased temperatures there was considerable unbinding and rebinding of biotin-analogues observed. Following from the observations of Jones and Kurzban then, a better approach might involve preparation of SA:BXN at a 1:3 ratio, followed by a short incubation at 50 °C to bias the distribution of species toward the desired SA(BXN)$_3$.

In summary, this method was the most promising approach toward preparing SA(Cel8A) complexes with a defined stoichiometry. SA(BXN)$_3$ was isolated here as a precursor to preparing Cel8A complexes of defined stoichiometry via the Co(III)-mediated interaction. Prior to complexation with Cel8A, however, the capability of M13-biotin to bind this scaffold was explored first. Following complexation onto M13, the resulting nanoscale scaffold would have NTA moieties (three per SA$_{tet}$)

presented along the length to allow further complexation of the His6-tagged Cel8A and subsequent oxidation with H_2O_2 to form the final complex. Next the efficiency of preparing a purified "monomeric" $SA(NTA)_3$ onto M13-biotin was explored.

3.3.3 Preparation of M13/$SA(NTA)_3$ scaffold

Following from the experiments which led to the isolation of an NTA-displaying SA component with a single free biotin-binding site ($SA(BXN)_3$), the ability to efficiently bind this component to M13-biotin was explored next. First, some considerations regarding the possible loading capacity and possible steric limitations relating to the total number of SA that could be theoretically loaded onto the phage scaffold will be discussed. Next, TEM evidence showing the resulting M13/$SA(NTA)_3$ complexes will be presented and discussed. This will be followed last by the experimental results from further complexation of these M13/$SA(NTA)_3$ scaffolds with Cel8A under the Co(III)-mediated complexation conditions.

3.3.3.1 *Estimating optimal packing of SA on M13-biotin*

In order to better assess the TEM images in the following section, the approximate sizes of the components were compared. Estimation of the maximal loading of protein onto M13 has been done for a protein of ~26.8 kDa (GFP); the maximum loading was based on the number of labelling sites occluded by attachment of a single GFP and was estimated to be ~385 GFP/M13 (Hess et al. 2012). It was expected to be useful to determine the theoretical maximum possible loading of SA onto M13 based on its geometry. M13 and SA (52 kDa) were approximated as a cylinder of ~7 nm diameter and a sphere of ~6 nm diameter respectively (**Figure 3.26**). For the M13-PEG_{12}-biotin scaffold, the length of the PEG_{12} linker will depend on how extended it is. For comparison, a relaxed PEG_{12} linker extended out ~2.6 nM from the biotin-binding site of SA while fully extended it measures ~3.8 nm from the binding site (**Figure 3.26**). The distance of SA from the surface of M13 would therefore fall somewhere below this when assembled. For simplicity, the following approximations consider the relative spacing

of N-termini on M13 to estimate the spacing of biotin moieties in M13-biotin, though it should be noted that Lys8 can also be modified by chemical acylation (K. Li et al. 2010). Thus, in the real biotinylated M13 particles, the actual spacing of biotin moieties would likely be shorter in some areas where Lys8 was labelled as well. Regardless, the simplified consideration of N-termini spacing will be suitable for an initial estimate of biotin spacing – which is expected to translate to how SA(BXN)$_3$ would be spaced on biotinylated phage.

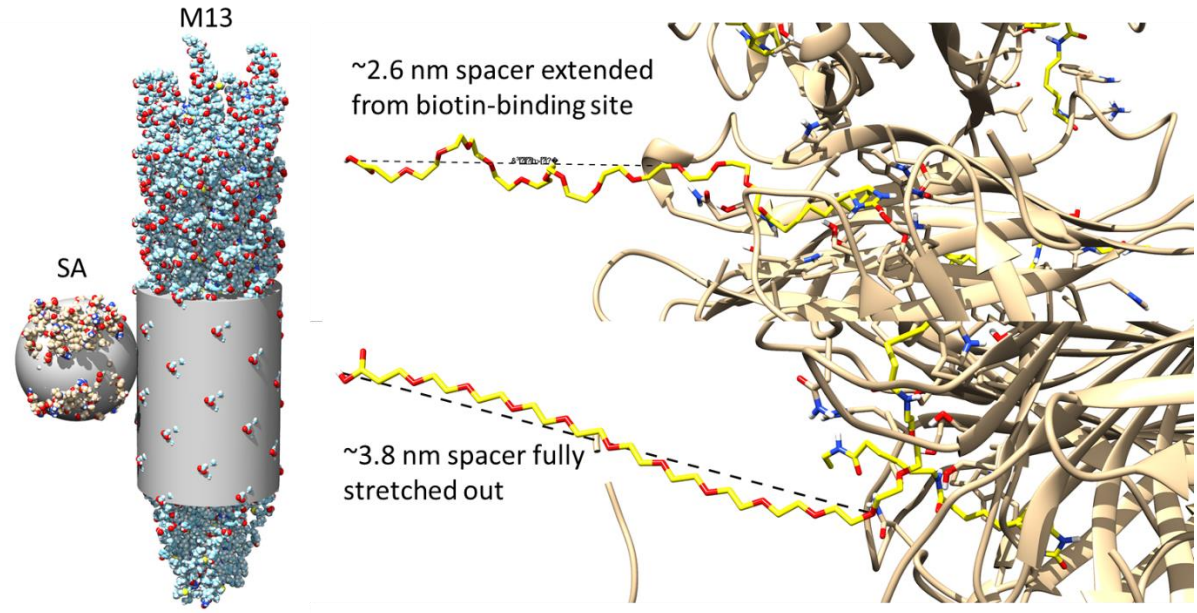

Figure 3.26: Approximating SA and M13 diameters as geometric shapes and the expected length of PEG$_{12}$-biotin bound to SA. (Left) SA was approximated as a 6 nm sphere, and M13 was approximated as a 7 nm cylinder. (Right) The biotin-PEG$_{12}$ linker length estimates were measured from PEG$_{12}$ built out from SA with biotin bound (PDB: 3RY2) using Maestro (Schrödinger). The linkers were measured and presented using UCSF Chimera.

The majority of the M13 viral coat is formed by the major coat protein p8 which provides a surface with regularly spaced amines that can be functionalized. In the preparation of M13-biotin, these amines were reacted with TFP-PEG$_{12}$-biotin. From literature data, the positioning of each p8 subunit can be approximated as stacks of planes, each with five subunits positioned and rotated ~36° between planes with spacing of 1.66 nm between each plane (**Figure 3.27A**)(Morag et al. 2015). This information gives one an approximate idea of the expected spacing of TFP-PEG$_{12}$-biotin reacted to p8. Knowledge of the symmetry of the subunits therefore gives an indication of how the biotin moieties

might be spaced in assembled M13, and where SA might bind. Down the length of the bacteriophage, one can estimate that the approximate spacing between subunit functional groups is about 3.3 nm (**Figure 26B**). Therefore, binding of SA (recall, 6 nm diameter sphere), would block binding of SA to a directly adjacent p8 subunit, however, it would permit binding to the next subunit. This enables a prediction of what the spacing of SA on the bacteriophage coat might look like and how they might be spaced. This information will be useful to draw on when interpreting the TEM data.

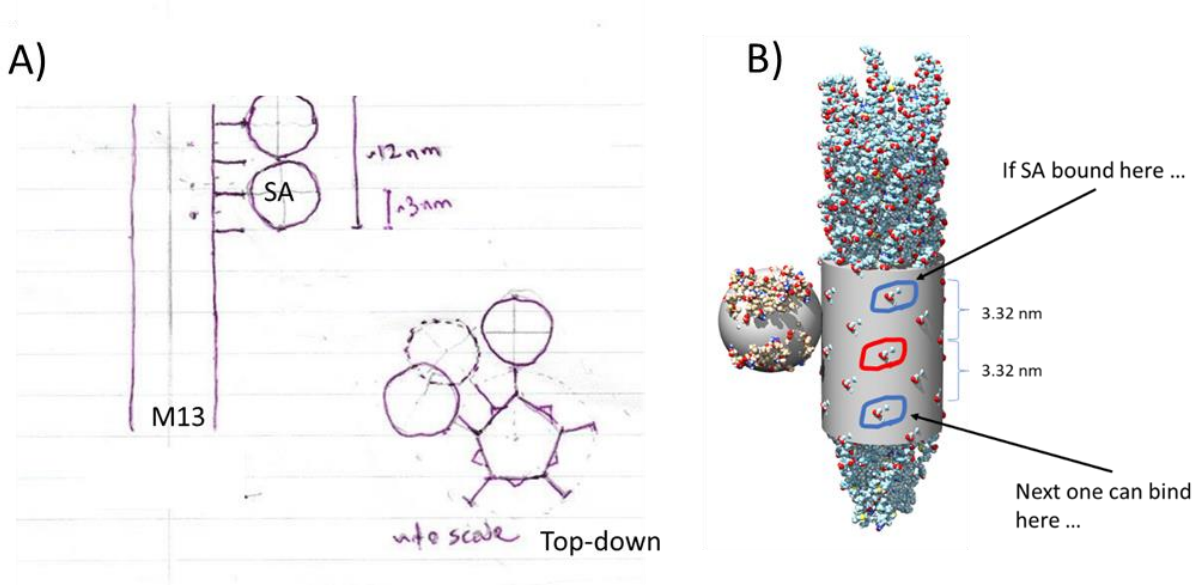

Figure 3.27: Estimating the probable spacing of PEG_{12}-biotin moieties reacted to M13 p8 viral coat proteins. A) Schematic highlighting the approximate spacing and symmetry of p8 subunit and how bound SA might be oriented. B) Diagram showing possible spacing of SA on the surface of M13 and how many adjacent subunits of p8 might be blocked.

First, M13-PEG_{12}-biotin on its own was analyzed by TEM to obtain a baseline diameter that could be later compared to the samples complexed with $SA(BXN)_3$. M13-PEG_{12}-biotin was adhered to TEM grids and stained with PTA as a negative stain (**Figure 3.28**). The diameters at multiple points along the length of multiple M13 were chosen and manually measured using image analysis tools. From these measurements, a histogram was prepared showing the distribution of measured diameters (**Figure 3.29**). The estimated mean diameter of M13-PEG_{12}-biotin was 7.6 nm. This was slightly higher than typical literature estimates of M13 diameter which are around 6 – 6.5 nm (Cao, Xu, and Mao 2011; D. Marvin 1998). The slightly expanded diameter measured might be from the attached PEG_{12} molecules

forming a zone that somewhat excludes the PTA heavy metal negative stain. Regardless, this gave a baseline measure of diameter with which to compare M13 complexed with SA.

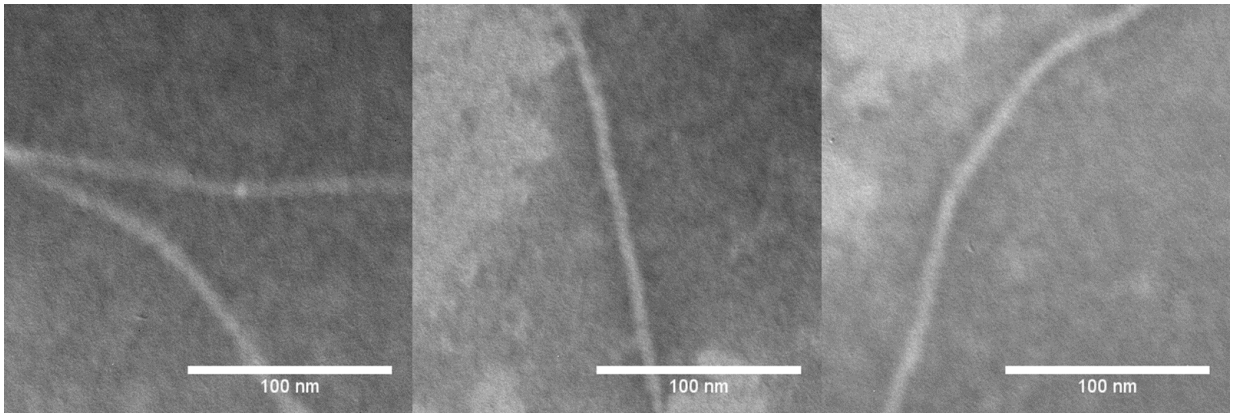

Figure 3.28: Representative TEM images of M13-PEG$_{12}$-biotin negatively stained with 1% phosphotungstic acid (PTA).

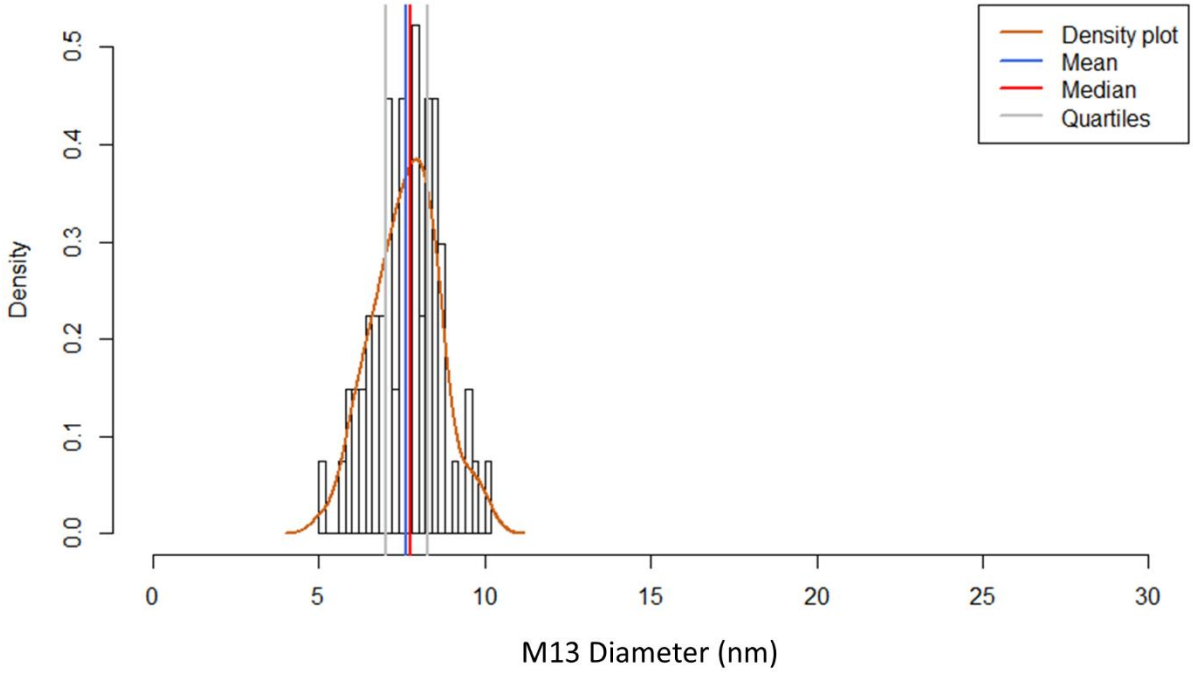

Figure 3.29: Histogram with density plot of M13-PEG$_{12}$-biotin diameters estimated from TEM images. Estimated using ImageJ image analysis software (n = 67).

A good test of the predicted spacing of SA based on the above discussion regarding the M13 major coat protein geometry is to use a monovalent SA (single biotin-binding site) and observe the apparent packing of SA by TEM. In this case, the monovalent SA was the SA(BXN)$_3$ prepared in **Section 3.3.2.3**. Here are the results from complexing M13-PEG$_{12}$-biotin with SA(BXN)$_3$ collected

from IEC. In this discussion, the spacing and apparent packing of the SA molecules are noted, measured and compared to the expected spacing based on the theoretical estimate of optimal packing discussed above. Two main variations of this experiment were done: one with excess $SA(BXN)_3$ added and a second experiment with slightly less than a stoichiometric amount of $SA(BXN)_3$ compared to the total amount of p8 subunits present.

First, M13-PEG_{12}-biotin with an excess of added $SA(BXN)_3$ was imaged by TEM. M13-PEG_{12}-biotin at 1.2 μM p8 subunits was incubated with 2 μM $SA(BXN)_3$ prepared from IEC. The diameter of M13-biotin incubated with excess $SA(BXN)_3$ was visibly thicker than M13-PEG_{12}-biotin on its own (**Figure 3.30**). The bound SA gave the surface of the bacteriophage a bumpy appearance, as the phages appeared to be almost uniformly coated with $SA(BXN)_3$. Once again, the diameter of M13-PEG_{12}-biotin with bound $SA(BXN)_3$ was measured at multiple points along the length of imaged phages to compare with the expected diameter increase for M13 with bound SA. This was once again represented as a histogram of diameter measurements (**Figure 3.31**). The mean diameter of these phages estimated by image analysis was 16.4 nm from 390 observations. This was slightly lower than the predicted diameter which would have been 19 nm based on the approximate shapes laid side-by-side (7 nm for M13, 6 nm for SA; **Figure 3.26**). However, SA is not perfectly spherical and the estimate above of 6 nm may overestimate the true diameter along some of the axes of SA. Overall the observations were reasonably consistent with the expected diameter increase from SA bound to either side of M13.

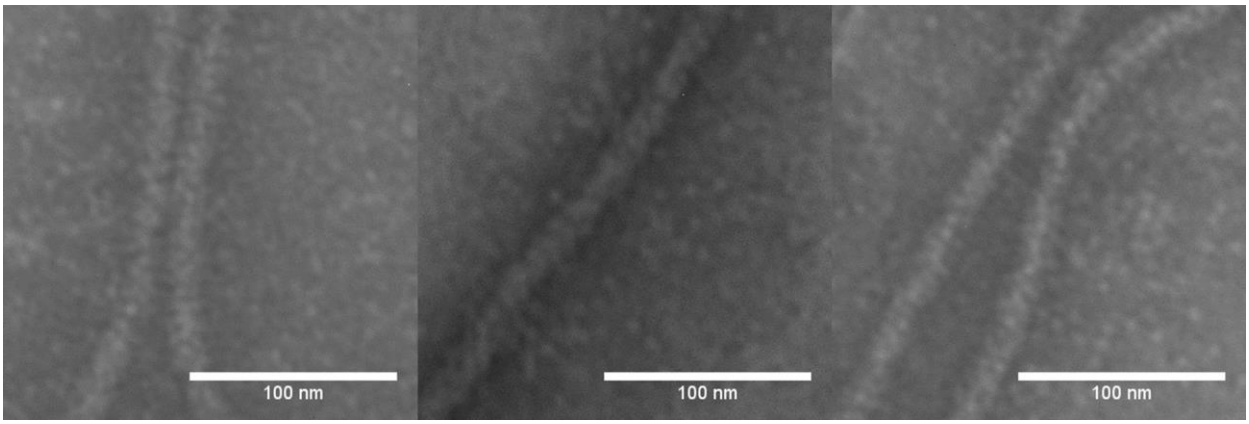

Figure 3.30: Representative TEM images of M13-PEG$_{12}$-biotin and bound SA(BXN)$_3$ negatively stained with 1% PTA. M13 complexes were prepared at a p8:SA(BXN)$_3$ ratio of 1:2.

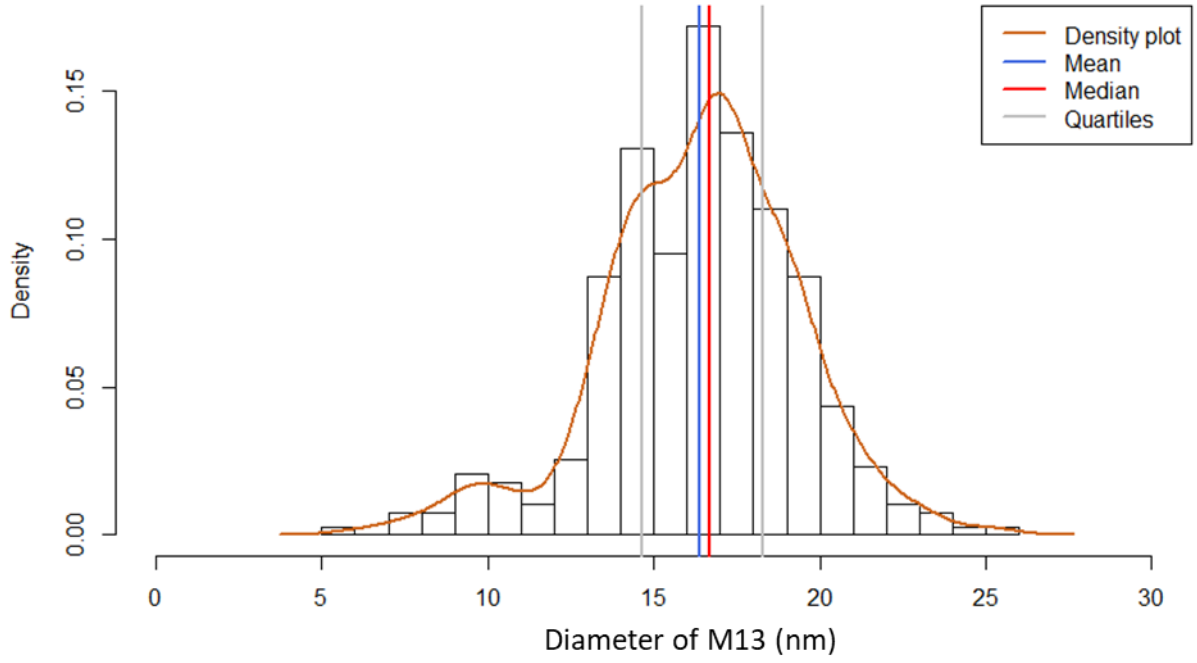

Figure 3.31: Histogram with density plot of M13 complex (M13-PEG$_{12}$-biotin mixed with SA(BXN)$_3$ at a ratio of 1:2 p8:SA(BXN)$_3$) diameters estimated from TEM images. Estimated using ImageJ image analysis software (n = 390).

Secondly, M13-biotin incubated with a nearly stoichiometric amount of SA(BXN)$_3$ was also imaged. There was greater variation in the diameter of these M13 phages, though they were still clearly of a greater thickness than M13-PEG$_{12}$-biotin on its own (**Figure 3.32**). The diameters were measured at various points along the length of phages and showed two populations of phage widths (**Figure 3.33**). The histogram density plot showed one population with a mean around 16 nm, and another

population around 11 nm (106 observations). The wider diameter population, as seen above, likely corresponded to M13-biotin with SA bound on both sides. The smaller width population likely corresponded to areas where SA was bound on only one side of the phage.

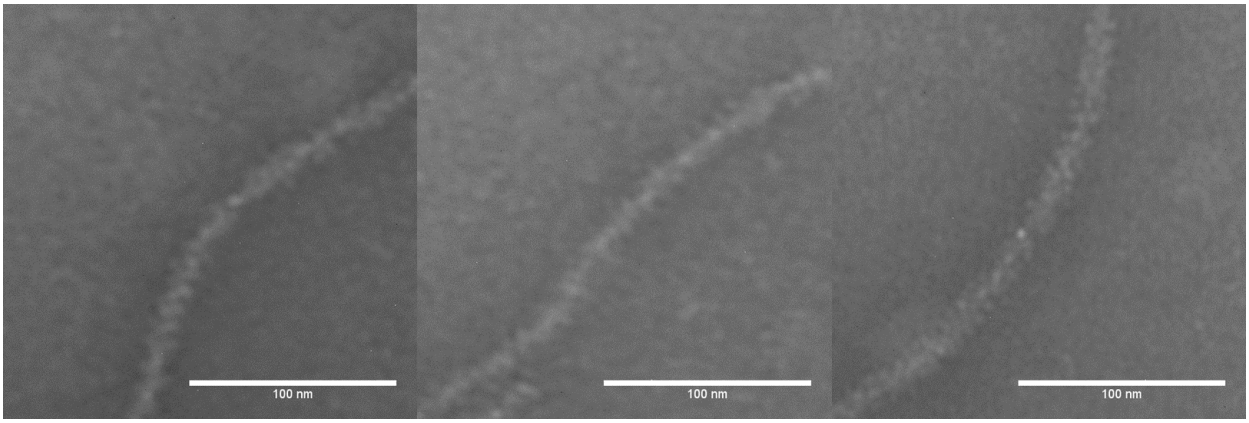

Figure 3.32: Representative TEM images of M13-PEG$_{12}$-biotin and bound SA(BXN)$_3$ negatively stained with 1% PTA. M13 complexes were prepared at a p8:SA(BXN)$_3$ ratio of 1:1.

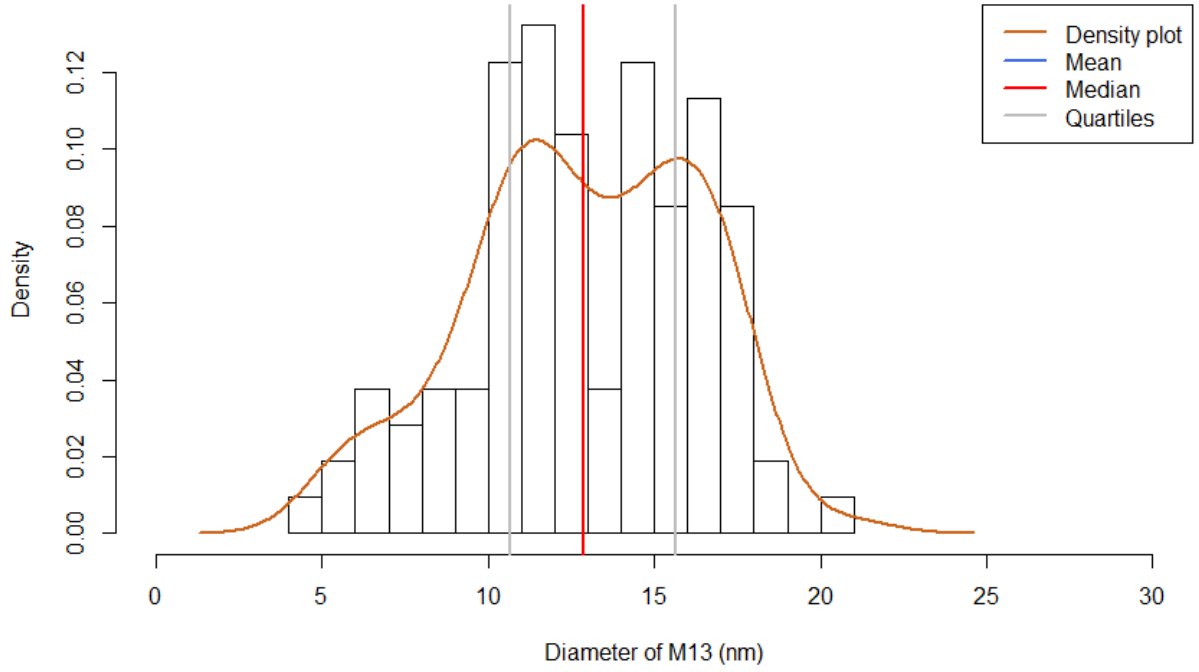

Figure 3.33: Histogram with density plot of M13 complex (M13-PEG$_{12}$-biotin mixed with SA(BXN)$_3$ at a ratio of 1:1 p8:SA(BXN)$_3$) diameters estimated from TEM images. Estimated using ImageJ image analysis software (n = 106).

Lastly, since the quality of the TEM data was good enough to resolve individual SA tetramers, a comparison was made to the SA packing model proposed at the start of this section. Where the SA molecules were well-resolved on M13, one gets a good impression of the well-ordered spacing between adjacent SA (**Figure 3.34A**). In particular, it was possible to measure the end-to-end distance of individually resolved, adjacent SA molecules to compare with what would be expected for optimal packing. After measuring this distance multiple times, the mean end-to-end distance of adjacent SA molecules was about 12.4 nm (**Figure 3.34B**). The range of these measurements was consistent with the predicted spacing of SA where each bound SA blocked binding to the directly adjacent biotin moiety. As the spacing of biotin moieties was estimated to be roughly 3.3 nm and the diameter of SA itself was ~6 nm, each SA along the length of the phage should be packed almost directly against its neighbor, as observed.

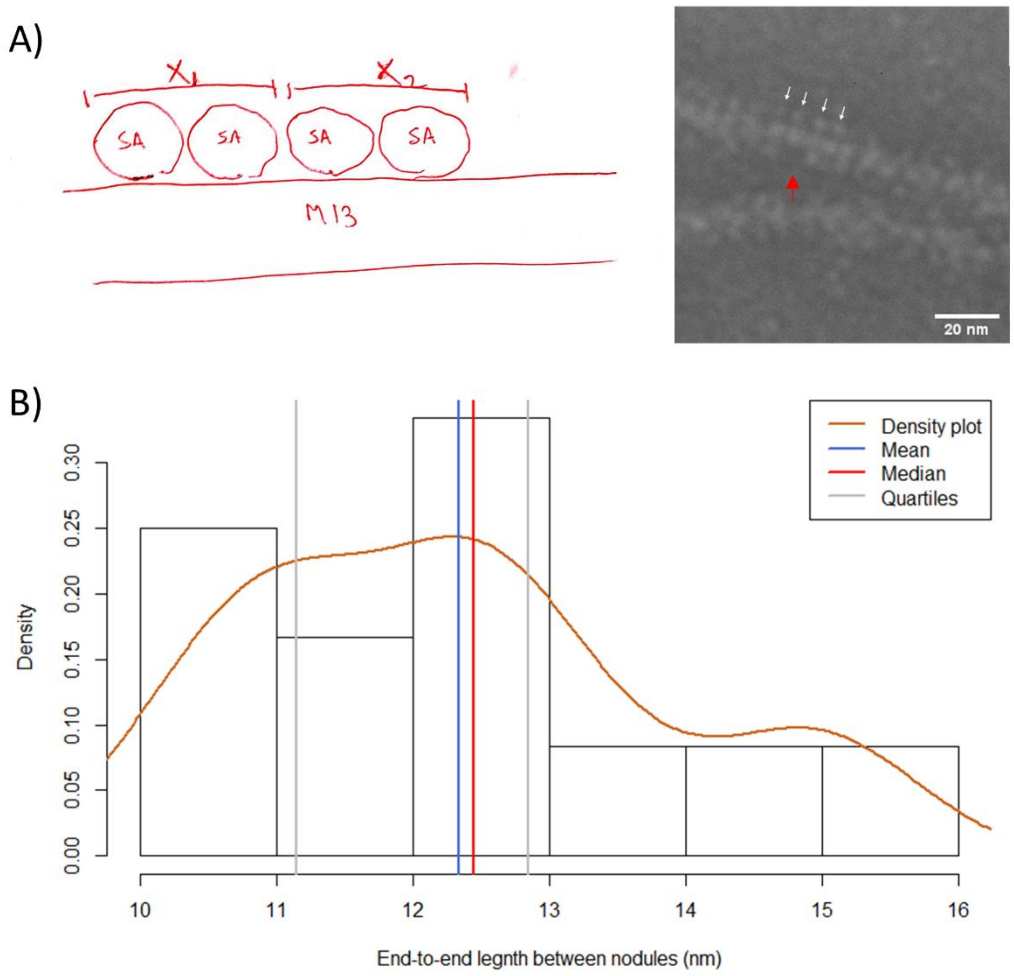

Figure 3.34: Determining approximate longitudinal spacing of SA tetramers packed on M13-PEG$_{12}$-biotin. A) Schematic showing how distance was measured: end-to-end distance of adjacent SA tetramers. B) Examples of areas of ordered SA(BXN)$_3$ on M13-PEG$_{12}$-biotin (TEM, 1% PTA negative stain). White arrows point to individual SA tetramers; red arrow points to gap in SA packing. C) Histogram with density plot longitudinal end-to-end distances of adjacent SA tetramers (n = 12).

To better explain this, the potential packing arrangement observed was modeled coarsely in 3D. The model was built using the measurements made from structural data on M13 p8 symmetry (Morag et al. 2015). In particular, based on the authors' explanation of p8 symmetry, 6 nm spheres were arranged with 5-fold symmetry around a 7 nm cylinder (**Figure 3.35A**). Three stacks of rings with 5-fold symmetry were shown to give an idea of how such dense packing may be possible. For comparison, a well-resolved section of SA(BXN)$_3$ loaded M13 is shown as well, showing a packing pattern of SA reminiscent of the 3D model (**Figure 3.35B**). As a single adjacent site for SA binding appears to be occluded when a single SA binds, the optimal loading density appears to be ~1 SA for

every 2 p8 subunits – giving a possible loading of ~1350 SA per M13. This would be one of the highest loading capacities observed for binding of a protein onto an M13 scaffold thus far. For reference, SA loaded with GFP was estimated to have a theoretical maximal loading of 385 GFP/M13, with ~91 GFP/M13 actually measured (Hess et al. 2012). As the GFP was reacted to M13 enzymatically (using sortase), there could conceivable be steric limitations for reaction with the enzyme. Given that the M13-biotin scaffold used here was not uniformly biotinylated, the actual loading would likely be lower than the estimated 1 SA per 2 p8. In the TEM images; this was observed as the occasional "missing SA" in an otherwise densely packed phage (see red arrow in **Figure 3.34**). Regardless, these experiments were able to give a semi-stochastic snapshot of how these SA are loaded onto biotinylated M13 scaffolds.

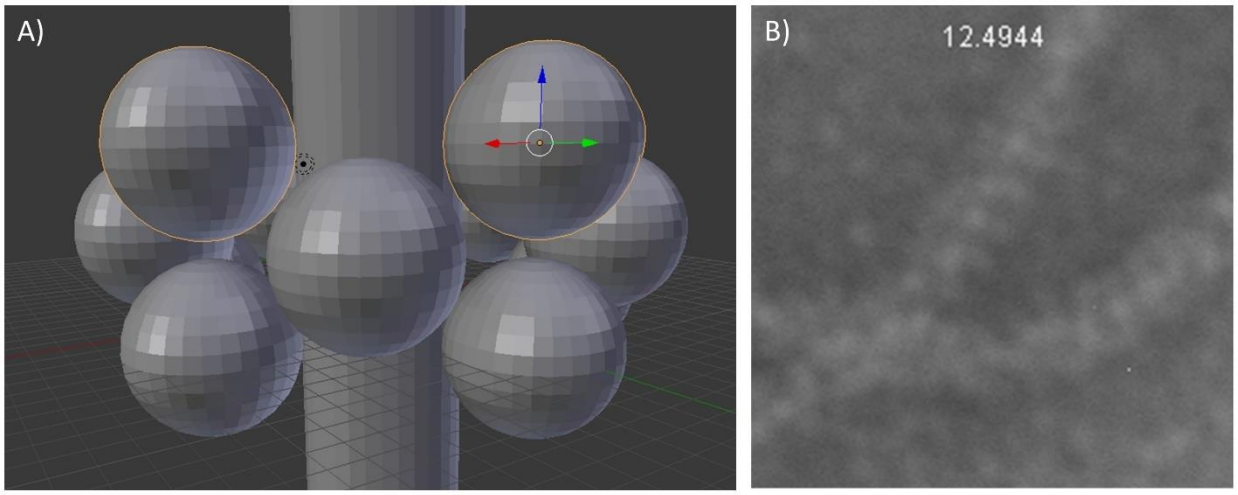

Figure 3.35: Visualizing the possible packing of SA tetramers onto the surface of M13-biotin. A) A 3D model of 15 spheres (d = 6 units) stacked in three layers (5 spheres per layer) with 5-fold symmetry around a cylinder (7 units). Each layer is spaced 3.3 units and rotated 36° to roughly represent symmetry of p8 coat proteins highlighted in figure 3.27. B) TEM image showing highly ordered packing of SA(BXN)$_3$ on M13-PEG$_{12}$-biotin (stained with 1% PTA).

In summary, the packing of monovalent SA onto biotinylated M13 was assessed by TEM. From the TEM observations, loading of monovalent SA onto biotinylated M13 occurred very efficiently. The resulting complexes were anticipated to have ~3 NTA moieties per SA for a maximum of ~4000 NTA per M13. This was expected to be particularly useful for further complexation to His-tagged protein using the Co(III)-mediated approach (Wegner and Spatz 2013). In the following section, some of the efforts to detect complexed Cel8A using this approach will be presented.

3.3.3.2 *Further complexation of Cel8A with M13/SA(NTA)$_3$ scaffold*

After demonstrating that SA(BXN)$_3$ could be uniformly bound to M13-PEG$_{12}$-biotin to prepare an NTA-bearing nanoscale scaffold, further complexation was tested. Initially this was done by negative staining of TEM grids with PTA as done in the previous section; however, any differences in diameter of M13 complexes were not easily observed. An immuno-gold labelling approach was devised to attempt to detect Cel8A complexed to the phage. Lastly, some considerations regarding the kinetics and expected equilibrium kinetics of Cel8A bound to NTA via coordination complex with Co(II) will be discussed.

Binding of His6-tagged Cel8A was initially assessed by negatively stained TEM to see if there might be a noticeable diameter increase from the binding of Cel8A. SA(BXN)$_3$ was bound to M13-biotin as done in the previous section. These were subsequently incubated with a stoichiometric amount of Co(II), and 3 Cel8A for every SA(BXN)$_3$. The complexes were oxidized for 10 min with 10 mM H_2O_2. These samples were adhered to TEM grids and negatively stained with PTA. Under these conditions, the M13 complexes looked very similar to the M13 bound to SA(BXN)$_3$ in the previous section (**Figure 3.36**). The adhered layer of protein appeared uniformly wide with few obvious "bulges" or nodules that might indicate the presence of bound Cel8A (expected diameter of cellulase domain is ~5 nm based on the crystal structure). Overall, multiple measures of the diameter of these samples were consistent with the width of M13 with SA(BXN)$_3$ bound (**Figure 3.37**). The mean diameter was measured to be 15.4 nm – consistent with the diameter of the M13/ SA(BXN)$_3$ without any added Cel8A. Given the infrequent occurrence of irregularities along the length of the phages, it would be questionable to try and assign them as complexed Cel8A. Therefore, alternate means would be necessary to confirm that Cel8A was present associated with the coat of M13.

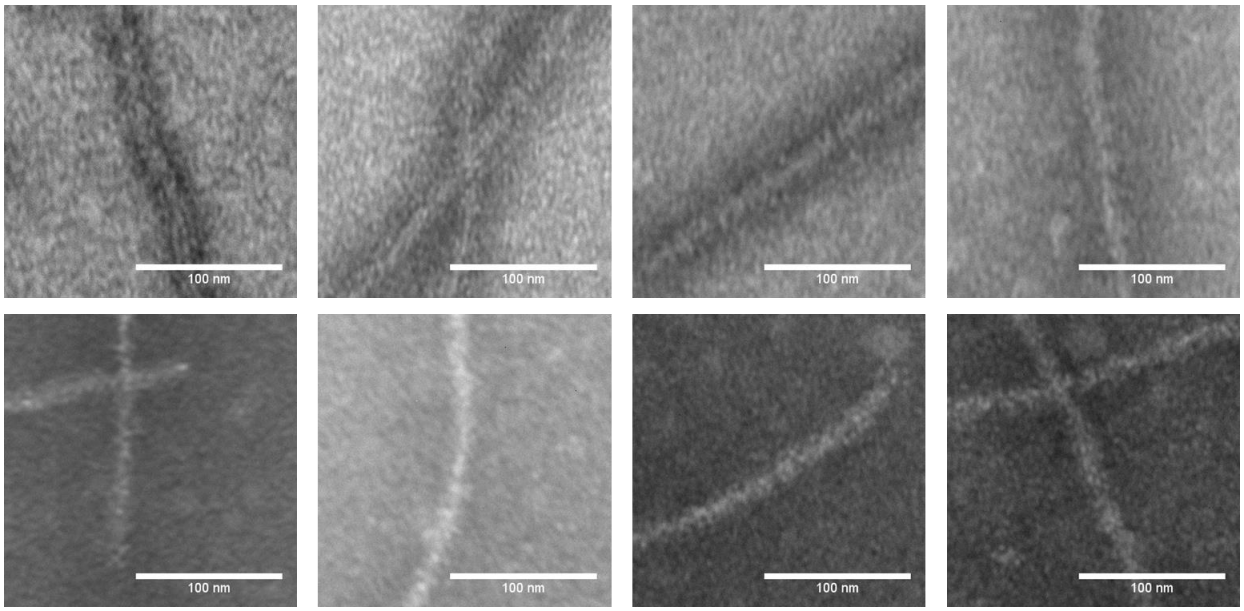

Figure 3.36: Representative TEM images of M13-PEG$_{12}$-biotin (1 µM p8) and bound 1 µM SA(BXN)$_3$ reacted to 3 µM Cel8A via Co(III)-mediated approach. Negatively stained with 1% PTA. The panels show different phage particles from the same TEM grid.

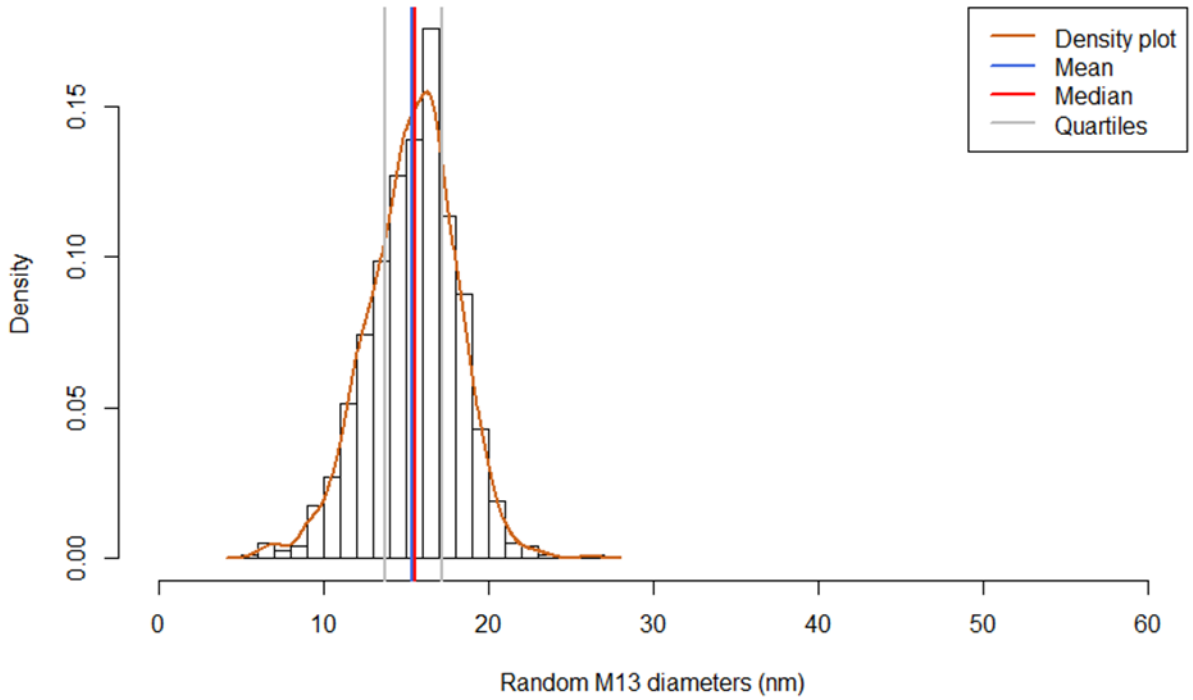

Figure 3.37: Histogram with density plot of M13 Cel8A complex (M13-PEG$_{12}$-biotin (1 µM p8) and bound 1 µM SA(BXN)$_3$ reacted to 3 µM Cel8A via Co(III)-mediated approach) diameters estimated from TEM images. Estimated using ImageJ image analysis software (n = 740).

To identify whether any Cel8A was associated with the M13 scaffold under the Co(III)-mediated complexation conditions, immunostaining for TEM was attempted. A hapten was selected with which Cel8A would be modified and then bound with an appropriate antibody. Then, a secondary antibody conjugated to a 5 nm gold nanoparticle (**GNP**) was added to visualize Cel8A by TEM. TAMRA was selected initially, as Cel8A could be modified and then quantified easily by absorbance spectroscopy to confirm it was labelled efficiency (**Figure 3.38A**). Labelling of Cel8A with NHS-TAMRA as described in the Methods resulted in a labelling efficiency of 97%.

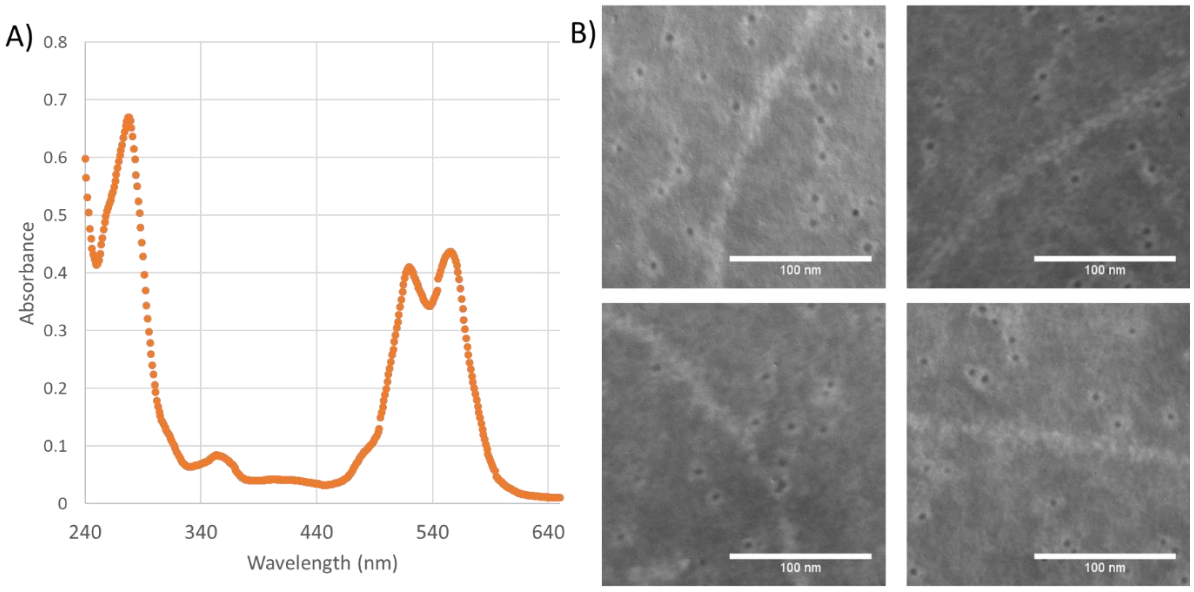

Figure 3.38: Anti-TAMRA detection of Cel8A-TAMRA bound to M13-SA(NTA) scaffold. A) Absorbance spectrum of 80 µM Cel8A-TAMRA reacted to 5-fold NHS-TAMRA for 3 h at 23 °C. B) Representative TEM images of M13-PEG$_{12}$-biotin (1 µM p8) and bound 1 µM SA(BXN)$_3$ reacted to 3 µM Cel8A-TAMRA via Co(III)-mediated approach. Immunolabelled with anti-TAMRA primary antibody and 5 nm GNP-conjugated secondary antibody and negatively stained with 1% PTA. The panels show different phage particles from the same TEM grid.

Overall, this approach failed due to the high background from 5 nm GNPs bound to the grid. The M13 had a thickened width from the binding of SA(BXN)$_3$ and could be clearly observed (**Figure 3.38B**). However, the selectivity of the immunogold labelling method was poor as the secondary antibody GNPs could be observed spread throughout the grid. Additionally, the GNPs were only rarely imaged in the vicinity of M13 making it difficult to ascertain whether it was by chance or specific

binding of the primary antibody to Cel8A-TAMRA. In order to draw conclusions, the background noise needed to be reduced.

Several controls were carried out to determine the reason for the high background and reduce it. First, the immunostaining procedure was done with M13-PEG_{12}-biotin on its own to determine the extent to which there was non-specific binding of either the primary or secondary antibody. There was little non-specific binding of the GNPs on the grid (**Figure 3.39A**). From this it was apparent that the 0.1% BSA was adequate to block non-specific binding of the antibodies or coated GNPs. Overall, non-specific binding of the antibody to the grid after blocking was unlikely the reason for the high background. Additionally, a positive control using M13 covalently labelled with NHS-TAMRA was stained using the same protocol (**Figure 3.39B**). The immunolabelling protocol was clearly identified the dye covalently labeled to the phage showing the antibody pair was indeed capable of specifically binding to TAMRA reacted to biomolecules.

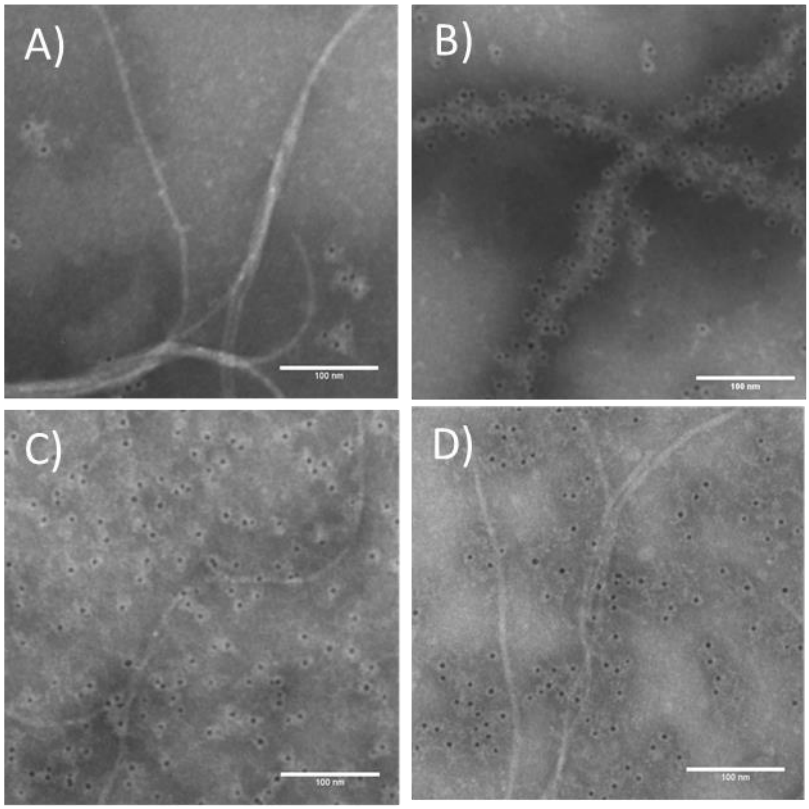

Figure 3.39: Representative TEM images of anti-TAMRA immunolabelling protocol troubleshooting. A) M13-PEG$_{12}$-biotin negative control. B) M13 covalently labelled with NHS-TAMRA. C) M13-PEG$_{12}$-biotin first added to the grid. Following a blocking step with 0.1% BSA, Cel8A-TAMRA (with 0.1% BSA) was added to grid for 30 min. D) M13-PEG$_{12}$-biotin was first added to the grid. Following a blocking step with 0.1% BSA, TAMRA-COO$^-$ (with 0.1% BSA) was added to grid for 30 min. TEM samples adhered to grids as indicated were immunolabelled with anti-TAMRA primary antibody and 5 nm GNP-conjugated secondary antibody and negatively stained with 1% PTA.

A change to the immunostaining protocol was made to account for the possibility that the high background came from Cel8A-TAMRA adsorbed to the grid prior to blocking and staining. The grid was incubated with M13-biotin first, blocked with 0.1% BSA, then incubated with Cel8A-TAMRA and finally subjected to the immunostaining protocol. M13 could be observed here at a width consistent with naked M13 (no coat of SA present; **Figure 3.39C**). There was a heavy background of GNPs observed here despite first blocking the grid with BSA before adding Cel8A-TAMRA. This blocking step should have prevented the non-specific binding of Cel8A, but clearly some non-specific interaction of Cel8A-TAMRA with the grid was possible.

An alternative possibility is that there was some free TAMRA present in the Cel8A-TAMRA preparation. While the Cel8A-TAMRA was extensively dialyzed, TAMRA is quite hydrophobic and its

removal may not have been complete. Consider a 3 μM TAMRA-Cel8A solution: even if one assumes 1% unreacted TAMRA that was not adequately removed by dialysis, that would result in ~30 nM free dye. Any unreacted TAMRA present in the preparation may in fact be quite significant. To test this, the grids were first incubated with M13, blocked with BSA and then incubated with a 30 nM TAMRA-COO^- prior to immunostaining. There was considerable background from including the grid with as little as 30 nM TAMRA-COO^- (**Figure 3.39D**). When imaged by TEM, the secondary antibody GNPs showed up ubiquitously.

It seems apparent that non-specific binding of the dye molecule itself was the issue with this approach. It is possible that unreacted TAMRA binds first to the layer of BSA on the grid, and then primary antibody is binding to that. There are known interactions between hydrophobic dyes and BSA where a specific binding between the two components can be measured (Jameson et al. 2016). BSA has several high-affinity binding sites for anionic lipids which might also bind dye molecules (Kragh-Hansen et al. 2001). The exact number of detergent binding sites depends on the nature of the hydrophobic molecule that interacts with BSA. A dye related to TAMRA, rhodamine B (which has 4 ethyl groups rather than 4 methyl groups) has specific binding to a particular detergent binding site on BSA (Cai et al. 2010). The hydrophobic properties of certain fluorescent dyes are a known potential problem in experiments that rely on stochastic measurement, such as single molecule tracking experiments (Zanetti-Domingues et al. 2013). Thus, TAMRA as a hapten molecule to use in immunostaining procedures should be carefully considered as it was observed here to result in considerable background noise. An alternate primary/secondary antibody pair would have been a possible solution; however, the Co(III)-mediated approach to complex Cel8A to the M13 scaffold was not pursued further for the reasons highlighted below.

Despite the high efficiency of loading $SA(BXN)_3$ onto M13-biotin, the subsequent loading step of His-tagged protein would likely not be efficient enough. In particular, a key part of this strategy was the oxidation of Co(II) to Co(III) to form a stable complex with a slow off-rate (Wegner and Spatz

2013). Prior to oxidation there must be complexation of Co(II), NTA and the His-tagged protein. Unfortunately, the interaction between NTA:Co(II) and His6 peptides is weak – the association constant (K_a) is about 2290 M^{-1} (Mehlenbacher et al. 2015). Using this K_a, the amounts of NTA:Co(II):Cel8A expected to form under typical conditions tested were modelled with a simple protein ligand binding equilibrium (**Figure 3.40**). Specifically, the concentration of NTA (found in $SA(BXN)_3$) was set to 3 µM and the amounts of complex that would be expected to form at a range of Cel8A concentrations were calculated. For the typical conditions used in preparing samples for TEM, 3 µM Cel8A was used. In the model, only ~1 % of the NTA present on M13 would be expected to be complexed under these conditions and was consistent with the lack of obvious change to the width of M13 complexes in the TEM images.

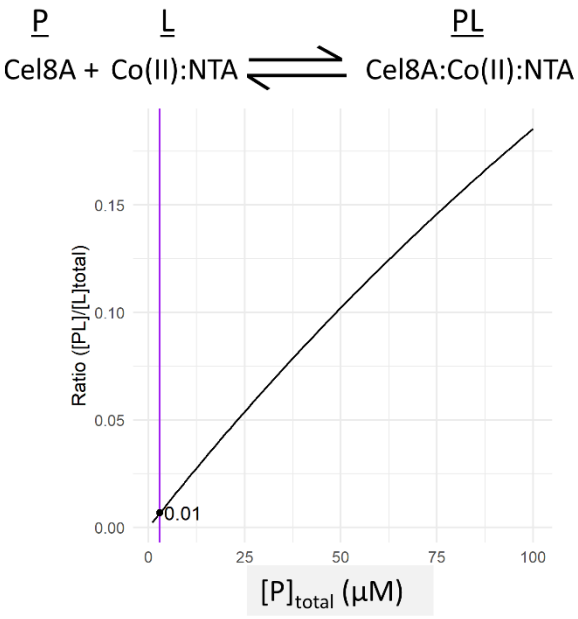

Figure 3.40: Simulated binding equilibria between Cel8A and Co(II):BXN at a range of Cel8A concentrations. Co(II):BXN was treated as a single component due to its presumed tight binding (k_D = 4 x 10^{-11} M for Co(II) and NTA (Anderegg 2009)). The simulation assumed a [L] = 3 µM and association constant of 2290 M^{-1} (from (Mehlenbacher et al. 2015)). The purple line indicates typical concentrations of Cel8A used for preparing Cel8A bound to SA(BXN)-coated M13 (3 µM).

Due to the weak association constant expected for Co(II), a very large excess of Cel8A would be necessary to load appreciable amounts of the enzyme on the M13-$SA(BXN)_3$ scaffold. This was not ideal from a modularity and applicability point of view, as this would necessitate further purification after complexation. While this is not a problem from the point of view of characterizing the system, in

developing a nanoscale scaffold with broad applicability, the low efficiency of this step would reduce the potential utility of this platform.

3.4 Conclusions

It became apparent that efficient interactions would be necessary at each step in order to prepare a nanoscale scaffold densely loaded with a particular protein of interest. Consider that one of the big advantages of using a viral scaffold is the exact and reproducible positioning of functional groups with known and predictable symmetry. This was seen with the efficient loading of $SA(BXN)_3$ onto M13-biotin – the SA was positioned with regular and dense packing, following the symmetry of p8 subunit packing. The subsequent complexation of His-tagged protein and NTA:Co(II) was unfortunately not efficient and by utilizing an interaction that results in poor coverage of the phage scaffold, the platform is not being used to its greatest advantage. In the ideal case there would be near complete complexation, producing a multi-enzyme construct with precisely positioned enzymes, ready for characterization.

There may however be modifications to this approach that may improve the efficiency of the His6-protein loading step. The standard NTA:Ni(II) interaction with a His6-tagged protein has a dissociation constant of around 10 μM (Bartoschik et al. 2018). While better than the interaction with Co(II), this would still be unlikely to produce an efficiently loaded, multi-enzyme construct. Several groups have developed modified NTA analogues with either improved binding with His-tagged proteins, or cleverly make use of a subsequent covalent reaction with the His-tagged protein (**Figure 3.41**). In one example of this, the NTA reagent is photo-reactive – after complexation, exposing the complex to light results in covalent reaction with the probe of interest (Hintersteiner et al. 2008). In a second example, an NTA analogue with a reactive tosyl group was observed to react over the course of 12 h only with protein containing a His-tag (Uchinomiya et al. 2009). It was thought that the nearby coordinated Ni(II) enhanced the reaction with the tosyl group.

A different type of analogue is an NTA variant with tighter binding through avidity effects. This molecule had three NTA moieties, and resulted in a noncovalent interaction with a <1 nM dissociation constant (Lata et al. 2006). While this would be a non-covalent interaction, the enhanced binding from avidity affects would be expected to make interaction with the resulting M13 scaffold much more efficient and long-lived (Vauquelin and Charlton 2013). In particular, the use of a biotinylated tris-NTA would likely be an improvement over the design used here, by virtue of its low dissociation constant with His-tagged proteins and potential to interface with SA (Reichel et al. 2007). These potential improvements would be more likely to result in a generalized approach to binding His-tagged proteins to a M13 scaffold that could be carried out more efficiently.

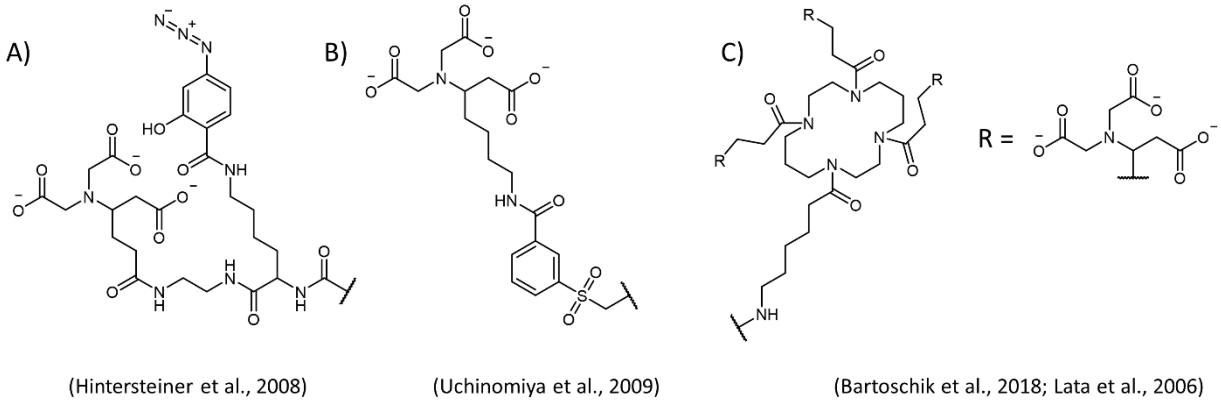

Figure 3.41: NTA-based molecules for forming A, B) covalent and C) non-covalent interactions with oligo-His-tags on proteins. A) Photoreactive NTA analogue (Hintersteiner et al. 2008). B) Reactive NTA analogue mediated by proximity of chelated Ni(II) (Uchinomiya et al. 2009). C) Tris-NTA with improved binding from avidity effects (Bartoschik et al. 2018).

In characterizing the SA(BXN:Co(II):Cel8A) complexes by SEC, a biotinylated Cel8A was used as a positive control to aid in interpreting the chromatograms. It was apparent from the shift to increased mass and subsequent disappearance of the SA peak that complexation occurred very well. Also, from TEM analysis of SA bound to M13-biotin, it was found that SA packed efficiently onto the surface of M13. The size of SA matched well with the anticipated spacing of biotin moieties on M13-biotin. Thus, given the efficient binding of SA to M13-biotin and apparent efficient binding of Cel8A-biotin to SA, the use of directly biotinylated enzymes bound to M13 via a SA adaptor molecule was pursued as a follow-up strategy.

Chapter 4 Multi-enzyme assembly using streptavidin as an adaptor molecule for biotinylated proteins

4.1 Introduction

Given the positive results seen when using Cel8A covalently biotinylated with TFP-PEG_{12}-biotin as a positive control in **Chapter 3**, it became apparent that it would be more efficient to bind Cel8A-biotin directly to SA. When used as a positive control in troubleshooting the His-tag mediated approach, complexation was particularly clear. In the following section, methodologies to prepare complexes of biotinylated protein onto M13 using SA as an adaptor molecule will be discussed.

First, in order to aid the interpretation of results, Cel8A-biotin was characterized by a fluorescence-based assay, to assess the extent of biotinylation, and mass spectrometry, to assess the distribution of Cel8A-biotin species present (**Figure 4.1**). Given the multivalent nature of the components, M13-biotin (maximum of 2700 biotin) and SA (four ligand binding sites), there was the potential for the formation of aggregates without defined control of the positioning of components – the methods were designed such that loading of enzyme could be done in a controllable manner while reducing random aggregation. Two different approaches were taken to prepare the complexes: 1) Cel8A-biotin was complexed with SA to form a mixture of $SA(Cel8A\text{-}biotin)_N$ complexes with some free biotin-binding sites to allow complexation to M13-biotin in a second step, and 2) M13 with a coating of SA (**SA-coated M13**) was pre-formed in an initial step, and complexation of Cel8A-biotin was done in a second step.

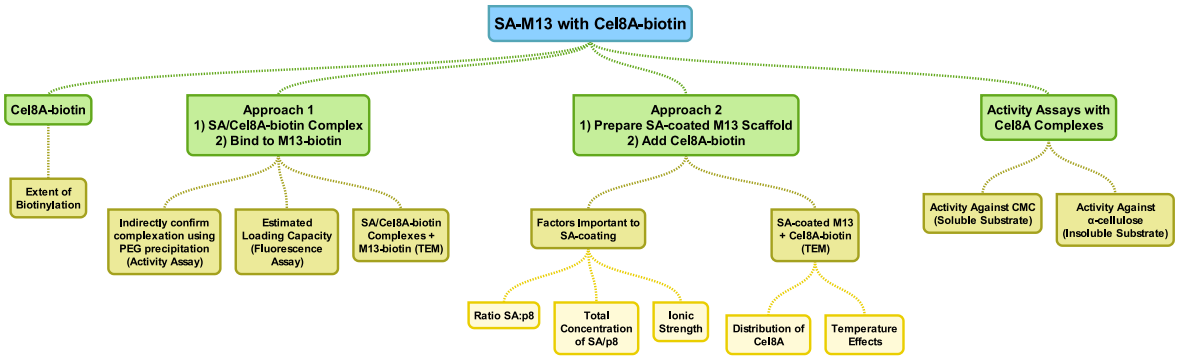

Figure 4.1: Chapter topic overview for the formation of Cel8A multienzyme complexes on M13 using SA as an adaptor molecule. The topics in the mind map diagram will be presented in order from left-to-right.

From experimentation with SA/Cel8A-biotin complexes in **Section 3.3.2,** it was apparent that SEC would be incapable of isolating SA/Cel8A-biotin with defined stoichiometry. Therefore, an approach using an ensemble of SA/Cel8A-biotin species with average stoichiometry determined by the ratio of SA and Cel8A-biotin used was first tested. This ensemble of SA/Cel8A-biotin species would then be mixed with M13-biotin to form a nanoscale arrangement of the Cel8A components on M13 (**Figure 4.2**). As discussed in **Section 3.3.1.1**, directly binding biotin to SA can result in a distribution that is skewed toward fully bound and full unoccupied SA(biotin) species. Therefore, desthiobiotin-saturated SA was used throughout this section to slow the binding of biotin to SA when mixing Cel8A-biotin species to SA. The ratios of SA and Cel8A-biotin should furthermore be prepared in such a way that on average SA(Cel8A-biotin) species have some free biotin-binding sites for further complexation onto M13-biotin. A fluorescence assay utilizing B4F was devised to indirectly monitor the complexation of SA(Cel8A-biotin) species onto M13-biotin.

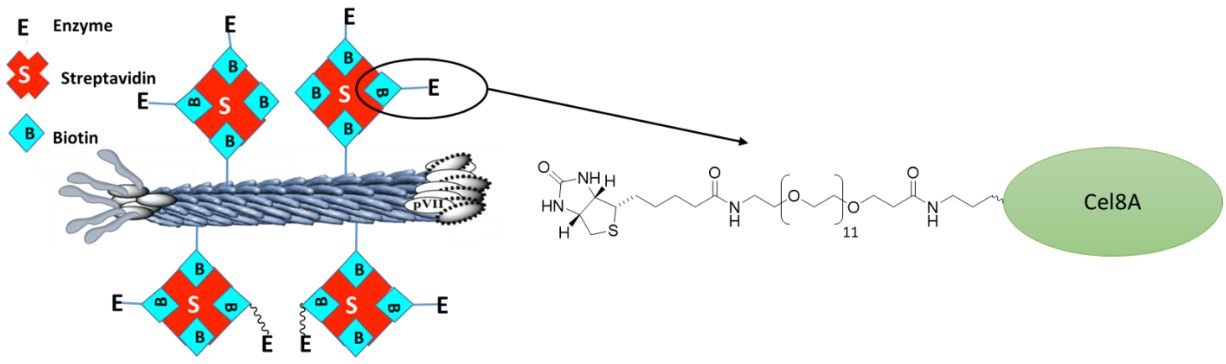

Figure 4.2: Schematic representation of multi-enzyme complex assembly using biotinylated enzyme and SA as an adaptor molecule.

For the second approach, where M13-biotin was first coated with SA, it was found that there were certain conditions under which SA and M13-biotin could be mixed without unwanted crosslinking and aggregation. The different conditions for preparing SA-coated M13 were assessed by TEM and will be discussed first, followed by the results of further complexation of SA-coated M13 with Cel8A-biotin. Additionally, factors that impacted the stability of the formed complexes on M13 will be presented. In the last section, the results of activity assays against cellulosic substrates utilizing the formed M13/Cel8A complexes will be shown. In some of these assays, a cellulose binding module-cohesin fusion protein (**CBM-Coh**) was included to bind to the free dockerin domains of Cel8A to furthermore add a targeting component to the assembled complexes.

4.2 Materials and methods

4.2.1 General

SA (>95% purity according to the supplier; Cedarlane, Burlington, Canada) was supplied as a lyophilized protein (from 10 mM potassium phosphate buffer pH 6.5) and was resuspended up to 5 mg/mL in MQH_2O. The concentration of SA was determined by its estimated monomer extinction coefficient at 280 nm of 41940 M^{-1} cm^{-1} (ProtParam, ExPASy). Low viscosity carboxymethylcellullose (**CMC**) sodium salt (Millipore Sigma, Oakville, Canada) was prepared freshly as a 1% solution (w/v) in

0.1 M sodium citrate pH 5.8 and α-cellulose (Millipore Sigma, Oakville, Canada) was similarly prepared freshly as a 2% (w/v) solution in 0.1 M sodium citrate pH 5.8.

4.2.2 Protein expression and purification

4.2.2.1 *General statement*

Details on purification of the following relevant components can be found in Chapter 3 methods: Cel8A and M13KE.

4.2.2.2 *CBM-Coh expression and purification*

CBM-Coh was expressed from pET28a-ybbR-HIS-CBM-CohI (Addgene plasmid # 58709) from Hermann Gaub (Otten et al. 2014). Briefly, the plasmid was cloned into BL21 *E. coli* which was grown to ~0.8 OD at 37 ºC in LB media with 50 µg/mL kanamycin. Protein expression was induced at 37 ºC with 1 mM IPTG for 3 h, at which point the cells were collected by centrifugation at 5000 *g* for 15 min at 4 ºC.

To cell pellet from 1 L of culture, 30 mL of lysis buffer (25 mM Tris, 137 mM NaCl, 2.7 mM NaCl, 5 mM imidazole) supplemented with 0.5 mM PMSF was added. The resuspended pellet was passed three times through a high-pressure (>10,000 psi) homogenizer to lyse the cells. The lysate was incubated at 60 ºC for 30 min and then centrifuged at 20,000 *g* for 30 min at 4 ºC. The protein was purified by IMAC. The cleared lysate was loaded onto a 1 mL HisTrap™ (GE Healthcare, Chicago, USA), washed with 5 mL of wash buffer (25 mM Tris, 137 mM NaCl, 2.7 mM NaCl, 10 mM imidazole), and eluted over a 5 mL gradient from 5 to 250 mM imidazole. The sample was dialyzed against 50 mM sodium acetate pH 6 using a 12400 Da MWCO dialysis membrane (Millipore Sigma, Oakville, Canada). The purified protein was flash frozen in liquid nitrogen and stored at -80 ºC. CBM-Coh was quantified by measuring its absorbance at 280 nm and using its theoretical extinction coefficient of 48485 M^{-1} cm^{-1} calculated by ProtParam (Gasteiger et al. 2005).

4.2.3 Bioconjugation methods

4.2.3.1 *Preparing Cel8A-PEG$_{12}$-biotin (variable)*

Cel8A was diluted to 110.8 µM in 100 mM sodium phosphate buffer pH 7.46. To this solution, either 110.8, 277, or 554 µM TFP-PEG$_{12}$-biotin was added to initiate the reaction. The total amount of DMSO present in each reaction was 10% (v/v). The reaction was carried out for 18 h at 23 ºC. After reaction, labeled Cel8A samples were dialyzed for a total of three 2 L dialysis exchanges (6 h minimum, 23 ºC) employing 12400 kDa MWCO dialysis tubing (Millipore Sigma, Oakville, Canada) against 1x PBS pH 7.4.

Labelled Cel8A-PEG$_{12}$-biotin samples were prepared for ESI-MS by employing filtration through C18 ZipTips (Millipore Sigma, Oakville, Canada). Sample preparation by spin filtration (with 10 kDa MWCO filters) was unsuccessful, as samples were poorly recovered after several spins, resulting in insufficient material to obtain good spectra. The Cel8A-PEG$_{12}$-biotin samples were at ~60 µM and were spiked to a formic acid (FA) concentration of 0.5% (v/v) prior to binding to the ZipTip. With a pipette set to 10 µL, the tip was aspirated: in 100% ACN 7 times, 0.1% FA 7 times, the sample 15 times, 0.1% FA 7 times (discarding into waste each time), and finally aspirating into 50 µL 1:1 MeOH:H_2O with 0.1 % FA. The desalted sample was directly infused into a ThermoFisher™ Q-Exactive ESI-MS Orbitrap in positive mode.

4.2.3.2 *Preparing M13-PEG$_4$-biotin*

Tetrafluorophenyl-PEG$_{12}$-biotin (**TFP-PEG$_4$-biotin**) was first prepared at a 10 mM concentration in anhydrous dimethyl formamide (**DMF**). The final reaction concentrations were 100 µM p8, 1 mM TFP-PEG$_4$-biotin in 1x PBS pH 7.46 with 20% DMF. Reactions were carried out over 18 h at 4 ºC. These were then dialyzed 6 times against 2 L of 1x PBS pH 7.46 in 12.4 kDa MWCO regenerated cellulose dialysis tubing (Millipore Sigma, Oakville, Canada). M13-PEG$_4$-biotin were flash

frozen with liquid nitrogen and stored at -80 ºC. The concentration of M13-PEG_4-biotin was determined according to its A_{269} absorbance as described in **Section 3.2.2.1**.

4.2.4 Preparation of Cel8A-biotin complexes on M13

4.2.4.1 *Preparation of SA(Cel8A-biotin) complexes onto M13-biotin*

This method describes the general approach and conditions for preparing SA(Cel8A-biotin) complexes followed by subsequent complexation onto M13-PEG_{12}-biotin. All steps were carried out at 23 ºC. Saturated SA was first prepared at 25 µM SA and 100 µM desthiobiotin and equilibrated for 10 min in 1x PBS pH 7.4. Cel8A-biotin was added to desthiobiotin-saturated SA as indicated; typical concentrations were, Cel8A-biotin (0.74 biotin/Cel8A) added to a concentration of 33.8 µM Cel8A (25 µM biotin moieties) and equilibrated for 60 min. M13-PEG_{12}-biotin was added to a final p8 concentration as indicated; typical concentrations were 16 µM p8 subunits added to 1.48 µM SA(Cel8A-biotin)$_N$ complexes to ensure complete binding of SA(Cel8A-biotin)$_N$ species over the course of 1 h.

Where CBM-Coh was added to these complexes, an additional step where the complexes were diluted down to 350 nM Cel8A subunits and incubated with 700 nM CBM-Coh in 0.1 M citrate pH 5.8 supplemented with 2 mM EDTA and 12 mM $CaCl_2$ for 2 h at 37 ºC was carried out.

4.2.4.2 *Preparation of SA-coated M13 and complexation with Cel8A-biotin*

This method describes the general approach taken to coat M13-PEG_4-biotin with SA, followed by subsequent complexation with Cel8A-biotin. SA-coated M13 was typically prepared with M13-PEG_4-biotin at 2 µM p8 subunits and SA at 2 µM in MQH_2O. M13-PEG_4-biotin was added to the solution first and mixed before adding SA which was further mixed immediately by pipetting.

For complexation with Cel8A-biotin, prepared SA-coated M13 was first pre-bound to desthiobiotin. Typically, desthiobiotin was added to a final concentration of 8 µM to the complexes to

saturate biotin-binding sites and given 15 min to equilibrate. After, Cel8A-biotin (0.74 biotin/Cel8A) was added to 3.2 µM Cel8A (2.36 µM biotin) to SA-coated M13 at a SA tetramer concentration of 1.6 µM unless otherwise indicated. These were allowed to interact for 1 h at 23 ^{o}C before further manipulation.

4.2.4.3 *Drop dialysis of SA-coated M13 complexes*

Clean-up of SA-coated M13 complexes was tested with two approaches: by drop dialysis and by differential centrifugation. SA(Cel8A-biotin) complexes with M13-biotin were prepared as described. Drop dialysis was carried out on MF-Millipore Membrane filters with 0.05 µM pore size (Millipore Sigma, Oakville, Canada). Filters were floated onto MQH_2O or 1x TBS (25 mM Tris, 137 mM NaCl, 2.7 mM KCl pH 7.4). The sample (100 µL) was pipetted gently onto filters that were floated on MQH_2O or 1x TBS pH 7.4 and allowed to dialyze at 23 ^{o}C for up to 4 h (**Figure 4.3**). Small aliquots of MQH_2O or 1x TBS pH 7.4 were added over time to bring up the volume to 100 µL with some gentle mixing by pipetting. The final volume was brought back to 100 µL by mass. The change in SA concentration over time was determined by monitoring the biotin-binding activity of the solution using B4F. Briefly, samples containing SA were diluted into 400 nM B4F in 1x PBS pH 7.4 and the change in fluorescence, when compared to a B4F fluorescence standard curve, was used to determine biotin-binding activity of the sample. The biotin-binding activity was proportional to the amount of SA in solution and used to calculate the relative concentrations of SA over time. Where M13 was monitored, the concentration was too low to monitor spectrophotometrically; M13 was instead monitored by its titer (PFU/mL). M13 was diluted up to 10^9-fold in sterile MQH2O and plated on a lawn of *E. coli* ER2738 plated on LB agar supplemented with 12 µg/mL tetracycline. These were incubated overnight at 37 ^{o}C and plaques formed were used to calculate the amount of M13 present over time.

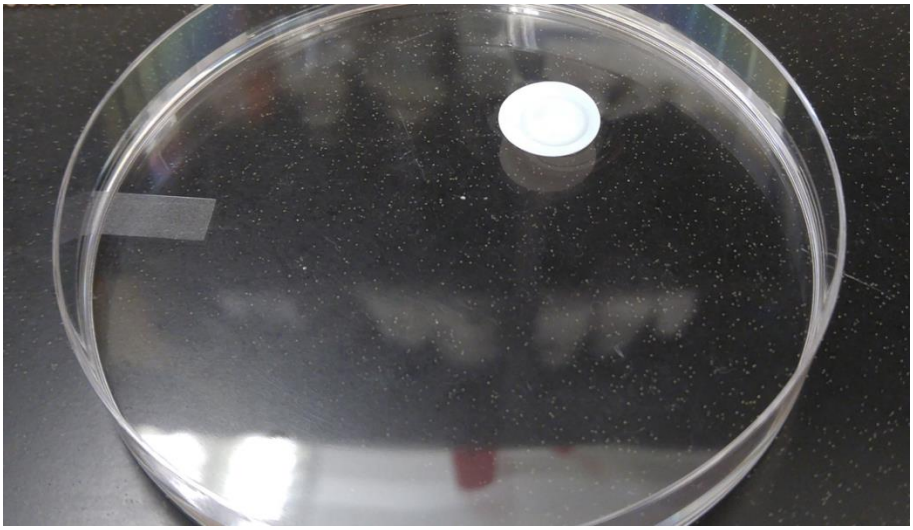

Figure 4.3: Drop dialysis setup showing membrane filter with a solution to be dialyzed floating on buffer in a Petri plate.

4.2.5 Analysis methods

4.2.5.1 *Estimating Cel8A biotinylation by mass spectrometry*

It is possible to determine the labelling efficiency of a multiply labelled protein by treating reactive amine observed to be labelled (m) with a probability (p) of being labelled and fitting to a binomial distribution as shown in **Equation 4.1** (Wojcik et al. 2008). The relative intensities of biotinylated Cel8A peaks in deconvoluted mass spectra were fit to a binomial distribution using a least squares minimization approach to obtain an estimate of the extent of biotinylation of Cel8A-biotin samples. Absolute quantitation by MS would require running each component separately to determine relative ionization efficiencies – this method is simplified in that it assumes the ionization efficiency of each Cel8A-biotin species is similar.

$$P(n;m;p) = \frac{m!}{n!(m-n)!}p^n(1-p)^{m-n} \quad (4.1)$$

In this distribution, m represents the total number of Lys residues that can be labelled, p is the probability of a Lys being labelled (value to be fitted), and n is the number of amines observed to be labelled. The value of m was determined from the maximumly labelled species observed (m = 3). The

peaks that were used in fitting were the parent peaks (with no ion adducts). For Cel8A(biotin)$_0$, this was the peak at 50276 Da with each subsequently-labelled peak have an additional mass of 827.02 Da.

Each peak intensity was divided by the sum of all peak intensities to obtain a relative frequency (0 – 1) for each Cel8A(biotin)$_N$ species. The value of p that best fit the relative frequencies of each Cel8A(biotin)$_N$ species to a binomial distribution was determined by least squares minimization. Analysis was performed in R (version 3.5.1).

4.2.5.2 *Estimating Cel8A biotinylation by B4F titration*

A B4F titration was carried out as described in **Chapter 3** in order to determine the total biotin per Cel8A in bioconjugate preparations. First, the concentration of Cel8A was determined by its estimated extinction coefficient at 280 nm of 104420 M^{-1} cm^{-1} calculated by ProtParam (Gasteiger et al. 2005). The concentration of SA was determined by its estimated monomer extinction coefficient at 280 nm of 41940 M^{-1} cm^{-1}. Biotin-4-fluorescein (**B4F**) was diluted 250-fold from a DMSO stock into 1x PBS pH 7.4 and standardized using its extinction coefficient of 68000 M^{-1} cm^{-1} at 495 nm (Ebner et al. 2008). For the titration, Cel8A-biotin samples were first mixed with SA at a concentration of 2.5 µM SA_{tet} and 2.5 µM Cel8A-biotin in 1x PBS pH 7.4. The complexed protein was further diluted: 5 µL into 495 µL 1x PBS pH 7.4 to a SA_{tet} concentration of 25 nM. The fluorescence of this mixture was measured at 490 nm excitation and 525 nm emission with a 515 nm cut-off filter after each 5 µL addition of 1 µM B4F. B4F was added until a breakpoint was clearly observed. A control titration with just SA to determine the number of open biotin-binding sites in the absence of biotinylated protein was also carried out as described above.

4.2.5.3 *Monitoring complexation of SA(Cel8A-biotin)$_N$ to M13-biotin using B4F*

This assay was devised to monitor complexation of SA (and SA(Cel8A-biotin) complexes) to biotinylated M13 indirectly by monitoring the total number of free biotin-binding sites before and after adding SA(Cel8A-biotin) to M13-biotin. The total amount of free biotin-binding sites at each step was

determined by adding a known amount of B4F to SA; B4F is quenched upon binding to SA, therefore the difference in B4F fluorescence before and after adding a SA-containing sample is proportional to the number of biotin-binding sites present. The absolute molar amount of free B4F before and after was determined using a fluorescence standard curve. A fluorescence standard curve was made using the same prepared buffers used for each experiment.

First, the SA(Cel8A-biotin)$_N$ complexes are prepared. SA was first pre-saturated with an equivalent amount of desthiobiotin (25 µM SA_{tet} and 100 µM desthiobiotin) in 1x PBS pH 7.4. Cel8A-biotin (0.74 biotin/Cel8A) was added to a final concentration of 33.78 µM Cel8A (equivalent to 25 µM biotin). After the addition of desthiobiotin, the mixture was incubated 15 min at room temperature. After the addition of Cel8A-biotin and 1x PBS, the mixture was incubated for 1 hour at room temperature. At this stage, the complexes with varying amounts of Cel8A-biotin (and residual desthiobiotin) bound to SA will be referred to generally as "SA(Cel8A-biotin)". As these species are likely to be an ensemble of SA(Cel8A-biotin)$_N$ species, the specific ratios or concentrations of SA and Cel8A-biotin used in preparing SA(Cel8A-biotin) complexes will be referred to where relevant.

The ensemble of SA(Cel8A-biotin)$_N$ species, as prepared above, were diluted to 2 µM of SA_{tet} and then bound to an M13-PEG_{12}-biotin concentration such that 16, 8 or 4 µM of p8 subunits were present (assuming 2700 p8/M13 particle). Controls with SA(Cel8A-biotin) diluted an equivalent amount in 1x PBS pH 7.4 were also prepared. This complexation mixture was also incubated for 1 hour to allow time for the desthiobiotin to be displaced by the biotin on the M13. Lastly, the complex was diluted to 75 nM of SA_{tet} (expected free biotin-binding sites 225 nM) and mixed with 350 nM of B4F in 1x PBS pH 7.4. These solutions were equilibrated for 2 hours at room temperature prior to measuring the retained fluorescence at 490 nm excitation, 525 nm emission with a 515 nm cut-off. Fluorescence data was collected on a SpectraMax® M5 (Molecular Devices, San Jose, USA) with the photomultiplier tube sensitivity set to high.

4.2.5.4 *PEG precipitation of SA(Cel8A-biotin)$_N$ complexes prepared on M13-biotin*

PEG precipitation of M13 phages was carried out to qualitatively assess the presence of SA(Cel8A-biotin) complexes bound to M13. Complexation of Cel8A-biotin (attached to SA) to M13 was carried out in two steps: first Cel8A-biotin was complexed to SA to form an ensemble of SA(Cel8A-biotin) complexes, followed by complexation to the M13-biotin scaffold. SA at a concentration of 15 µM was bound to 60 µM desthiobiotin in 1x PBS pH 7.4. After 30 min, Cel8A-biotin (2.04 biotin/Cel8A) was added to a final concentration of 15 µM Cel8A (30.6 µM biotin) and incubated for 60 min at 23 ^{o}C in 1x PBS pH 7.4. The prepared SA(Cel8A-biotin) ensemble was further diluted to 1.5 µM SA_{tet} in 1x PBS pH 7.4. For the M13-biotin containing sample, M13-biotin was added to a final concentration of 36 µM p8 subunits. For the control without M13-biotin an equal quantity of buffer was added. PEG/NaCl (20% PEG-8000, 2.5 M NaCl) was added at 200 µL PEG/NaCl per 1 mL of SA(Cel8A-biotin) with or without M13-PEG12-biotin. This was precipitated for 1 hour at 23 ^{o}C and then centrifuged at 15000 *g* for 10 min. The pellet fraction was brought back to its original volume with 1x PBS pH 7.4.

Initial aliquots of SA(Cel8A-biotin) (with or without M13-biotin) before centrifugation, as well as aliquots of the pellet and supernatant fractions were assayed for endocellulase activity. The aliquots taken were diluted such that the final concentration of Cel8A would be 50 nM if one were to assume that the total amount of Cel8A added was retained in that respective fraction. The reactions were carried out with 0.5% CMC in 0.1 M citrate pH 5.8 at 50 ^{o}C for 10 min. Reducing ends produced were detected with DNS reagent (as prepared in **section 3.2.4.1.**) and compared to a glucose standard curve to convert the values to a molar quantity of reducing ends produced. Briefly, aliquots of the reaction were mixed 1:1 with DNS reagent and boiled 5 min. The resulting absorbances were read at 540 nm.

4.2.5.5 *PASC pull-down assay*

This assay was carried out to confirm that association between CBM-Coh and the biotinylated Cel8A could occur. Phosphoric acid-swollen cellulose (**PASC**) was produced for this assay according to literature methods (Hsieh et al. 2015). First, 4 g Avicel® PH101 was incubated with 100 mL of ice-cold 85% phosphoric acid. Mechanical disruption with a glass stir rod was used to break up the cellulose and after 2.5 h the syrupy solution was poured into 1.9 L of ice-cold distilled deionized water. The cellulose fibres were allowed to settle and the water carefully decanted off for a total of 4 x 2L water washes. Similarly, the fibres were washed with 2 x 2 L of $NaHCO_3$ (10 g/L, not pH adjusted). Three more 2 L water washes were carried out and the final volume was brought down to about 100 mL. The PASC was quantified gravimetrically by evaporating the water *in vacuo*.

This procedure was carried out according to literature methods for cellulose-based pull-down assays (Yael Vazana et al. 2012). However, rather than analyze bound and unbound fractions solely by SDS-PAGE, the fraction of unbound protein was assessed by its activity against CMC. Additionally, PASC was used as it has a higher binding capacity for cellulose-binding proteins than other forms of insoluble cellulose (Lamed et al. 1985). Mixtures of Cel8A-biotin were prepared with CBM-Coh at 350 nM Cel8A and corresponding ratios of CBM-Coh. Solutions were equilibrated for 2 h at 37 ^{o}C in 0.1 M citrate pH 5.8 supplemented with 2 mM ethylenediaminetetraacetic acid (**EDTA**) and 12 mM $CaCl_2$. These solutions were further incubated with PASC at a final concentration of 0.12 % w/v on ice for 1 h. The solutions were centrifuged at 12700 *g* for 5 min.

Supernatants were diluted down to 10 nM Cel8A (based on the initial concentration of Cel8A-biotin in the solution prior to centrifugation) and reacted with 0.5 % CMC (w/v) in 0.1 M sodium citrate pH 5.8 at 65 ^{o}C for various time intervals. Endpoints were analyzed by mixing aliquots of the reaction 1:1 with DNS reagent (as prepared in **Section 3.2.5.1**) and boiling for 5 min. The absorbance of the solution was read at 540 nm and compared to a *D*-glucose standard curve reacted with DNS in the same way. The initial rates were determined from time points taken during the linear portion of the reaction.

4.2.5.6 *Endocellulase assays*

For assays against CMC, complexes were diluted such that there was either 100 nM Cel8A for reactions at 23 ºC, or 10 nM Cel8A for reactions at 50 ºC unless otherwise noted. Reactions were carried out with 0.5 % CMC in 0.1 M citrate pH 5.8. These concentrations were chosen such that the linear range of the reaction could be monitored over 20 – 30 min. Aliquots were removed and mixed with 1:1 with DNS reagent (prepared as described in **Section 3.2.5.1.**) and boiled 5 min. The absorbance of the resulting solution read at 540 nm and compared to a *D*-glucose standard curve to determine the produced reducing ends.

For assays against α-cellulose, reactions were carried out in test tubes floated in a jacketed beaker attached to a water bath to maintain the temperature at 50 ºC. The jacketed beaker was set on a stir plate to allow stirring of the reactions to ensure dispersion of α-cellulose particles throughout the reaction. Complexes were diluted such that there was 100 nM Cel8A. Reactions were carried out with 1 % w/v α-cellulose in 0.1 M citrate pH 5.8 at 50 ºC with constant stirring. Due to the insolubility of the substrate, removing equal aliquots by pipette was inconsistent; thus, each endpoint represents a single test tube which was mixed 1:1 with DNS reagent and boiled for 10 min. Tubes were cooled for 1 min before centrifuging at 15000 *g* for 5 min to remove α-cellulose particles and the absorbance of the supernatant was read at 540 nm and compared to a glucose standard curve to determine reducing ends.

4.2.5.7 *TEM staining conditions (regular staining with PTA)*

Phosphotungstic acid (**PTA**) was prepared fresh before each experiment by diluting PTA in water to 1% (w/v) and then adding 1.12 mL 2 M NaOH per 1 g of PTA that was weighed out to neutralize the stain (Phillips 1950).

M13 phage containing samples were typically adhered to TEM grids at a concentration of 1.5 – 4.5 x 10^{11} M13 particles/mL in sterile MQH_2O (M13 typically exchanged into MQH_2O from 1x PBS buffer by dilution of ~100-fold). Grids used were carbon/formvar 400 mesh (Ted Pella, etc.) or ultrathin

carbon film supported by lacey carbon 400 mesh (Ted Pella, etc.) where indicated. Grids were prepared by placing grids onto prepared drops of sample/wash solution. A typical grid preparation is as follows: a 10 µL drop of M13 was adhered to the grid for 1 min, followed by two brief washes (a few seconds) on 50 µL drops of sterile MQH_2O, and lastly, staining for 20 sec on a 20 µL drop of 1% PTA. Excess solution was wicked away with filter paper after each step. Grids were dried overnight.

4.2.5.8 *TEM staining conditions (TEM immunostaining procedure)*

This staining procedure was carried out to specifically bind 5 nm gold nanoparticles (**GNP**) to the His6-tag of Cel8A present on M13 scaffolds. The primary antibody used to bind the His6-tag was a 6x-His tag monoclonal mouse IgG antibody (ThermoFisher Scientific, Waltham, USA). The stock solution was at 1 mg/mL. The secondary antibody was goat anti-mouse IgG 5 nm GNP conjugate (Cytodiagnostics, Burlington, Canada). The stock solution was at 3 OD (~1.64×10^{14} particles/mL according to the manufacturer).

The protocol for immunogold staining was adapted from literature methods with some changes (X. Li et al. 2016). The TEM grids used were carbon/formvar 400 mesh. In order to adhere phage samples to the grid, M13 was diluted down to $1.5 – 4.5 \times 10^{11}$ M13 particles/mL in sterile MQH_2O, and a 10 µL droplet to each grid and let sit for 1 min before removing the excess with filter paper. The grid was touched to 50 µL water droplets (~2 sec) to wash and the excess was removed with filter paper. The grid was blocked by incubation of the grid with 50 µL droplet of blocking buffer (0.1 % BSA in 1x TBS pH 7.4) for 10 min to prevent non-specific binding of antibodies. The excess solution was removed with filter paper. The grid was incubated on 50 µL droplet containing primary antibody (diluted 1:20 into blocking buffer) for 60 min. This was washed 5 x 3 min on 50 µL droplets of blocking buffer. The grid was incubated on 50 µL droplet containing the secondary antibody GNP conjugate (diluted 1:30 into blocking buffer) for 60 min. This was washed 3 x 3 min on 50 µL droplets of blocking buffer, followed by 3 x 3 min on 50 µL droplets of 1x TBS pH 7.4, and lastly, with 4 x 30 s on 50 µL droplets of sterile MQH_2O. The excess solution was removed with filter paper. Lastly, the

grids were stained on 20 µL droplets of 1% (w/v) PTA for 1 min and then the excess stain was removed with filter paper.

4.3 Results and discussion

There were two main approaches taken to complexing biotinylated Cel8A (referred to generally as **Cel8A-biotin**) to M13-biotin using SA as an adaptor protein. The main difference in these two approaches was whether or not Cel8A-biotin was complexed to SA before further complexation onto M13-biotin, or if M13-biotin was first bound to SA followed by complexation with the biotinylated enzyme. There were benefits and drawbacks to both approaches that will be highlighted in this section. Furthermore, each approach highlights different aspects and considerations that are generally applicable to the formation of a high density, multi-enzyme complex on an M13 scaffold, and perhaps for other filamentous phages.

4.3.1 Estimated extents of biotinylation of Cel8A-biotin

Characterization of Cel8A-biotin will be discussed here prior to discussing the results of complexation onto M13-biotin. The results here are relevant to all of the approaches used to prepare Cel8A/M13 complexes using SA as an adaptor molecule in this chapter, and thus will be presented first. Specifically, the method used to biotinylate Cel8A was expected to produce a mixture of Cel8A-biotin species. Therefore, the characterization in this section covers the estimation of the total extent of biotinylation of Cel8A-biotin samples and the distribution of Cel8A(biotin)$_N$ (multiply labelled) species by mass spectrometry. Here, Cel8A(biotin)$_N$ refers to the total number of times a particular Cel8A was modified with biotin.

Cel8A-biotin was prepared by reacting free amines on the protein with the activated ester TFP-PEG$_{12}$-biotin. After reaction, excess reagents and hydrolyzed side product were removed by dialysis with 12400 Da MWCO dialysis tubing. About 40 % of Cel8A was lost over the course of the dialysis

step for each sample (**Table 4-1**). This was possibly due to association of the cellulase with the regenerated cellulose dialysis membrane; some affinity to cellulose-based membranes might be expected. However, the recovered yields after dialysis were acceptable.

Table 4-1: Summary of reaction conditions for preparing biotinylated Cel8A and recovered sample after dialysis (n = 4).

Sample Name	[Cel8A] (µM)	[TFP PEG_{12}-biotin] (µM)	[Cel8A] After dialysis (µM)	% Recovered
Cel8A-biotin (1 eq TFP-biotin)	111	111	64.8 ± 2.5	58.5 ± 2.3
Cel8A-biotin (2.5 eq TFP-biotin)	111	277	63.0 ± 3.0	56.9 ± 2.7
Cel8A-biotin (5 eq TFP-biotin)	111	554	63.8 ± 2.4	57.6 ± 2.2

One of the methods used to estimate the extent of biotinylation was by competitive titration with the fluorescent biotin analogue, biotin-4-fluorescein (**B4F**), against streptavidin (**SA**). From three different concentrations of TFP-PEG_{12}-biotin initially added to Cel8A, a range of labelling efficiencies from 32 – 171 % labelling were estimated (**Table 4-2**). The extent of biotinylation increased as the equivalents of TFP-PEG_{12}-biotin in the reaction increased. An example of the calculations used to estimate the extent of biotinylation from a competitive B4F titration are highlighted in **Table 4-2**. The maximum sites per SA were determined from a control (SA at the same concentration), titrated with B4F to determine the total biotin-binding sites present in the absence of Cel8A-biotin. From the breakpoint of the titration, one can estimate the number of biotin present in the unknown samples from which the biotin per Cel8A is calculated (described in more details in **Methods 4.2.5.2.**).

Table 4-2: Summary of B4F fluorescence titration breakpoint estimates (mean and SD; n=3). From left-to-right the columns highlight how the breakpoints of the B4F titrations were converted into biotinylation estimates.

Sample	Breakpoint	Max sites/SA monomer	Fraction of occupied sites	[biotin]* (nM)	biotin/Cel8A ≠
Cel8A:TFP-biotin 1:1	0.754 ± 0.045	0.835	0.0813	8.13	0.32 ± 0.18
Cel8A:TFP-biotin 1:2.5	0.650 ± 0.017	0.835	0.185	18.5	0.74 ± 0.07
Cel8A:TFP-biotin 1:5	0.407 ± 0.007	0.835	0.428	42.8	1.71 ± 0.028

Dialysis buffer (control)	0.832 ± 0.018	0.835	0.003	0.3	0.01 ± 0.070

**Total concentration of biotin binding sites was 100 nM; the fraction of occupied sites multiplied by 100 nM gives [biotin].*
⁄Concentration of Cel8A-biotin added was 25 nM.

In the initial survey of ESI-MS of Cel8A-biotin, it was possible to resolve the individual biotinylated species of Cel8A-biotin. The expected average isotopic mass of unlabeled Cel8A is 50276.70 Da and corresponds well to the measured mass (**Figure 4.4A**). The increase in mass expected for the aminolysis reaction was 827.02 Da (**Figure 4.4B**). The species detected at 51102.06, 51928.13 and 52753.03 Da correspond well to Cel8A(biotin), Cel8A(biotin)$_2$ and Cel8A(biotin)$_3$ respectively. As there are several surface-exposed Lys residues present, multiply labelled Cel8A is expected (19 surface-exposed Lys residues on cellulase domain; **Figure 4.5**), though, many of the Lys residues appear to be interacting as salt bridges according to the crystal structure (PDB: 1CEM; (Alzari, ne Souchon, and Dominguez 1996)). It is commonly the case for thermostable proteins to have a network of ionic bonding on the surface of the protein (Chan, Yu, and Wong 2011). At pH 7.46, these salt bridges mean that it is possible that only a small subset of these Lys residues is reactive.

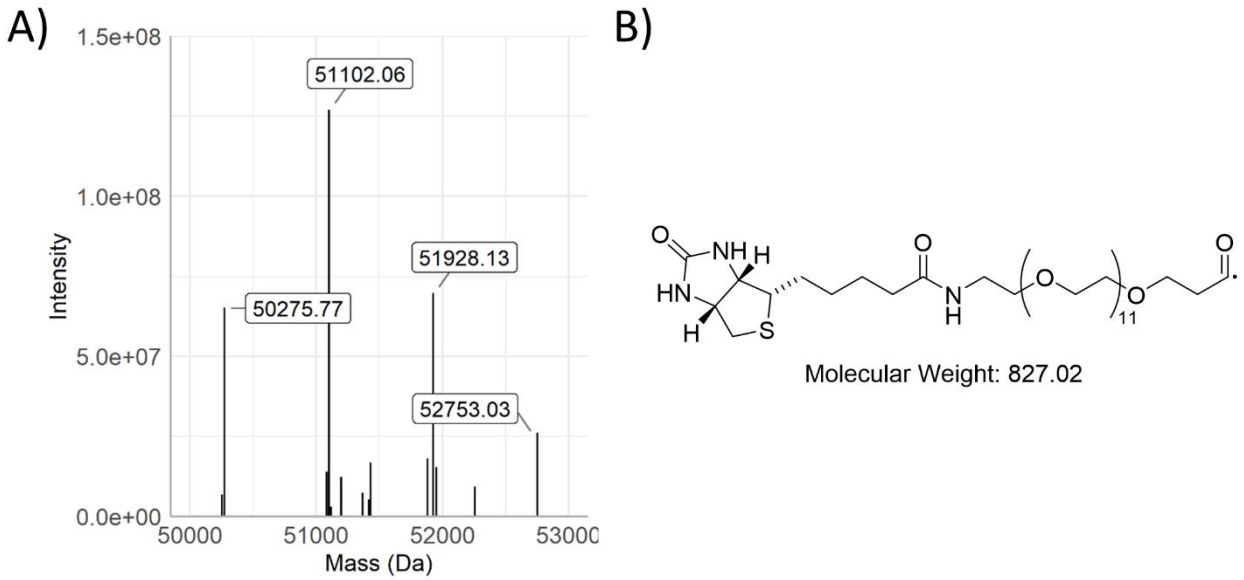

Figure 4.4: Typical ESI-MS of Cel8A-biotin samples. A) Deconvoluted ESI mass spectrum of Cel8A-biotin (0.74 biotin/protein) run in 1:1 MeOH:H2O + 0.1% FA on a Thermo Q-Exactive ESI mass spectrometer and deconvoluted using BioPharma Finder™ (ThermoScientific, v.3.0). B) Fragment of TFP-PEG$_{12}$-biotin showing expected mass increase upon acylation of Cel8A primary amines.

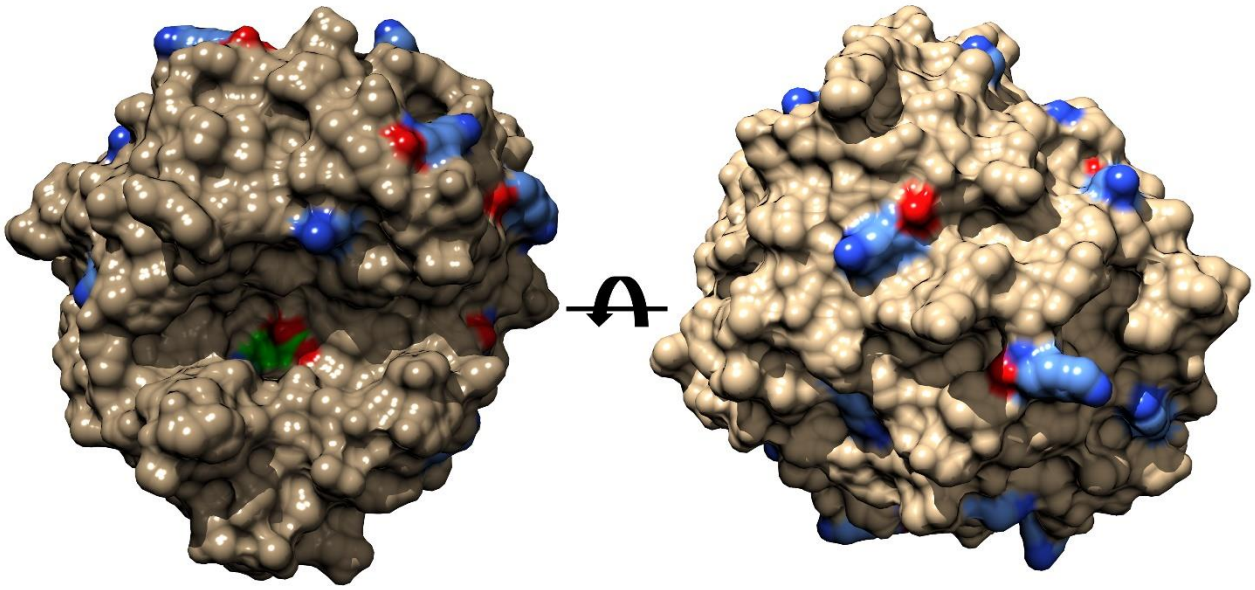

Figure 4.5: Crystal structure of Cel8A (cellulase domain) highlighting Lys residues (blue) and potential ionic interactions with acidic residues, Asp and Glu (red). PDB: 1CEM (Alzari, ne Souchon, and Dominguez 1996)).

If one assumes that the ionization efficiency is the same for each of the multiply biotinylated Cel8A species, and the reactive Lys residues are equivalent in their reactivity, then the data should fit well to a binomial distribution. The main peak for each Cel8A(biotin)$_N$ species (parent ion; no adducts) was taken from the deconvoluted spectra and then fit to a binomial distribution (**Figure 4.6**). The spectra fit reasonably well to the binomial distributions, indicating that the reacted Lys residues are likely similar in their reactivity. More practically, the fitted values for p could be used to determine the percent labelling of each Cel8A-biotin sample. The estimates of percent labelling from the mass spectra ranged from 57 – 189 % labelling. Though it was possible to estimate percent labelling from the B4F competitive titration experiment, knowledge of the distribution of multiply biotinylated species is important for understanding complexation to SA and M13 downstream. The batch of biotinylated Cel8A-biotin (unless otherwise indicated) used in subsequent experiments in this chapter was the Cel8A-biotin prepared such that there was an approximate ratio of 0.74 biotin per Cel8A.

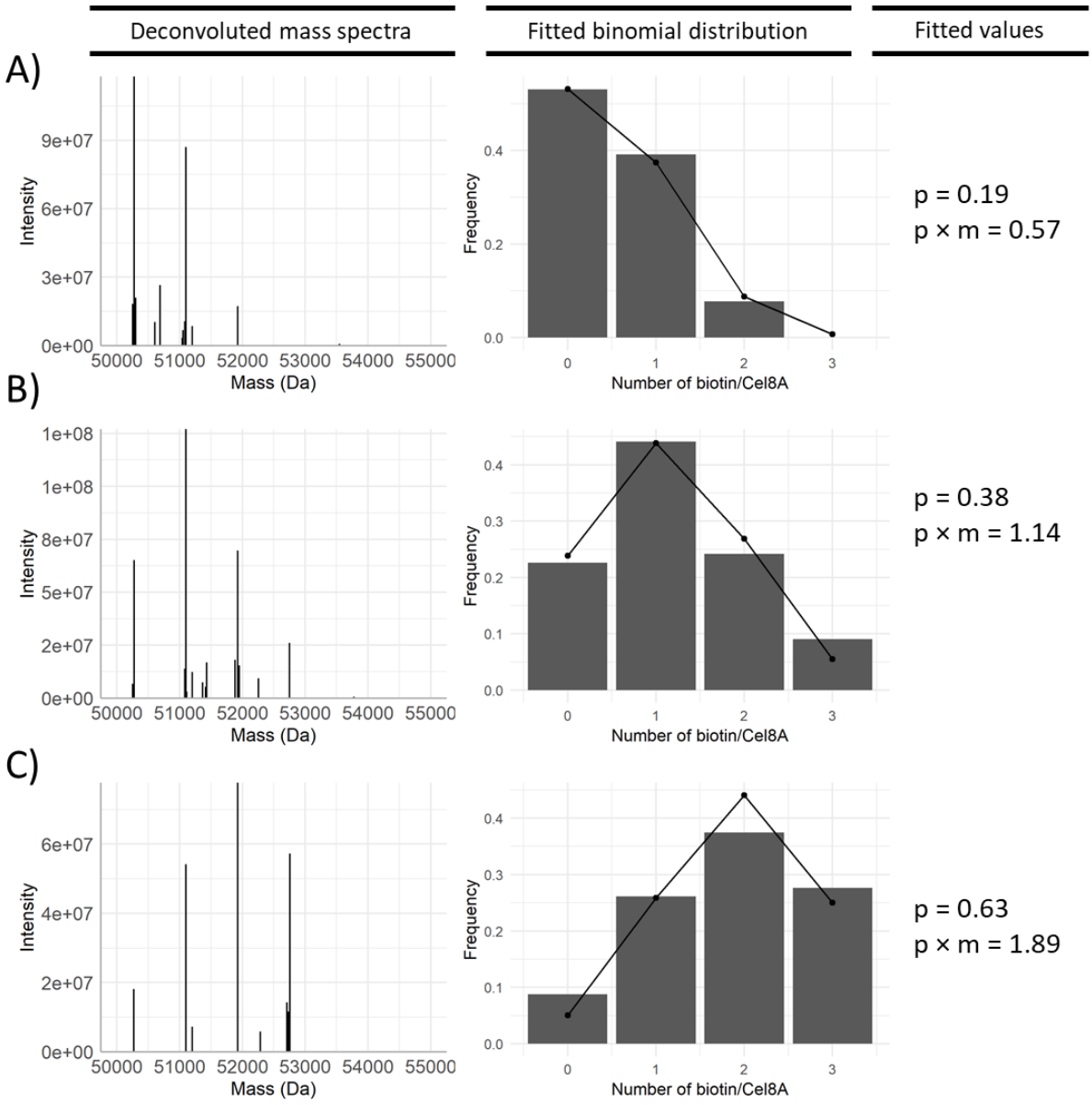

Figure 4.6: Estimating extent of biotinylation from mass spectra of Cel8A-biotin. Deconvoluted ESI mass spectra of Cel8A-biotin (left column) from reactions of Cel8A (110.8 µM) with increasing equivalents of TFP-PEG$_{12}$-biotin: A) 110.8 µM, B) 277 µM, and C) 554 µM TFP-PEG$_{12}$-biotin. Peak intensity (bars) from mass spectra were fit to a binomial distribution (fitted line) as described in the Methods (middle column). The value of p fitted from the binomial distribution was multiplied by total reactive residues (m) to obtain the average biotin per Cel8A (right column). Single spectra (n = 1) were fit to obtain values.

The estimations of extent of biotinylation of Cel8A by ESI-MS were higher than by the B4F titration method discussed above. If the ionization efficiencies being different was the reason for the difference between the ESI-MS estimates and the B4F estimates, one would expect the estimates to be lower by ESI-MS. It should be considered that the spectrum is run in positive ion mode and each subsequent labelling would reduce the overall positive charge on the protein surface, and hence it is

likely that this would reduce the ionization efficiency of the biotinylated species and hence underestimate their true amount. It is possible that the B4F titration method underestimates the total biotin present. Since the assay relies on binding analyte to SA, if not all of the biotin is capable of binding to SA (due to steric factors), the total amount could be underestimated by this method.

In summary, Cel8A-biotin prepared through the acylation of primary amines with an activated biotin ester was characterized by fluorescence titration and ESI-MS. From this, an estimate of the extent of biotinylation and distribution of Cel8A(biotin)$_N$ species was determined. Further studies could employ tandem mass spectrometry sequencing to specifically localize the position(s) of the biotin; however the purpose of demonstrating that multienzyme complexes could be controllably fabricated on a filamentous phage, determination of the exact location(s) of the biotin modification(s) were not pursued at this stage.

4.3.2 Method 1: complexation of SA(Cel8A-biotin)$_N$ species to M13-biotin

This section covers analysis and results of preparing an ensemble of SA(Cel8A-biotin) species with relative amounts of SA and Cel8A-biotin, such that the resulting mixture of SA(Cel8A-biotin)$_N$ species would have, on average, one or more open biotin-binding sites on each SA. In a subsequent step, these SA(Cel8A-biotin)$_N$ species were adhered to biotin-M13 (**Figure 4.7**). Successful complexation was indirectly confirmed using PEG precipitation followed by monitoring Cel8A activity in supernatant or pellet fractions. Additionally, B4F was utilized as a probe to follow complexation by monitoring loss of free biotin-binding sites upon addition of M13-biotin – allowing binding of SA(Cel8A-biotin) complexes to M13 to be inferred. While Cel8A was confirmed to be bound to the M13 scaffold, the arrangement of Cel8A components were not as designed or intended. Analysis of the results of TEM experiments demonstrated that SA(Cel8A-biotin) complexation occurred in a non-uniform fashion and it was likely that aggregates of SA(Cel8A-biotin) formed that were incapable of binding to the M13-biotin scaffold. However, this section highlights some factors and considerations in

assessing the successful formation of multi-enzyme complexes on a nanoscale scaffold – and some useful methodologies for assessing and monitoring the binding of enzymes to this scaffold.

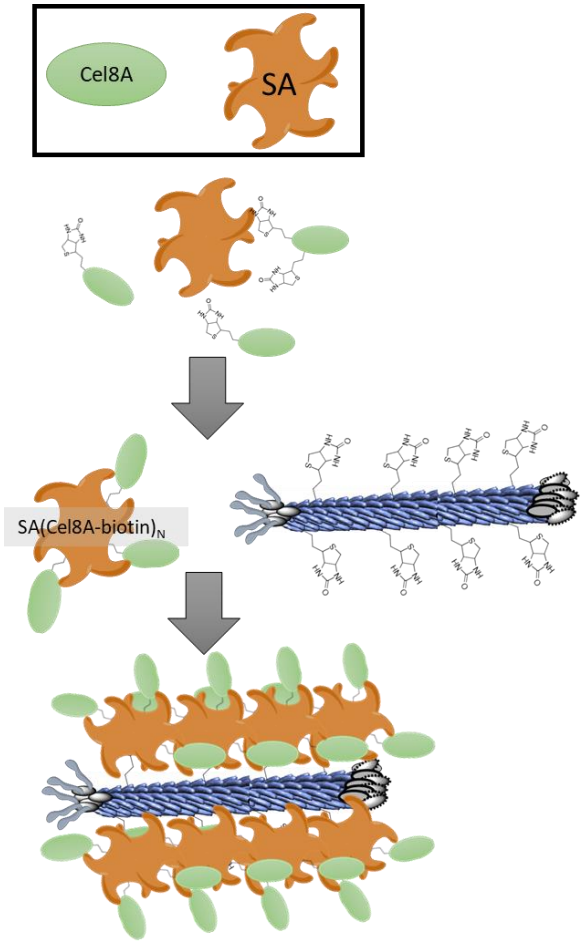

Figure 4.7: Schematic representation of methodology whereby SA(Cel8A-biotin) complexes are first formed and then further complexed onto M13-PEG$_{12}$-biotin.

4.3.2.1 *Confirming complexation of Cel8A by indirect methods (PEG precipitation)*

Assessing the success of complexation of Cel8A onto M13 using the approach outlined in **Figure 4.7** was accomplished employing two different methodologies. One was to determine whether cellulase activity could be found associated with M13 scaffolds after separating M13 from other components. The second approach was to use the fluorescent biotin analogue, B4F, to probe the average free biotin-binding sites on SA before and after complexation with M13-biotin. This was

furthermore used to estimate the number of SA(Cel8A-biotin) complexes that could be bound per M13-biotin scaffold.

Initially, complexation to M13-biotin was assessed by determining whether endocellulase activity followed the separation of M13 from other components. This experiment took advantage of the ability to precipitate M13 by incubation with PEG-8000/NaCl followed by centrifugation. In this way, binding of SA(Cel8A-biotin)$_N$ complexes to M13-biotin could be confirmed by the presence of endocellulase activity in the pellet and loss from the supernatant. An excess amount of M13-biotin was added to prepared solutions of SA(Cel8A-biotin) to ensure complete binding to the M13 scaffold and so that binding of SA(Cel8A-biotin) would be unlikely to be limited by available M13 surface area to bind to. As a control, this was compared with the same SA(Cel8A-biotin) complexes in the absence of M13-biotin to confirm that M13 was indeed necessary for fractionation of SA(Cel8A-biotin) to the pellet fraction.

The activity of Cel8A was monitored using carboxymethyl cellulose (**CMC**), a soluble cellulose substrate useful for monitoring the activity of endocellulases. This cellulose derivative contains carboxymethyl (-CH_2-COOH) groups attached to a subset of the hydroxyl groups of the glucose residues in the cellulose biopolymer. Cleavage of the substrate over time was monitored via the dinitrosalicylic acid (**DNS**) assay for detecting reducing ends of sugars – with each additional reducing end produced corresponding to a single cut by Cel8A. In order to assess the presence of the enzyme in either the supernatant fraction or pellet fraction following PEG-8000 precipitation of M13, activity in the pellet and SN fractions was compared to the total activity prior to PEG precipitation. Samples were diluted such that the final concentration of enzyme would be equal if 100% of the Cel8A were found in that fraction. Thus, the activity in each fraction would be proportional to the amount of Cel8A.

First, Cel8A on its own did not precipitate under the conditions used to precipitate M13 (**Figure 4.8**). However, after preparing Cel8A-biotin with SA the properties might be expected to change; therefore, samples with all components except for M13-biotin were tested as well to determine

that they would not also precipitate. This control was run alongside the same sample containing M13-biotin as well for a direct comparison. In comparing the pellet fractions, endocellulase activity was found in the pellet only when M13-biotin was added to SA(Cel8A-biotin) mixtures (**Figure 4.8**). Given that endocellulase activity was in the pellet only with added M13-biotin, it was inferred that this activity comes from SA(Cel8A-biotin) associated with M13-biotin.

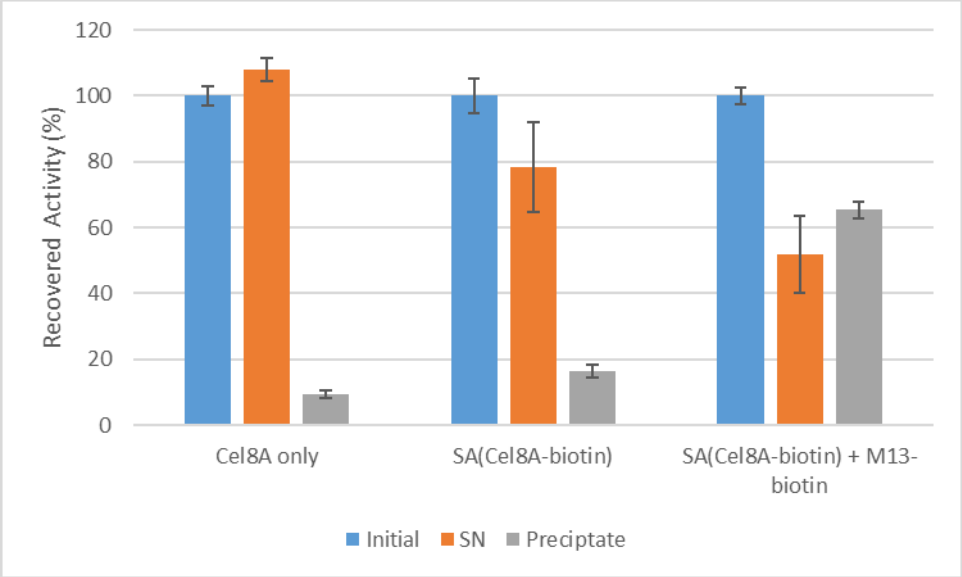

*Figure 4.8: M13-specific PEG precipitation of SA(Cel8A) complexed bound to M13-biotin. SA(Cel8A-biotin)$_N$ complexes were first prepared and precipitated as described in the Methods section (**Section 4.2.7**). Endocellulase activity was monitored with 0.5% CMC reacted for 10 min with end-point analysis of produced reducing ends with DNS at 65 ^oC (mean and SD; n = 3). The percent of recovered activity was determined from the initial activity of the solution before precipitation. "SN" refers to the supernatant fraction.*

Some additional information might also be inferred from this experiment. First, not all of the endocellulase activity was fractionated to the pellet in the presence of M13-biotin. One possibility was that there may have been incomplete precipitation of any M13-SA(Cel8A-biotin) complexes that formed. The efficiency of recovering M13-biotin after PEG precipitation was tested and found to be dependent upon the concentration of M13. M13 phages were titered before and after PEG precipitation and the amount of M13-biotin recovered from a single round of PEG precipitation was 89 % for M13 at 10^{11} particles/mL and 16 % for M13 at 10^{10} particles/mL. The concentration of M13 with complexed SA(Cel8A-biotin) was at ~8 x 10^{12} particles/mL – it is therefore expected that the majority of M13 could be precipitated under these conditions. A second possibility considers the labelling efficiency of

the Cel8A-biotin (74% labelled) used in preparing the solutions of SA(Cel8A-biotin). From ESI-MS estimations of the distribution of Cel8A(biotin)$_N$ species presented earlier, 21% in this sample exists as Cel8A(biotin)$_0$. This should account for a portion of the endocellulase activity found in the supernatant.

4.3.2.2 *Confirming complexation of Cel8A by indirect methods (Fluorescence assay)*

It was determined that Cel8A was associated with M13 by following Cel8A activity after PEG precipitation. However, this was unable to answer how many SA(Cel8A-biotin) complexes might be bound to M13-biotin. To explore this question, a fluorescence assay using B4F was devised to probe for unoccupied biotin-binding sites on SA(Cel8A-biotin) complexes before and after the addition of M13-biotin.

This assay directly measures the amount of free B4F by its fluorescence, which is quenched when bound to SA. In this experiment, SA is present among the various SA(Cel8A-biotin)$_N$ species in solution. Therefore, analyzing the amount of biotin-binding sites initially present in a solution of SA and Cel8A-biotin using B4F would inform on the average free biotin-binding sites per SA tetramer. Upon adding M13-biotin, the change in the average number of free biotin-binding sites would inform on the extent to which those SA(Cel8A-biotin) were bound to the M13 scaffold. The biotin-binding sites present in each mixture were determined indirectly by the addition of a known quantity of B4F – quenching of B4F fluorescence is proportional to the number of biotin-binding sites. In this way, one can indirectly estimate the extent of loading of SA(Cel8A-biotin) onto M13-biotin. The fluorescence of the mixture is therefore inversely proportional to the quantity of SA(Cel8A-biotin) not bound to M13. By assaying several different ratios of SA(Cel8A-biotin):M13, the number of complexes that can be loaded onto M13 can be estimated.

In presenting the results of preparing different ratios of SA(Cel8A-biotin) ensembles with M13-biotin, M13 will be referred to in terms of p8 subunits (2700 p8/M13) and “SA(Cel8A-biotin)” refers to the total amount of SA tetramers in the solution. For example, a 1:8 mixture of SA(Cel8A-biotin):p8

would refer to a mixture of SA and Cel8A-biotin complexes where an amount of M13-biotin was added such that the concentration of p8 was 8 times the concentration of SA tetramers in the solution. In the 1:8 SA(Cel8A-biotin):p8 mixture no biotin-binding sites were detected after adding M13-biotin (**Figure 4.9A, B**). This suggests that the biotin present on M13-biotin was sufficient to fully bind all SA(Cel8A-biotin) complexes in that mixture. This would correspond to roughly 340 SA(Cel8A-biotin) complexes loaded per phage. At lower concentrations of M13, it is apparent that there is not enough surface area to bind all SA(Cel8A-biotin) complexes (**Figure 4.9C, E**). For these samples the number of available biotin-binding sites estimated for the SA(Cel8A-biotin) before and after adding M13-biotin can be estimated.

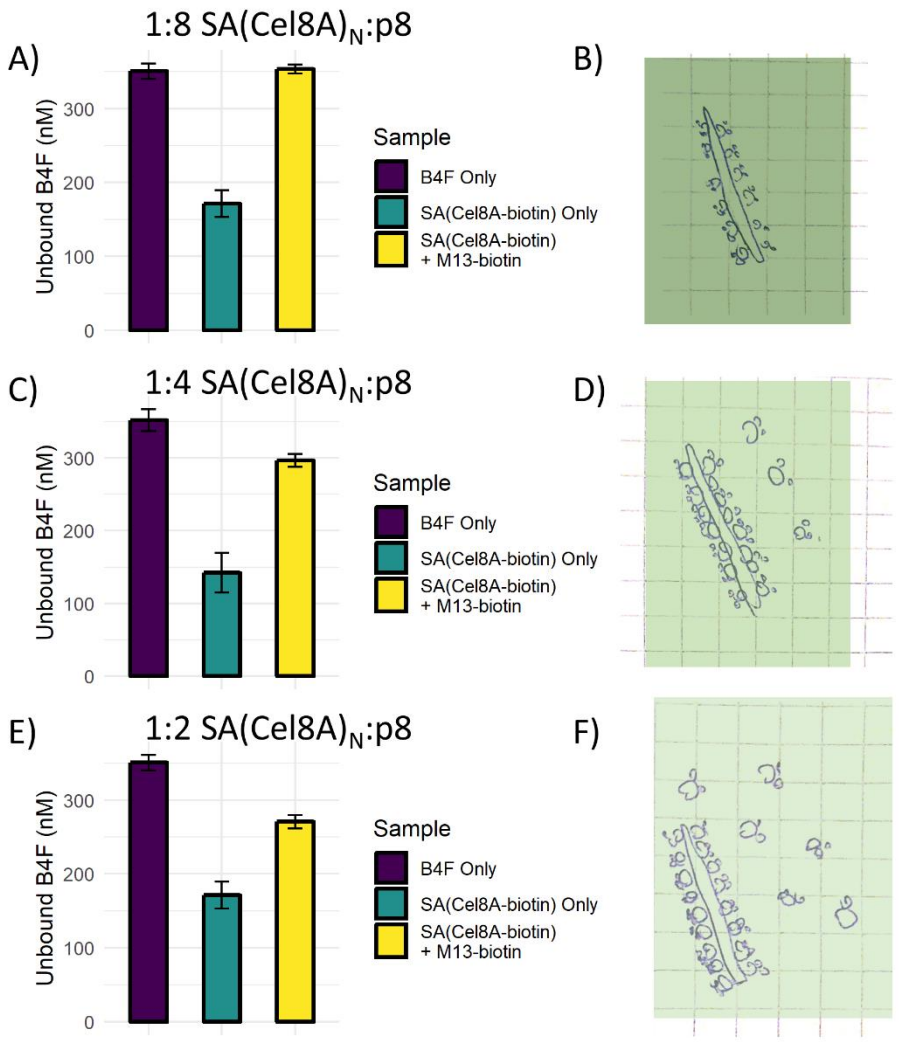

Figure 4.9: Free B4F in mixtures of 1:1 SA:Cel8A (0.74 biotin/protein) complexes and M13-PEG$_{12}$-biotin. The y-axis indicates the amount of unbound B4F when 350 nM was mixed with assembled complexes (mean and SD; n = 3). In the different data sets, different amounts of M13-biotin (referred to in terms of major coat protein concentration assuming 2700 p8/M13). SA(Cel8A-biotin)$_1$ (75 nM) was mixed with A) 600 nM p8, C) 300 nM p8, or E) 150 nM p8. The interpretation of the fluorescence data is shown in panels B, D, F.

The difference in free B4F between the B4F only controls and the SA(Cel8A-biotin) samples reflects the amount of available biotin-binding sites on the SA(Cel8A-biotin) complexes before adding M13-biotin. By dividing this value by the total number of SA tetramers (75 nM), one can obtain the average number of free biotin-binding sites per SA after complexing with Cel8A-biotin (**Table 4-3**). The difference between the B4F only control and the SA(Cel8A-biotin) complexes mixed with M13-biotin reflects any open biotin-binding sites on SA(Cel8A-biotin) that have not been bound to M13-biotin. By dividing this value by the average open biotin-binding sites per SA(Cel8A-biotin), one can

calculate the total number of unbound SA(Cel8A-biotin) in the mixture, which can then be used to infer the SA(Cel8A-biotin) complexes that are therefore bound to M13. By dividing this number by the total number of p8 subunits present in the mixture, the number of SA(Cel8A-biotin) complexes bound to M13 can be estimated as a percent ($[SA]_{bound}$/[p8] x 100%).

Table 4-3: Estimate of loading capacity of M13-PEG$_{12}$-biotin for SA(Cel8A-biotin)$_N$ complexes prepared from 1:1 SA:Cel8A(0.74 biotin/Cel8A). Mean and SD for n = 3 shown.

SA(Cel8A-biotin):p8	Fraction open biotin sites per SA_{tet}	Unbound SA_{tet} (nM)	SA_{tet} complexes bound to M13 (nM)	Loading capacity (% SA complexes/p8)
1:8	0.598 ± 0.038	-1.23 ± 6.22	76.2 ± 6.22	12.7 ± 1.0
1:4	0.700 ± 0.101	19.7 ± 7.7	55.2 ± 7.7	18.4 ± 2.6
1:2	0.598 ± 0.038	33.4 ± 5.86	41.6 ± 5.86	27.8 ± 4.9

Since the 1:8 SA(Cel8A)$_N$:p8 sample was able to bind all SA(Cel8A-biotin), this gives a lower bound estimate of how many SA(Cel8A-biotin) complexes can be loaded onto M13-biotin. The other samples where not all complexes are bound can be used to calculate an upper bound for the loading capacity. If the SA(Cel8A-biotin)$_N$ species are uniform in steric size (size of SA(Cel8A-biotin)$_N$ complexes, number of biotin-binding sites per complex) then the estimate between the 1:4, and 1:2 SA(Cel8A-biotin):p8 samples should be similar. However, the estimates were quite different, with the 1:4 sample giving a lower estimate of 18% loading and the 1:2 sample giving a higher estimate of 28 % loading (**Table 4-3**). This is an indication that the SA(Cel8A-biotin) complexes are likely not uniform and exist in a distribution of different sizes and valencies, as might be expected.

There are two important considerations in making sense of the differing loading capacity estimates: 1) that the off-rate of SA and biotin is very slow, and 2) if the SA(Cel8A-biotin)$_N$ complexes exist as a distribution of different sizes, these could reasonably be expected to have differing rates of diffusion. The first consideration predicts that once bound to M13, the SA(Cel8A-biotin) would be slow to rearrange to a more optimal packing. For the second consideration, the smaller configurations of SA(Cel8A-biotin) might be expected to bind the M13 first, leaving little space for the larger

configurations to then diffuse in and bind (**Figure 4.10**). There would unlikely be much difference between a SA with three versus two Cel8A bound; however, a proportion of Cel8A-biotin species are biotinylated >1 and therefore there is potential for complexes of SA and Cel8A-biotin with more than one SA molecule participating, resulting in a distribution of particle sizes. If the total number of biotin-binding sites was skewed such that the smaller configurations of SA(Cel8A-biotin) have more open sites per complex, then binding of these smaller species would result in a higher estimate for the loading capacity, where M13 surface area is limited. Thus, as more M13-biotin is added, the change in the estimated number of complexes bound to M13, which was determined by the change in total biotin-binding sites after adding M13-biotin, would not scale linearly with increasing M13 surface area.

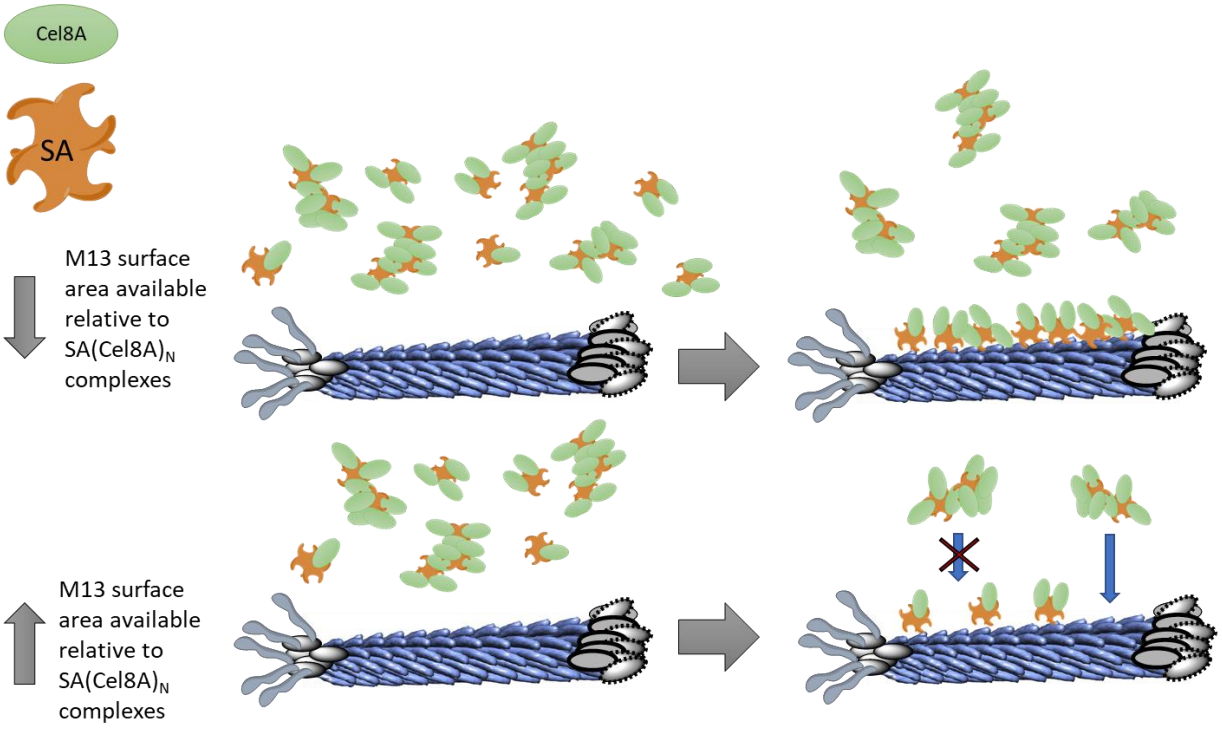

Figure 4.10: Illustration of complexes with varying size loading onto an M13 scaffold at higher, and lower loading ratios (complex:M13). In the top of the figure, there is only limited space available on M13 and once bound to M13, the formed complex is kinetically stable. In the bottom of the figure, as more space opens on the M13 coat, larger complexes might bind – however, the packing becomes less efficient and hence, the estimate for the loading capacity decreases.

In summary, it is possible to first prepare a mixture of SA(Cel8A-biotin) and in a subsequent step, bind to M13-biotin; though only a portion of the Cel8A activity can be associated to the phage scaffold in this way. When preparing M13/SA(Cel8A-biotin) complexes for PEG precipitation, an

excess amount of M13-biotin (~113 SA/Cel8A complexes per M13) was used to ensure maximal binding of SA(Cel8A-biotin). It was found that Cel8A activity could be found associated with the M13 scaffold and indirectly suggested that complexation was occurring. In order to better quantitate the amount of SA(Cel8A-biotin) bound to M13, a fluorescence-based assay was devised to assess binding to M13. This assay was able to provide a lower limit for the loading capacity onto M13 of roughly 340 complexes per M13 using this approach. This gives an idea of the minimum amount of M13-biotin that should be used to ensure that limited surface area on M13 is a negligible factor. Furthermore, the results suggest that there exists a distribution of SA(Cel8A-biotin)$_N$ species with differing valencies (ligand binding sites/molecule) and sizes. This would be confirmed by later experiments examining prepared complexes by TEM.

4.3.2.3 *Visualization of SA(Cel8A-biotin) complexes by TEM*

The indirect assays in the previous section were able to confirm that SA(Cel8A-biotin) could be prepared and then be complexed onto the M13-biotin scaffold in a subsequent step. In order to further understand the arrangement of SA(Cel8A-biotin) complexes on M13, the resulting supramolecular complexes were analyzed by TEM. Cel8A was labelled with antibody-conjugated gold nanoparticles (**GNPs**) to make the localization of Cel8A on M13 scaffolds more obvious. A primary antibody that recognized the His6-tag on Cel8A was paired with a secondary antibody conjugated to a 5 nm GNP. This would be useful in determining the distribution of Cel8A along the length of M13 and would further confirm that SA(Cel8A-biotin) complexes were indeed bound.

SA(Cel8A-biotin) was first prepared by mixing SA and Cel8A-biotin as described in the Methods and then subsequently bound to an excess of M13-PEG$_{12}$-biotin; the resulting complexes were then analyzed by TEM. The appearance of M13-biotin after complexation with SA(Cel8A-biotin) was roughened and bumpy (**Figure 4.11A**). Additionally, it was apparent that there were some particles roughly 10 – 20 nm in diameter and irregularly shaped on the background of the grid. Staining with the antibody-conjugated GNPs revealed that the bumpy protrusions on the surface of M13 were indeed

complexes of SA(Cel8A-biotin) bound to the surface of the phage (**Figure 4.11B**). However, these were irregularly spaced along the length of M13 and the size of the protrusions varied. The background particles observed on the unstained grid were also reactive to the antibody-conjugated GNPs, indicating that Cel8A must be present (**Figure 4.11C**). The average area of the background particles was 130 nm^2 and seemed to be composed of at least two populations of ~190 and 80 nm^2 (**Figure 4.12**). It was not unexpected that there would be some unbound Cel8A – from the ESI-MS estimates, ~23 % of the Cel8A in the Cel8A-biotin (0.74 biotin/Cel8A) sample was unlabeled. However, it is clear from the size of these particles in the non-immunostained image that they are composed of more than a single Cel8A molecule, as Cel8A is ~5 nm in diameter for the cellulase domain. These are therefore likely small aggregates of SA(Cel8A-biotin).

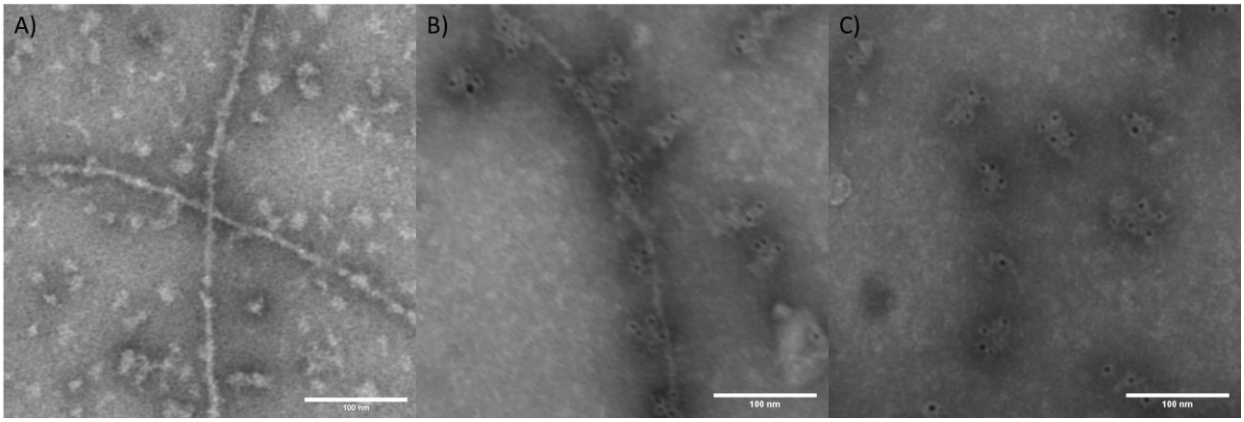

Figure 4.11: Representative TEM images of SA(Cel8A-biotin)$_N$ complexes bound to M13-PEG$_{12}$-biotin. SA(Cel8A-biotin)$_N$ complexes were prepared at 1:1 Cel8A-biotin:SA$_{tet}$ and then bound to 16 µM M13-PEG$_{12}$-biotin. Samples were stained for TEM either with A) 1% PTA, or B, C) immunogold antibody labelling against His6-tag as described in the Methods. White scale bars show 100 nm.

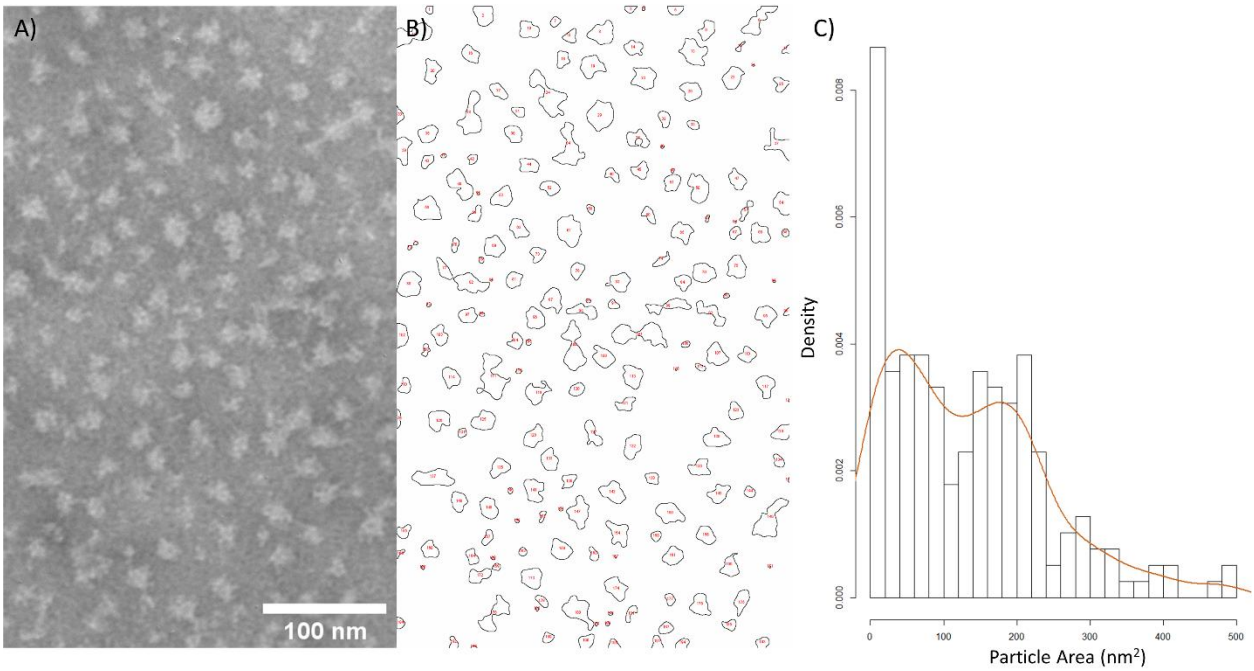

Figure 4.12: Particle analysis of background particles observed on TEM grids of SA(Cel8A-biotin)$_N$ complexes bound to M13-PEG$_{12}$-biotin. A) Representative image of background particles in 1% PTA stained TEM sample. B) Outlines of particles detected using particle analysis tool in ImageJ (version 1.52n). C) Histogram of particle areas measured using ImageJ with associated density plot (n = 196).

In combination with the results of the indirect assays in the previous section, a more complete picture of the M13-SA(Cel8A-biotin) complexes formed by this approach can be elucidated. The results obtained by TEM need to be reconciled with the results obtained from the PEG precipitation assays and the fluorescent B4F assay. First, the PEG precipitation assays were done in order to determine whether endocellulase activity could be found associated M13 phages. This is consistent with the visual evidence of clusters of SA(Cel8A-biotin) bound to the surface of M13 by TEM. Furthermore, it was found that not all the endocellulase activity was associated with M13, as the resulting SN after PEG precipitation still contained Cel8A activity. This would be consistent with the unbound Cel8A in the TEM images.

Second, the B4F assays suggested that all biotin-binding sites present in solutions of SA(Cel8A-biotin) were occupied upon subsequent addition of M13-biotin. However, it is clear from the TEM that SA (in the form of SA(Cel8A-biotin) aggregates) remains unbound. In order to be consistent with the B4F results, these small aggregates of SA(Cel8A-biotin) which are not bound to M13-biotin

must therefore have no accessible biotin-binding sites. Additionally, an excess of M13 ([p8] = 16 µM, $[SA]_{complexes}$ = 1.48 µM) was added to the SA(Cel8A-biotin) complexes in preparing these samples for TEM. From the B4F fluorescence experiments, it was determined that a 1:8 ratio of SA(Cel8A):p8 was sufficient to occupy all detected biotin-binding sites. Inspection of the TEM images show much of the surface area of M13 unoccupied – it is unlikely that steric effects were preventing binding of the unbound SA(Cel8A-biotin). Therefore, it is inferred that upon preparing SA(Cel8A-biotin) complexes in the initial step that a mixture of SA(Cel8A-biotin) clusters with and without available biotin-binding sites form – though the relative concentrations of SA and Cel8A-biotin were such that each SA would have, on average, 3 open biotin-binding sites.

In summary, though the indirect methods of assaying the nature of complexes formed from first preparing SA(Cel8A-biotin) followed by subsequent addition of M13-biotin were promising – imaging of the M13-SA(Cel8A-biotin) complexes by TEM revealed the complexes were not formed as anticipated. Loading Cel8A-biotin onto M13 in this way was inefficient, with much of the Cel8A bound up in small aggregates of SA/Cel8A-biotin that were not capable of binding to M13-biotin. For the Cel8A-biotin batch with 0.74 biotin/Cel8A, though the most abundant species was singly biotinylated Cel8A, ~30% of the Cel8A-biotin species according to the mass spectra have two or more biotin per Cel8A. Future directions taking this approach should carefully consider the extent of biotinylation of the protein of interest. In particular, methods of labelling that can ensure only a single biotin per protein would be preferable. Possible alternative methods that could be recommended are maleimide labeling of free Cys (if a single Cys can be added to the protein of interest) or enzymatic labelling methods that utilizes an incorporated biotinylation recognition peptide sequence.

4.3.3 Method 2: binding Cel8A-biotin to SA-coated M13 scaffold

In a second approach to preparing multi-enzyme scaffolds on M13, the phages were first coated with SA. In the subsequent step, Cel8A-biotin would be bound to the SA-coated M13 scaffold (**Figure 4.13**). Highlighted in this section are some of the factors found to be important in preparing complexes

of M13 with bound SA (referred to generally in this section as **SA-coated M13**). Notably, since both the SA and M13-biotin were capable of forming multiple affinity interactions, there was the potential for a crosslinking side reaction between two or more M13-biotin with SA as a "crosslinker". This was a particularly obvious concern – surprisingly, directly adding SA to biotinylated M13 *under the appropriate conditions* was found to form SA-coated M13 with a low degree of crosslinking observed. Two main factors were explored in preparing SA-coated M13: the ratio of SA:p8 subunits and total concentration of SA/p8 subunits used. These two factors were critical in forming SA-coated M13 without considerable crosslinking "side reactions". The subsequent binding of Cel8A-biotin to this scaffold was demonstrated via TEM analysis to be quite uniform. Further design considerations regarding the stability and dynamic nature of the formed complexes will also be discussed.

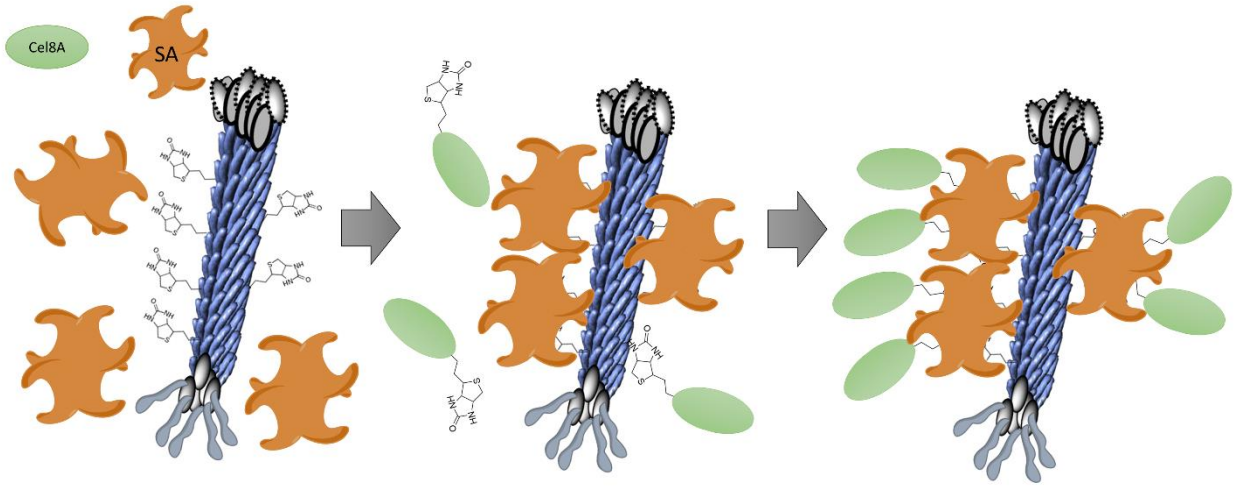

Figure 4.13: Scheme showing assembly of SA onto M13-PEG4-biotin to produce SA-coated M13 followed by assembly of biotinylated Cel8A onto the resulting scaffold.

4.3.3.1 *Preparation of SA-coated M13: SA-coating protects from crosslinking*

Based on the geometry and symmetry of SA, it seemed possible to prepare M13-biotin in such a way that SA was only capable of binding at the adjacent *cis* biotin-binding sites, leaving the opposing two (*trans*) biotin-binding sites for further loading with Cel8A-biotin. This was predicted based on the relative positioning of the biotin-binding sites on SA: two pairs of approximately adjacent ligand-binding sites exist on opposite sides of the molecule (**Figure 4.14A**). A shorter PEG_4 linker (as opposed

to the PEG_{12} linker used in all previous experiments with biotinylated M13) was used in preparing biotinylated M13 (**Figure 4.14B**). This was to reduce the chance of p8-biotin binding to all four biotin-binding sites on SA, as the shorter PEG linker would be expected to restrict the SA to a greater extent.

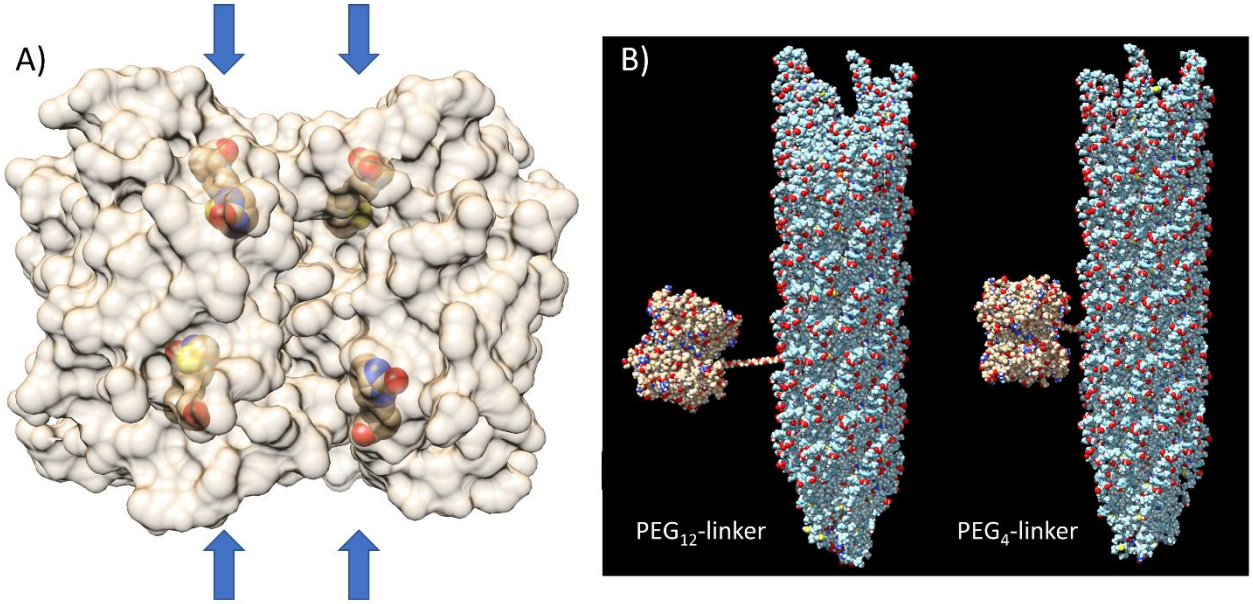

Figure 4.14: Geometrical and size considerations for SA and expected relative lengths of PEG linkers on M13. A) Relative positioning of biotin-binding sites on SA with bound biotin molecules (PDB: 3RY2 (Le Trong et al. 2011)). The arrows show where the openings to the ligand-binding sites are. B) Comparison of relative lengths and spacing expected for M13-PEG_{12}-biotin and M13-PEG_4-biotin with a SA molecule bound to biotin moiety (PDB: 1PFI (D. J. Liu and Day 1994)). The PEG linkers were built out from biotin bound to SA using Maestro (Schrödinger).

It was hypothesized that with an excess of SA, M13-PEG_4-biotin would bind to free SA at a higher probability than SA already bound to M13-PEG_4-biotin – which would be expected to diffuse more slowly in solution. This was considered from the fact that SA binds to free biotin with an on-rate near the limit of diffusion (~130 x 10^6 s^{-1} M^{-1}; (Deng, Kitova, and Klassen 2013)). Furthermore, the slow off-rate of SA was predicted to allow a solution containing SA-coated M13 to be stable once formed. In this way, it might be possible to mix SA and M13-biotin without significant aggregate formation, in contrast to what might be intuitively expected when mixing two multivalent components (SA: 4 ligand-biotin sites, M13: 2700 p8 subunits). Additionally, it was earlier observed that packing of SA onto M13 is quite efficient and has a theoretical optimal packing density of roughly one SA_{tet} for every two p8 subunits (based on TEM observations; **Section 3.3.3.1**). Therefore, if sufficient SA is

added such that M13 is completely coated with SA, there would be little free biotin-p8 to form inter-M13 crosslinks after the initial formation of SA-coated M13. However, if not enough SA is provided to fully cover the surface area of M13, exposed p8-biotin on one M13 could bind to a different SA-coated M13 and aggregate.

Based on this initial hypothesis, if the concentration of SA must indeed be high enough to protect M13-biotin from crosslinking, then at lower ratios of SA:p8, one should expect to see a higher degree of crosslinking and hence phage aggregate formation. At a ratio of 0.25:1 SA:p8, there was poor dispersion of singly SA-coated M13 on the TEM grid (**Figure 4.15A**). Furthermore, where M13 could be found, they existed in large dense aggregates. Indeed, before even spotting the samples to the TEM grids, the solutions had formed aggregates that precipitated out of solution. However, at a 1:1 ratio of SA:p8 (recall, ~1 SA can optimally fit for every two p8 coat proteins), SA-coated M13 were found to be well-dispersed throughout the grid (**Figure 4.15B**). Occasional small aggregates were visible, but the SA-coated M13 visualized on the grid were clearly more dispersed here. Furthermore, no visible aggregation could be seen in solution by visual inspection. Samples were also prepared at a 0.5:1 ratio of SA:p8 (the amount of SA that could be maximally loaded onto M13 with no excess); however, this was similarly prone to aggregation as with the 0.25:1 loading ratio (not shown). Aggregation was seen both by TEM (as in **Figure 4.15A**) and immediately seen after mixing solutions.

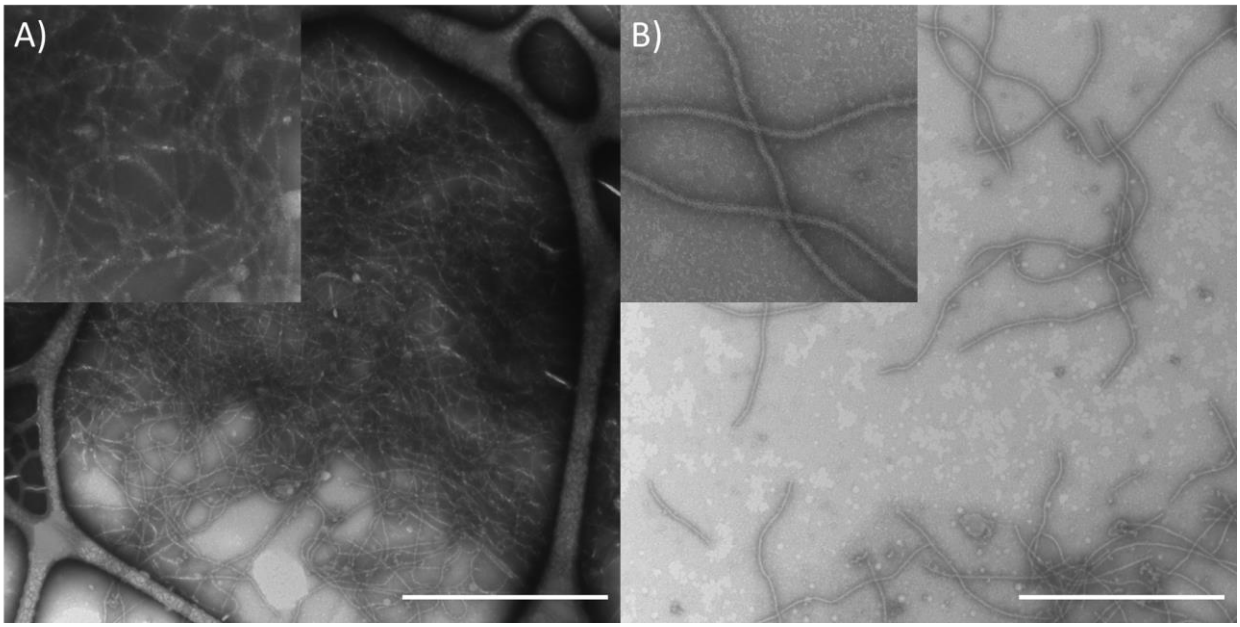

Figure 4.15: Representative TEM micrographs of SA-coated M13 prepared at different ratios of SA:p8. Complexes were prepared at a final concentration of 2 µM p8 and A) 0.5 µM SA_{tet} and, B) 2 µM SA_{tet}. Stained with 1% PTA. White scale bars represent 1 µm. The insets show a 500 x 500 nm area of the same grid.

Interestingly, when preparing SA-coated M13 at even higher ratios of SA:p8 (2:1) an additional side pathway was observed. It was found that preparing SA-coated M13 with too much of an excess of SA resulted in an apparent deformation of the assembled virus itself. When these samples were observed by TEM, there were several instances where the M13 particles appeared to collapse and twist in upon themselves (**Figure 4.16**). Several representative species along this apparent pathway were captured in a series of TEM images from this grid. First, the coat toward one of the ends of the phage was observed to curve and separate from the rest of the phage (**Figure 4.16, panel 1**). The following steps give the impression that as additional p8-biotin become exposed, the SA is able to bind and further force the phage into an arrangement that is more compact. It has been observed that under certain solvent conditions, chloroform in particular, that the major coat protein adopts a very different packing structure referred to as open-form phage (Griffith, Manning, and Dunn 1981; D. A. Marvin, Symmons, and Straus 2014). While unlikely that the mechanism is the same, this example does highlight that p8 subunits have been observed to radically change their packing structure under specific conditions. Something analogous might be occurring here, but instead of a change in solvent conditions

inducing a different packing structure of the major coat protein, the tight binding of SA might force the biotinylated p8 coat proteins into a different conformation. Importantly, these altered phage were infrequently observed where the ratio of SA:p8 was 1:1 and so these conditions were used in future preparations of SA-coated M13.

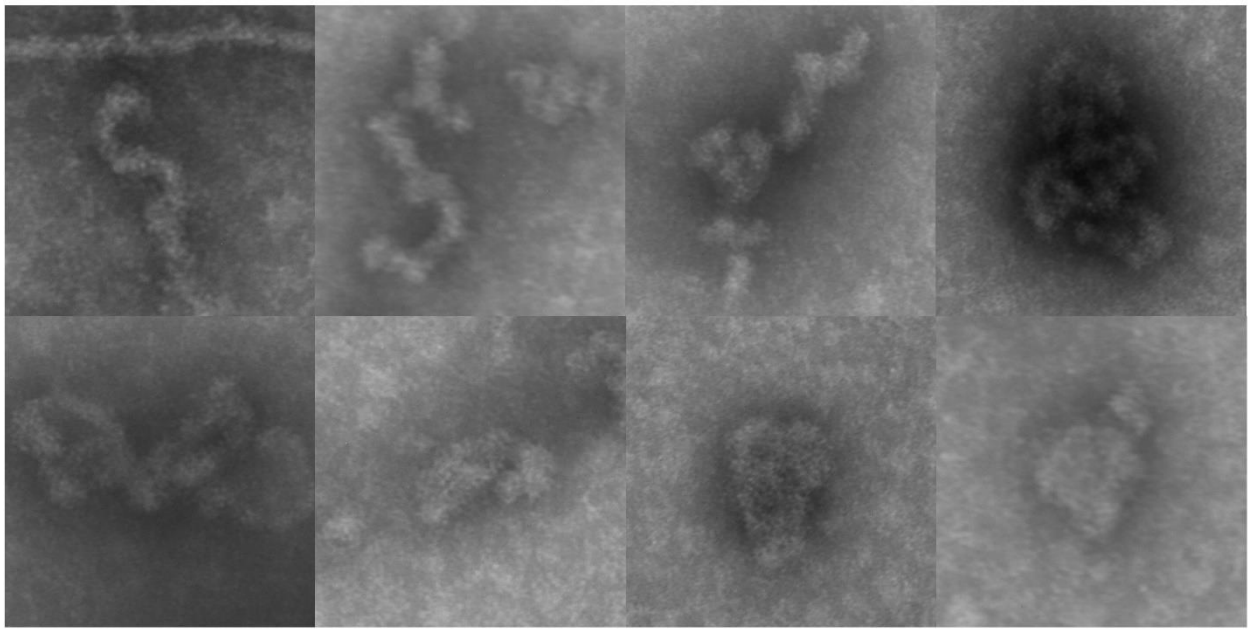

Figure 4.16: Representative TEM images showing SA-coated M13 (prepared from M13-PEG$_4$-biotin at 2 µM p8 subunits and 4 µM SA$_{tet}$) with altered packing structure. Stained with 1% PTA. Each panel is 200 by 200 nm.

If the complexes were able to form as predicted – with two *cis*-facing biotin-binding sites attached to M13-biotin, and two outward facing – then, upon adding Cel8A-biotin, the enzyme should be able to bind to the SA-coated M13 complex. After preparing these complexes with an approximately stoichiometric amount of Cel8A-biotin (according to number of biotin and expected biotin-binding sites in the SA-coated M13 sample), they were adhered to TEM grids and were immunostained with GNPs against the His6-tag on Cel8A. The surface of the phage was rough with very obvious "nodules" which protruded from the phage (**Figure 4.17A**). When these were labelled with antibody GNPs, Cel8A was detected ubiquitously along the length of SA-coated M13 (**Figure 4.17B**). Notably, the Cel8A was detected uniformly distributed along the entire length of the phage. Though it was apparent that there was a considerable amount of Cel8A unbound to the SA-coated M13 scaffold, this was anticipated,

given that an excess of SA was used in preparing SA-coated M13. Therefore, upon adding Cel8A-biotin, some would bind the scaffold, and some would bind SA that was free in solution. This demonstrated that after coating with SA there still existed available biotin-binding sites with which to further complex with biotinylated enzyme. Importantly, being able to produce a multi-enzyme complex on M13 that was extensively and uniformly loaded was one of the main goals of this work.

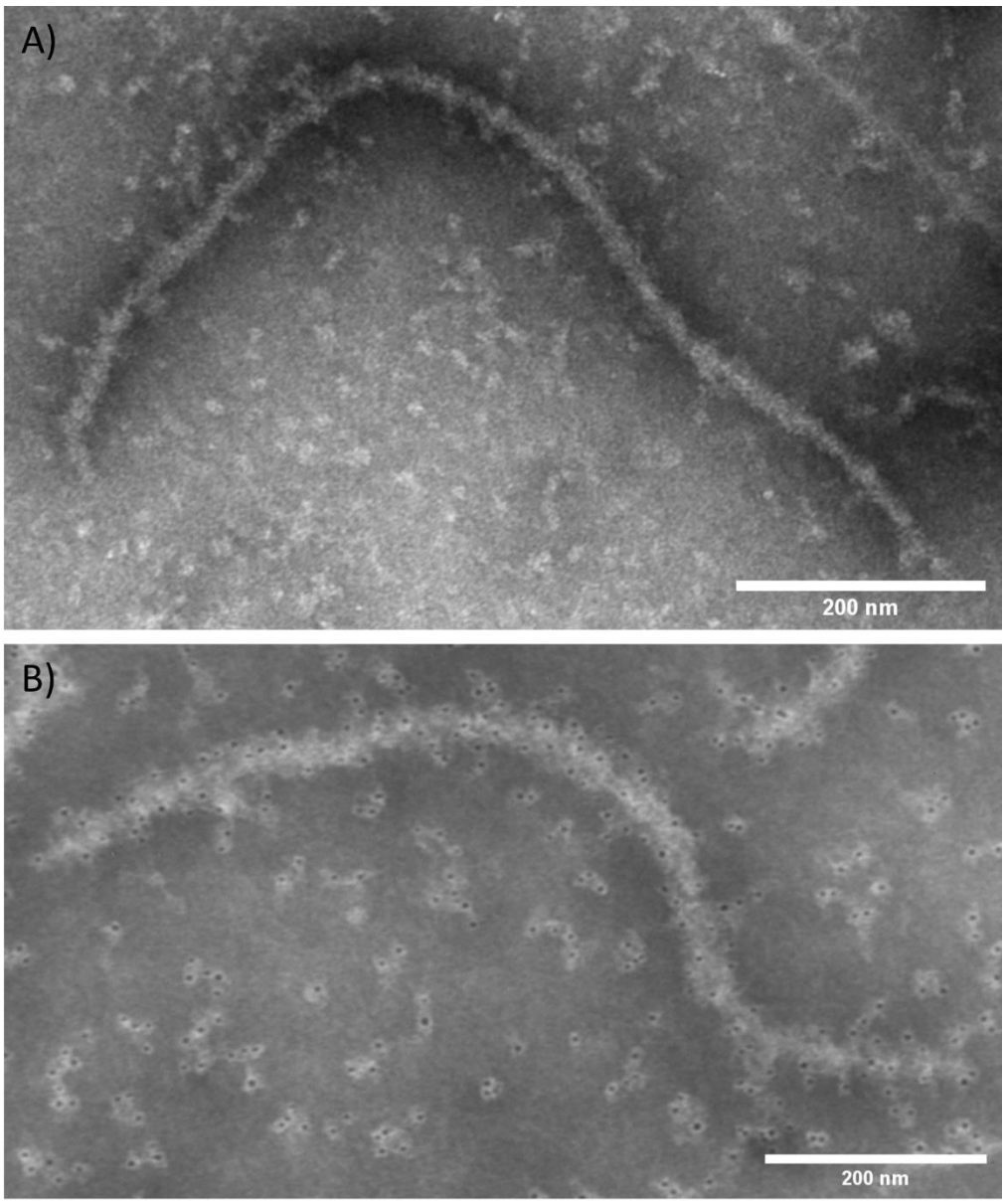

Figure 4.17: Representative TEM images of Cel8A -biotin bound to SA-coated M13 nanoscale scaffold. SA-coated M13 was prepared with 2 µM p8-PEG$_4$-biotin and 2 µM SA$_{tet}$ and then mixed with 8 µM desthiobiotin. Cel8A-PEG$_{12}$-biotin (0.74 biotin/Cel8A) was added to a final concentration of 3.2 µM. TEM samples were stained with A) 1% PTA, and B) immunostained with anti-His6 primary antibody, and 5 nm secondary antibody GNP followed by staining with 1% PTA.

Studies on the binding of SA to biotinylated lipid surfaces is relevant to the discussion of this SA-coated M13 complex. While dissolved in solution, M13 can be thought of as a high curvature surface. A comprehensive study of the residual valency to a lipid surface demonstrated several important considerations for the binding of SA to a surface (Dubacheva et al. 2017). One relevant result in particular was the relationship between packing density (of SA on a biotinylated surface) and the resulting valency of SA binding to that biotinylated surface. A residual valency (free biotin-binding sites on SA) of two was favored in the likely case where steric interactions between surface-bound SA may have prevented binding to a third site. Or in other words, a high density of SA bound to a surface sterically prevents neighboring SA from binding more than twice to that surface. Considering that the SA-coated M13 produced here was able to further bind to Cel8A-biotin and that SA were densely packed suggests a residual valency of two in SA-coated M13.

Furthermore, there was a recommendation that a binding valency of two be made in order to ensure stable interaction of SA with a surface. It was found that SA bound by two or more biotin to the surface could not be washed away easily, showing increased stability and lifetime of SA on the surface (Dubacheva et al. 2017). This consideration is also relevant here, as it is desirable to have a long-lived interaction of SA with the biotinylated surface of M13 to ensure stable binding in subsequent steps after adding biotinylated enzyme to the scaffold. In summary, the idea to directly bind SA to M13-biotin was initially counterintuitive based on the potential for crosslinking and aggregation. Interestingly, the fast binding of SA to the surface of M13, and dense packing that can be achieved made this a viable strategy for decorating the surface of M13 with “sticky” ligand binding sites for the binding of additional components. Some additional considerations and potential challenges with this system are presented in the following sections.

4.3.3.2 *Low concentration of SA and M13-PEG$_4$-biotin are required to reduce crosslinking behavior*

It was anticipated that the concentrations of SA and M13-biotin would be an important factor in forming SA-coated M13 without too much aggregation. In particular, at higher concentrations of M13-

biotin, the chance of a "crosslink" occurring would likely be higher, as the average distance between M13 particles in solution would be reduced and this might translate to a higher degree of aggregation when SA is added. This was tested by preparing 1:1 ratios of SA:p8 at 2, 10 and 20 µM (for each component) and qualitatively assessing the mixtures by TEM. For SA-coated M13 prepared at the lowest concentration tested (2 µM), M13 phages were overall well-dispersed and uniformly bound to the TEM grid (**Figure 4.18A**). In the samples prepared at either of the higher concentrations, M13 was poorly dispersed on the grid (**Figure 4.18B, C**). Large, dark aggregates were also visible, though the electrons penetrated poorly due to the thickness of these aggregates – these could only be visualized as dark shapes, sometimes with the ends of phage visible at the periphery. Though this approach to characterizing the extent of aggregation was only qualitative, it does seem to indicate the importance of preparing SA-coated M13 at lower concentrations.

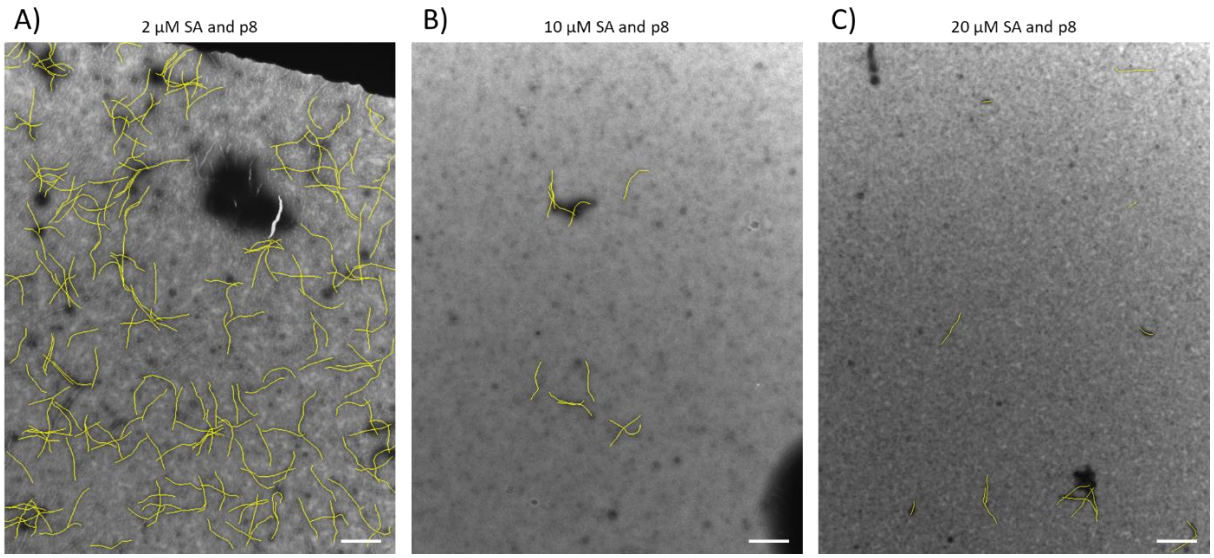

Figure 4.18: TEM micrographs of SA-coated M13 at a 1:1 ratio of SA:p8 at different concentrations. Samples were further complexed with Cel8A-PEG$_{12}$-biotin (0.74 biotin/cel8A) so that the samples could be stained with immunogold as described. A) SA-coated M13 prepared at 2 µM SA and 2 µM p8. B) SA-coated M13 prepared at 10 µM SA and 10 µM p8. C) SA-coated M13 prepared at 20 µM SA and 20 µM p8. SA-coated M13 complexes were diluted down to 2 µM SA, and Cel8A-PEG$_{12}$-biotin (0.74 biotin/Cel8A) was added to a final concentration of 3.2 µM. M13 were highlighted individually using ImageJ image analysis software to aid visibility. Scale-bars represent 1 µM.

Analysis of the results in terms of expected average distance between M13 particles at different concentrations can aid in understanding these interactions. As the concentration of the two components is increased, there is a higher likelihood that two M13-biotin$(SA)_N$ (M13 with some amount of SA

bound) to meet and form a crosslink. As the concentrations decrease, the average distance between any M13 increases and the likelihood of two particles meeting would be expected to decrease. There is likely an interplay between the rate at which diffusing SA can quickly and efficiently coat the M13-biotin (covering up any "sticky" p8 biotin patches), and the rate at which two M13 phages come into contact resulting in some crosslinking side product. This unfortunately does preclude the possibility of preparing SA-coated M13 at higher concentrations initially. However, given the tight binding of SA and biotin, it is quite possible to get complete complexation with biotinylated target without having to employ high concentrations.

4.3.3.3 *Dynamic behavior and stability at higher temperature*

It is expected based on the increased off-rate of SA/biotin at higher temperatures (half-life of ~46 min at 44.8 ºC, compared to 35 h at 22 ºC (Deng, Kitova, and Klassen 2013)) that some dynamics will occur at higher temperatures. This was also seen in **Section 3.3.1.2** where $SA(BXN)_4$ was found to exchange BXN molecules for B4F molecules over time at elevated (50 ºC), but not at ambient (23 ºC) temperatures. In particular, those dynamics could include potential unbinding and rebinding of Cel8A-biotin, or even SA from the surface of M13-biotin. It was conceivable then, that at higher temperatures, complexes of Cel8A-biotin prepared on the surface of SA-coated M13 might tend to aggregate over time as these components rearrange themselves. This aggregation could occur either via a) p8-biotin binding to a different SA-coated M13 or, b) Cel8A-biotin forming a crosslink between two SA-coated M13. The effects of incubation at 50 ºC were tested to see whether and how this affected the overall structure of the M13/Cel8A complexes over time. This was further relevant to reactions carried out with Cel8A which are typically carried out at temperatures at or greater than 50 ºC for efficient hydrolysis of cellulose.

SA-coated M13 with Cel8A-biotin bound were visualized by TEM to make a comparison of how quickly they might tend toward larger aggregates over time when incubated at 50 ºC. Samples were observed after 0, 1 and 4 h incubation at 50 ºC. Over the timeframe observed, Cel8A-biotin was

observed to be ubiquitously bound to M13 particles (**Figure 4.19**). The appearance of individual phages with Cel8A-biotin bound were similar between the incubation times used. In order to give a representative overview of these TEM grids, several images were taken at low magnification (13,000x) in order to qualitatively assess the extent of aggregation of these samples (**Figure 4.20**). There did seem to be a larger number of electon-dense aggregates that formed at 4 h incubation time, but surprisingly, the dispersion of SA-coated M13 with bound Cel8A-biotin was still quite good. Given the dynamic nature of the components expected at 50 ºC, and the number of possible interactions (mediated by SA and biotin) that could potentially form between two phages, it is remarkable that the extent of aggregation overtime is not more noticeable.

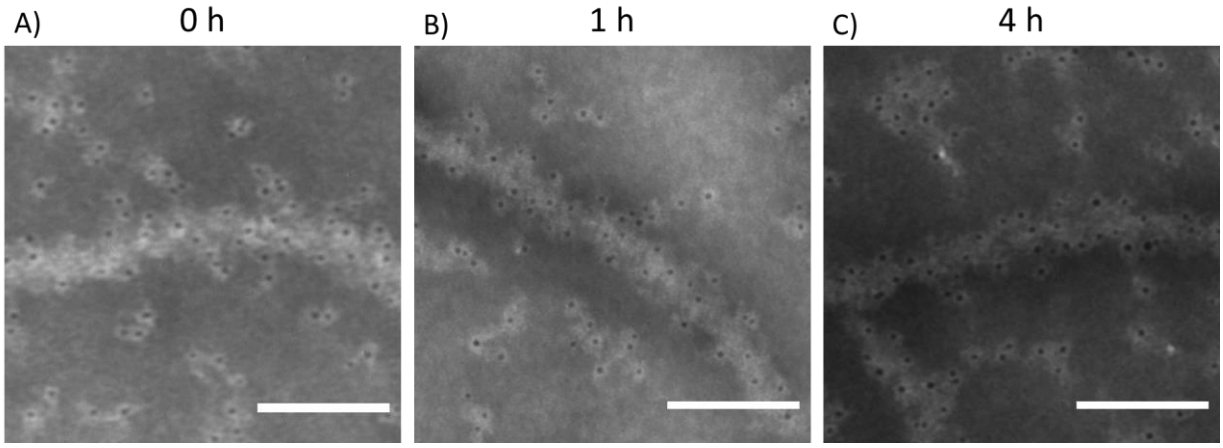

Figure 4.19: Effect of incubation of SA-coated M13 with Cel8A-biotin at 50 ºC. SA-coated M13 was prepared with 2 µM p8-PEG$_4$-biotin and 2 µM SA$_{tet}$ and then mixed with 8 µM desthiobiotin. Cel8A-PEG$_{12}$-biotin (0.74 biotin/Cel8A) was added to a final concentration of 3.2 µM. These were incubated at 50 ºC for A) 0 h, B) 1 h, and C) 4 h. Samples were labelled with primary antibody against His6-tag and 5 nm secondary antibody GNP. White scale-bars represent 100 nm.

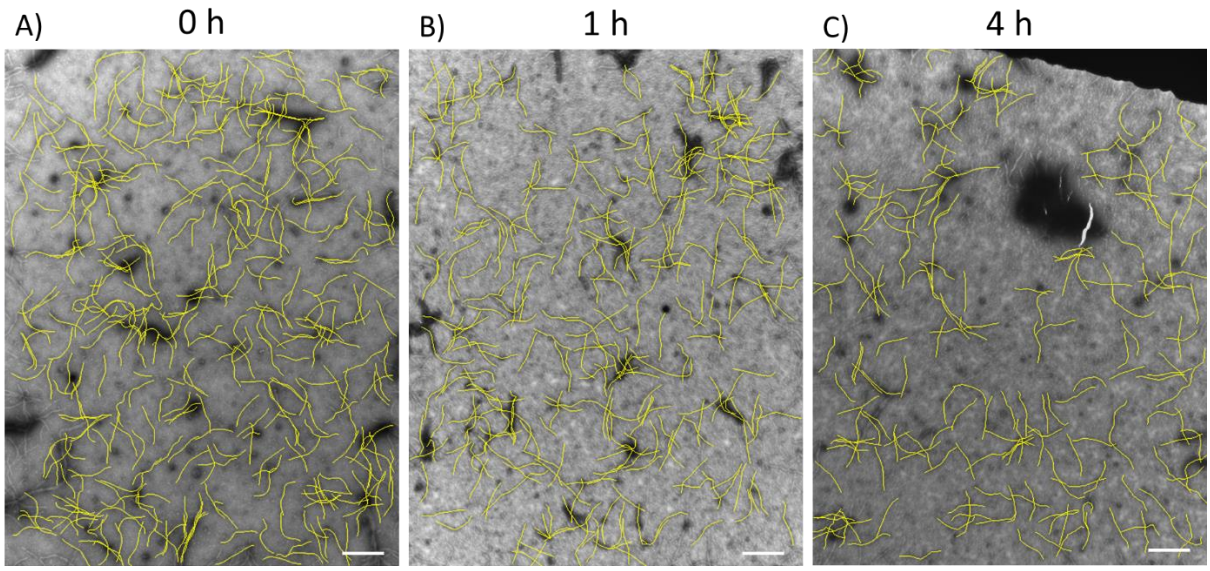

Figure 4.20: Effect of incubation of SA-coated M13 with Cel8A-biotin at 50 °C (wide view). SA-coated M13 was prepared with 2 µM p8-PEG$_4$-biotin and 2 µM SA$_{tet}$ and then mixed with 8 µM desthiobiotin. Cel8A-PEG$_{12}$-biotin (0.74 biotin/Cel8A) was added to a final concentration of 3.2 µM. These were incubated at 50 °C for A) 0 h, B) 1 h, and C) 4 h. Samples were labelled with primary antibody against His6-tag and 5 nm secondary antibody GNP. M13 phages were highlighted individually using ImageJ image analysis software to aid visibility. Scale bars represent 1 µM.

It was expected that there would be some dynamic behavior among the components used to prepare a multi-enzyme complex on M13, and all the possible interactions expected to occur in this mixture of components are quite complex. There are three different components (M13-biotin, SA and Cel8A-biotin) which are all capable of binding to each other in various configurations. It is because of this complexity that the observations made in this data set were so surprising. One aspect of these findings that should be considered is the idea of avidity; that the same SA molecule is capable of binding at two of its biotin-binding sites on the same biotinylated M13 surface. It is typically found that avidity interactions can greatly increase the lifetime of a protein ligand interaction through rebinding (Vauquelin and Charlton 2013). The idea is that forced proximity can promote rebinding of a protein to a nearby ligand, and thereby increase resident time. While a single biotin bound to SA may be expected to dynamically exchange, SA bound "bivalently" to the biotin-M13 surface could exhibit a longer-lived interaction. Recall from **Section 3.3.3.1** that the expected spacing of two adjacent biotin on the surface of M13 would be ~3 nm, which is certainly short enough distance for bivalent binding to SA (diameter of SA is ~6 nm). This could have a very significant impact on the lifetime and stability of a single,

particular SA bound to the surface of biotinylated M13. While the off-rate of biotin/SA increases at higher temperature, for SA to be liberated from the surface of M13 when in such a configuration both biotin would need to dissociate before rebinding occurs.

A second consideration is that free SA (or SA(Cel8A-biotin) in solution plays a protective role. Upon forming SA-coated M13, there is an excess of free SA in solution (recall from **Section 4.3.3.1** that this is necessary for forming SA-coated M13 without aggregation). This free SA may be playing a protective role, quickly replacing any SA displaced from the surface of M13-biotin. Consider what might occur when a SA or SA(Cel8A-biotin) dissociates from the surface of M13-biotin; the exposed patch of M13-biotin would either encounter another SA-coated M13, or one of the free SA present in the solution. If the exposed patch binds to SA present on a separate phage, aggregation may occur. Thus, the excess SA may protect from aggregation by quickly binding to any exposed p8-biotin patches before the formation of a crosslink with another SA-coated M13.

If having an excess of SA is required for the stability of formed SA-coated M13 multi-enzyme complexes, it would be expected that this would make removal of unbound components (excess SA, and Cel8A) detrimental. However, it should be noted that in cellulosomal arrangements of enzymes, there is expected to be considerable dynamics, as the cohesin-dockerin interaction is itself non-covalent. Thus, it might be sufficient that a proportion of Cel8A exists bound to the designed nanoscale scaffold with a defined lifetime – with individual cellulases docking and releasing back into solution dynamically. In this way, there would be an increased concentration of cellulase localized on the surface of phage on average. This would of course depend on a number of parameters, such as the lifetime of residence of a single docked enzyme. Regardless, the apparent stability of SA-coated M13 with complexed enzyme at increased temperature was an interesting phenomenon, though the potential requirement for excess SA to be present could be a potential challenge in some applications.

4.3.3.4 *Importance of ionic strength*

Lastly, it was discovered that the ionic strength of the solution used when preparing SA-coated M13 from M13-PEG_4-biotin and SA affected the stability of the resulting SA/M13 complex. When prepared in water, the SA-coated M13 formed with the expected dimensions (**Figure 4.21A**). Furthermore, the phages were well-dispersed on the grid and easy to locate. However, when preparing SA-coated M13 in a buffered solution, the samples had a few notable differences when observed by TEM. Even though the samples were prepared at the same concentrations, there were few phages observed on the grid. Furthermore, phages that were found on the grid had a "bushy" appearance – as if they were falling apart (**Figure 4.21B, C**). The appearance of these "damaged" phages could be consistent with the lack of phage observed on the grid, as they degrade over time. The conclusion was that the phages prepared in 1x TBS were not stable and peeled apart into smaller particles.

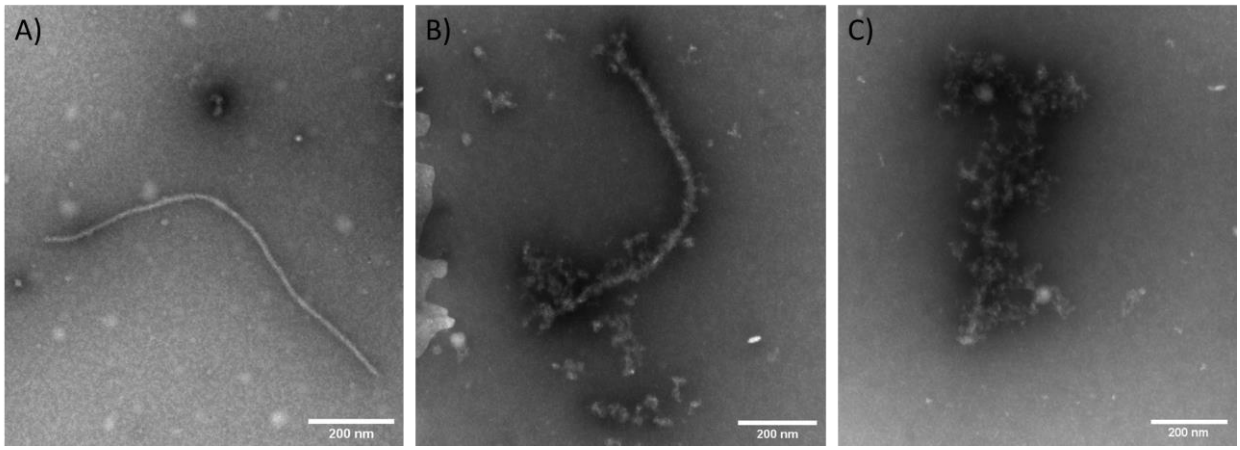

Figure 4.21: Representative TEM images showing the effect of ionic strength in structure of SA-coated M13. Complexes were prepared at a final concentration of 2 µM p8 and 2 µM SA_{tet} in A) water, and B, C) 1x TBS pH 7.4. Stained with 1% PTA.

Firstly, though designed to only bind bivalently to one side of SA at the adjacent *cis* ligand-binding sites, it is feasible that adjacent p8-biotin might be capable of binding to ligand-binding sites of SA in the *trans* configuration. If this occurs, it could force or restrict the flexibility of the M13 particle in a way that starts to destabilize the intermolecular interactions between p8 subunits. This is reminiscent of the collapsing phage observed in **Section 4.3.3.1** where it was hypothesized that SA bound more than twice to the same M13-biotin surface could start to deform or destabilize the packing of p8 coat proteins. The binding of SA to three or more p8-biotin on the same phage SA could act as an

initial trigger for this "collapse", as it could force curvature which in turn could position additional p8-biotin to re-bind to SA on the same phage particle further pulling the subunits apart.

Given that one difference between preparing the SA-coated M13 in 1x TBS versus water would be the ionic strength of those solutions, it is reasonable to consider possible electrostatic effects. The overall charge on the surface of M13 is negative (pI of 4.2 (Zimmermann et al. 1986)) and SA has a theoretical pI of 6.09 (negative at neutral pH; calculated using ProtParam (Gasteiger et al. 2005)). It is therefore conceivable that in low ionic strength solutions there is an electrostatic barrier (repulsion) to SA orienting in such a way that allows binding to one of the *trans* biotin-binding sites. However, upon switching to a solution with greater ionic strength, the range of that electrostatic repulsion could be reduced by charge screening, allowing SA bound to the surface of M13 to re-orient such that neighboring p8-biotin can bind to the *trans* biotin-binding sites, triggering the process leading to the degradation observed in the TEM images above. This leads to an additional design consideration that was not initially apparent: that of potential electrostatic contributions to the stability of the formed complexes on M13. Though it might be possible that binding of an additional component (i.e., Cel8A-biotin) might "cap off" the phage and have a stabilizing effect on the entire structure. Consider the SA-coated complexes with Cel8A-biotin in **Section 4.3.3.3** at 50 °C; despite the higher dynamics that occur at this temperature, the complexes remained stable for at least 4 h. While there is instability apparently present with SA-coated M13, further complexation with Cel8A-biotin may be stabilizing.

4.3.3.5 *Attempts to purify SA-coated M13 from other components*

Due to the multi-component nature of the M13 complexes, a gentle method was sought to remove unbound components (SA and Cel8A-biotin) from Cel8A-biotin mixtures complexed to SA-coated M13. In particular, a method that utilizes a small surface area would hopefully reduce the loss of materials from non-specific binding. Due to the requirement of low µM SA and p8 concentrations when assembling SA-coated M13, typical separation methods such as chromatography were expected to result in a considerable loss of any material applied to a column. Drop dialysis, a method analogous to

conventional dialysis, was tested as a purification procedure. In drop dialysis, a filter membrane is floated on a dialysis buffer and solution to be dialyzed is pipetted on top of the filter. This method has been reported to be useful for dialyzing small volumes of biomolecules, with DNA and protein recovery being reported as high at 98% (Marusyk and Sergeant 1980). This approach has been used to desalt proteins for mass spectrometry (Cancilla et al. 2000; Lehmann Renato Zenobi and Vetter 1999) and for removal of reactants in reactions with biomolecules (Brin et al. 2000). In particular, there is evidence that over time, proteins will also be removed by drop dialysis (Görisch 1988). A half-life of about 85 min was reported for ribonuclease by drop dialysis. Thus, if the relatively small SA could be removed at a rate faster than M13, this approach could be suitable.

The envisioned clean-up procedure was as follows: SA-coated M13 would be first prepared as described, followed by removal of excess SA. The resulting solution would be expected to contain only biotin-binding sites associated with M13 and thus, would be used as the base material for stoichiometric complexation of Cel8A-biotin. This procedure was initially tested with the individual components SA and M13. An exponential decrease over time ($t_{½}$ ~ 1.3 h) was observed with SA on its own (**Figure 4.22A**). The loss of M13KE titer was slower than the loss of SA over the course of 4 h. While complete removal of free SA would be unlikely, the resulting drop-dialyzed solution would be enriched with M13. To further test this, SA either in the presence of M13KE (no interaction) or with M13-PEG_4-biotin (to prepare SA-coated M13) was monitored overtime by drop dialysis. The decrease in biotin-binding sites over time when SA was mixed with biotinylated M13 was slower than with the nonbiotinylated control (**Figure 4.22B**). This suggested that perhaps the fraction of SA that was bound to M13-PEG_4-biotin might dialyze out at a slower rate than free SA. A time point of 3 h was chosen to examine dialyzed solutions, as this seemed a good compromise between removing SA and retaining some M13 particles. Since the concentrations of components were low in these mixtures, the samples which were drop dialyzed were immediately adhered to TEM grids and analyzed by TEM. However, no

recovered samples were visible on any of the TEM grids – typically, at this order of magnitude of phage concentration (~10^{11} particles/mL), phage particles uniformly coat the grids.

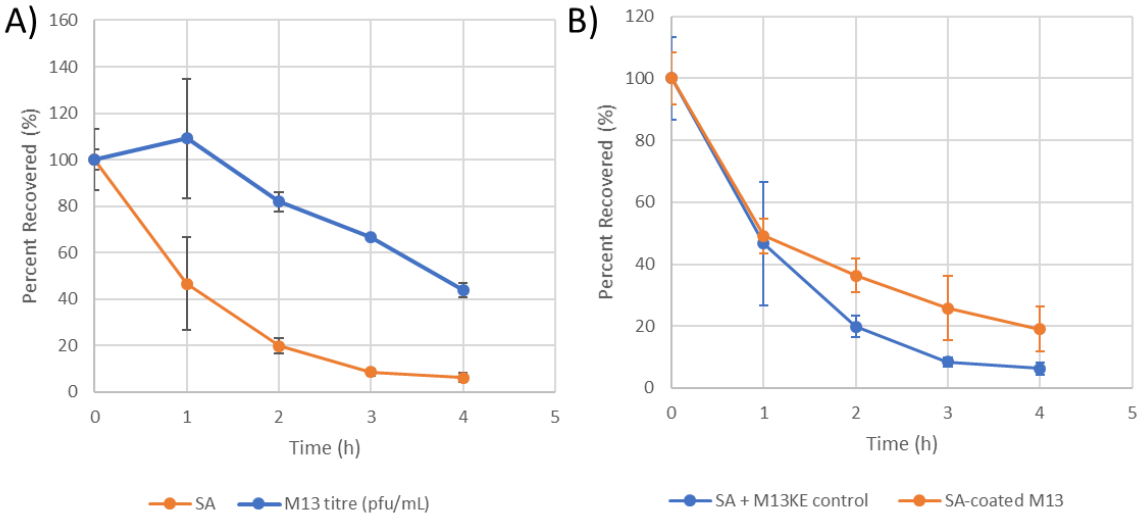

Figure 4.22: Testing the suitability of drop dialysis for cleaning up SA from SA-coated M13 preparations. A) Recovered M13KE (no biotin) and SA from a mixture of SA and M13KE applied to drop dialysis over 1x TBS pH 7.4. The percent recovery for M13 was based on the titer (plated twice per time point) of a single trial. The percent recovery for SA was determined from its biotin-binding activity using B4F (determined three times per time point) for a single trial. B) Recovered SA mixed with either M13KE (no biotin) or M13-PEG$_4$-biotin and applied to drop dialysis over 1x TBS pH 7.4. The recovered SA was determined according to its biotin-binding activity using B4F (determined three times per time point) for a single trial. Mean values and SD are shown.

As it was observed that ionic strength was detrimental to the stability of SA-coated M13 particles (**Section 4.3.3.4.**), drop dialysis procedures were briefly tested in MQH$_2$O. Drop dialysis of SA over MQH$_2$O was carried out and SA concentration was observed to decrease at a similar rate to SA in 1x TBS pH 7.4 (not shown) and so it was expected that 3 h of drop dialysis would still be appropriate before analyzing the resulting mixtures by TEM. SA-coated M13 with complexed Cel8A-biotin was dialyzed over water for 3 h and then the resulting solutions analyzed by TEM. An aliquot of the prepared SA-coated M13 with Cel8A-biotin was removed prior to drop dialysis as a control. The control was consistent with the appearance of other SA-coated M13 with bound Cel8A-biotin that were shown in previous sections (**Figure 4.23A**). The M13 particles had a roughened surface from bound Cel8A and unbound SA(Cel8A-biotin) particles were observed as well. Additionally, these were well-distributed on the TEM grid as seen previously. However, after 3 h of drop dialysis there were far less

M13 particles that could be imaged (**Figure 4.23B**). The M13 that could be found were typically bundled together in small aggregates. One possibility is that too many M13 particles were lost over the course of drop dialysis – possibly due to adsorption to the membrane used for drop dialysis, as the 0.05 µM pore diameter should have prevented transfer through the membrane. A second possibility is that some amount of excess SA is necessary for the stability of the SA-coated M13 particles. If a SA were to dissociate from the surface of M13-biotin, having an excess of SA would make it more likely that a different SA diffuses in to bind to the empty spot, rather than it encountering a second SA-coated M13. Regardless of the reason, this was found to be unsuitable for cleaning up preparations of SA-coated M13.

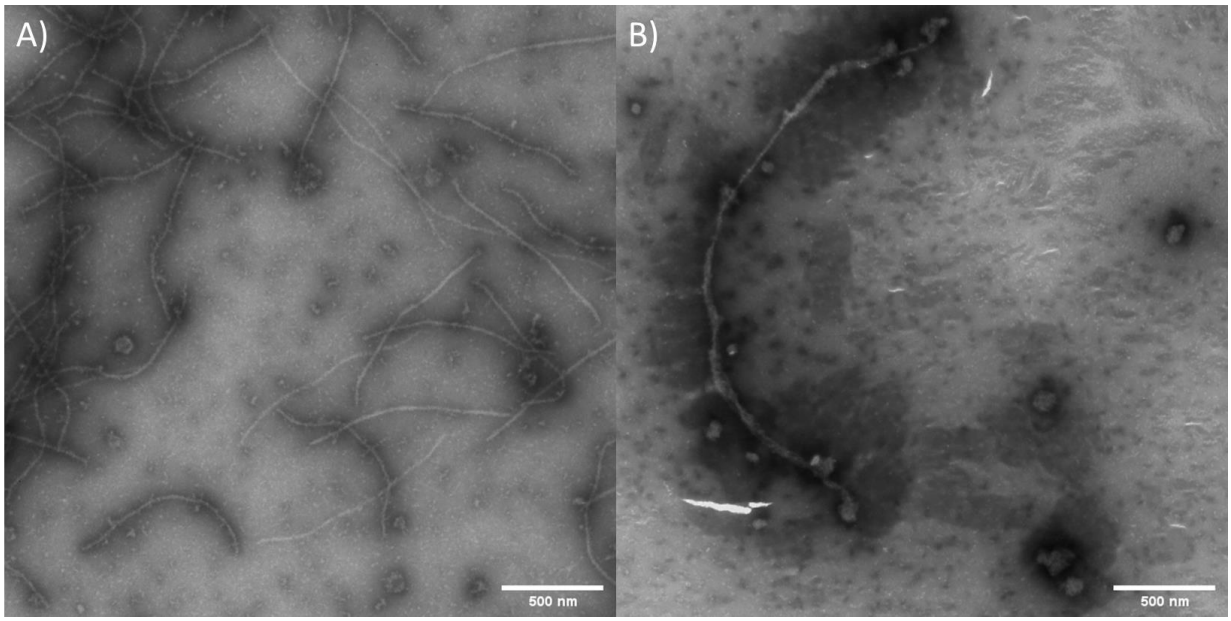

Figure 4.23: SA-coated M13 with bound Cel8A-biotin recovered from drop dialysis. SA-coated M13 complexes with Cel8A-biotin were prepared as described in the methods and subjected to drop dialysis on water for A) 0 h, and B) 3h. After that time, the samples were removed and adhered to TEM grids which were stained with 1% PTA.

A second approach was tested to clean up SA-coated M13 preparations. Given the difference in size between SA-coated M13 and individual SA(Cel8A-biotin) particles, differential centrifugation was attempted. This was carried out at 4 ºC in order to reduce the chance of SA/biotin dissociation, followed by potential inter-phage links forming. Prepared SA-coated M13 were centrifuged at 15000 *g* for 3 h. When the resulting pellet was resuspended and analyzed by TEM, phage that were observed were in

large aggregates (**Figure 4.24A**). M13 particles that were tangled together were of a diameter consistent with that expected for SA-coated M13 (**Figure 4.24B**). Given that centrifugation would ultimately cause the average distance between SA-coated M13 to decrease as they form a pellet, it is not surprising that they ultimately aggregated together in this way.

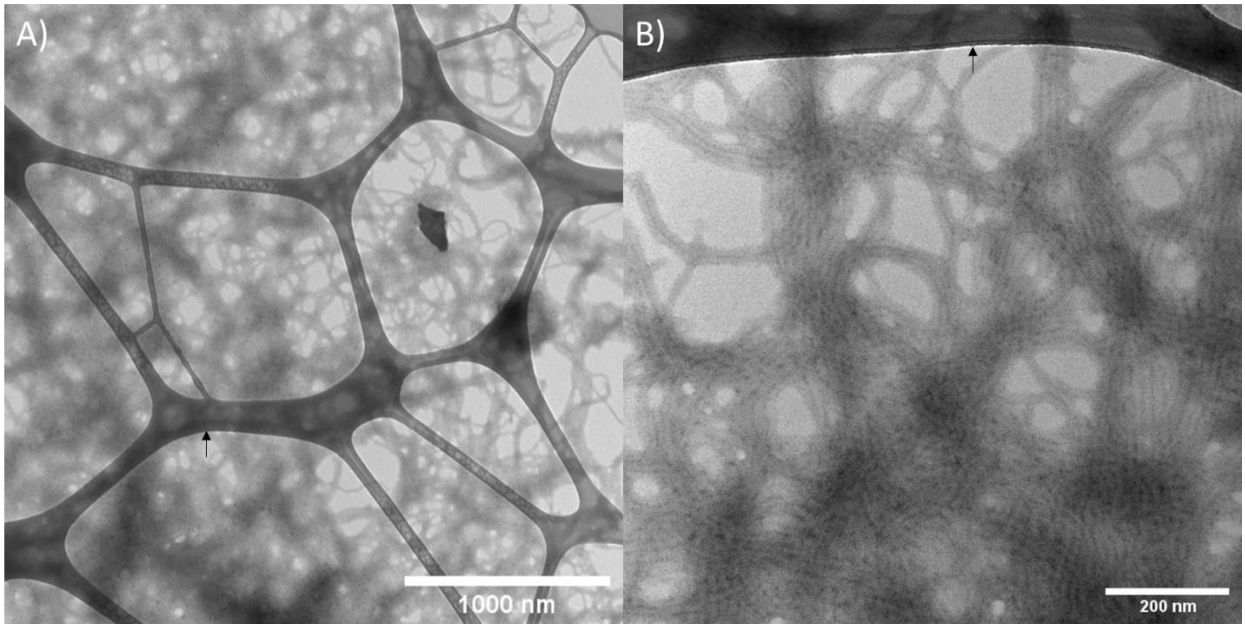

Figure 4.24: TEM of SA-coated M13 recovered from the pellet after differential centrifugation. A) Wide view of tangled M13 particles. B) Higher magnification image of a section of M13 tangle. The black arrows show the lacey carbon from the grid itself.

In summary, two methods were tested to try to remove unbound SA from SA-coated M13 preparations: drop dialysis and differential centrifugation. Neither of these approaches were successful; however, the drop dialysis results did ultimately highlight some factors that appeared to be important to phage stability. The apparent instability of SA-coated M13 in salt-containing solutions was first noticed when analyzing samples drop dialyzed over buffered solution (discussed more in **Section 4.3.3.4**). However, even when carried out in water, there were few recovered phages to be imaged – perhaps due to adsorption to the membrane, or some other factor involving lowered stability in the absence of some amount of free SA. Despite the unfortunate difficulties here, recall that SA-coated M13 with bound Cel8A-biotin was stable at 50 ºC for up to at least 4 h (**Section 4.3.3.3.**). Given that SA-coated M13

with bound Cel8A-biotin remains stable without removal of unbound particles, it would potentially be worth testing the activity of these complexes against cellulose substrates.

4.3.4 Cellulase activity assays SA(Cel8A-biotin) complexes on M13-biotin

Despite the difficult in purifying the M13 complexes from the unbound components, it was desired to at least evaluate what kind of activity these complexes had against cellulosic substrates. It has been observed that a good proportion of Cel8A-biotin exists bound to the phage scaffolds produced by the two methods used in this chapter (SA(Cel8A-biotin) bound to M13-biotin in **Section 4.3.2**; SA-coated M13 with bound Cel8A-biotin in **Section 4.3.3**). If there is a considerable rate enhancement from Cel8A-biotin complexed onto phage scaffold, this might be observed even in the presence of unbound components. Furthermore, since the SA-coated M13 was shown to maintain its structure over the course of at least 4 hours at 50 ^{o}C when in the presence of unbound SA(Cel8A-biotin), it might be beneficial to the stability of SA-coated M13 particles to carry out reactions without removal of those excess components. Thus, the mixture of components would be likely to exist as a dynamic system with SA(Cel8A-biotin) dissociating and rebinding over the course of a reaction. Considering that the off-rate for SA/biotin at 44 ^{o}C is ~2.5 x 10^{-4} s^{-1} (Deng, Kitova, and Klassen 2013), it is still expected that docked Cel8A-biotin would have a relatively long-lived interaction with the biotinylated M13-biotin scaffold.

Indeed, extensive consideration on the necessary interactions in the native cellulosome suggest a conformationally flexible arrangement of cellulases where considerable dynamics of the cellulase-laden scaffold occurs (S. P. Smith and Bayer 2013). For example, with type 1 cohesin-dockerin interactions (**Section 1.4**) binding can occur in two modes (oriented ~180^{o} to each other) and it has been speculated that the ability of the cellulases to dock in a way that allows flexibility in orientation over the course of degrading cellulose could be important for efficient activity. As it is unlikely that the cellulosome itself is a static system, it is potentially worth exploring the cellulolytic activity of these nanoscale complexes, where a dynamic equilibrium likely exists between docked and free cellulase. Therefore, the systems explored here and the results should be considered within the context that these

comprise scaffolded as well as some proportion of freely diffusing complexes of SA(Cel8A-biotin) or Cel8A-biotin.

For some of the reactions in this section, an additional component was included. As the Cel8A used here contains a C-terminal dockerin (**Doc**) domain, it is possible to bind this to a cohesin (**Coh**) from the same organism (**Section 1.4**). CBM-Coh was obtained, expressed and purified as described in the Methods. The CBM domain binds strongly to cellulose and has furthermore been shown to enhance activity against cellulose (Mansfield, Mooney, and Saddler 1999). Furthermore, using an affinity pull-down assay, the interaction between CBM-Coh and Cel8A was confirmed (Yael Vazana et al. 2012). By incubating CBM-Coh with Cel8A, the extent of the interaction can be determined by assessing the fraction of cellulase activity that associates with cellulose. The cellulose was removed by centrifugation and the activity of the supernatant is assessed. At increasing concentrations of CBM-Coh, less Cel8A activity was recovered in the supernatant when incubated with phosphoric-acid swollen cellulose (**PASC**; **Figure 4.25A**). At a 1:1 ratio of CBM-Coh to Cel8A, 80 % of Cel8A activity was lost from the supernatant fraction, and at a 3:1 ratio (excess CBM-Coh), 90% removal of activity was the maximum decrease observed. The initial rates correspond to the fraction of Cel8A associated with CBM-Coh. SDS-PAGE on the pelleted PASC showed a trend of increasing Cel8A-biotin associated at higher concentrations of CBM-Coh (**Figure 4.25B**). There was some association of Cel8A to the PASC fraction observed in the absence of CBM-Coh. This was consistent with the observed loss of activity in the supernatant fraction of Cel8A-biotin mixed with PASC compared to the activity of Cel8A-biotin on its own. However, the trend clearly shows association under the conditions later used for binding CBM-Coh to Cel8A in some of the assays. PASC pull-down assays were tried for SA(Cel8A-biotin) complexes as well; however, there was so much binding of these complexes to PASC in the absence of CBM-Coh that the trend was more difficult to measure (not shown).

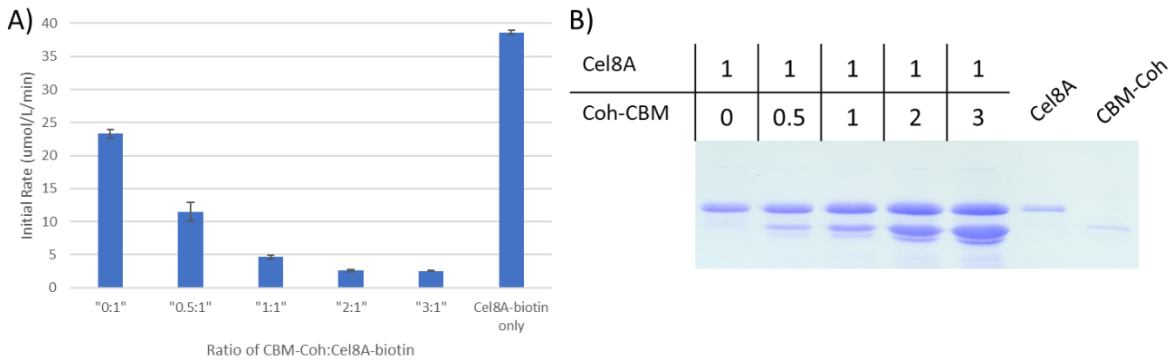

Figure 4.25: PASC pull-down assay to confirm association of Cel8A-biotin with CBM-Coh. A) Endocellulase activity measured against 0.5 % CMC at 65 ºC of diluted supernatant after removal of PASC/CBM by centrifugation (mean and SD shown; n = 3). B) SDS-PAGE of PASC pellets after incubation with CBM-containing complexes. Control lanes with purified Cel8A and CBM-Coh run separately.

The activity against a simple cellulose substrate, CMC, and a complex cellulose substrate, α-cellulose, were investigated utilizing complexes produced by either 1) preparing SA(Cel8A-biotin) followed by docking onto M13-PEG_{12}-biotin, or 2) preparing SA-coated M13 (biotin-PEG_4 linker) and binding Cel8A-biotin to it, without further removal of unbound components. Initially, activity against the soluble substrate, CMC, was tested to confirm that mixtures with the phage scaffolds were active. Specifically, activity against CMC was measured at two temperatures – 50 ºC, where considerable dynamics would be expected, and 23 ºC, where little rearrangement of SA/biotin affinity interactions would be expected. Typically, at 23 ºC there was a loss of activity observed compared to free cellulase (**Figure 4.26A, C**). This was observed in samples from both approaches to preparing complexes on M13-biotin. As the orientation of complexed Cel8A-biotin was not known here, it is possible that the loss of activity compared to free Cel8A-biotin comes from occlusion of the enzyme active site. For complexes of SA(Cel8A-biotin) bound to M13-biotin, further binding of CBM-Coh was also tested – this was found to hinder the mixtures of enzymes to a greater extent (**Figure 4.26A, B**). It is possible that the presence of the additional CBM-Coh component hindered access of the CMC to the Cel8A active sites without offering further enhancement to rate. This might be due to the simple nature of the substrate – it is soluble and therefore has no real surface with which the CBM domain might bind. Conversely, at high temperature, the difference between free Cel8A-biotin and complexed Cel8A-biotin

was minimal (**Figure 4.26B, D**). The similarity in rate of CMC hydrolysis to free Cel8A at 50 ºC, which was present in solution at the same concentrations that were present in all assembled complexes, likely reflects the rearrangement of SA/biotin affinity interactions allowing a greater fraction of complexed Cel8A to make their active sites accessible to the substrate.

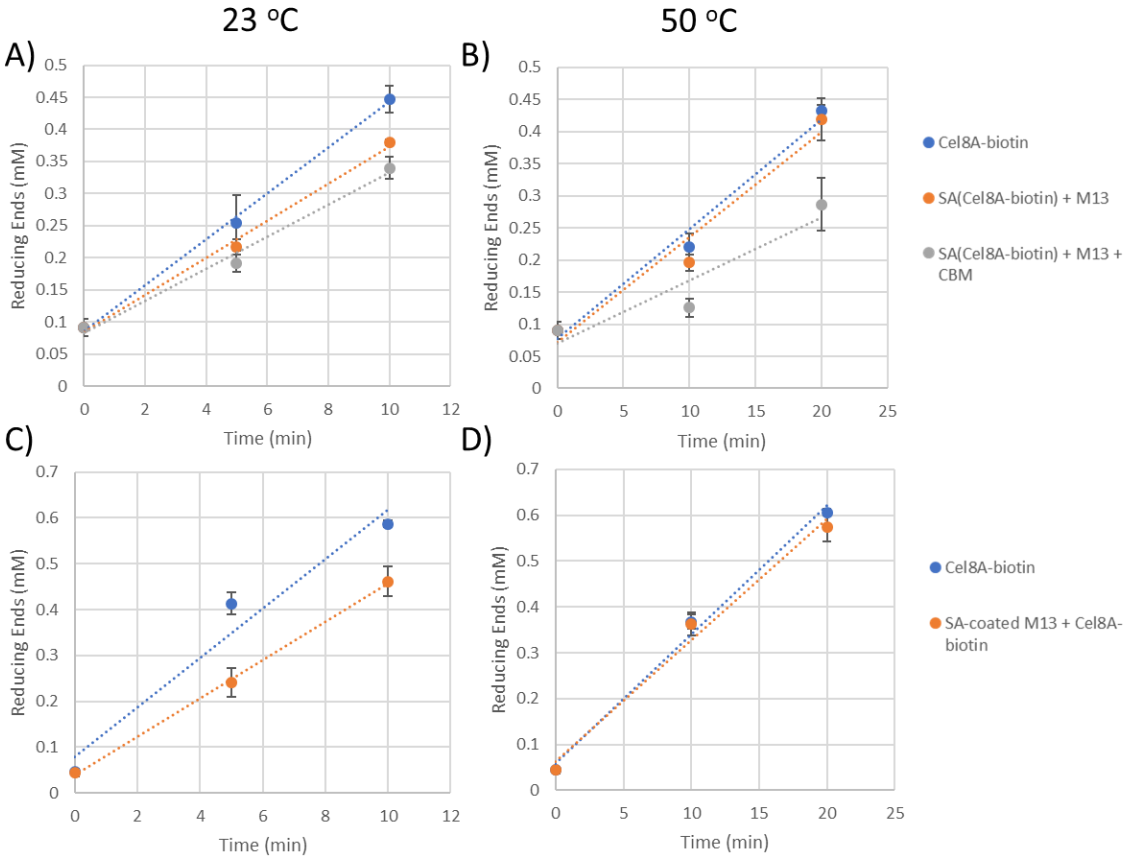

Figure 4.26: CMC hydrolysis of Cel8A-biotin bound to SA/M13 scaffolds. SA/M13 scaffolds were prepared either by A, B) first preparing SA(Cel8A-biotin) and binding to M13-PEG$_{12}$-biotin or C, D) preparing SA-coated M13 and adding Cel8A-biotin. The reactions were carried out at A, C) 23 ºC or B, D) 50 ºC against 0.5% CMC in 0.1 M citrate pH 5.8. The reducing ends produced were measured using the DNS assay described in the Methods (mean and SD shown; n = 3). Additional complexation with CBM-Coh was done as described in the Methods.

Given that assemblies of Cel8A onto M13 had activity against the simple substrate, activity against a complex substrate, α-cellulose was tested. This substrate was insoluble and required that reaction mixtures be individually stirred over the course of the reaction to ensure complete dispersal of the substrate. Detection of hydrolysis activity was done by measuring the total reducing ends produced over time using DNS detection. Total reducing ends were measured on whole α-cellulose particles, and

therefore would include both solubilized reducing ends in solution, and hydrolysis on the surface of the cellulose particles. To determine a reasonable endpoint for the reactions with the complexes, the substrate was initially reacted with free Cel8A over the course of 48 h at 50 ºC (**Figure 4.27A**). There was little hydrolysis beyond 24 h. Based on the results of this initial survey, the endpoints at 8 and 24 hours were used to compare different arrangements of Cel8A.

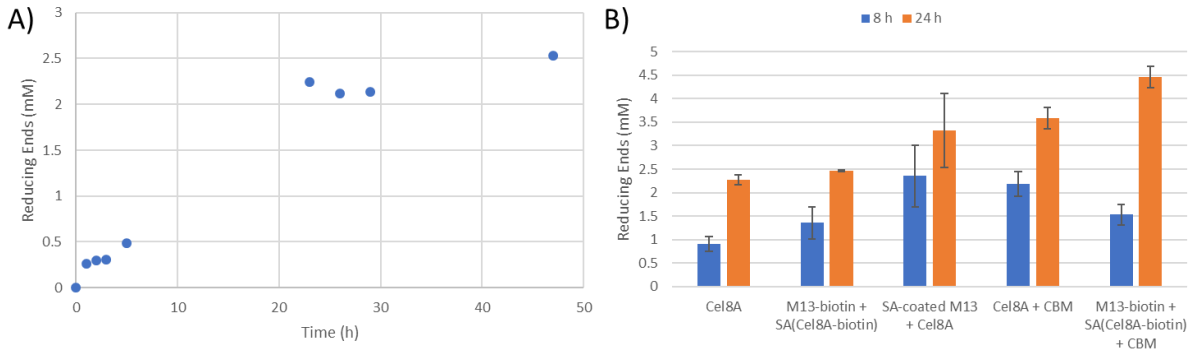

Figure 4.27: Endocellulase activity against 1% (w/v) α-cellulose in 0.1 M sodium citrate pH 5.8. A) Time course of reducing ends produced when α-cellulose was reacted with 100 nM Cel8A-biotin. B) Survey of 8 and 24 h endpoints of α-cellulose reacted to 100 nM Cel8A complexed to SA and M13 as described in the Methods. The reducing ends produced show SD from n = 2 trials (or n = 4 for SA-coated M13).

Overall, between Cel8A, SA(Cel8A-biotin) bound to M13, and Cel8A-biotin bound to SA-coated M13, there was very little difference in activity between these arrangements (**Figure 4.27B**). Given the insoluble nature of the substrate, these assays were unfortunately prone to high variability between reactions set up in separate test tubes. This makes determination of whether there was any true difference between activity of free Cel8A and complexed Cel8A difficult. The further complexation of a second component, CBM-Coh, was also carried out. CBM domains are known to enhance activity by two means: through affinity of the CBM domain with the cellulose surface, and by making individual cellulose chains more accessible to enzymes (Mansfield, Mooney, and Saddler 1999). The most noticeable rate enhancement came from inclusion of this additional component. For free Cel8A, 1.5-fold more reducing ends were produced at 24 hours when CBM-Coh was included (**Figure 4.27B**). For the complexed arrangement of cellulases there were 1.8-fold more reducing ends produced when CBM-Coh was added. Still, these were only modest enhancements to the rate.

Overall, the activity was quite low – consider that for a 1% solution of α-cellulose (10 mg/mL), and at a monomer MW of 162.14 g/mol per glucose unit in the polymer, there would be 62 mM of potential reducing ends that could be produced at maximum. Among all the configurations of Cel8A tested, only 4 – 7% of total hydrolysis of α-cellulose was observed. The activity of Cel8A was estimated to be 5 μmol/min/(μmol Cel8A) against other insoluble cellulose substrates (Schwarz, Gräbnitz, and Staudenbauer 1986). Based on this activity, ~0.7 mM reducing ends might be expected at 24 h. Within the context of this known activity of Cel8A, production of 2.5 mM reducing ends at 24 h is reasonable.

Enhancement of cellulase activity via complexation onto the nanoscale scaffolds used here was not observed. It has been noted already that without purification the total activity comes from a mixture of docked and free cellulases – even so, if complexation were to enhance activity, some increase still may have been observed here. Therefore, there are additional considerations that relate more directly to the nature of the scaffold and cellulase used here. In research on artificial cellulosomes, it was found that a simple two-component mixtures of CBM and endocellulase (Cel5A from *Thermobifida fusca*) complexed on a DNA scaffold did exhibit synergy together (Mori et al. 2013). There were some key differences that might account for the lack of synergy observed here. Firstly, the cellulase was covalently reacted to the DNA scaffold and the CBM domain was expressed as a fusion to the endoglucanase (Mori et al. 2013). The covalent and defined position of the CBM relative to the endoglucanase could be a critical factor to the observed synergy upon complexation. Additionally, the flexibility of the scaffolds would be expected to be quite different. The persistence length gives a measure of flexibility, with smaller values being more flexible: the persistence lengths of M13 and DNA are 1265 and 34 nm respectively (Gross et al. 2011; Khalil et al. 2007). Conformational flexibility is likely a critical factor to the high cellulosome activity seen in nature (S. P. Smith and Bayer 2013). Thus, the M13 scaffold may not be flexible enough to allow the optimal positioning of docked cellulases. Furthermore, in the Cel5A/CBM system mentioned above, there existed an optimal density

of Cel5A on the DNA scaffolds for rate enhancement to be observed (Mori et al. 2013). At densities in excess of this, there was a decrease in activity. With that in mind, it may be that this nanoscale arrangement of cellulases were too densely loaded onto the M13 scaffold.

Lastly, it might be that the use of a single enzymatic component was too simplistic to truly observe rate enhancement against a complex substrate such as cellulose. Typically, true cellulosomal activity requires additional components, such as exoglucanases (Artzi, Bayer, and Moraïs 2017). Initially, a single enzyme was used due to there being literature examples of synergy with endocellulase and CBM domains through proximity effects (Honda, Tanaka, and Yoshino 2015; Mori et al. 2013; Q. Sun et al. 2014). This would therefore have been a simple proof of concept; however, inclusion of an exoglucanase as well, while increasing the complexity of the scaffold, would test whether co-complexation of the two types of cellulases resulted in endo-/exo- synergy observed in cellulosomes (Mansfield, Mooney, and Saddler 1999). However, the use of a single component initially was important as it allowed more facile characterization of binding and complexation. It is conceivable that the application of a mixture of biotinylated Cel8A and a biotinylated exo-cellulase to the SA-coated scaffold could be carried out based on the principles learned here.

4.4 Conclusions

In this chapter, SA was used as an adaptor protein between biotinylated M13 and biotinylated Cel8A. While simple in concept, there were several subtleties that revealed more complex interactions between the components. The initial goal was to devise a nanoscale scaffold and methodology for preparing large, multi-enzyme complexes and use the endocellulase, Cel8A, to form an artificial cellulosome as a proof-of concept; the process of characterizing the complexation methodology has led to some subtle and interesting characteristics of this system.

The challenge addressed initially was how one might take a defined arrangement of SA and Cel8A-biotin and bind this to M13-biotin without unwanted crosslinking between the M13 and SA.

This challenge was approached in two different ways. The first methodology was to first prepare SA(Cel8A-biotin) in such a way that there would be biotin-binding sites available for complexation onto M13-biotin. However, this is complicated by the fact that binding of biotin to SA is rapid, and results in the formation of a non-equilibrium distribution of SA(biotin) species (Jones and Kurzban 1995). However, as highlighted in Chapter 3, SA pre-saturated with desthiobiotin could be used to bias the distribution of $SA(biotin)_N$ species toward a more statistically predictable one by slowing down the binding of biotin to SA. This was used extensively here in the preparation of SA(Cel8A-biotin) complexes to avoid biasing the distribution toward SA with biotin-binding sites fully occupied with Cel8A-biotin. Using this method, cellulase activity could be detected associated with M13 particles – however, they were found to be non-uniformly loaded with SA(Cel8A) upon analysis by TEM. The main drawback was that mixing SA with Cel8A-biotin where multiply biotinylated species were present (recall that ~30% of Cel8A-biotin species in the 0.74 biotin/Cel8A batch were biotinylated twice or more) resulted in aggregates that could not bind to M13-biotin. Thus, this approach might be more suitable for singly biotinylated components via maleimide labeling or a specific recognition peptide, such AviTag for *E. coli* biotin ligase labelling (Y. Li and Sousa 2012). In this way, the number of possible interactions that might occur between components would be simplified.

Of particular interest was the discovery that directly mixing M13-biotin with unmodified SA, rather than resulting in highly disordered aggregates, could form uniformly coated M13 under the right conditions. This scaffold, referred to throughout as SA-coated M13, was prepared using a shorter PEG_4-linker that was thought to restrict SA binding to the two *cis*-facing biotin-binding sites. In support of this, SA-coated M13 were capable of binding Cel8A-biotin in a subsequent step – supporting the existence of unoccupied *trans*-biotin binding sites. Initially, this appeared to be a very good way to prepare a nanoscale arrangement of SA with biotin-binding activity for subsequent binding of enzymes – as binding of Cel8A-biotin was uniform when observed by TEM. Furthermore, when directly subjected to incubation at higher temperature, the filamentous ordering of components persisted.

Careful observation led to the discovery of an instability in the assembled structures whereby SA binding could destabilize p8 monomer packing. It was speculated that this process was triggered by binding of SA at its *trans*-ligand binding sites to the same phage, putting strain on attached p8 subunits. Since this degradation process was enhanced when SA-coated M13 were prepared at higher ionic strength, it was further speculated that the charge repulsion between SA and the M13 surface might act as a barrier to binding at the *trans*-biotin binding site. This strained configuration might then further cause the shedding or rearrangement of packed p8 subunits as observed.

Possible strategies for improving upon the SA-coated M13 scaffold would seek to resolve the instability. Given the likely role of electrostatics in this process, engineering p8 to be more negative might provide a higher barrier to unfavorable binding configurations. Numerous p8 variants exist with additional glutamates for the purpose of binding cations or otherwise placing greater negative charge on the coat of M13 for device applications (Jeong et al. 2013; B. Y. Lee et al. 2012; Nam 2006). By tailoring the surface of M13 in this way, the resulting SA-coated M13 might be stabilized better in buffered solutions. Another possibility is to use a SA variant with even tighter binding to biotin, such as traptavidin (Chivers et al. 2011). In this variant, the off-rate is 10-fold slower than wildtype SA. By increasing the lifetime of the SA-biotin interaction on the scaffold, the chance for a particular SA to unbind from the M13-biotin surface, followed by a neighboring SA binding in a configuration that destabilizes the p8 packing structure, should be reduced. Lastly, by using a bifurcated biotin analogue to bind additional components to the SA-coated M13 scaffold, the entire assembly might be better stabilized. Such an analogue should space the biotin moieties such that they span the distance between two *cis*-binding sites. First, given the multivalent nature of such a reagent, there would be avidity effects making attachment particularly stable; furthermore, this might essentially “cap” off any remaining biotin-binding sites, preventing any destabilizing binding configurations between the biotin-binding sites opposite to the ones bound to p8-biotin.

The initial goals set out were to design a scaffold that would form multi-enzyme complexes utilizing a nanoscale scaffold. Through exploring different methodologies for preparing multi-enzyme complexes on M13 design principles important to preparing this scaffold were learned, and furthermore, complexes with endocellulolytic activity were successfully prepared. Though several possible improvements to this system were highlighted in this chapter summary, it is encouraging that the complexes do indeed have activity against cellulose.

Chapter 5 Conclusions and future research

Over the course of this thesis research several strategies were explored for preparing densely loaded multi-enzyme complexes on M13. This goal was not a simple one; in particular, positioning multiple biological components in a controlled way by manipulating their properties, concentrations and the interactions that can form between them is a real challenge. Furthermore, there were several characteristics that were desired in the resulting complex: that it was densely and uniformly loaded with enzyme, retained enzymatic activity, could be prepared using a methodology that could be broadly applicable and not specific to a particular enzyme, and utilized the properties of the phage scaffold itself. In the end, M13 particles densely loaded with enzyme were observed. In this summary, some of the notable aspects of this work and challenges that became apparent will be highlighted.

A range of designs were conceived and modified throughout the course of this work and these touched on the above-mentioned desirable properties, while having their own subtleties and challenges. By highlighting these challenges and discussing them, even where designs were unsuccessful, concepts that were found to be important or improvements to design methodologies could be highlighted in a way that pushes the field further and helps in the design and preparation of multi-enzyme complexes in a general sense. Initially, an M13 platform with Coh2 domains conjugated to p8 to controllably bind dockerin-bearing enzymes was designed. An advantage of using such an adaptor was that it would control the orientation of the docked proteins via engineering of a dockerin-domain either at the N- or C-terminus of the protein of interest as needed. The Coh2 would be attached to the M13 scaffold via literature methods for enzyme-mediated conjugation to M13 (Hess et al. 2012). However, it was found that the application of this technique was somewhat protein-dependent as efficient cyclization was observed to occur with Coh2, rather than formation of the desired p8 adduct. The cyclization side reaction is known to occur and modification to the N-terminus of the protein to prevent it is recommended (Guimaraes et al. 2013); however, these side-reactions were still observed. Furthermore,

it was determined that an enzyme-mediated approach would be unlikely to produce a densely loaded scaffold, likely due to steric effects creating an upper limit for the total protein per M13 that could be achieved. Thus, after consideration, a redesign was pursued where the first step involved efficient modification of the viral coat directly by chemical means followed by protein complexation.

For the second broad approach, M13 particles were labelled with biotin molecules with different spacer lengths (PEG_4 and PEG_{12}) and an "adaptor" molecule, SA, was used. Importantly, this would ultimately allow for high capacity loading of the adaptor molecule – up to ~1350 SA per M13 was estimated. In terms of extending the methodology to be broadly applicable, the initial design involved further complexation of the protein of interest by utilizing a His6-tag. To have the resulting complexes form stably, a methodology for oxidizing Co(II) to Co(III) coordinated with His-tagged proteins was utilized (Wegner and Spatz 2013). In this thesis, SA tetramers with three bound NTA moieties for binding the His6-tagged protein and a single open biotin-binding site to bind to biotinylated M13 were realized. However, it was later found that the loading step was not very efficient, and high loading of the biotinylated protein was not observed. Interestingly, the positioning and spacing of the adaptor molecule followed from the symmetry and packing of p8 monomers. One of the interesting aspects with respect to utilizing viral particles in assembling components on the nanoscale are the well-defined positioning of functional groups via the symmetry of the viral coat itself. This has been noted as one of the attractive aspects of viruses as nanoscale scaffolds (L. A. Lee and Wang 2006). Thus, the data demonstrating the nearly ideal packing of the SA adaptor on the surface of M13 particles reflects this concept well – importantly, the size of SA was well-suited to its positioning with the ~5-fold symmetry of p8, and allowed it to be positioned almost directly adjacent to neighboring SA molecules.

This nearly ideal packing later led to the conception of an approach whereby M13-biotin could be directly mixed with SA under appropriate conditions producing SA-coated M13 with residual valency for further complexation of a biotinylated biomolecule. This approach was particularly

attractive for several reasons: 1) this led to M13 uniformly loaded with Cel8A, 2) the core scaffold was composed of two core components, SA and M13-biotin – which are straightforward in their preparation, and 3) this was anticipated to be highly modular. For the first point, of the methods explored in this thesis, the highest loading density was achieved using this SA-coated M13 scaffold as indicated by TEM micrographs. This was only possible with efficient interactions at each step in assembling the complexes – in this case, the tight binding between biotin and SA. The second point relates to the idea of accessibility – the core scaffold, SA-coated M13, is prepared from two highly accessible components which has good implications for potential applicability. Lastly, as the core scaffold is essentially a filamentous array of biotin-binding sites, the modularity comes down to whether a particular biomolecule can be biotinylated.

As discussed in the summary of **Chapter 4**, there are many ways to biotinylate biomolecules – for proteins, particular expression systems even obviate the need for bioconjugate techniques entirely by biotinylating the protein as it is expressed (Y. Li and Sousa 2012). Thus, the requirement that the biomolecule be biotinylated is any easy one to meet. As carried out here, biotinylation of reactive amino acids is another straightforward method of preparing a component to be docked onto this scaffold. However, this can lead to multiply biotinylated proteins (depending on the chemistry utilized), increasing the number of potential interactions with the SA adaptor protein. This system was characterized using a biotinylated enzyme with multiply biotinylated species present (though the most abundant species was singly labelled Cel8A, ~30% of species had ≥2 biotin per Cel8A), representing this more challenging case; with multivalence comes the potential for crosslinking side reactions and aggregation. Yet it was found that even with such a component here, the resulting enzyme-laden M13 were still well-dispersed, and not observed to aggregate. This may be due to the high-density of biotin-binding sites presented to a multiply biotinylated molecule as it approaches this highly curved SA-coated M13 surface: once bound at one of its biotin moieties, the rest are likely to find a place to bind in neighboring SA molecules bound to the phage surface, rather than bind to a separate phage particle.

The observations made in this thesis have important implications for the use of biotinylated viruses and SA-conjugated components in general. The utilization of SA/biotin interactions are common in approaches where specificity and stable interactions are desired, as highlighted in **Section 1.5**. With reference specifically to filamentous viruses, there have been examples of biotinylated phages utilizing the SA/biotin interaction for the purpose of signal enhancement (ELISA; (Brasino, Lee, and Cha 2015; S. Williams, Schulz, and Sierks 2015)) or sensor signal enhancement (field effect biosensor; (Poghossian et al. 2018)). In these applications, the biotinylated virus served as a mediator with which a particular sensing component conjugated to SA was bound after the phage was first adhered to a solid phase. These differ from the designs explored in this thesis in which M13-biotin in solution was complexed with SA and other components forming complexes which were soluble and dispersed; however, the concepts learned in this thesis are likely still applicable.

In particular, where a tight-binding, multivalent component such as SA is used to interact with a biotinylated multi-subunit scaffold (i.e., viruses), it is important to confirm that the resulting structures are indeed formed as intended, as it was highlighted that there is potential for the packing structure of multi-subunit viruses to be destabilized by SA binding (i.e.. SA-coated M13; **Section 4.3.3.4**). This is unlikely to impact the utilization of biotinylated viruses where monovalent SA are used to build onto the scaffold (i.e.. $SA(BXN)_3$ bound to M13-biotin; **Section 3.3.4**); however, this is likely to be an important consideration for SA conjugates (with multiple biotin-binding sites), where there exists the potential for multiple interactions to form. Indeed, it was demonstrated that the interactions that lead to these degradation pathways can be quite subtle, where factors such as the ionic strength of a solution may lead to destabilization when a multivalent component is bound. Whether this is a phenomenon specific to M13 would be an interesting fundamental avenue to explore, as this could highlight the way in which subunit packing and symmetry of a multi-subunit scaffold translates to the relative stability of a complex formed with a multivalent component such as SA. It is predicted that if

binding to more than two of the biotin-binding sites of SA by the same biotinylated scaffold is limited due its geometry and spacing of biotin moieties, the resulting complex may exhibit better stability.

In summary, multi-subunit particles such as viruses are an important part of the nanoscale toolbox – however, just as any single tool may not be optimal in all applications, one should consider that each naturally-occurring, or designed, multi-subunit scaffold may have different strengths. This thesis research focused particularly on methods for preparing large, multi-enzymes on a particular viral scaffold, M13, using tight-binding interactions. Among the various design considerations highlighted above, a particularly novel methodology that was devised was the rapid coating of M13-biotin with SA, forming arrays of SA with residual biotin-binding capability. In characterizing this, there was potential for high density loading of biotinylated enzymes, but also some challenges to be overcome with respect to the instability introduced to coat protein packing under certain conditions. It is expected that this methodology is not specific only to M13 and might be employed elsewhere with appropriately spaced biotin-binding moieties. Furthermore, the results here hint at the potential value of a thorough characterization of different multi-subunit scaffolds with varied geometries and spacing of reactive groups. Given the wealth of stable, multi-subunit structures that exist in nature there is much to be explored and it is hoped that the challenges highlighted in this thesis illustrate the value in building up a toolbox of carefully characterized nanoscale scaffolds.

Chapter 6 References

Adams, J. J., G. Pal, Z. Jia, and S. P. Smith. 2006. "Mechanism of Bacterial Cell-Surface Attachment Revealed by the Structure of Cellulosomal Type II Cohesin-Dockerin Complex." *Proceedings of the National Academy of Sciences* 103 (2): 305–10. https://doi.org/10.1073/pnas.0507109103.

Adhikari, Meena, Ulrich Strych, Jinsu Kim, Heather Goux, Sagar Dhamane, Mohan-Vivekanandan Poongavanam, Anna E. V. Hagström, Katerina Kourentzi, Jacinta C. Conrad, and Richard C. Willson. 2015. "Aptamer-Phage Reporters for Ultrasensitive Lateral Flow Assays." *Analytical Chemistry* 87 (23): 11660–65. https://doi.org/10.1021/acs.analchem.5b00702.

Aiba, Shuichi, Kazuo Kitai, and Tadayuki Imanaka. 1983. "Cloning and Expression of Thermostable α-Amylase Gene from Bacillus Stearothermophilus in Bacillus Stearothermophilus and Bacillus Subtilis." *Applied and Environmental Microbiology* 46 (5): 1059–65.

Alzari, Pedro M, Hélè ne Souchon, and Roberto Dominguez. 1996. "The Crystal Structure of Endoglucanase CelA, a Family 8 Glycosyl Hydrolase from Clostridium Thermocellum." *Structure* 4 (3): 265–75. https://doi.org/10.1016/S0969-2126(96)00031-7.

Anbar, Michael, Ozgur Gul, Raphael Lamed, Ugur O. Sezerman, and Edward A. Bayer. 2012. "Improved Thermostability of Clostridium Thermocellum Endoglucanase Cel8A by Using Consensus-Guided Mutagenesis." *Applied and Environmental Microbiology* 78 (9): 3458–64. https://doi.org/10.1128/AEM.07985-11.

Anderegg, Giorgio. 2009. "Critical Survey of Stability Constants of NTA Complexes." *Pure and Applied Chemistry* 54 (12): 2693–2758. https://doi.org/10.1351/pac198254122693.

Antos, John M., Maximilian Wei-Lin Popp, Robert Ernst, Guo-Liang Chew, Eric Spooner, and Hidde L. Ploegh. 2009. "A Straight Path to Circular Proteins." *Journal of Biological Chemistry* 284 (23): 16028–36. https://doi.org/10.1074/jbc.M901752200.

Arora, Mansi, Ragothaman M. Yennamalli, and Taner Z. Sen. 2018. "Application of Molecular Simulations Toward Understanding Cellulase Mechanisms." *BioEnergy Research* 11 (4): 850–67. https://doi.org/10.1007/s12155-018-9944-x.

Artzi, Lior, Edward A. Bayer, and Sarah Moraïs. 2017. "Cellulosomes: Bacterial Nanomachines for Dismantling Plant Polysaccharides." *Nature Reviews Microbiology* 15 (2): 83–95. https://doi.org/10.1038/nrmicro.2016.164.

Asztalos, Andrea, Marcus Daniels, Anurag Sethi, Tongye Shen, Paul Langan, Antonio Redondo, and Sandrasegaram Gnanakaran. 2012. "A Coarse-Grained Model for Synergistic Action of Multiple Enzymes on Cellulose." *Biotechnology for Biofuels* 5 (1): 55. https://doi.org/10.1186/1754-6834-5-55.

Avery, Kendra N., Janell E. Schaak, and Raymond E. Schaak. 2009. "M13 Bacteriophage as a Biological Scaffold for Magnetically-Recoverable Metal Nanowire Catalysts: Combining Specific and Nonspecific Interactions To Design Multifunctional Nanocomposites." *Chemistry of Materials* 21 (11): 2176–78. https://doi.org/10.1021/cm900869u.

Barile, Lucio, and Giuseppe Vassalli. 2017. "Exosomes: Therapy Delivery Tools and Biomarkers of Diseases." *Pharmacology & Therapeutics* 174 (June): 63–78. https://doi.org/10.1016/j.pharmthera.2017.02.020.

Bartoschik, Tanja, Stefanie Galinec, Christian Kleusch, Katarzyna Walkiewicz, Dennis Breitsprecher, Sebastian Weigert, Yves A. Muller, et al. 2018. "Near-Native, Site-Specific and Purification-Free Protein Labeling for Quantitative Protein Interaction Analysis by MicroScale Thermophoresis." *Scientific Reports* 8 (1): 4977. https://doi.org/10.1038/s41598-018-23154-3.

Bayer, Edward A, Eva Setter, and Raphael Lamed. 1985. "Organization and Distribution of the Cellulosome in Clostridium Thermocellum." *Journal of Bacteriology* 163: 8.

Berkowitz, Steven A., and Loren A. Day. 1976. “Mass, Length, Composition and Structure of the Filamentous Bacterial Virus Fd.” *Journal of Molecular Biology* 102 (3): 531–47. https://doi.org/10.1016/0022-2836(76)90332-6.

Bolivar, Juan M., and Bernd Nidetzky. 2012. “Positively Charged Mini-Protein Zbasic2 As a Highly Efficient Silica Binding Module: Opportunities for Enzyme Immobilization on Unmodified Silica Supports.” *Langmuir* 28 (26): 10040–49. https://doi.org/10.1021/la3012348.

Borne, Romain, Edward A. Bayer, Sandrine Pagès, Stéphanie Perret, and Henri-Pierre Fierobe. 2013. “Unraveling Enzyme Discrimination during Cellulosome Assembly Independent of Cohesin–Dockerin Affinity.” *The FEBS Journal* 280 (22): 5764–79. https://doi.org/10.1111/febs.12497.

Boulos, Stefano P., Tyler A. Davis, Jie An Yang, Samuel E. Lohse, Alaaldin M. Alkilany, Lisa A. Holland, and Catherine J. Murphy. 2013. “Nanoparticle–Protein Interactions: A Thermodynamic and Kinetic Study of the Adsorption of Bovine Serum Albumin to Gold Nanoparticle Surfaces.” *Langmuir* 29 (48): 14984–96. https://doi.org/10.1021/la402920f.

Brasino, Michael, Ju Hun Lee, and Jennifer N. Cha. 2015. “Creating Highly Amplified Enzyme-Linked Immunosorbent Assay Signals from Genetically Engineered Bacteriophage.” *Analytical Biochemistry* 470 (February): 7–13. https://doi.org/10.1016/j.ab.2014.10.006.

Brin, Elena, Jizu Yi, Anna Marie Skalka, and Jonathan Leis. 2000. “Modeling the Late Steps in HIV-1 Retroviral Integrase-Catalyzed DNA Integration.” *Journal of Biological Chemistry* 275 (50): 39287–95. https://doi.org/10.1074/jbc.M006929200.

Cai, Huai-Hong, Xing Zhong, Pei-Hui Yang, Wei Wei, Jianan Chen, and Jiye Cai. 2010. “Probing Site-Selective Binding of Rhodamine B to Bovine Serum Albumin.” *Colloids and Surfaces A: Physicochemical and Engineering Aspects* 372 (1–3): 35–40. https://doi.org/10.1016/j.colsurfa.2010.09.017.

Cancilla, Mark T., Michael D. Leavell, Jason Chow, and Julie A. Leary. 2000. “Mass Spectrometry and Immobilized Enzymes for the Screening of Inhibitor Libraries.” *Proceedings of the National Academy of Sciences* 97 (22): 12008–13. https://doi.org/10.1073/pnas.220403997.

Cao, Binrui, Hong Xu, and Chuanbin Mao. 2011. “Transmission Electron Microscopy as a Tool to Image Bio-Inorganic Nanohybrids: The Case of Phage-Gold Nanocomposites.” *Microscopy Research and Technique* 74 (7): 627–35. https://doi.org/10.1002/jemt.21030.

Caspi, J., Y. Barak, R. Haimovitz, D. Irwin, R. Lamed, D. B. Wilson, and E. A. Bayer. 2009. “Effect of Linker Length and Dockerin Position on Conversion of a Thermobifida Fusca Endoglucanase to the Cellulosomal Mode.” *Applied and Environmental Microbiology* 75 (23): 7335–42. https://doi.org/10.1128/AEM.01241-09.

Castellana, Michele, Maxwell Z. Wilson, Yifan Xu, Preeti Joshi, Ileana M. Cristea, Joshua D. Rabinowitz, Zemer Gitai, and Ned S. Wingreen. 2014. “Enzyme Clustering Accelerates Processing of Intermediates through Metabolic Channeling.” *Nature Biotechnology* 32 (10): 1011–18. https://doi.org/10.1038/nbt.3018.

Chaiet, Louis, and Frank J. Wolf. 1964. “The Properties of Streptavidin, a Biotin-Binding Protein Produced by Streptomycetes.” *Archives of Biochemistry and Biophysics* 106 (January): 1–5. https://doi.org/10.1016/0003-9861(64)90150-X.

Chan, Chi-Ho, Tsz-Ha Yu, and Kam-Bo Wong. 2011. “Stabilizing Salt-Bridge Enhances Protein Thermostability by Reducing the Heat Capacity Change of Unfolding.” *PLoS ONE* 6 (6). https://doi.org/10.1371/journal.pone.0021624.

Chappel, J.A., M. He, and A.S. Kang. 1998. “Modulation of Antibody Display on M13 Filamentous Phage.” *Journal of Immunological Methods* 221 (1–2): 25–34. https://doi.org/10.1016/S0022-1759(98)00094-5.

Chen, Po-Yen, Xiangnan Dang, Matthew T. Klug, Noémie-Manuelle Dorval Courchesne, Jifa Qi, Md Nasim Hyder, Angela M. Belcher, and Paula T. Hammond. 2015. “M13 Virus-Enabled Synthesis of Titanium Dioxide Nanowires for Tunable Mesoporous Semiconducting Networks.” *Chemistry of Materials* 27 (5): 1531–40. https://doi.org/10.1021/cm503803u.

Chen, Po-Yen, Xiangnan Dang, Matthew T. Klug, Jifa Qi, Noémie-Manuelle Dorval Courchesne, Fred J. Burpo, Nicholas Fang, Paula T. Hammond, and Angela M. Belcher. 2013. "Versatile Three-Dimensional Virus-Based Template for Dye-Sensitized Solar Cells with Improved Electron Transport and Light Harvesting." *ACS Nano* 7 (8): 6563–74. https://doi.org/10.1021/nn4014164.

Chen, Wenshuai, Haipeng Yu, Sang-Young Lee, Tong Wei, Jian Li, and Zhuangjun Fan. 2018. "Nanocellulose: A Promising Nanomaterial for Advanced Electrochemical Energy Storage." *Chemical Society Reviews* 47 (8): 2837–72. https://doi.org/10.1039/C7CS00790F.

Chidchob, Pongphak, and Hanadi F Sleiman. 2018. "Recent Advances in DNA Nanotechnology." *Current Opinion in Chemical Biology*, Synthetic Biology / Synthetic Biomolecules, 46 (October): 63–70. https://doi.org/10.1016/j.cbpa.2018.04.012.

Chilkoti, Ashutosh, and Patrick S. Stayton. 1995. "Molecular Origins of the Slow Streptavidin-Biotin Dissociation Kinetics." *Journal of the American Chemical Society* 117 (43): 10622–28. https://doi.org/10.1021/ja00148a003.

Chivers, Claire E., Estelle Crozat, Calvin Chu, Vincent T. Moy, David J. Sherratt, and Mark Howarth. 2010. "A Streptavidin Variant with Slower Biotin Dissociation and Increased Mechanostability." *Nature Methods* 7 (5): 391–93. https://doi.org/10.1038/nmeth.1450.

Chivers, Claire E., Apurba L. Koner, Edward D. Lowe, and Mark Howarth. 2011. "How the Biotin–Streptavidin Interaction Was Made Even Stronger: Investigation via Crystallography and a Chimaeric Tetramer." *Biochemical Journal* 435 (Pt 1): 55–63. https://doi.org/10.1042/BJ20101593.

Choi, Dong Shin, Hyo-Eon Jin, So Young Yoo, and Seung-Wuk Lee. 2014. "Cyclic RGD Peptide Incorporation on Phage Major Coat Proteins for Improved Internalization by HeLa Cells." *Bioconjugate Chemistry* 25 (2): 216–23. https://doi.org/10.1021/bc4003234.

Chundawat, Shishir P. S., Chad D. Paavola, Babu Raman, Matthieu Nouailler, Suzanne L. Chan, Jonathan R. Mielenz, Veronique Receveur-Brechot, Jonathan D. Trent, and Bruce E. Dale. 2016. "Saccharification of Thermochemically Pretreated Cellulosic Biomass Using Native and Engineered Cellulosomal Enzyme Systems." *Reaction Chemistry & Engineering* 1 (6): 616–28. https://doi.org/10.1039/C6RE00172F.

Chundawat, Shishir P.S., Gregg T. Beckham, Michael E. Himmel, and Bruce E. Dale. 2011. "Deconstruction of Lignocellulosic Biomass to Fuels and Chemicals." *Annual Review of Chemical and Biomolecular Engineering* 2 (1): 121–45. https://doi.org/10.1146/annurev-chembioeng-061010-114205.

Chung, Woo-Jae, Doe-Young Lee, and So Young Yoo. 2014. "Chemical Modulation of M13 Bacteriophage and Its Functional Opportunities for Nanomedicine." *International Journal of Nanomedicine* 9 (December): 5825–36. https://doi.org/10.2147/IJN.S73883.

Clarke, M., L. Maddera, R. L. Harris, and P. M. Silverman. 2008. "F-Pili Dynamics by Live-Cell Imaging." *Proceedings of the National Academy of Sciences* 105 (46): 17978–81. https://doi.org/10.1073/pnas.0806786105.

Courchesne, Noémie-Manuelle Dorval, Matthew T. Klug, Po-Yen Chen, Steven E. Kooi, Dong Soo Yun, Nina Hong, Nicholas X. Fang, Angela M. Belcher, and Paula T. Hammond. 2014. "Assembly of a Bacteriophage-Based Template for the Organization of Materials into Nanoporous Networks." *Advanced Materials* 26 (21): 3398–3404. https://doi.org/10.1002/adma.201305928.

Dai, Xiaolin, Alexander Böker, and Ulrich Glebe. 2019. "Broadening the Scope of Sortagging." *RSC Advances* 9 (9): 4700–4721. https://doi.org/10.1039/C8RA06705H.

Day, Loren A., Christopher J. Marzee, Stephen A. Reisberg, and Arturo Casadevall. 1988. "DNA Packing in Filamentous Bacteriophages." *Annual Review of Biophysics and Biophysical Chemistry* 17 (1): 509–39. https://doi.org/10.1146/annurev.bb.17.060188.002453.

De Plano, Laura M., Santi Scibilia, Maria Giovanna Rizzo, Sara Crea, Domenico Franco, Angela M. Mezzasalma, and Salvatore P. P. Guglielmino. 2018. "One-Step Production of Phage–Silicon

Nanoparticles by PLAL as Fluorescent Nanoprobes for Cell Identification." *Applied Physics A* 124 (3). https://doi.org/10.1007/s00339-018-1637-y.

Deng, Lu, Elena N. Kitova, and John S. Klassen. 2013. "Dissociation Kinetics of the Streptavidin–Biotin Interaction Measured Using Direct Electrospray Ionization Mass Spectrometry Analysis." *Journal of The American Society for Mass Spectrometry* 24 (1): 49–56. https://doi.org/10.1007/s13361-012-0533-5.

DePorter, Sandra M., and Brian R. McNaughton. 2014. "Engineered M13 Bacteriophage Nanocarriers for Intracellular Delivery of Exogenous Proteins to Human Prostate Cancer Cells." *Bioconjugate Chemistry* 25 (9): 1620–25. https://doi.org/10.1021/bc500339k.

Devaraj, Vasanthan, Jiye Han, Chuntae Kim, Yong-Cheol Kang, and Jin-Woo Oh. 2018. "Self-Assembled Nanoporous Biofilms from Functionalized Nanofibrous M13 Bacteriophage." *Viruses* 10 (6): 322. https://doi.org/10.3390/v10060322.

Dhakal, Soma, Matthew R. Adendorff, Minghui Liu, Hao Yan, Mark Bathe, and Nils G. Walter. 2016. "Rational Design of DNA-Actuated Enzyme Nanoreactors Guided by Single Molecule Analysis." *Nanoscale* 8 (5): 3125–37. https://doi.org/10.1039/C5NR07263H.

Doll, Tais A. P. F., Senthilkumar Raman, Raja Dey, and Peter Burkhard. 2013. "Nanoscale Assemblies and Their Biomedical Applications." *Journal of The Royal Society Interface* 10 (80): 20120740. https://doi.org/10.1098/rsif.2012.0740.

Douglas, Shawn M., Ido Bachelet, and George M. Church. 2012. "A Logic-Gated Nanorobot for Targeted Transport of Molecular Payloads." *Science* 335 (6070): 831–34. https://doi.org/10.1126/science.1214081.

Du, Yan, and Shaojun Dong. 2017. "Nucleic Acid Biosensors: Recent Advances and Perspectives." *Analytical Chemistry* 89 (1): 189–215. https://doi.org/10.1021/acs.analchem.6b04190.

Dubacheva, Galina V., Carolina Araya-Callis, Anne Geert Volbeda, Michael Fairhead, Jeroen Codée, Mark Howarth, and Ralf P. Richter. 2017. "Controlling Multivalent Binding through Surface Chemistry: Model Study on Streptavidin." *Journal of the American Chemical Society* 139 (11): 4157–67. https://doi.org/10.1021/jacs.7b00540.

Dueber, John E., Gabriel C. Wu, G. Reza Malmirchegini, Tae Seok Moon, Christopher J. Petzold, Adeeti V. Ullal, Kristala L. J. Prather, and Jay D. Keasling. 2009. "Synthetic Protein Scaffolds Provide Modular Control over Metabolic Flux." *Nature Biotechnology* 27 (8): 753–59. https://doi.org/10.1038/nbt.1557.

Dundas, Christopher M., Daniel Demonte, and Sheldon Park. 2013. "Streptavidin–Biotin Technology: Improvements and Innovations in Chemical and Biological Applications." *Applied Microbiology and Biotechnology* 97 (21): 9343–53. https://doi.org/10.1007/s00253-013-5232-z.

Ebner, Andreas, Markus Marek, Karl Kaiser, Gerald Kada, Christoph D. Hahn, Bernd Lackner, and Hermann J. Gruber. 2008. "Application of Biotin-4-Fluorescein in Homogeneous Fluorescence Assays for Avidin, Streptavidin, and Biotin or Biotin Derivatives." In *Avidin-Biotin Interactions: Methods and Applications*, edited by Robert J. McMahon, 73–88. Methods In Molecular Biology™. Totowa, NJ: Humana Press. https://doi.org/10.1007/978-1-59745-579-4_7.

Eigler, D. M., and E. K. Schweizer. 1990. "Positioning Single Atoms with a Scanning Tunnelling Microscope." *Nature* 344 (6266): 524. https://doi.org/10.1038/344524a0.

Eisenhawer, Martin, Serge Cattarinussi, Andreas Kuhn, and Horst Vogel. 2001. "Fluorescence Resonance Energy Transfer Shows a Close Helix−Helix Distance in the Transmembrane M13 Procoat Protein †." *Biochemistry* 40 (41): 12321–28. https://doi.org/10.1021/bi0107694.

Elcock, Adrian H., and J. Andrew McCammon. 1996. "Evidence for Electrostatic Channeling in a Fusion Protein of Malate Dehydrogenase and Citrate Synthase." *Biochemistry* 35 (39): 12652–58. https://doi.org/10.1021/bi9614747.

Erkelenz, Michael, Chi-Hsien Kuo, and Christof M. Niemeyer. 2011. “DNA-Mediated Assembly of Cytochrome P450 BM3 Subdomains.” *Journal of the American Chemical Society* 133 (40): 16111–18. https://doi.org/10.1021/ja204993s.

Fairhead, Michael, Gianluca Veggiani, Melissa Lever, Jun Yan, Dejan Mesner, Carol V. Robinson, Omer Dushek, P. Anton van der Merwe, and Mark Howarth. 2014. “SpyAvidin Hubs Enable Precise and Ultrastable Orthogonal Nanoassembly.” *Journal of the American Chemical Society* 136 (35): 12355–63. https://doi.org/10.1021/ja505584f.

Fierobe, H P, C Gaudin, A Belaich, M Loutfi, E Faure, C Bagnara, D Baty, and J P Belaich. 1991. “Characterization of Endoglucanase A from Clostridium Cellulolyticum.” *Journal of Bacteriology* 173 (24): 7956–62. https://doi.org/10.1128/jb.173.24.7956-7962.1991.

Fierobe, Henri-Pierre, Edward A. Bayer, Chantal Tardif, Mirjam Czjzek, Adva Mechaly, Anne Bélaïch, Raphael Lamed, Yuval Shoham, and Jean-Pierre Bélaïch. 2002. “Degradation of Cellulose Substrates by Cellulosome Chimeras. Substrate Targeting Versus Proximity of Enzyme Components.” *Journal of Biological Chemistry* 277 (51): 49621–30. https://doi.org/10.1074/jbc.M207672200.

Fierobe, Henri-Pierre, Florence Mingardon, Adva Mechaly, Anne Bélaïch, Marco T. Rincon, Sandrine Pagès, Raphael Lamed, Chantal Tardif, Jean-Pierre Bélaïch, and Edward A. Bayer. 2005. “Action of Designer Cellulosomes on Homogeneous *Versus* Complex Substrates: Controlled Incorporation of Three Distinct Enzymes Into a Defined Trifunctional Scaffoldin.” *Journal of Biological Chemistry* 280 (16): 16325–34. https://doi.org/10.1074/jbc.M414449200.

Fontes, Carlos M.G.A., and Harry J. Gilbert. 2010. “Cellulosomes: Highly Efficient Nanomachines Designed to Deconstruct Plant Cell Wall Complex Carbohydrates.” *Annual Review of Biochemistry* 79 (1): 655–81. https://doi.org/10.1146/annurev-biochem-091208-085603.

Fu, Jinglin, Yuhe Renee Yang, Alexander Johnson-Buck, Minghui Liu, Yan Liu, Nils G. Walter, Neal W. Woodbury, and Hao Yan. 2014. “Multi-Enzyme Complexes on DNA Scaffolds Capable of Substrate Channelling with an Artificial Swinging Arm.” *Nature Nanotechnology* 9 (7): 531–36. https://doi.org/10.1038/nnano.2014.100.

Funke, Jonas J., and Hendrik Dietz. 2016. “Placing Molecules with Bohr Radius Resolution Using DNA Origami.” *Nature Nanotechnology* 11 (1): 47–52. https://doi.org/10.1038/nnano.2015.240.

Gallizia, Anna, Claudia de Lalla, Errica Nardone, Paolo Santambrogio, Anna Brandazza, Alessandro Sidoli, and Paolo Arosio. 1998. “Production of a Soluble and Functional Recombinant Streptavidin InEscherichia Coli.” *Protein Expression and Purification* 14 (2): 192–96. https://doi.org/10.1006/prep.1998.0930.

García-Aljaro, Cristina, Francesc Xavier Muñoz, and Eva Baldrich. 2009. “Captavidin: A New Regenerable Biocomponent for Biosensing?” *The Analyst* 134 (11): 2338. https://doi.org/10.1039/b905050g.

Gasteiger, Elisabeth, Christine Hoogland, Alexandre Gattiker, S’everine Duvaud, Marc R. Wilkins, Ron D. Appel, and Amos Bairoch. 2005. “Protein Identification and Analysis Tools on the ExPASy Server.” In *The Proteomics Protocols Handbook*, edited by John M. Walker, 571–607. Totowa, NJ: Humana Press. https://doi.org/10.1385/1-59259-890-0:571.

Gaudin, C., A. Belaich, S. Champ, and J.-P. Belaich. 2000. “CelE, a Multidomain Cellulase from Clostridium Cellulolyticum: A Key Enzyme in the Cellulosome?” *Journal of Bacteriology* 182 (7): 1910–15. https://doi.org/10.1128/JB.182.7.1910-1915.2000.

Glover, Dominic J., and Douglas S. Clark. 2016. “Protein Calligraphy: A New Concept Begins To Take Shape.” *ACS Central Science* 2 (7): 438–44. https://doi.org/10.1021/acscentsci.6b00067.

Görisch, Helmut. 1988. “Drop Dialysis: Time Course of Salt and Protein Exchange.” *Analytical Biochemistry* 173 (2): 393–98. https://doi.org/10.1016/0003-2697(88)90205-9.

Green, Nm. 1963. “Avidin. 1. the Use of [14c]Biotin for Kinetic Studies and for Assay.” *Biochemical Journal* 89 (3): 585–91. https://doi.org/10.1042/bj0890585.

Gregory, Ann C., Ahmed A. Zayed, Nádia Conceição-Neto, Ben Temperton, Ben Bolduc, Adriana Alberti, Mathieu Ardyna, et al. 2019. “Marine DNA Viral Macro- and Microdiversity from Pole to Pole.” *Cell* 177 (5): 1109-1123.e14. https://doi.org/10.1016/j.cell.2019.03.040.

Griffith, Jack, Marcia Manning, and Kathi Dunn. 1981. “Filamentous Bacteriophage Contract into Hollow Spherical Particles upon Exposure to a Chloroform-Water Interface.” *Cell* 23 (3): 747–53. https://doi.org/10.1016/0092-8674(81)90438-4.

Gross, Peter, Niels Laurens, Lene B. Oddershede, Ulrich Bockelmann, Erwin J. G. Peterman, and Gijs J. L. Wuite. 2011. “Quantifying How DNA Stretches, Melts and Changes Twist under Tension.” *Nature Physics* 7 (9): 731–36. https://doi.org/10.1038/nphys2002.

Guérin, Diego M.A, Marie-Bernard Lascombe, Marcelo Costabel, Hélène Souchon, Victor Lamzin, Pierre Béguin, and Pedro M Alzari. 2002. “Atomic (0.94 Å) Resolution Structure of an Inverting Glycosidase in Complex with Substrate.” *Journal of Molecular Biology* 316 (5): 1061–69. https://doi.org/10.1006/jmbi.2001.5404.

Guimaraes, Carla P, Martin D Witte, Christopher S Theile, Gunes Bozkurt, Lenka Kundrat, Annet E M Blom, and Hidde L Ploegh. 2013. “Site-Specific C-Terminal and Internal Loop Labeling of Proteins Using Sortase-Mediated Reactions.” *Nature Protocols* 8 (9): 1787–99. https://doi.org/10.1038/nprot.2013.101.

Haack, Richard A., Kerry M. Swift, Qiaoqiao Ruan, Richard J. Himmelsbach, and Sergey Y. Tetin. 2017. “The Photostability of the Commonly Used Biotin-4-Fluorescein Probe.” *Analytical Biochemistry* 531 (August): 78–82. https://doi.org/10.1016/j.ab.2017.05.019.

Hajian, Alireza, Stefan B. Lindström, Torbjörn Pettersson, Mahiar M. Hamedi, and Lars Wågberg. 2017. “Understanding the Dispersive Action of Nanocellulose for Carbon Nanomaterials.” *Nano Letters* 17 (3): 1439–47. https://doi.org/10.1021/acs.nanolett.6b04405.

Han, Lei, Changxu Shao, Bo Liang, and Aihua Liu. 2016. “Genetically Engineered Phage-Templated MnO_2 Nanowires: Synthesis and Their Application in Electrochemical Glucose Biosensor Operated at Neutral PH Condition.” *ACS Applied Materials & Interfaces* 8 (22): 13768–76. https://doi.org/10.1021/acsami.6b03266.

He, Didi, and Jon Marles-Wright. 2015. “Ferritin Family Proteins and Their Use in Bionanotechnology.” *New Biotechnology* 32 (6): 651–57. https://doi.org/10.1016/j.nbt.2014.12.006.

Henry, Kevin A., Mehdi Arbabi-Ghahroudi, and Jamie K. Scott. 2015. “Beyond Phage Display: Non-Traditional Applications of the Filamentous Bacteriophage as a Vaccine Carrier, Therapeutic Biologic, and Bioconjugation Scaffold.” *Frontiers in Microbiology* 6. https://doi.org/10.3389/fmicb.2015.00755.

Hess, Gaelen T., Juan J. Cragnolini, Maximilian W. Popp, Mark A. Allen, Stephanie K. Dougan, Eric Spooner, Hidde L. Ploegh, Angela M. Belcher, and Carla P. Guimaraes. 2012. “M13 Bacteriophage Display Framework That Allows Sortase-Mediated Modification of Surface-Accessible Phage Proteins.” *Bioconjugate Chemistry* 23 (7): 1478–87. https://doi.org/10.1021/bc300130z.

Hiller, Y, J M Gershoni, E A Bayer, and M Wilchek. 1987. “Biotin Binding to Avidin. Oligosaccharide Side Chain Not Required for Ligand Association.” *Biochemical Journal* 248 (1): 167–71.

Hintersteiner, Martin, Thomas Weidemann, Thierry Kimmerlin, Nimet Filiz, Christof Buehler, and Manfred Auer. 2008. “Covalent Fluorescence Labeling of His-Tagged Proteins on the Surface of Living Cells.” *ChemBioChem* 9 (9): 1391–95. https://doi.org/10.1002/cbic.200800089.

Hirano, Katsuaki, Masahiro Kurosaki, Satoshi Nihei, Hiroki Hasegawa, Suguru Shinoda, Mitsuru Haruki, and Nobutaka Hirano. 2016. “Enzymatic Diversity of the Clostridium Thermocellum Cellulosome Is Crucial for the Degradation of Crystalline Cellulose and Plant Biomass.” *Scientific Reports* 6 (1). https://doi.org/10.1038/srep35709.

Hirano, Katsuaki, Satoshi Nihei, Hiroki Hasegawa, Mitsuru Haruki, and Nobutaka Hirano. 2015. “Stoichiometric Assembly of the Cellulosome Generates Maximum Synergy for the Degradation of Crystalline Cellulose, as Revealed by In Vitro Reconstitution of the Clostridium

Thermocellum Cellulosome." *Applied and Environmental Microbiology* 81 (14): 4756–66. https://doi.org/10.1128/AEM.00772-15.
Hirsch, James D, Leila Eslamizar, Brian J Filanoski, Nabi Malekzadeh, Rosaria P Haugland, Joseph M Beechem, and Richard P Haugland. 2002. "Easily Reversible Desthiobiotin Binding to Streptavidin, Avidin, and Other Biotin-Binding Proteins: Uses for Protein Labeling, Detection, and Isolation." *Analytical Biochemistry* 308 (2): 343–57. https://doi.org/10.1016/S0003-2697(02)00201-4.
Hofmann, Klaus, Gail Titus, Judith A. Montibeller, and Frances M. Finn. 1982. "Avidin Binding of Carboxyl-Substituted Biotin and Analogs." *Biochemistry* 21 (5): 978–84. https://doi.org/10.1021/bi00534a024.
Honda, Toru, Tsuyoshi Tanaka, and Tomoko Yoshino. 2015. "Stoichiometrically Controlled Immobilization of Multiple Enzymes on Magnetic Nanoparticles by the Magnetosome Display System for Efficient Cellulose Hydrolysis." *Biomacromolecules* 16 (12): 3863–68. https://doi.org/10.1021/acs.biomac.5b01174.
Howarth, Mark, Daniel J-F Chinnapen, Kimberly Gerrow, Pieter C Dorrestein, Melanie R Grandy, Neil L Kelleher, Alaa El-Husseini, and Alice Y Ting. 2006. "A Monovalent Streptavidin with a Single Femtomolar Biotin Binding Site." *Nature Methods* 3 (4): 267–73. https://doi.org/10.1038/nmeth861.
Hsieh, Chia-wen C., David Cannella, Henning Jørgensen, Claus Felby, and Lisbeth G. Thygesen. 2015. "Cellobiohydrolase and Endoglucanase Respond Differently to Surfactants during the Hydrolysis of Cellulose." *Biotechnology for Biofuels* 8 (1): 52. https://doi.org/10.1186/s13068-015-0242-y.
Huang, Yu, Chung-Yi Chiang, Soo Kwan Lee, Yan Gao, Evelyn L. Hu, James De Yoreo, and Angela M. Belcher. 2005. "Programmable Assembly of Nanoarchitectures Using Genetically Engineered Viruses." *Nano Letters* 5 (7): 1429–34. https://doi.org/10.1021/nl050795d.
Hwang, Inseong. 2014. "Virus Outbreaks in Chemical and Biological Sensors." *Sensors* 14 (8): 13592–612. https://doi.org/10.3390/s140813592.
Idan, Ofer, and Henry Hess. 2013. "Origins of Activity Enhancement in Enzyme Cascades on Scaffolds." *ACS Nano* 7 (10): 8658–65. https://doi.org/10.1021/nn402823k.
Irwin, Diana C., Michael Spezio, Larry P. Walker, and David B. Wilson. 1993. "Activity Studies of Eight Purified Cellulases: Specificity, Synergism, and Binding Domain Effects." *Biotechnology and Bioengineering* 42 (8): 1002–13. https://doi.org/10.1002/bit.260420811.
Jameson, Laramie P., Nicholas W. Smith, Onofrio Annunziata, and Sergei V. Dzyuba. 2016. "Interaction of BODIPY Dyes with Bovine Serum Albumin: A Case Study on the Aggregation of a Click-BODIPY Dye." *Physical Chemistry Chemical Physics* 18 (21): 14182–85. https://doi.org/10.1039/C6CP00420B.
Jeong, Chang Kyu, Insu Kim, Kwi-Il Park, Mi Hwa Oh, Haemin Paik, Geon-Tae Hwang, Kwangsoo No, Yoon Sung Nam, and Keon Jae Lee. 2013. "Virus-Directed Design of a Flexible $BaTiO_3$ Nanogenerator." *ACS Nano* 7 (12): 11016–25. https://doi.org/10.1021/nn404659d.
Jindou, Sadanari, Akane Soda, Shuichi Karita, Tsutomu Kajino, Pierre Béguin, J. H. David Wu, Minoru Inagaki, Tetsuya Kimura, Kazuo Sakka, and Kunio Ohmiya. 2004. "Cohesin-Dockerin Interactions within and between *Clostridium Josui* and *Clostridium Thermocellum*: Binding Selectivity Between Cognate Dockerin and Cohesin Domains and Species Specificity." *Journal of Biological Chemistry* 279 (11): 9867–74. https://doi.org/10.1074/jbc.M308673200.
Jones, M. Lisa, and Gary P. Kurzban. 1995. "Noncooperativity of Biotin Binding to Tetrameric Streptavidin." *Biochemistry* 34 (37): 11750–56. https://doi.org/10.1021/bi00037a012.
Jung, Sung Mi, Jifa Qi, Dahyun Oh, Angela Belcher, and Jing Kong. 2017. "M13 Virus Aerogels as a Scaffold for Functional Inorganic Materials." *Advanced Functional Materials* 27 (4): 1603203. https://doi.org/10.1002/adfm.201603203.
Kada, Gerald, Heinz Falk, and Hermann J. Gruber. 1999. "Accurate Measurement of Avidin and Streptavidin in Crude Biofluids with a New, Optimized Biotin–Fluorescein Conjugate."

Biochimica et Biophysica Acta (BBA) - General Subjects 1427 (1): 33–43. https://doi.org/10.1016/S0304-4165(98)00178-0.

Kang, Wei, Jiahui Liu, Jianpeng Wang, Yunyu Nie, Zhihong Guo, and Jiang Xia. 2014. "Cascade Biocatalysis by Multienzyme–Nanoparticle Assemblies." *Bioconjugate Chemistry* 25 (8): 1387–94. https://doi.org/10.1021/bc5002399.

Karan, Sumanta Kumar, Sandip Maiti, Owoong Kwon, Sarbaranjan Paria, Anirban Maitra, Suman Kumar Si, Yunseok Kim, Jin Kon Kim, and Bhanu Bhusan Khatua. 2018. "Nature Driven Spider Silk as High Energy Conversion Efficient Bio-Piezoelectric Nanogenerator." *Nano Energy* 49 (July): 655–66. https://doi.org/10.1016/j.nanoen.2018.05.014.

Kargarzadeh, Hanieh, Marcos Mariano, Deepu Gopakumar, Ishak Ahmad, Sabu Thomas, Alain Dufresne, Jin Huang, and Ning Lin. 2018. "Advances in Cellulose Nanomaterials." *Cellulose* 25 (4): 2151–89. https://doi.org/10.1007/s10570-018-1723-5.

Khalil, A. S., J. M. Ferrer, R. R. Brau, S. T. Kottmann, C. J. Noren, M. J. Lang, and A. M. Belcher. 2007. "Single M13 Bacteriophage Tethering and Stretching." *Proceedings of the National Academy of Sciences* 104 (12): 4892–97. https://doi.org/10.1073/pnas.0605727104.

Kim, Do-Myoung, Mitsuo Umetsu, Kyo Takai, Takashi Matsuyama, Nobuhiro Ishida, Haruo Takahashi, Ryutaro Asano, and Izumi Kumagai. 2011. "Enhancement of Cellulolytic Enzyme Activity by Clustering Cellulose Binding Domains on Nanoscaffolds." *Small* 7 (5): 656–64. https://doi.org/10.1002/smll.201002114.

Kim, Jinsu, Meena Adhikari, Sagar Dhamane, Anna E. V. Hagström, Katerina Kourentzi, Ulrich Strych, Richard C. Willson, and Jacinta C. Conrad. 2015. "Detection of Viruses By Counting Single Fluorescent Genetically Biotinylated Reporter Immunophage Using a Lateral Flow Assay." *ACS Applied Materials & Interfaces* 7 (4): 2891–98. https://doi.org/10.1021/am5082556.

Kim, Jungok, Youngwoo Rheem, Bongyoung Yoo, Youhoon Chong, Krassimir N. Bozhilov, Daehee Kim, Michael J. Sadowsky, Hor-Gil Hur, and Nosang V. Myung. 2010. "Peptide-Mediated Shape- and Size-Tunable Synthesis of Gold Nanostructures." *Acta Biomaterialia* 6 (7): 2681–89. https://doi.org/10.1016/j.actbio.2010.01.019.

King, Neil P., William Sheffler, Michael R. Sawaya, Breanna S. Vollmar, John P. Sumida, Ingemar André, Tamir Gonen, Todd O. Yeates, and David Baker. 2012. "Computational Design of Self-Assembling Protein Nanomaterials with Atomic Level Accuracy." *Science* 336 (6085): 1171–74. https://doi.org/10.1126/science.1219364.

Klug, A. 1999. "The Tobacco Mosaic Virus Particle: Structure and Assembly." *Philosophical Transactions of the Royal Society B: Biological Sciences* 354 (1383): 531–35.

Knez, Karel, Wim Noppe, Nick Geukens, Kris P. F. Janssen, Dragana Spasic, Jeroen Heyligen, Kim Vriens, et al. 2013. "Affinity Comparison of P3 and P8 Peptide Displaying Bacteriophages Using Surface Plasmon Resonance." *Analytical Chemistry* 85 (21): 10075–82. https://doi.org/10.1021/ac402192k.

Koh, Eun Hye, ChaeWon Mun, ChunTae Kim, Sung-Gyu Park, Eun Jung Choi, Sun Ho Kim, Jaejeung Dang, et al. 2018. "M13 Bacteriophage/Silver Nanowire Surface-Enhanced Raman Scattering Sensor for Sensitive and Selective Pesticide Detection." *ACS Applied Materials & Interfaces* 10 (12): 10388–97. https://doi.org/10.1021/acsami.8b01470.

Kostylev, Maxim, and David Wilson. 2013. "Two-Parameter Kinetic Model Based on a Time-Dependent Activity Coefficient Accurately Describes Enzymatic Cellulose Digestion." *Biochemistry* 52 (33): 5656–64. https://doi.org/10.1021/bi400358v.

Kragh-Hansen, Ulrich, Florence Hellec, Béatrice de Foresta, Marc le Maire, and Jesper V. Møller. 2001. "Detergents as Probes of Hydrophobic Binding Cavities in Serum Albumin and Other Water-Soluble Proteins." *Biophysical Journal* 80 (6): 2898–2911. https://doi.org/10.1016/S0006-3495(01)76255-8.

Krauss, Jan, Vladimir V. Zverlov, and Wolfgang H. Schwarz. 2012. "*In Vitro* Reconstitution of the Complete Clostridium Thermocellum Cellulosome and Synergistic Activity on Crystalline

Cellulose." *Applied and Environmental Microbiology* 78 (12): 4301–7. https://doi.org/10.1128/AEM.07959-11.
Kruger, Nicholas J. 1994. "The Bradford Method for Protein Quantitation." In *Basic Protein and Peptide Protocols*, edited by John M. Walker, 9–15. Methods in Molecular Biology™. Totowa, NJ: Humana Press. https://doi.org/10.1385/0-89603-268-X:9.
Kuhn, Misty L., Bozena Zemaitaitis, Linda I. Hu, Alexandria Sahu, Dylan Sorensen, George Minasov, Bruno P. Lima, et al. 2014. "Structural, Kinetic and Proteomic Characterization of Acetyl Phosphate-Dependent Bacterial Protein Acetylation." *PloS One* 9 (4): e94816. https://doi.org/10.1371/journal.pone.0094816.
Kumar, Deepak, and Ganti S Murthy. 2013. "Stochastic Molecular Model of Enzymatic Hydrolysis of Cellulose for Ethanol Production." *Biotechnology for Biofuels* 6 (May): 63. https://doi.org/10.1186/1754-6834-6-63.
Kuzmič, Petr. 2009. "Chapter 10 - DynaFit—A Software Package for Enzymology." In *Methods in Enzymology*, 467:247–80. Academic Press. https://doi.org/10.1016/S0076-6879(09)67010-5.
Laitinen, O. H., V. P. Hytönen, H. R. Nordlund, and M. S. Kulomaa. 2006. "Genetically Engineered Avidins and Streptavidins." *Cellular and Molecular Life Sciences CMLS* 63 (24): 2992–3017. https://doi.org/10.1007/s00018-006-6288-z.
Lamed, Raphael, Rina Kenig, Eva Setter, and Edward A. Bayer. 1985. "Major Characteristics of the Cellulolytic System of Clostridium Thermocellum Coincide with Those of the Purified Cellulosome." *Enzyme and Microbial Technology* 7 (1): 37–41. https://doi.org/10.1016/0141-0229(85)90008-0.
Lamed, Raphael, Eva Setiter, and Edward A Bayer. 1983. "Characterization of a Cellulose-Binding, Cellulase-Containing Complex in Clostridium Thermocellum." *Journal of Bacteriology* 156: 9.
Langan, Paul, S. Gnanakaran, Kirk D. Rector, Norma Pawley, David T. Fox, Dae Won Cho, and Kenneth E. Hammel. 2011. "Exploring New Strategies for Cellulosic Biofuels Production." *Energy & Environmental Science* 4 (10): 3820–33. https://doi.org/10.1039/C1EE01268A.
Lata, Suman, Martynas Gavutis, Robert Tampé, and Jacob Piehler. 2006. "Specific and Stable Fluorescence Labeling of Histidine-Tagged Proteins for Dissecting Multi-Protein Complex Formation." *Journal of the American Chemical Society* 128 (7): 2365–72. https://doi.org/10.1021/ja0563105.
Le Trong, Isolde, Zhizhi Wang, David E. Hyre, Terry P. Lybrand, Patrick S. Stayton, and Ronald E. Stenkamp. 2011. "Streptavidin and Its Biotin Complex at Atomic Resolution." *Acta Crystallographica Section D: Biological Crystallography* 67 (Pt 9): 813–21. https://doi.org/10.1107/S0907444911027806.
Lee, Bo-Ram, Ho Kyung Ko, Ju Hee Ryu, Keum Young Ahn, Young-Ho Lee, Se Jin Oh, Jin Hee Na, et al. 2016. "Engineered Human Ferritin Nanoparticles for Direct Delivery of Tumor Antigens to Lymph Node and Cancer Immunotherapy." *Scientific Reports* 6 (October): 35182. https://doi.org/10.1038/srep35182.
Lee, Byung Yang, Jinxing Zhang, Chris Zueger, Woo-Jae Chung, So Young Yoo, Eddie Wang, Joel Meyer, Ramamoorthy Ramesh, and Seung-Wuk Lee. 2012. "Virus-Based Piezoelectric Energy Generation." *Nature Nanotechnology* 7 (6): 351–56. https://doi.org/10.1038/nnano.2012.69.
Lee, Dong Jae, Hyun Su Park, Kunmo Koo, Jeong Yong Lee, Yoon Sung Nam, Wonhee Lee, and Moon Young Yang. 2019. "Gold Binding Peptide Identified from Microfluidic Biopanning: An Experimental and Molecular Dynamics Study." *Langmuir* 35 (2): 522–28. https://doi.org/10.1021/acs.langmuir.8b02563.
Lee, Eun Jung. 2018. "Recent Advances in Protein-Based Nanoparticles." *Korean Journal of Chemical Engineering* 35 (9): 1765–78. https://doi.org/10.1007/s11814-018-0102-0.
Lee, Hee-Sook, Jeong-In Kang, Woo-Jae Chung, Do Hoon Lee, Byung Yang Lee, Seung-Wuk Lee, and So Young Yoo. 2018. "Engineered Phage Matrix Stiffness-Modulating Osteogenic Differentiation." *ACS Applied Materials & Interfaces* 10 (5): 4349–58. https://doi.org/10.1021/acsami.7b17871.

Lee, Hye-Eun, Hwa Kyoung Lee, Hyejin Chang, Hyo-Yong Ahn, Norov Erdene, Ho-Young Lee, Yoon-Sik Lee, Dae Hong Jeong, Junho Chung, and Ki Tae Nam. 2014. "Virus Templated Gold Nanocube Chain for SERS Nanoprobe." *Small* 10 (15): 3007–11. https://doi.org/10.1002/smll.201400527.

Lee, Jae Yoon, Woo-Jae Chung, and GeunHyung Kim. 2016. "A Mechanically Improved Virus-Based Hybrid Scaffold for Bone Tissue Regeneration." *RSC Advances* 6 (60): 55022–32. https://doi.org/10.1039/C6RA07054J.

Lee, Ju Hun, Benson Fan, Tuan D. Samdin, David A. Monteiro, Malav S. Desai, Olivia Scheideler, Hyo-Eon Jin, Soyoun Kim, and Seung-Wuk Lee. 2017. "Phage-Based Structural Color Sensors and Their Pattern Recognition Sensing System." *ACS Nano* 11 (4): 3632–41. https://doi.org/10.1021/acsnano.6b07942.

Lee, L. Andrew, and Qian Wang. 2006. "Adaptations of Nanoscale Viruses and Other Protein Cages for Medical Applications." *Nanomedicine: Nanotechnology, Biology and Medicine* 2 (3): 137–49. https://doi.org/10.1016/j.nano.2006.07.009.

Lehmann Renato Zenobi, Edda, and Stefan Vetter. 1999. "Matrix-Assisted Laser Desorption/Ionization Mass Spectra Reflect Solution-Phase Zinc Finger Peptide Complexation." *Journal of the American Society for Mass Spectrometry* 10 (1): 27–34. https://doi.org/10.1016/S1044-0305(98)00116-0.

Levary, David A., Ranganath Parthasarathy, Eric T. Boder, and Margaret E. Ackerman. 2011. "Protein-Protein Fusion Catalyzed by Sortase A." Edited by Joseph Najbauer. *PLoS ONE* 6 (4): e18342. https://doi.org/10.1371/journal.pone.0018342.

Li, Kai, Yi Chen, Siqi Li, Huong Giang Nguyen, Zhongwei Niu, Shaojin You, Charlene M. Mello, Xiaobing Lu, and Qian Wang. 2010. "Chemical Modification of M13 Bacteriophage and Its Application in Cancer Cell Imaging." *Bioconjugate Chemistry* 21 (7): 1369–77. https://doi.org/10.1021/bc900405q.

Li, Xuehua, Cengiz Koç, Petra Kühner, York-Dieter Stierhof, Bernhard Krismer, Mark C. Enright, José R. Penadés, et al. 2016. "An Essential Role for the Baseplate Protein Gp45 in Phage Adsorption to Staphylococcus Aureus." *Scientific Reports* 6 (May): 26455. https://doi.org/10.1038/srep26455.

Li, Yifeng, and Rui Sousa. 2012. "Expression and Purification of E. Coli BirA Biotin Ligase for in Vitro Biotinylation." *Protein Expression and Purification* 82 (1): 162–67. https://doi.org/10.1016/j.pep.2011.12.008.

Lin, Jyun-Liang, Leidy Palomec, and Ian Wheeldon. 2014. "Design and Analysis of Enhanced Catalysis in Scaffolded Multienzyme Cascade Reactions." *ACS Catalysis* 4 (2): 505–11. https://doi.org/10.1021/cs401009z.

Liu, David J., and Loren A. Day. 1994. "Pf1 Virus Structure: Helical Coat Protein and DNA with Paraxial Phosphates." *Science* 265 (5172): 671–74.

Liu, Fang, Scott Banta, and Wilfred Chen. 2013. "Functional Assembly of a Multi-Enzyme Methanol Oxidation Cascade on a Surface-Displayed Trifunctional Scaffold for Enhanced NADH Production." *Chemical Communications* 49 (36): 3766–68. https://doi.org/10.1039/C3CC40454D.

Liu, Minghui, Jinglin Fu, Christian Hejesen, Yuhe Yang, Neal W. Woodbury, Kurt Gothelf, Yan Liu, and Hao Yan. 2013. "A DNA Tweezer-Actuated Enzyme Nanoreactor." *Nature Communications* 4 (July): 2127. https://doi.org/10.1038/ncomms3127.

Liu, Yuwei, Tadeusz L. Ogorzalek, Pei Yang, McKenna M. Schroeder, E. Neil G. Marsh, and Zhan Chen. 2013. "Molecular Orientation of Enzymes Attached to Surfaces through Defined Chemical Linkages at the Solid–Liquid Interface." *Journal of the American Chemical Society* 135 (34): 12660–69. https://doi.org/10.1021/ja403672s.

Ma, Wenjuan, Yuxi Zhan, Yuxin Zhang, Xiaoru Shao, Xueping Xie, Chenchen Mao, Weitong Cui, et al. 2019. "An Intelligent DNA Nanorobot with in Vitro Enhanced Protein Lysosomal Degradation of HER2." *Nano Letters*, June. https://doi.org/10.1021/acs.nanolett.9b01320.

Malam, Yogeshkumar, Marilena Loizidou, and Alexander M. Seifalian. 2009. “Liposomes and Nanoparticles: Nanosized Vehicles for Drug Delivery in Cancer.” *Trends in Pharmacological Sciences* 30 (11): 592–99. https://doi.org/10.1016/j.tips.2009.08.004.

Mansfield, Shawn D., Caitriona Mooney, and John N. Saddler. 1999. “Substrate and Enzyme Characteristics That Limit Cellulose Hydrolysis.” *Biotechnology Progress* 15 (5): 804–16. https://doi.org/10.1021/bp9900864.

Mao, C. 2004. “Virus-Based Toolkit for the Directed Synthesis of Magnetic and Semiconducting Nanowires.” *Science* 303 (5655): 213–17. https://doi.org/10.1126/science.1092740.

Marraffini, L. A., A. C. DeDent, and O. Schneewind. 2006. “Sortases and the Art of Anchoring Proteins to the Envelopes of Gram-Positive Bacteria.” *Microbiology and Molecular Biology Reviews* 70 (1): 192–221. https://doi.org/10.1128/MMBR.70.1.192-221.2006.

Marusyk, R., and A. Sergeant. 1980. “A Simple Method for Dialysis of Small-Volume Samples.” *Analytical Biochemistry* 105 (1): 403–4. https://doi.org/10.1016/0003-2697(80)90477-7.

Marvin, D. A., R. D. Hale, C. Nave, and M. Helmer Citterich. 1994. “Molecular Models and Structural Comparisons of Native and Mutant Class I Filamentous Bacteriophages: Ff (Fd, F1, M13), If1 and IKe.” *Journal of Molecular Biology* 235 (1): 260–86. https://doi.org/10.1016/S0022-2836(05)80032-4.

Marvin, DA. 1998. “Filamentous Phage Structure, Infection and Assembly.” *Current Opinion in Structural Biology* 8 (2): 150–58. https://doi.org/10.1016/S0959-440X(98)80032-8.

Marvin, D.A., M.F. Symmons, and S.K. Straus. 2014. “Structure and Assembly of Filamentous Bacteriophages.” *Progress in Biophysics and Molecular Biology* 114 (2): 80–122. https://doi.org/10.1016/j.pbiomolbio.2014.02.003.

Matsumoto, Takuya, Yuki Isogawa, Kosuke Minamihata, Tsutomu Tanaka, and Akihiko Kondo. 2016. “Twigged Streptavidin Polymer as a Scaffold for Protein Assembly.” *Journal of Biotechnology* 225 (May): 61–66. https://doi.org/10.1016/j.jbiotec.2016.03.030.

Meadows, David L., Jules S. Shafer, and Jerome S. Schultz. 1991. “Determining the Extent of Labeling for Tetramethylrhodamine Protein Conjugates.” *Journal of Immunological Methods* 143 (2): 263–72. https://doi.org/10.1016/0022-1759(91)90051-G.

Mehlenbacher, Matthew R., Fadi Bou-Abdallah, Xing Xin Liu, and Artem Melman. 2015. “Calorimetric Studies of Ternary Complexes of Ni(II) and Cu(II) Nitrilotriacetic Acid and N-Acetyloligohistidines.” *Inorganica Chimica Acta* 437 (October): 152–58. https://doi.org/10.1016/j.ica.2015.08.009.

Merzlyak, Anna, and Seung-Wuk Lee. 2009. “Engineering Phage Materials with Desired Peptide Display: Rational Design Sustained through Natural Selection.” *Bioconjugate Chemistry* 20 (12): 2300–2310. https://doi.org/10.1021/bc900303f.

Miles, Edith Wilson, Sangkee Rhee, and David R. Davies. 1999. “The Molecular Basis of Substrate Channeling.” *Journal of Biological Chemistry* 274 (18): 12193–96. https://doi.org/10.1074/jbc.274.18.12193.

Mitsuzawa, Shigenobu, Hiromi Kagawa, Yifen Li, Suzanne L. Chan, Chad D. Paavola, and Jonathan D. Trent. 2009. “The Rosettazyme: A Synthetic Cellulosome.” *Journal of Biotechnology* 143 (2): 139–44. https://doi.org/10.1016/j.jbiotec.2009.06.019.

Molek, Peter, and Tomaž Bratkovič. 2015. “Bacteriophages as Scaffolds for Bipartite Display: Designing Swiss Army Knives on a Nanoscale.” *Bioconjugate Chemistry* 26 (3): 367–78. https://doi.org/10.1021/acs.bioconjchem.5b00034.

Moon, Robert J., Ashlie Martini, John Nairn, John Simonsen, and Jeff Youngblood. 2011. “Cellulose Nanomaterials Review: Structure, Properties and Nanocomposites.” *Chemical Society Reviews* 40 (7): 3941–94. https://doi.org/10.1039/C0CS00108B.

Moradi, Maryam, Jae Chul Kim, Jifa Qi, Kang Xu, Xin Li, Gerbrand Ceder, and Angela M. Belcher. 2016. “A Bio-Facilitated Synthetic Route for Nano-Structured Complex Electrode Materials.” *Green Chemistry* 18 (9): 2619–24. https://doi.org/10.1039/C6GC00273K.

Morag, Omry, Nikolaos G. Sgourakis, David Baker, and Amir Goldbourt. 2015. “The NMR–Rosetta Capsid Model of M13 Bacteriophage Reveals a Quadrupled Hydrophobic Packing Epitope.” *Proceedings of the National Academy of Sciences* 112 (4): 971–76. https://doi.org/10.1073/pnas.1415393112.

Mori, Yutaro, Shiori Ozasa, Momoko Kitaoka, Shuhei Noda, Tsutomu Tanaka, Hirofumi Ichinose, and Noriho Kamiya. 2013. “Aligning an Endoglucanase Cel5A from Thermobifida Fusca on a DNA Scaffold: Potent Design of an Artificial Cellulosome.” *Chemical Communications* 49 (62): 6971. https://doi.org/10.1039/c3cc42614a.

Muggeo, Vito M. R. 2003. “Estimating Regression Models with Unknown Break-Points.” *Statistics in Medicine* 22 (19): 3055–71. https://doi.org/10.1002/sim.1545.

Murugesan, Murali, Gopal Abbineni, Susan L. Nimmo, Binrui Cao, and Chuanbin Mao. 2013. “Virus-Based Photo-Responsive Nanowires Formed By Linking Site-Directed Mutagenesis and Chemical Reaction.” *Scientific Reports* 3 (1). https://doi.org/10.1038/srep01820.

Nakazawa, Hikaru, Do-Myoung Kim, Takashi Matsuyama, Nobuhiro Ishida, Akinori Ikeuchi, Yuri Ishigaki, Izumi Kumagai, and Mitsuo Umetsu. 2013. “Hybrid Nanocellulosome Design from Cellulase Modules on Nanoparticles: Synergistic Effect of Catalytically Divergent Cellulase Modules on Cellulose Degradation Activity.” *ACS Catalysis* 3 (6): 1342–48. https://doi.org/10.1021/cs400012v.

Nam, K. T. 2006. “Virus-Enabled Synthesis and Assembly of Nanowires for Lithium Ion Battery Electrodes.” *Science* 312 (5775): 885–88. https://doi.org/10.1126/science.1122716.

Nelson, James W., Alexander G. Chamessian, Patrick J. McEnaney, Ryan P. Murelli, Barbara I. Kazmiercak, and David A. Spiegel. 2010. “A Biosynthetic Strategy for Re-Engineering the *Staphylococcus Aureus* Cell Wall with Non-Native Small Molecules.” *ACS Chemical Biology* 5 (12): 1147–55. https://doi.org/10.1021/cb100195d.

Niu, Zhongwei, Michael A. Bruckman, Brandon Harp, Charlene M. Mello, and Qian Wang. 2008. “Bacteriophage M13 as a Scaffold for Preparing Conductive Polymeric Composite Fibers.” *Nano Research* 1 (3): 235–41. https://doi.org/10.1007/s12274-008-8027-2.

Oh, Jin-Woo, Woo-Jae Chung, Kwang Heo, Hyo-Eon Jin, Byung Yang Lee, Eddie Wang, Chris Zueger, et al. 2014. “Biomimetic Virus-Based Colourimetric Sensors.” *Nature Communications* 5 (1). https://doi.org/10.1038/ncomms4043.

Otten, Marcus, Wolfgang Ott, Markus A. Jobst, Lukas F. Milles, Tobias Verdorfer, Diana A. Pippig, Michael A. Nash, and Hermann E. Gaub. 2014. “From Genes to Protein Mechanics on a Chip.” *Nature Methods* 11 (11): 1127–30. https://doi.org/10.1038/nmeth.3099.

Pagès, Sandrine, Anne Bélaïch, Jean-Pierre Bélaïch, Ely Morag, Raphael Lamed, Yuval Shoham, and Edward A. Bayer. 1997. “Species-Specificity of the Cohesin-Dockerin Interaction between Clostridium Thermocellum and Clostridium Cellulolyticum: Prediction of Specificity Determinants of the Dockerin Domain.” *Proteins: Structure, Function, and Bioinformatics* 29 (4): 517–27. https://doi.org/10.1002/(SICI)1097-0134(199712)29:4<517::AID-PROT11>3.0.CO;2-P.

Park, Joseph P., Minjae Do, Hyo-Eon Jin, Seung-Wuk Lee, and Haeshin Lee. 2014. “M13 Bacteriophage Displaying DOPA on Surfaces: Fabrication of Various Nanostructured Inorganic Materials without Time-Consuming Screening Processes.” *ACS Applied Materials & Interfaces* 6 (21): 18653–60. https://doi.org/10.1021/am506873g.

Petrenko, V.A., G.P. Smith, X. Gong, and T. Quinn. 1996. “A Library of Organic Landscapes on Filamentous Phage.” *Protein Engineering, Design and Selection* 9 (9): 797–801. https://doi.org/10.1093/protein/9.9.797.

Petrescu, Dan Stefan, and Amy Szuchmacher Blum. 2018. “Viral-Based Nanomaterials for Plasmonic and Photonic Materials and Devices.” *Wiley Interdisciplinary Reviews: Nanomedicine and Nanobiotechnology* 10 (4): e1508. https://doi.org/10.1002/wnan.1508.

Pham, Thi Hoa, Dinh Thi Quyen, Ngoc Minh Nghiem, and Thu Doan Vu. 2011. “Cloning, Expression, Purification, and Properties of an Endoglucanase Gene (Glycosyl Hydrolase Family 12) from

Aspergillus Niger VTCC-F021 in Pichia Pastoris." *Journal of Microbiology and Biotechnology* 21 (10): 1012–20. https://doi.org/10.4014/jmb.1104.04030.
Phillips, M. A. 1950. "The Preparation of Phosphotungstic Acid and of Sodium and Barium Phosphotungstates." *Journal of the Society of Chemical Industry* 69 (9): 282–84. https://doi.org/10.1002/jctb.5000690906.
Pieper, Ursula, Benjamin M. Webb, Guang Qiang Dong, Dina Schneidman-Duhovny, Hao Fan, Seung Joong Kim, Natalia Khuri, et al. 2014. "ModBase, a Database of Annotated Comparative Protein Structure Models and Associated Resources." *Nucleic Acids Research* 42 (D1): D336–46. https://doi.org/10.1093/nar/gkt1144.
Poghossian, Arshak, Melanie Jablonski, Claudia Koch, Thomas S. Bronder, David Rolka, Christina Wege, and Michael J. Schöning. 2018. "Field-Effect Biosensor Using Virus Particles as Scaffolds for Enzyme Immobilization." *Biosensors and Bioelectronics* 110 (July): 168–74. https://doi.org/10.1016/j.bios.2018.03.036.
Pollheimer, Philipp, Barbara Taskinen, Andreas Scherfler, Sergey Gusenkov, Marc Creus, Philipp Wiesauer, Dominik Zauner, et al. 2013. "Reversible Biofunctionalization of Surfaces with a Switchable Mutant of Avidin." *Bioconjugate Chemistry* 24 (10): 1656–68. https://doi.org/10.1021/bc400087e.
Qureshi, Mohammad Hassan, and Sui-Lam Wong. 2002. "Design, Production, and Characterization of a Monomeric Streptavidin and Its Application for Affinity Purification of Biotinylated Proteins." *Protein Expression and Purification* 25 (3): 409–15. https://doi.org/10.1016/S1046-5928(02)00021-9.
Race, Paul R., Matthew L. Bentley, Jeff A. Melvin, Allister Crow, Richard K. Hughes, Wendy D. Smith, Richard B. Sessions, Michael A. Kehoe, Dewey G. McCafferty, and Mark J. Banfield. 2009. "Crystal Structure of *Streptococcus Pyogenes* Sortase A: Implications for Sortase Mechanism." *Journal of Biological Chemistry* 284 (11): 6924–33. https://doi.org/10.1074/jbc.M805406200.
Rakonjac, Jasna, Nicholas J. Bennett, Julian Spagnuolo, Dragana Gagic, and Marjorie Russel. 2011. "Filamentous Bacteriophage: Biology, Phage Display and Nanotechnology Applications." *Current Issues in Molecular Biology*. https://doi.org/10.21775/cimb.013.051.
Reichel, Annett, Dirk Schaible, Natalie Al Furoukh, Mati Cohen, Gideon Schreiber, and Jacob Piehler. 2007. "Noncovalent, Site-Specific Biotinylation of Histidine-Tagged Proteins." *Analytical Chemistry* 79 (22): 8590–8600. https://doi.org/10.1021/ac0714922.
Reverbel-Leroy, C, S Pages, A Belaich, J P Belaich, and C Tardif. 1997. "The Processive Endocellulase CelF, a Major Component of the Clostridium Cellulolyticum Cellulosome: Purification and Characterization of the Recombinant Form." *Journal of Bacteriology* 179 (1): 46–52. https://doi.org/10.1128/jb.179.1.46-52.1997.
Roos, Tilmann, Dorothee Kiefer, Stephanie Hugenschmidt, Anastassios Economou, and Andreas Kuhn. 2001. "Indecisive M13 Procoat Protein Mutants Bind to SecA but Do Not Activate the Translocation ATPase." *Journal of Biological Chemistry*, August. https://doi.org/10.1074/jbc.M105483200.
Rothemund, Paul W. K. 2006. "Folding DNA to Create Nanoscale Shapes and Patterns." *Nature* 440 (7082): 297. https://doi.org/10.1038/nature04586.
Sachdeva, Gairik, Abhishek Garg, David Godding, Jeffrey C. Way, and Pamela A. Silver. 2014. "In Vivo Co-Localization of Enzymes on RNA Scaffolds Increases Metabolic Production in a Geometrically Dependent Manner." *Nucleic Acids Research* 42 (14): 9493–9503. https://doi.org/10.1093/nar/gku617.
Sakka, Kazutaka, Yuka Sugihara, Sadanari Jindou, Makiko Sakka, Minoru Inagaki, Kazuo Sakka, and Tetsuya Kimura. 2011. "Analysis of Cohesin–Dockerin Interactions Using Mutant Dockerin Proteins." *FEMS Microbiology Letters* 314 (1): 75–80. https://doi.org/10.1111/j.1574-6968.2010.02146.x.

Samuelson, James C., Fenglei Jiang, Liang Yi, Minyong Chen, Jan-Willem de Gier, Andreas Kuhn, and Ross E. Dalbey. 2001. “Function of YidC for the Insertion of M13 Procoat Protein in *Escherichia Coli*: Translocation of Mutants That Show Differences in Their Membrane Potential Dependence and Sec Requirement.” *Journal of Biological Chemistry* 276 (37): 34847–52. https://doi.org/10.1074/jbc.M105793200.

Sano, T., and C. R. Cantor. 1990a. “Expression of a Cloned Streptavidin Gene in Escherichia Coli.” *Proceedings of the National Academy of Sciences* 87 (1): 142–46. https://doi.org/10.1073/pnas.87.1.142.

———. 1990b. “Cooperative Biotin Binding by Streptavidin. Electrophoretic Behavior and Subunit Association of Streptavidin in the Presence of 6 M Urea.” *Journal of Biological Chemistry* 265 (6): 3369–73.

Sano, T., S. Vajda, C. L. Smith, and C. R. Cantor. 1997. “Engineering Subunit Association of Multisubunit Proteins: A Dimeric Streptavidin.” *Proceedings of the National Academy of Sciences* 94 (12): 6153–58. https://doi.org/10.1073/pnas.94.12.6153.

Schoeler, Constantin, Klara H. Malinowska, Rafael C. Bernardi, Lukas F. Milles, Markus A. Jobst, Ellis Durner, Wolfgang Ott, et al. 2014. “Ultrastable Cellulosome-Adhesion Complex Tightens under Load.” *Nature Communications* 5 (1). https://doi.org/10.1038/ncomms6635.

Schoffelen, Sanne, Jules Beekwilder, Marjoke F. Debets, Dirk Bosch, and Jan C. M. van Hest. 2013. “Construction of a Multifunctional Enzyme Complex via the Strain-Promoted Azide–Alkyne Cycloaddition.” *Bioconjugate Chemistry* 24 (6): 987–96. https://doi.org/10.1021/bc400021j.

Schwarz, Wolfgang H., Folke Gräbnitz, and Walter L. Staudenbauer. 1986. “Properties of a Clostridium Thermocellum Endoglucanase Produced in Escherichia Coli.” *Applied and Environmental Microbiology* 51 (6): 1293–99.

Seker, Urartu Ozgur Safak, and Hilmi Volkan Demir. 2011. “Material Binding Peptides for Nanotechnology.” *Molecules* 16 (2): 1426–51. https://doi.org/10.3390/molecules16021426.

Sharma, Hitesh, Mark J. Landau, Melissa A. Vargo, Krasimir A. Spasov, and Karen S. Anderson. 2013. “First Three-Dimensional Structure of Toxoplasma Gondii Thymidylate Synthase–Dihydrofolate Reductase: Insights for Catalysis, Interdomain Interactions, and Substrate Channeling.” *Biochemistry* 52 (41): 7305–17. https://doi.org/10.1021/bi400576t.

Sheldon, Roger A. 2007. “Enzyme Immobilization: The Quest for Optimum Performance.” *Advanced Synthesis & Catalysis* 349 (8–9): 1289–1307. https://doi.org/10.1002/adsc.200700082.

Shi, Jiafu, and Zhongyi Jiang. 2014. “An Efficient and Recyclable Enzyme Catalytic System Constructed through the Synergy between Biomimetic Mineralization and Polyamine–Salt Aggregate Assembly.” *Journal of Materials Chemistry B* 2 (28): 4435–41. https://doi.org/10.1039/C4TB00440J.

Shi, Jinjun, Philip W. Kantoff, Richard Wooster, and Omid C. Farokhzad. 2017. “Cancer Nanomedicine: Progress, Challenges and Opportunities.” *Nature Reviews Cancer* 17 (1): 20–37. https://doi.org/10.1038/nrc.2016.108.

Shimon, Linda JW, Edward A. Bayer, Ely Morag, Raphael Lamed, Sima Yaron, Yuval Shoham, and Felix Frolow. 1997. “A Cohesin Domain from Clostridium Thermocellum: The Crystal Structure Provides New Insights into Cellulosome Assembly.” *Structure* 5 (3): 381–90. https://doi.org/10.1016/S0969-2126(97)00195-0.

Shin, Dong-Myeong, Hye Ji Han, Won-Geun Kim, Eunjong Kim, Chuntae Kim, Suck Won Hong, Hyung Kook Kim, Jin-Woo Oh, and Yoon-Hwae Hwang. 2015. “Bioinspired Piezoelectric Nanogenerators Based on Vertically Aligned Phage Nanopillars.” *Energy & Environmental Science* 8 (11): 3198–3203. https://doi.org/10.1039/C5EE02611C.

Shoseyov, Oded, Ziv Shani, and Ilan Levy. 2006. “Carbohydrate Binding Modules: Biochemical Properties and Novel Applications.” *Microbiology and Molecular Biology Reviews* 70 (2): 283–95. https://doi.org/10.1128/MMBR.00028-05.

Sidhu, S. S., G. A. Weiss, and J. A. Wells. 2000. “High Copy Display of Large Proteins on Phage for Functional Selections.” *Journal of Molecular Biology* 296 (2): 487–95. https://doi.org/10.1006/jmbi.1999.3465.

Slutzki, Michal, Dan Reshef, Yoav Barak, Rachel Haimovitz, Shahar Rotem-Bamberger, Raphael Lamed, Edward A. Bayer, and Ora Schueler-Furman. 2015. “Crucial Roles of Single Residues in Binding Affinity, Specificity, and Promiscuity in the Cellulosomal Cohesin-Dockerin Interface.” *Journal of Biological Chemistry* 290 (22): 13654–66. https://doi.org/10.1074/jbc.M115.651208.

Smeal, Steven W., Margaret A. Schmitt, Ronnie Rodrigues Pereira, Ashok Prasad, and John D. Fisk. 2017a. “Simulation of the M13 Life Cycle I: Assembly of a Genetically-Structured Deterministic Chemical Kinetic Simulation.” *Virology* 500 (January): 259–74. https://doi.org/10.1016/j.virol.2016.08.017.

———. 2017b. “Simulation of the M13 Life Cycle II: Investigation of the Control Mechanisms of M13 Infection and Establishment of the Carrier State.” *Virology* 500 (January): 275–84. https://doi.org/10.1016/j.virol.2016.08.015.

Smith, G. P. 1985. “Filamentous Fusion Phage: Novel Expression Vectors That Display Cloned Antigens on the Virion Surface.” *Science* 228 (4705): 1315–17. https://doi.org/10.1126/science.4001944.

Smith, Mark L., John A. Lindbo, Stephan Dillard-Telm, Paul M. Brosio, Amanda B. Lasnik, Alison A. McCormick, Long V. Nguyen, and Kenneth E. Palmer. 2006. “Modified Tobacco Mosaic Virus Particles as Scaffolds for Display of Protein Antigens for Vaccine Applications.” *Virology* 348 (2): 475–88. https://doi.org/10.1016/j.virol.2005.12.039.

Smith, Steven P, and Edward A Bayer. 2013. “Insights into Cellulosome Assembly and Dynamics: From Dissection to Reconstruction of the Supramolecular Enzyme Complex.” *Current Opinion in Structural Biology* 23 (5): 686–94. https://doi.org/10.1016/j.sbi.2013.09.002.

Spolaore, Barbara, Nunzio Damiano, Samanta Raboni, and Angelo Fontana. 2014. “Site-Specific Derivatization of Avidin Using Microbial Transglutaminase.” *Bioconjugate Chemistry* 25 (3): 470–80. https://doi.org/10.1021/bc400378h.

Stern, Johanna, Amaranta Kahn, Yael Vazana, Melina Shamshoum, Sarah Moraïs, Raphael Lamed, and Edward A. Bayer. 2015. “Significance of Relative Position of Cellulases in Designer Cellulosomes for Optimized Cellulolysis.” Edited by Eric A. Johnson. *PLOS ONE* 10 (5): e0127326. https://doi.org/10.1371/journal.pone.0127326.

Su, Zhengding, Tong Leung, and John F. Honek. 2006. “Conformational Selectivity of Peptides for Single-Walled Carbon Nanotubes.” *The Journal of Physical Chemistry B* 110 (47): 23623–27. https://doi.org/10.1021/jp065837g.

Sun, Jiayu, Jiechao Ge, Weimin Liu, Minhua Lan, Hongyan Zhang, Pengfei Wang, Yanming Wang, and Zhongwei Niu. 2014. “Multi-Enzyme Co-Embedded Organic–Inorganic Hybrid Nanoflowers: Synthesis and Application as a Colorimetric Sensor.” *Nanoscale* 6 (1): 255–62. https://doi.org/10.1039/C3NR04425D.

Sun, Qing, and Wilfred Chen. 2016. “HaloTag Mediated Artificial Cellulosome Assembly on a Rolling Circle Amplification DNA Template for Efficient Cellulose Hydrolysis.” *Chemical Communications* 52 (40): 6701–4. https://doi.org/10.1039/C6CC02035F.

Sun, Qing, Bhawna Madan, Shen-Long Tsai, Matthew P. DeLisa, and Wilfred Chen. 2014. “Creation of Artificial Cellulosomes on DNA Scaffolds by Zinc Finger Protein-Guided Assembly for Efficient Cellulose Hydrolysis.” *Chemical Communications* 50 (12): 1423–25. https://doi.org/10.1039/C3CC47215A.

Tamerler, Candan, Ersin Emre Oren, Memed Duman, Eswaranand Venkatasubramanian, and Mehmet Sarikaya. 2006. “Adsorption Kinetics of an Engineered Gold Binding Peptide by Surface Plasmon Resonance Spectroscopy and a Quartz Crystal Microbalance.” *Langmuir* 22 (18): 7712–18. https://doi.org/10.1021/la0606897.

Taskinen, Barbara, Dominik Zauner, Soili I. Lehtonen, Masi Koskinen, Chloe Thomson, Niklas Kähkönen, Sampo Kukkurainen, et al. 2014. “Switchavidin: Reversible Biotin–Avidin–Biotin Bridges with High Affinity and Specificity.” *Bioconjugate Chemistry* 25 (12): 2233–43. https://doi.org/10.1021/bc500462w.

Tausig, Fred, and Frank J. Wolf. 1964. “Streptavidin—A Substance with Avidin-like Properties Produced by Microorganisms.” *Biochemical and Biophysical Research Communications* 14 (3): 205–9. https://doi.org/10.1016/0006-291X(64)90436-X.

Theile, Christopher S, Martin D Witte, Annet E M Blom, Lenka Kundrat, Hidde L Ploegh, and Carla P Guimaraes. 2013. “Site-Specific N-Terminal Labeling of Proteins Using Sortase-Mediated Reactions.” *Nature Protocols* 8 (9): 1800–1807. https://doi.org/10.1038/nprot.2013.102.

Tian, Feng, Meng-Lin Tsao, and Peter G. Schultz. 2004. “A Phage Display System with Unnatural Amino Acids.” *Journal of the American Chemical Society* 126 (49): 15962–63. https://doi.org/10.1021/ja045673m.

Tsai, Shen-Long, Miso Park, and Wilfred Chen. 2013. “Size-Modulated Synergy of Cellulase Clustering for Enhanced Cellulose Hydrolysis.” *Biotechnology Journal* 8 (2): 257–61. https://doi.org/10.1002/biot.201100503.

Tsunoda, S., Y. Tsutsumi, and S. Imai. 2008. “Effect of Protein Properties on Display Efficiency Using the M13 Phage Display System.” *Die Pharmazie-An International Journal of Pharmaceutical Sciences* 63 (10): 760–764. https://doi.org/10.1691/ph.2008.8132.

Uchinomiya, Sho-hei, Hiroshi Nonaka, Sho-hei Fujishima, Shinya Tsukiji, Akio Ojida, and Itaru Hamachi. 2009. “Site-Specific Covalent Labeling of His-Tag Fused Proteins with a Reactive Ni(II)–NTA Probe.” *Chemical Communications* 0 (39): 5880–82. https://doi.org/10.1039/B912025D.

Urquhart, Taylor, Elisabeth Daub, and John Frank Honek. 2016. “Bioorthogonal Modification of the Major Sheath Protein of Bacteriophage M13: Extending the Versatility of Bionanomaterial Scaffolds.” *Bioconjugate Chemistry* 27 (10): 2276–80. https://doi.org/10.1021/acs.bioconjchem.6b00460.

Vauquelin, Georges, and Steven J Charlton. 2013. “Exploring Avidity: Understanding the Potential Gains in Functional Affinity and Target Residence Time of Bivalent and Heterobivalent Ligands: Exploring Bivalent Ligand Binding Properties.” *British Journal of Pharmacology* 168 (8): 1771–85. https://doi.org/10.1111/bph.12106.

Vazana, Y., S. Morais, Y. Barak, R. Lamed, and E. A. Bayer. 2010. “Interplay between Clostridium Thermocellum Family 48 and Family 9 Cellulases in Cellulosomal versus Noncellulosomal States.” *Applied and Environmental Microbiology* 76 (10): 3236–43. https://doi.org/10.1128/AEM.00009-10.

Vazana, Yael, Yoav Barak, Tamar Unger, Yoav Peleg, Melina Shamshoum, Tuval Ben-Yehezkel, Yair Mazor, Ehud Shapiro, Raphael Lamed, and Edward A Bayer. 2013. “A Synthetic Biology Approach for Evaluating the Functional Contribution of Designer Cellulosome Components to Deconstruction of Cellulosic Substrates.” *Biotechnology for Biofuels* 6 (1): 182. https://doi.org/10.1186/1754-6834-6-182.

Vazana, Yael, Sarah Moraïs, Yoav Barak, Raphael Lamed, and Edward A. Bayer. 2012. “Designer Cellulosomes for Enhanced Hydrolysis of Cellulosic Substrates.” In *Methods in Enzymology*, 510:429–52. Elsevier. https://doi.org/10.1016/B978-0-12-415931-0.00023-9.

Vm, Muggeo. 2008. “Segmented: An R Package to Fit Regression Models with Broken-Line Relationships.” *R NEWS* 8/1: 20–25.

Wang, Jianglin, Mingying Yang, Ye Zhu, Lin Wang, Antoni P. Tomsia, and Chuanbin Mao. 2014. “Phage Nanofibers Induce Vascularized Osteogenesis in 3D Printed Bone Scaffolds.” *Advanced Materials* 26 (29): 4961–66. https://doi.org/10.1002/adma.201400154.

Wang, Nuo, and J. Andrew McCammon. 2016. “Substrate Channeling between the Human Dihydrofolate Reductase and Thymidylate Synthase.” *Protein Science* 25 (1): 79–86. https://doi.org/10.1002/pro.2720.

Wegner, Seraphine V., and Joachim P. Spatz. 2013. “Cobalt(III) as a Stable and Inert Mediator Ion between NTA and His6-Tagged Proteins.” *Angewandte Chemie International Edition* 52 (29): 7593–96. https://doi.org/10.1002/anie.201210317.

Wei, Yang, Aby A. Thyparambil, Yonnie Wu, and Robert A. Latour. 2014. “Adsorption-Induced Changes in Ribonuclease A Structure and Enzymatic Activity on Solid Surfaces.” *Langmuir* 30 (49): 14849–58. https://doi.org/10.1021/la503854a.

Whaley, Sandra R., D. S. English, Evelyn L. Hu, Paul F. Barbara, and Angela M. Belcher. 2000. “Selection of Peptides with Semiconductor Binding Specificity for Directed Nanocrystal Assembly.” *Nature* 405 (6787): 665. https://doi.org/10.1038/35015043.

Williams, Karen A., Mira Glibowicka, Zuomei Li, Hong Li, Amir R. Khan, Yvonne M.Y. Chen, Jing Wang, Donald A. Marvin, and Charles M. Deber. 1995. “Packing of Coat Protein Amphipathic and Transmembrane Helices in Filamentous Bacteriophage M13: Role of Small Residues in Protein Oligomeriza Tion.” *Journal of Molecular Biology* 252 (1): 6–14. https://doi.org/10.1006/jmbi.1995.0469.

Williams, Stephanie, Philip Schulz, and Michael R. Sierks. 2015. “A Sensitive Phage-Based Capture ELISA for Sub-Femtomolar Detection of Protein Variants Directly from Biological Samples.” *Biotechnology Progress* 31 (1): 289–98. https://doi.org/10.1002/btpr.1987.

Wojcik, Roza, Kristian E. Swearingen, Jane A. Dickerson, Emily H. Turner, Lauren M. Ramsay, and Norman J. Dovichi. 2008. “Reaction of Fluorogenic Reagents with Proteins I. Mass Spectrometric Characterization of the Reaction with 3-(2-Furoyl)Quinoline-2-Carboxaldehyde, Chromeo P465, and Chromeo P503.” *Journal of Chromatography. A* 1194 (2): 243–48. https://doi.org/10.1016/j.chroma.2008.04.042.

Wong, Ngo Yin, Hang Xing, Li Huey Tan, and Yi Lu. 2013. “Nano-Encrypted Morse Code: A Versatile Approach to Programmable and Reversible Nanoscale Assembly and Disassembly.” *Journal of the American Chemical Society* 135 (8): 2931–34. https://doi.org/10.1021/ja3122284.

Wu, Fei, and Shelley Minteer. 2015. “Krebs Cycle Metabolon: Structural Evidence of Substrate Channeling Revealed by Cross-Linking and Mass Spectrometry.” *Angewandte Chemie International Edition* 54 (6): 1851–54. https://doi.org/10.1002/anie.201409336.

Xia, Xin-Rui, Nancy A. Monteiro-Riviere, and Jim E. Riviere. 2010. “An Index for Characterization of Nanomaterials in Biological Systems.” *Nature Nanotechnology* 5 (9): 671–75. https://doi.org/10.1038/nnano.2010.164.

Xu, Lingling, Marie-Laurence Tremblay, Kathleen E. Orrell, Jérémie Leclerc, Qing Meng, Xiang-Qin Liu, and Jan K. Rainey. 2013. “Nanoparticle Self-Assembly by a Highly Stable Recombinant Spider Wrapping Silk Protein Subunit.” *FEBS Letters* 587 (19): 3273–80. https://doi.org/10.1016/j.febslet.2013.08.024.

Xu, Qi, Shi-You Ding, Roman Brunecky, Yannick J Bomble, Michael E Himmel, and John O Baker. 2013. “Improving Activity of Minicellulosomes by Integration of Intra- and Intermolecular Synergies.” *Biotechnology for Biofuels* 6 (1): 126. https://doi.org/10.1186/1754-6834-6-126.

Yan, Yiran, Miluo Zhang, Chung Hee Moon, Heng-Chia Su, Nosang V Myung, and Elaine D Haberer. 2016. “Viral-Templated Gold/Polypyrrole Nanopeapods for an Ammonia Gas Sensor.” *Nanotechnology* 27 (32): 325502. https://doi.org/10.1088/0957-4484/27/32/325502.

Yaron, Sima, Ely Morag, Edward A Bayer, Raphael Lamed, and Yuval Shoham. 1995. “Expression, Purification and Subunit-Binding Properties of Cohesins 2 and 3 of the *Clostridium Thermocellum* Cellulosome.” *FEBS Letters* 360 (2): 121–24. https://doi.org/10.1016/0014-5793(95)00074-J.

Yoon, Hyun C., Mi-Young Hong, and Hak-Sung Kim. 2001. “Reversible Association/Dissociation Reaction of Avidin on the Dendrimer Monolayer Functionalized with a Biotin Analogue for a Regenerable Affinity-Sensing Surface.” *Langmuir* 17 (4): 1234–39. https://doi.org/10.1021/la001373g.

You, Chun, Suwan Myung, and Y.-H. Percival Zhang. 2012. “Facilitated Substrate Channeling in a Self-Assembled Trifunctional Enzyme Complex.” *Angewandte Chemie International Edition* 51 (35): 8787–90. https://doi.org/10.1002/anie.201202441.

Zaman, Mohammed Shahriar, and Elaine D. Haberer. 2014. “Mineralization and Optical Characterization of Copper Oxide Nanoparticles Using a High Aspect Ratio Bio-Template.” *Journal of Applied Physics* 116 (15): 154308. https://doi.org/10.1063/1.4898809.

Zanetti-Domingues, Laura C., Christopher J. Tynan, Daniel J. Rolfe, David T. Clarke, and Marisa Martin-Fernandez. 2013. “Hydrophobic Fluorescent Probes Introduce Artifacts into Single Molecule Tracking Experiments Due to Non-Specific Binding.” *PLOS ONE* 8 (9): e74200. https://doi.org/10.1371/journal.pone.0074200.

Zhang, Fang, Meitao Wang, Chao Liang, Huangyong Jiang, Jian Shen, and Hexing Li. 2014. “Thin-Layer Polymer Wrapped Enzymes Encapsulated in Hierarchically Mesoporous Silica with High Activity and Enhanced Stability.” *Scientific Reports* 4 (March): 4421. https://doi.org/10.1038/srep04421.

Zhang, Mingzhen, Changlong Xu, Liuqing Wen, Moon Kwon Han, Bo Xiao, Jun Zhou, Yuchen Zhang, Zhan Zhang, Emilie Viennois, and Didier Merlin. 2016. “A Hyaluronidase Responsive Nanoparticle-Based Drug Delivery System for Targeting Colon Cancer Cells.” *Cancer Research* 76 (24): 7208–18. https://doi.org/10.1158/0008-5472.CAN-16-1681.

Zhang, Yan, Jingyan Zhang, Xuelei Huang, Xuejiao Zhou, Haixia Wu, and Shouwu Guo. 2012. “Assembly of Graphene Oxide–Enzyme Conjugates through Hydrophobic Interaction.” *Small* 8 (1): 154–59. https://doi.org/10.1002/smll.201101695.

Zhou, Wenhu, Runjhun Saran, and Juewen Liu. 2017. “Metal Sensing by DNA.” *Chemical Reviews* 117 (12): 8272–8325. https://doi.org/10.1021/acs.chemrev.7b00063.

Zimmermann, K., H. Hagedorn, C. C. Heuck, M. Hinrichsen, and H. Ludwig. 1986. “The Ionic Properties of the Filamentous Bacteriophages Pf1 and Fd.” *Journal of Biological Chemistry* 261 (4): 1653–55.

Zore, Omkar V., Ajith Pattammattel, Shailaja Gnanaguru, Challa V. Kumar, and Rajeswari M. Kasi. 2015. “Bienzyme–Polymer–Graphene Oxide Quaternary Hybrid Biocatalysts: Efficient Substrate Channeling under Chemically and Thermally Denaturing Conditions.” *ACS Catalysis* 5 (9): 4979–88. https://doi.org/10.1021/acscatal.5b00958.

Zverlov, Vladimir V., Nikolaus Schantz, and Wolfgang H. Schwarz. 2005. “A Major New Component in the Cellulosome of *Clostridium Thermocellum* Is a Processive Endo-Î²-1,4-Glucanase Producing Cellotetraose.” *FEMS Microbiology Letters* 249 (2): 353–58. https://doi.org/10.1016/j.femsle.2005.06.037.

Letters of copyright permission

Copyright use for Figure 1.4

This Agreement between University of Waterloo -- Taylor Urquhart ("You") and Elsevier ("Elsevier") consists of your license details and the terms and conditions provided by Elsevier and Copyright Clearance Center.

License Number	4626060593073
License date	Jul 11, 2019
Licensed Content Publisher	Elsevier
Licensed Content Publication	Virology
Licensed Content Title	Simulation of the M13 life cycle I: Assembly of a genetically-structured deterministic chemical kinetic simulation
Licensed Content Author	Steven W. Smeal,Margaret A. Schmitt,Ronnie Rodrigues Pereira,Ashok Prasad,John D. Fisk
Licensed Content Date	Jan 1, 2017
Licensed Content Volume	500
Licensed Content Issue	n/a
Licensed Content Pages	16
Start Page	259
End Page	274
Type of Use	reuse in a thesis/dissertation
Intended publisher of new work	other
Portion	figures/tables/illustrations
Number of figures/tables /illustrations	1
Format	both print and electronic
Are you the author of this Elsevier article?	No
Will you be translating?	No
Original figure numbers	Figure 2
Title of your thesis/dissertation	Bacteriophage M13 as a Template for Multi-Enzyme Assembly
Publisher of new work	University of Waterloo
Expected completion date	Sep 2019

Copyright use for Figure 1.5

PERMISSION/LICENSE IS GRANTED FOR YOUR ORDER AT NO CHARGE

This type of permission/license, instead of the standard Terms & Conditions, is sent to you because no fee is being charged for your order. Please note the following:

- Permission is granted for your request in both print and electronic formats, and translations.
- If figures and/or tables were requested, they may be adapted or used in part.
- Please print this page for your records and send a copy of it to your publisher/graduate school.
- Appropriate credit for the requested material should be given as follows: "Reprinted (adapted) with permission from (COMPLETE REFERENCE CITATION). Copyright (YEAR) American Chemical Society." Insert appropriate information in place of the capitalized words.
- One-time permission is granted only for the use specified in your request. No additional uses are granted (such as derivative works or other editions). For any other uses, please submit a new request.

If credit is given to another source for the material you requested, permission must be obtained from that source.

Copyright use for Figure 1.7A

ACS Publications
Most Trusted. Most Cited. Most Read.

Title: Virus-Directed Design of a Flexible BaTiO3 Nanogenerator
Author: Chang Kyu Jeong, Insu Kim, Kwi-Il Park, et al
Publication: ACS Nano
Publisher: American Chemical Society
Date: Dec 1, 2013
Copyright © 2013, American Chemical Society

LOGIN

If you're a copyright.com user, you can login to RightsLink using your copyright.com credentials.
Already **a RightsLink user** or want to learn more?

PERMISSION/LICENSE IS GRANTED FOR YOUR ORDER AT NO CHARGE

This type of permission/license, instead of the standard Terms & Conditions, is sent to you because no fee is being charged for your order. Please note the following:

- Permission is granted for your request in both print and electronic formats, and translations.
- If figures and/or tables were requested, they may be adapted or used in part.
- Please print this page for your records and send a copy of it to your publisher/graduate school.
- Appropriate credit for the requested material should be given as follows: "Reprinted (adapted) with permission from (COMPLETE REFERENCE CITATION). Copyright (YEAR) American Chemical Society." Insert appropriate information in place of the capitalized words.
- One-time permission is granted only for the use specified in your request. No additional uses are granted (such as derivative works or other editions). For any other uses, please submit a new request.

If credit is given to another source for the material you requested, permission must be obtained from that source.

BACK CLOSE WINDOW

Copyright use for Figure 1.7B

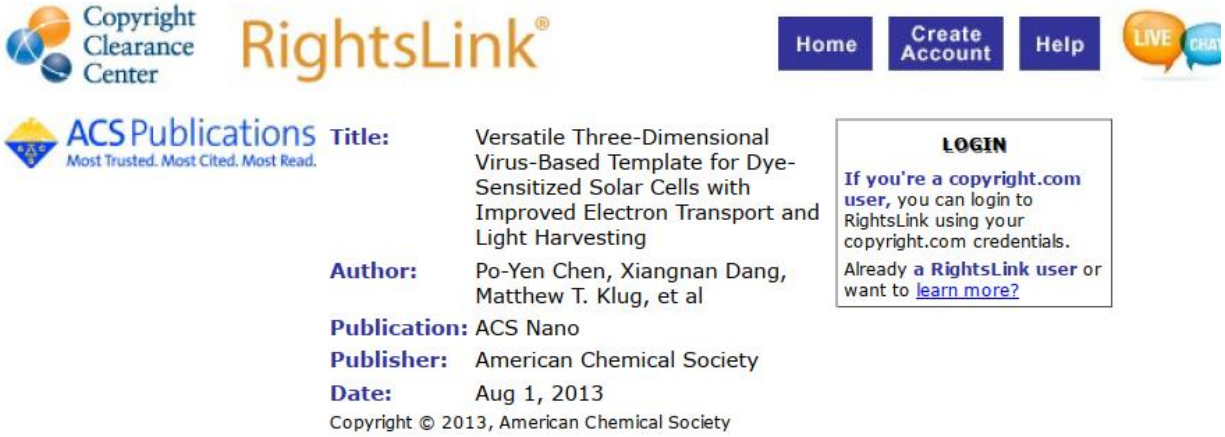

Copyright Clearance Center RightsLink®

Home | Create Account | Help | LIVE CHAT

ACS Publications
Most Trusted. Most Cited. Most Read.

Title: Versatile Three-Dimensional Virus-Based Template for Dye-Sensitized Solar Cells with Improved Electron Transport and Light Harvesting

Author: Po-Yen Chen, Xiangnan Dang, Matthew T. Klug, et al

Publication: ACS Nano

Publisher: American Chemical Society

Date: Aug 1, 2013

Copyright © 2013, American Chemical Society

LOGIN

If you're a copyright.com user, you can login to RightsLink using your copyright.com credentials.

Already **a RightsLink user** or want to learn more?

PERMISSION/LICENSE IS GRANTED FOR YOUR ORDER AT NO CHARGE

This type of permission/license, instead of the standard Terms & Conditions, is sent to you because no fee is being charged for your order. Please note the following:

- Permission is granted for your request in both print and electronic formats, and translations.
- If figures and/or tables were requested, they may be adapted or used in part.
- Please print this page for your records and send a copy of it to your publisher/graduate school.
- Appropriate credit for the requested material should be given as follows: "Reprinted (adapted) with permission from (COMPLETE REFERENCE CITATION). Copyright (YEAR) American Chemical Society." Insert appropriate information in place of the capitalized words.
- One-time permission is granted only for the use specified in your request. No additional uses are granted (such as derivative works or other editions). For any other uses, please submit a new request.

If credit is given to another source for the material you requested, permission must be obtained from that source.

BACK | CLOSE WINDOW

Copyright use for Figure 1.9B

This is a License Agreement between University of Waterloo -- Taylor Urquhart ("You") and Royal Society of Chemistry ("Royal Society of Chemistry") provided by Copyright Clearance Center ("CCC"). The license consists of your order details, the terms and conditions provided by Royal Society of Chemistry, and the payment terms and conditions.

All payments must be made in full to CCC. For payment instructions, please see information listed at the bottom of this form.

License Number	4626040393928
License date	Jul 11, 2019
Licensed Content Publisher	Royal Society of Chemistry
Licensed Content Title	Journal of materials chemistry. B, Materials for biology and medicine
Licensed Content Date	Jan 1, 2013
I would like to...	Thesis/Dissertation
Requestor type	Academic institution
Format	Print, Electronic
Portion	chart/graph/table/figure
Number of charts/graphs /tables/figures	1
The requesting person/organization is:	Taylor Urquhart
Title or numeric reference of the portion(s)	Figure 1
Title of the article or chapter the portion is from	An efficient and recyclable enzyme catalytic system constructed through the synergy between biomimetic mineralization and polyamine–salt aggregate assembly
Editor of portion(s)	N/A
Author of portion(s)	Jiafu Shi and Zhongyi Jiang
Volume of serial or monograph.	2
Page range of the portion	4435-4441
Publication date of portion	May 13, 2014
Rights for	Main product
Duration of use	Life of current edition
Creation of copies for the disabled	no
With minor editing privileges	no
For distribution to	Canada
In the following language(s)	Original language of publication
With incidental promotional use	no
The lifetime unit quantity of new product	Up to 499
Title	Bacteriophage M13 as a Template for Multi-Enzyme Assembly
Institution name	University of Waterloo

Copyright use for Figure 1.10

This Agreement between University of Waterloo -- Taylor Urquhart ("You") and Springer Nature ("Springer Nature") consists of your license details and the terms and conditions provided by Springer Nature and Copyright Clearance Center.

License Number	4626040865829
License date	Jul 11, 2019
Licensed Content Publisher	Springer Nature
Licensed Content Publication	Nature
Licensed Content Title	Folding DNA to create nanoscale shapes and patterns
Licensed Content Author	Paul W. K. Rothemund
Licensed Content Date	Mar 16, 2006
Type of Use	Thesis/Dissertation
Requestor type	academic/university or research institute
Format	print and electronic
Portion	figures/tables/illustrations
Number of figures/tables /illustrations	2
High-res required	no
Will you be translating?	no
Circulation/distribution	<501
Author of this Springer Nature content	no
Title	Bacteriophage M13 as a Template for Multi-Enzyme Assembly
Institution name	University of Waterloo
Expected presentation date	Sep 2019
Portions	Figure 1e, Figure 2

Copyright use for Figure 11A

This Agreement between University of Waterloo -- Taylor Urquhart ("You") and Springer Nature ("Springer Nature") consists of your license details and the terms and conditions provided by Springer Nature and Copyright Clearance Center.

License Number	4626041077764
License date	Jul 11, 2019
Licensed Content Publisher	Springer Nature
Licensed Content Publication	Nature Communications
Licensed Content Title	A DNA tweezer-actuated enzyme nanoreactor
Licensed Content Author	Minghui Liu, Jinglin Fu, Christian Hejesen, Yuhe Yang, Neal W. Woodbury et al.
Licensed Content Date	Jul 3, 2013
Licensed Content Volume	4
Type of Use	Thesis/Dissertation
Requestor type	academic/university or research institute
Format	print and electronic
Portion	figures/tables/illustrations
Number of figures/tables /illustrations	1
High-res required	no
Will you be translating?	no
Circulation/distribution	<501
Author of this Springer Nature content	no
Title	Bacteriophage M13 as a Template for Multi-Enzyme Assembly
Institution name	University of Waterloo
Expected presentation date	Sep 2019
Portions	figure 1a

Copyright use for Figure 11B

This Agreement between University of Waterloo -- Taylor Urquhart ("You") and Springer Nature ("Springer Nature") consists of your license details and the terms and conditions provided by Springer Nature and Copyright Clearance Center.

License Number	4626041236829
License date	Jul 11, 2019
Licensed Content Publisher	Springer Nature
Licensed Content Publication	Nature Nanotechnology
Licensed Content Title	Multi-enzyme complexes on DNA scaffolds capable of substrate channelling with an artificial swinging arm
Licensed Content Author	Jinglin Fu, Yuhe Renee Yang, Alexander Johnson-Buck, Minghui Liu, Yan Liu et al.
Licensed Content Date	May 25, 2014
Licensed Content Volume	9
Licensed Content Issue	7
Type of Use	Thesis/Dissertation
Requestor type	academic/university or research institute
Format	print and electronic
Portion	figures/tables/illustrations
Number of figures/tables /illustrations	1
High-res required	no
Will you be translating?	no
Circulation/distribution	<501
Author of this Springer Nature content	no
Title	Bacteriophage M13 as a Template for Multi-Enzyme Assembly
Institution name	University of Waterloo
Expected presentation date	Sep 2019
Portions	Figure 4a

Copyright use for Figure 12A

This is a License Agreement between University of Waterloo -- Taylor Urquhart ("You") and Annual Reviews, Inc ("Annual Reviews, Inc") provided by Copyright Clearance Center ("CCC"). The license consists of your order details, the terms and conditions provided by Annual Reviews, Inc, and the payment terms and conditions.

All payments must be made in full to CCC. For payment instructions, please see information listed at the bottom of this form.

License Number	4626050736789
License date	Jul 11, 2019
Licensed Content Publisher	Annual Reviews, Inc
Licensed Content Title	Annual review of biochemistry
Licensed Content Date	Jan 1, 1932
I would like to...	Thesis/Dissertation
Requestor type	Academic institution
Format	Print, Electronic
Portion	image/photo
Number of images/photos requested	3
The requesting person/organization is:	Taylor Urquhart
Title or numeric reference of the portion(s)	Figure 1, Figure 2, Figure 3
Title of the article or chapter the portion is from	Cellulosomes: Highly Efficient Nanomachines Designed to Deconstruct Plant Cell Wall Complex Carbohydrates
Editor of portion(s)	N/A
Author of portion(s)	Carlos M.G.A. Fontes and Harry J. Gilbert
Volume of serial or monograph.	79
Page range of the portion	655–81
Publication date of portion	April 7, 2010
Rights for	Main product
Duration of use	Life of current edition
Creation of copies for the disabled	no
With minor editing privileges	no
For distribution to	Canada
In the following language(s)	Original language of publication
With incidental promotional use	no
The lifetime unit quantity of new product	Up to 499
Title	Bacteriophage M13 as a Template for Multi-Enzyme Assembly
Institution name	University of Waterloo

Copyright use for Figure 13A

This Agreement between University of Waterloo -- Taylor Urquhart ("You") and John Wiley and Sons ("John Wiley and Sons") consists of your license details and the terms and conditions provided by John Wiley and Sons and Copyright Clearance Center.

License Number	4626051262827
License date	Jul 11, 2019
Licensed Content Publisher	John Wiley and Sons
Licensed Content Publication	Angewandte Chemie International Edition
Licensed Content Title	Facilitated Substrate Channeling in a Self-Assembled Trifunctional Enzyme Complex
Licensed Content Author	Chun You, Suwan Myung, Y.-H. Percival Zhang
Licensed Content Date	Jul 23, 2012
Licensed Content Volume	51
Licensed Content Issue	35
Licensed Content Pages	4
Type of Use	Dissertation/Thesis
Requestor type	University/Academic
Format	Print and electronic
Portion	Figure/table
Number of figures/tables	1
Original Wiley figure/table number(s)	Figure 1
Will you be translating?	No
Title of your thesis / dissertation	Bacteriophage M13 as a Template for Multi-Enzyme Assembly
Expected completion date	Sep 2019

Copyright use for Figure 13B

This Agreement between University of Waterloo -- Taylor Urquhart ("You") and Springer Nature ("Springer Nature") consists of your license details and the terms and conditions provided by Springer Nature and Copyright Clearance Center.

License Number	4626051422176
License date	Jul 11, 2019
Licensed Content Publisher	Springer Nature
Licensed Content Publication	Nature Biotechnology
Licensed Content Title	Synthetic protein scaffolds provide modular control over metabolic flux
Licensed Content Author	John E Dueber, Gabriel C Wu, G Reza Malmirchegini, Tae Seok Moon, Christopher J Petzold et al.
Licensed Content Date	Aug 2, 2009
Licensed Content Volume	27
Licensed Content Issue	8
Type of Use	Thesis/Dissertation
Requestor type	academic/university or research institute
Format	print and electronic
Portion	figures/tables/illustrations
Number of figures/tables /illustrations	1
High-res required	no
Will you be translating?	no
Circulation/distribution	<501
Author of this Springer Nature content	no
Title	Bacteriophage M13 as a Template for Multi-Enzyme Assembly
Institution name	University of Waterloo
Expected presentation date	Sep 2019
Portions	Figure 3A

Copyright use for Figure 14

This Agreement between University of Waterloo -- Taylor Urquhart ("You") and Springer Nature ("Springer Nature") consists of your license details and the terms and conditions provided by Springer Nature and Copyright Clearance Center.

License Number	4626060040833
License date	Jul 11, 2019
Licensed Content Publisher	Springer Nature
Licensed Content Publication	Nature Biotechnology
Licensed Content Title	Enzyme clustering accelerates processing of intermediates through metabolic channeling
Licensed Content Author	Michele Castellana, Maxwell Z Wilson, Yifan Xu, Preeti Joshi, Ileana M Cristea et al.
Licensed Content Date	Sep 28, 2014
Licensed Content Volume	32
Licensed Content Issue	10
Type of Use	Thesis/Dissertation
Requestor type	academic/university or research institute
Format	print and electronic
Portion	figures/tables/illustrations
Number of figures/tables /illustrations	2
High-res required	no
Will you be translating?	no
Circulation/distribution	<501
Author of this Springer Nature content	no
Title	Bacteriophage M13 as a Template for Multi-Enzyme Assembly
Institution name	University of Waterloo
Expected presentation date	Sep 2019
Portions	Figure 1, Figure 2B

Copyright use for Figure 15

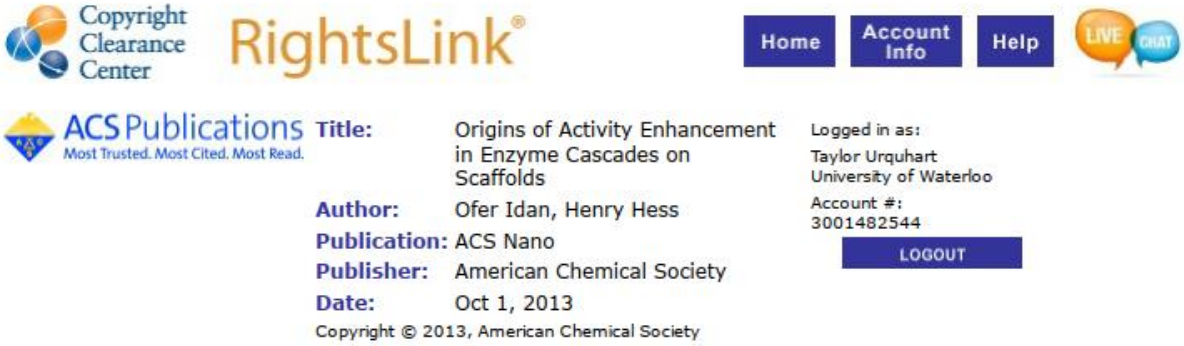

Copyright Clearance Center RightsLink®

Home | Account Info | Help | LIVE CHAT

ACS Publications Most Trusted. Most Cited. Most Read.

Title: Origins of Activity Enhancement in Enzyme Cascades on Scaffolds

Author: Ofer Idan, Henry Hess

Publication: ACS Nano

Publisher: American Chemical Society

Date: Oct 1, 2013

Copyright © 2013, American Chemical Society

Logged in as:
Taylor Urquhart
University of Waterloo
Account #:
3001482544

LOGOUT

PERMISSION/LICENSE IS GRANTED FOR YOUR ORDER AT NO CHARGE

This type of permission/license, instead of the standard Terms & Conditions, is sent to you because no fee is being charged for your order. Please note the following:

- Permission is granted for your request in both print and electronic formats, and translations.
- If figures and/or tables were requested, they may be adapted or used in part.
- Please print this page for your records and send a copy of it to your publisher/graduate school.
- Appropriate credit for the requested material should be given as follows: "Reprinted (adapted) with permission from (COMPLETE REFERENCE CITATION). Copyright (YEAR) American Chemical Society." Insert appropriate information in place of the capitalized words.
- One-time permission is granted only for the use specified in your request. No additional uses are granted (such as derivative works or other editions). For any other uses, please submit a new request.

If credit is given to another source for the material you requested, permission must be obtained from that source.

BACK | CLOSE WINDOW

Copyright use for Figure 18

This is a License Agreement between University of Waterloo -- Taylor Urquhart ("You") and Annual Reviews, Inc ("Annual Reviews, Inc") provided by Copyright Clearance Center ("CCC"). The license consists of your order details, the terms and conditions provided by Annual Reviews, Inc, and the payment terms and conditions.

All payments must be made in full to CCC. For payment instructions, please see information listed at the bottom of this form.

License Number	4626050736789
License date	Jul 11, 2019
Licensed Content Publisher	Annual Reviews, Inc
Licensed Content Title	Annual review of biochemistry
Licensed Content Date	Jan 1, 1932
I would like to...	Thesis/Dissertation
Requestor type	Academic institution
Format	Print, Electronic
Portion	image/photo
Number of images/photos requested	3
The requesting person/organization is:	Taylor Urquhart
Title or numeric reference of the portion(s)	Figure 1, Figure 2, Figure 3
Title of the article or chapter the portion is from	Cellulosomes: Highly Efficient Nanomachines Designed to Deconstruct Plant Cell Wall Complex Carbohydrates
Editor of portion(s)	N/A
Author of portion(s)	Carlos M.G.A. Fontes and Harry J. Gilbert
Volume of serial or monograph.	79
Page range of the portion	655–81
Publication date of portion	April 7, 2010
Rights for	Main product
Duration of use	Life of current edition
Creation of copies for the disabled	no
With minor editing privileges	no
For distribution to	Canada
In the following language(s)	Original language of publication
With incidental promotional use	no
The lifetime unit quantity of new product	Up to 499
Title	Bacteriophage M13 as a Template for Multi-Enzyme Assembly
Institution name	University of Waterloo

Copyright use for Figure 19

This Agreement between University of Waterloo -- Taylor Urquhart ("You") and Elsevier ("Elsevier") consists of your license details and the terms and conditions provided by Elsevier and Copyright Clearance Center.

License Number	4626060852409
License date	Jul 11, 2019
Licensed Content Publisher	Elsevier
Licensed Content Publication	Journal of Biotechnology
Licensed Content Title	The rosettazyme: A synthetic cellulosome
Licensed Content Author	Shigenobu Mitsuzawa,Hiromi Kagawa,Yifen Li,Suzanne L. Chan,Chad D. Paavola,Jonathan D. Trent
Licensed Content Date	Aug 20, 2009
Licensed Content Volume	143
Licensed Content Issue	2
Licensed Content Pages	6
Start Page	139
End Page	144
Type of Use	reuse in a thesis/dissertation
Intended publisher of new work	other
Portion	figures/tables/illustrations
Number of figures/tables /illustrations	1
Format	both print and electronic
Are you the author of this Elsevier article?	No
Will you be translating?	No
Original figure numbers	Figure 1C
Title of your thesis/dissertation	Bacteriophage M13 as a Template for Multi-Enzyme Assembly
Publisher of new work	University of Waterloo
Expected completion date	Sep 2019
Estimated size (number of pages)	1

Appendix A – Sequence Information

Cel8A

MAGVPFNTKYPYGPTSIADNQSEVTAMLKAEWEDWKSKRITSNGAGGYKRVQRDASTNYDT
VSEGMGYGLLLAVCFNEQALFDDLYRYVKSHFNGNGLMHWHIDANNNVTSHDGGDGAATD
ADEDIALALIFADKLWGSSGAINYGQEARTLINNLYNHCVEHGSYVLKPGDRWGGSSVTNPSY
FAPAWYKVYAQYTGDTRWNQVADKCYQIVEEVKKYNNGTGLVPDWCTASGTPASGQSYDY
KYDATRYGWRTAVDYSWFGDQRAKANCDMLTKFFARDGAKGIVDGYTIQGSKISNNHNASFI
GPVAAASMTGYDLNFAKELYRETVAVKDSEYYGYYGNSLRLLTLLYITGNFPNPLSDLSGQPT
PPSNPTPSLPPQVVYGDVNGDGNVNSTDLTMLKRYLLKSVTNINREAADVNRDGAINSSDMTI
LKRYLIKSIPHLPYLEHHHHHH

Coh2 variants

Coh2-LPETG

MAHHHHHHAAGVVVEIGKVTGSVGTTVEIPVYFRGVPSKGIANCDFVFRYDPNVLEIIGIDPGD
IIVDPNPTKSFDTAIYPDRKIIVFLFAEDSGTGAYAITKDGVFAKIRATVKSSAPGYITFDEVGGF
ADNDLVEQKVSFIDGGVNVGGSLPETG

Coh2-LPETAG

MAHHHHHHAAGVVVEIGKVTGSVGTTVEIPVYFRGVPSKGIANCDFVFRYDPNVLEIIGIDPGD
IIVDPNPTKSFDTAIYPDRKIIVFLFAEDSGTGAYAITKDGVFAKIRATVKSSAPGYITFDEVGGF
ADNDLVEQKVSFIDGGVNVGGSLPETAG

A2S-Coh2-LPETAG

MSHHHHHHAAGVVVEIGKVTGSVGTTVEIPVYFRGVPSKGIANCDFVFRYDPNVLEIIGIDPGD
IIVDPNPTKSFDTAIYPDRKIIVFLFAEDSGTGAYAITKDGVFAKIRATVKSSAPGYITFDEVGGF
ADNDLVEQKVSFIDGGVNVGGSLPETAG

A2S-Coh2-GGGGS-LPETAG

MSHHHHHHAAGVVVEIGKVTGSVGTTVEIPVYFRGVPSKGIANCDFVFRYDPNVLEIIGIDPGD
IIVDPNPTKSFDTAIYPDRKIIVFLFAEDSGTGAYAITKDGVFAKIRATVKSSAPGYITFDEVGGF
ADNDLVEQKVSFIDGGVNVGGSGGGGSLPETAG

CBM-Coh

MGTDSLEFIASKLALEVLFQGPLQHHHHHHPWTSASMCNTVSGNLKVEFYNSNPSDTTNSINP
QFKVTNTGSSAIDLSKLTLRYYYTVDGQKDQTFWCDHAAIIGSNGSYNGITSNVKGTFVKMSS
STNNADTYLEISFTGGTLEPGAHVQIQGRFAKNDWSNYTQSNDYSFKSASQFVEWDQVTAYL
NGVLVWGKEPGGSVVPSTQPVTTPPATTKPPATTIPPSDDPNAGSDGVVVEIGKVTGSVGTTVE
IPVYFRGVPSKGIANCDFVFRYDPNVLEIIGIDPGDIIVDPNPTKSFDTAIYPDRKIIVFLFAEDSGT
GAYAITKDGVFAKIRATVKSSAPGYITFDEVGGFADNDLVEQKVSFIDGGVNVGNAT

M13

- Highlighted sections correspond to the mature p8 coat protein.

M13KE (p8)

MKKSLVLKASVAVATLVPMLSFAAEGDDPAKAAFNSLQASATEYIGYAWAMVVVIVGATIGI
KLFKKFTSKAS

M13-A2G4 (p8)

MKKSLVLKASVAVATLVPMLSFAAAGGGGDPAK AAFNSLQASA TEYIGYAWAM
VVVIVGATIG IKLFKKFTSK AS